

**Chemical Modulation of Phospho-Signaling Pathways Involved in Cancer**

by

Sameer D. Phadke

A dissertation submitted in partial fulfillment  
of the requirements for the degree of  
Doctor of Philosophy  
(Chemistry)  
in the University of Michigan  
2015

Doctoral Committee:

Assistant Professor Matthew B. Soellner, Chair  
Assistant Professor Amanda L. Garner  
Professor Anna K. Mapp  
Professor E. Neil G. Marsh

© Sameer D. Phadke 2015

## ACKNOWLEDGEMENTS

Graduate school can be a difficult time without the support of your advisor, colleagues, friends, and family. I've been very fortunate to have had constant support and encouragement from all of these sources making the last six years a very enjoyable experience. Acknowledging everyone responsible for the production of this dissertation seems an impossible and unfair act, since it means so many people who have had an impact on me in small and big ways are invariably left out. So I'll stick to the people directly responsible for my progress while in graduate school.

I'd like to thank my advisor Dr. Matthew Soellner for his guidance over the last six years. A student's experience in graduate school is largely dictated by the lab environment and Matt, you've done an excellent job setting up your lab over the last 7 years making it very conducive for learning and a fun place to be in. Developing projects from the ground up and seeing them to fruition under your mentorship has been an incredible education that I'm very fortunate to have had. The freedom you offered me to pursue my own ideas and the attention you provided has kept me motivated and is directly responsible for my development as an independent scientist. I'm looking very excited about and looking forward to seeing the direction you take your lab takes over the next several years.

I've had very positive experiences interacting with faculty members at the University of Michigan. I'm very thankful to my committee members, Dr. Anna Mapp, Dr. Neil Marsh, and Dr. Amanda Garner for their guidance. I'm especially grateful for Dr. Anna Mapp, who in addition to being a fantastic asset for my committee has been a pleasure to teach with. Additionally, I've had the pleasure of being a graduate student instructor for Dr. Kathleen Nolte and Dr. Mustapha Belh. Both of them deserve special recognition for their incredible efforts, diligence, and skills as lecturers, which in turn, always motivated me to be a better teacher.

Throughout my time in the Soellner lab, I've had the pleasure of working with some very talented and hard-working colleagues: Dr. Peter Barker, Dr. Sonali Kurup, Dr. Steven Bremmer, Christel Fox, Michael Steffey, Dr. Kris Brandvold, Dr. Shana Santos, Dr. Meghan Breen, Frank Kwarcinski, Kristin Ko, Taylor Johnson, Eric Lachacz, Michael Agius, and Omar Beleh.

In particular, I'd like to thank Peter for his patient and enthusiastic mentorship which is largely responsible for my skills as a chemist. Frank, you've been an excellent bench-mate for the last 5 years. Despite the fact that we never worked on the same project, you've been a fantastic resource for ideas and encouragement. More importantly, I'm thankful for our friendship which set up a great work environment. Additionally, I'd like to thank Taylor Johnson, Eric Lachacz, and Chris Fox for their direct contributions to my projects. In addition to being excellent colleagues, I'm fortunate to be friends with all the current members of the Soellner lab.

Outside of the lab, I've had the pleasure of meeting some incredible people. Chelsea and Joe, you've both been a constant source of entertainment, inspiration, and support. I'm glad to have been friends with you since our first year in graduate school making it a wonderful experience. Victoria, David, Renata, Nathan, and Cam, I'm very fortunate to have met you all. We've had a great time together and you've left me with memories that I will cherish.

Finally, none of this would have been possible without the support of my family – my parents, Anjali and Dilip, and my sister, Himani. Thank you for your unwavering love and encouragement. Everything I am is because of you.

## TABLE OF CONTENTS

ACKNOWLEDGEMENTS	ii
LIST OF FIGURES	vii
LIST OF TABLES	ix
LIST OF SCHEMES	x
LIST OF APPENDICES	xi
ABSTRACT	xii
CHAPTER	
<b>I. Targeted Therapy in the Treatment of Cancer</b>	<b>1</b>
1.1. Abstract	1
1.2. Molecular Causes of Cancer	1
1.3. Phospho-Signaling Pathways Involved in Cancer	2
1.4. Efforts at Targeting Ras	3
1.5. Current Targeted Therapy	4
1.6. Conclusions	5
1.7. References	6
<b>II. Development of a Selective Inhibitor of Abl Kinase that Targets the T315I Gatekeeper Mutation</b>	<b>8</b>
2.1 Abstract	8
2.2. Chronic Myelogenous Leukemia and Treatment with Imatinib	8
2.3. c-Abl and its conformations	9
2.4. Imatinib-Resistant CML and Second Generation Inhibitors	12
2.5. Ponatinib and c-Abl Inhibitors that Target the T315I Gatekeeper Mutation	14

2.6.	Selectivity for c-Abl over c-Src	16
2.7.	Development of Selective Inhibitors Bypassing the Gatekeeper Mutation	18
2.8.	Kinome Profiling of compound <b>2.4</b> .	21
2.9.	<i>In Cellulo</i> Results	25
2.10.	Conclusions	27
2.11.	Materials and Methods	28
2.12.	References	41
<b>III.</b>	<b>Development of Cyclic Peptides as Inhibitors of Grb2 SH2</b>	45
3.1	Abstract	45
3.2.	Role of Grb2 in Cell Signaling	46
3.3.	Grb2 as a Therapeutic Target in Cancer	48
3.4.	Current Inhibitors of Grb2	48
3.5.	Utilizing Conformational Constraint in the Development of Grb2 SH2 Inhibitors	51
3.6.	Macrocycle Optimization	51
3.7.	Use of Phosphotyrosine Mimetics	53
3.8.	Surface Plasmon Resonance Studies	54
3.9.	Isothermal Titration Calorimetry	56
3.10.	Inhibition of Cancer Cell Growth	58
3.11.	Conclusions	58
3.12.	Materials and Methods	59
3.13	References	63
<b>IV.</b>	<b>Development of Substrate-Competitive Irreversible Inhibitors of Akt1</b>	67
4.1	Abstract	67
4.2.	Inhibitors Targeting the ATP-Binding Site of Kinases	67
4.3.	Inhibitors Targeting the Substrate-Binding Site of Kinases	69
4.4.	Covalent Inhibitors of Protein Kinases	71
4.5.	Akt1 as a Therapeutic Target in Cancer	72

4.6.	Fragment Screening of an Electrophile Library	73
4.7.	Modification of the Electrophile	76
4.8.	Proposed Binding Mode	78
4.9.	Conclusions	78
4.10.	Materials and Methods	79
4.11.	References	85
<b>V.</b>	<b>Conclusions and Future Directions</b>	<b>88</b>
5.1	Abstract	88
5.2	Development of a Selective Inhibitor of Abl Kinase	88
5.3	Optimizing Entropic Gains for Developing Inhibitors of Specific Kinases	89
5.4	N-Scan of Core Scaffold Yields Substantial Differences in Selectivity	90
5.5	Leveraging the Selectivity of <b>2.4</b> for Developing Irreversible Inhibitors	91
5.6	Utilizing Conformational Constraint for Stabilizing Turns Other than $\alpha$ -Helices	93
5.7	Utilizing Cyclic Peptides to Identify Inhibitors of Other SH2 Domains	94
5.8	N-Methylation to Increase Permeability of Cyclic Peptides	95
5.9	Substrate Competitive Irreversible Inhibitors of Akt1	95
5.10	Conclusions	96
5.11	References	97
	APPENDICES	99

## LIST OF FIGURES

### FIGURE

2.1.	Key structural features of the kinase domain of c-Abl (PDB 2GQG).	10
2.2.	Active and inactive conformations of c-Abl.	11
2.3.	Binding conformation of Imatinib to c-Abl.	12
2.4.	FDA-approved drugs for the treatment of CML and the RET inhibitor AST-487.	13
2.5.	Design elements for circumventing the T315I mutation.	14
2.6.	Determining the selectivity of Imatinib for c-Abl over c-Src.	17
2.7.	Selectivity profile for compound <b>2.4</b> .	22
2.8.	A plot of the primary screen score versus $K_d$ values for individual targets.	40
3.1.	Grb2 is comprised of one SH2 domain flanked by two SH3 domains.	46
3.2.	Novartis scaffold and the analogs synthesized by Burke and coworkers.	49
3.3.	Examples of local (left) and global (right) conformational constraint in the development of Grb2 SH2 inhibitors.	50
3.4.	The thermodynamic rationale of ligand pre-organization.	51
3.5.	SPR kinetic data for cyclic peptide <b>3.10</b> .	55
3.6.	SPR kinetic data for linear peptide <b>3.15</b> .	56
3.7.	ITC comparison of the cyclic and linear peptides.	57
4.1.	Surface representation of Akt1 (PDB 3MV5).	70
4.2.	Fragment screening results of Akt1.	75
4.3.	Top 10 hits obtained from the fragment screen.	76
4.4.	Proposed binding mode of compound <b>4.1</b> to Akt1.	78



5.1	Potential development of Lck-selective Inhibitors.	91
5.2	Multiple sequence alignment of the targets of compound <b>2.4</b> .	92

## LIST OF TABLES

### TABLE

2.1.	$K_i$ values of compounds with an altered hinge-binding motif.	19
2.2.	$K_i$ values of compounds with an altered type-II tail.	21
2.3.	56 kinases inhibited by AST-487 with $K_d < 69$ nM.	24
2.4.	Targets of <b>2.4</b> , but not of Imatinib.	25
2.5.	<i>In cellulo</i> evaluation of compound <b>2.4</b> .	26
3.1.	Summary of $IC_{50}$ values of macrocycles of increasing size.	52
3.2.	$IC_{50}$ values of compounds with phosphotyrosine mimetics.	53
4.1.	$IC_{50}$ values obtained on varying the electrophile.	77

## LIST OF SHEMES

### SCHEME

2.1.	Synthesis of compounds <b>2.1 – 2.6.</b>	28
2.2.	Synthesis of compounds <b>2.7 – 2.9.</b>	36
4.1.	Synthesis of compounds <b>4.1 – 4.6.</b>	80

## LIST OF APPENDICES

### APPENDIX

<b>A.</b>	<b>Analytical Data and Supporting Information for Chapter II</b>	99
A.1.	Spectral Data for Compounds <b>2.1-2.25</b>	100
A.2.	Analytical Data for Determination of $K_i$ Values	115
A.3.	KinomeScan™ Data for Compound 2.4	121
<b>B.</b>	<b>Analytical Data and Supporting Information for Chapter III</b>	133
B.1.	Peptide Synthesis and Characterization	134
B.2.	Analytical Data for Determination of $IC_{50}$ Values	136
B.3.	$K_d$ Determination Using Equilibrium Analysis on SPR	142
<b>C.</b>	<b>Analytical Data and Supporting Information for Chapter IV</b>	143
C.1.	Spectral Data for Compounds <b>4.1-4.6</b>	144
C.2.	InFarmatik Electrophile Fragment Library	150
C.3.	Percent Inhibition Values from Fragment Screen	154
C.4.	Analytical Data for Determination of $IC_{50}$ Values	154

## ABSTRACT

Advancements in our understanding of the molecular causes of cancer have led to the therapeutic targeting of key enzymes involved in cell growth and proliferation. Despite these advancements, cancer is expected to be the leading cause of death in the U.S. by the year 2035. Over the same period, the number of new cases globally is projected to rise by about 70%, necessitating an urgent need for the exploration of novel targets and therapeutics for the treatment of cancer. Of the drugs in current clinical use, kinase inhibitors have been the most successful forms of targeted therapy for a select group of cancers. However, a comprehensive understanding of the biological roles of individual kinases is necessary for therapies to be effective in a majority of cancers. The development of selective kinase probes and inhibitors, is, therefore, essential, for continued improvement in cancer chemotherapy. Additionally, the identification and exploration of non-kinase targets will be indispensable in adding to the toolbox of effective anti-cancer agents. To aid in our understanding of the molecular causes of cancer and to increase the number of tools available for its treatment, we aimed to develop inhibitors for critical proteins involved in phospho-signaling pathways.

Our studies began with the development of a selective inhibitor of the fusion protein, Bcr-Abl, which is the primary driver of Chronic Myelogenous Leukemia (CML). Most current FDA-approved drugs are ineffective against a resistant form of CML bearing a T315I mutation in the kinase domain of Bcr-Abl. While one approved drug, Ponatinib, is effective in the treatment of resistant CML, it displays life-threatening, and often, fatal toxicity owing to its promiscuity at inhibiting a multitude of kinases. Through a hypothesis based on the prevailing model of selectivity for the Abl kinase domain, we developed a library of small molecules and identified a compound with high potency for both the wild-type and mutant forms of Abl. The potency was comparable to that of Ponatinib, with a significantly improved spectrum of selectivity.

An alternate, non-kinase, and under-explored target for the treatment of CML and other cancers is the adaptor protein Grb2. Current inhibitors of Grb2 suffer from poor cellular efficacy, which is likely a consequence of most such inhibitors being primarily based on a single scaffold. Our efforts for targeting Grb2 centered on the hypothesis that utilizing conformational constraint for inhibitor development could lead to compounds with increased potency due to a lowered entropic cost of binding. Through the systematic development of conformationally constrained cyclic peptides, we identified a novel scaffold for the inhibition of Grb2 with *in cellulo* efficacy in a CML cell line.

Lastly, while protein kinases have been traditionally targeted with small molecules directed to their ATP-binding site, targeting the peptide substrate-binding site of kinases offers an attractive alternative with several advantages. The nature of the substrate-binding site, however, typically requires the development of linear peptidic inhibitors that lack potency and suffer from poor cell permeability and stability. Our efforts attempted to circumvent the problems associated with substrate-competitive inhibitors by covalently inhibiting the target Akt1 kinase. Our lead compound could prove a valuable tool for the delineation of the roles of specific isoforms of the Akt kinases.

As a whole, results from this work should advance the development of potent and selective inhibitors and aid in the understanding of signaling pathways involved in cancer.

## **CHAPTER I**

### **Targeted Therapy in the Treatment of Cancer**

#### **1.1. Abstract**

The last two decades have witnessed tremendous advancements in our understanding of the molecular causes of cancer and targeted therapy directed towards certain types of cancer. Despite these advancements, cancer remains the second most common cause of death in the U.S. (after heart disease) and is expected to be the leading cause by the year 2035. Over the same period, the number of new cases globally is projected to rise by about 70%, necessitating an urgent need for the exploration of novel targets and therapeutics for the treatment of cancer. This chapter provides a brief overview of the developments that led to our current understanding of the molecular causes of cancer. Furthermore, it details some of the key signaling pathways involved in cancer and offers insights into the limitations of our current understanding of these pathways as well as strategies for the development of novel cancer therapeutics.

#### **1.2. Molecular Causes of Cancer**

In 1911, Peyton Rous described an agent isolated from chicken tumor cells that, when injected in healthy chickens, caused the growth of tumors.<sup>1</sup> His observations, though seminal, were looked upon with skepticism, since at the time, cancers were not known to be transmissible.<sup>2</sup> His work did, however, initiate one of the first inquiries into the cause of cancer and 40 years later it was incontrovertibly proven that the causative agent observed by him was a virus, which could, in fact, cause the growth of tumor cells.<sup>3</sup> By the 1940s, through epidemiological and experimental data, it was well understood that cancers could be initiated by exposure to radiation and certain chemicals. However, the exact mechanism through which such exposure caused cancer was unclear.<sup>4</sup>

Around the same time, the modern era of cancer chemotherapy was initiated through the findings of Louis Goodman and Alfred Gilman investigating the therapeutic potential of chemical warfare agents. To assess the cytotoxic effects of nitrogen mustards

on cancer cells, a single mouse transplanted with a tumor was administered with, what was then only disclosed as, ‘Chemical X’.<sup>5</sup> Remarkably, regression of the tumor to undetectable levels was observed, and the mouse lived eighty-four days after implantation. Studies in several different tumor-bearing mice, however, revealed that some, but not all mice, showed tumor regression to various extents. Their fortuity and success were reflected upon by their colleague, Thomas Dougherty in a correspondence with Gilman; “... the very first mouse treated turned out to give the best result ... in most of the murine leukemias, particularly those which metastasize readily, we frequently obtained no effect at all. I have often thought that if we had by accident chosen one of these leukemias, in which there was absolutely no therapeutic effect, we might possibly have dropped the whole project”.<sup>5</sup> In addition to paving the way for cytotoxic chemotherapy, these initial studies led to the key observation, articulated above by Thomas Dougherty, that the efficacy of chemotherapy was not universal and variations in response existed in different tumor types.<sup>5-6</sup>

The idea that all cancers are not alike led to a massive effort in trying to understand the underlying cause of different cancers; an effort that continues to this day. The discovery that Chronic Myelogenous Leukemia (CML) arises from a shortened chromosome 22<sup>7-9</sup>, and the subsequent discovery of proto-oncogenes<sup>10-11</sup> led to a fundamental change in the understanding of how mutations and translocations lead to cancer and genetic abnormalities in other cancers were studied. By the 1990s, advances in molecular biology led to the identification and mapping of several signaling pathways involved in tumor cell growth and set the stage for targeted therapy in cancer.

### **1.3. Phospho-Signaling Pathways Involved in Cancer**

One of the most important pathways involved in cell growth is the Ras-signaling pathway. The best-characterized model of this pathway involves a linear signaling cascade from the epidermal growth factor receptor (EGFR) to transcription factors. By the late 1980s, though it was well understood that the GTPase, Ras, was dependent on the activation of EGFR, the exact mechanism through which this occurred was unclear. The key missing components were identified in rapid succession in the early 1990s with the characterization of the adaptor protein Grb2, and the guanine-nucleotide exchange factor Sos.<sup>12</sup> (The role of Grb2 within this pathway is discussed in depth in **Chapter III**.) Receptor activation and phosphorylation leads to the recruitment of the Grb2-Sos complex



from the cytosol to the membrane. The localization of Sos to the membrane leads to the conversion of membrane-bound Ras from its inactive, GDP-bound state, to its active, GTP-bound state. This triggers the activation of an entire signaling cascade through the phosphorylation of downstream kinases Raf, Mek, and Erk, ultimately resulting in cell growth and proliferation.

Approximately 30% of all tumors have activating Ras mutations making them one of the most common genetic causes of cancer.<sup>13</sup> Activating Ras mutants contributes significantly to deregulated cell growth and, even tumors that lack Ras mutations, activate and deregulate the Ras-signaling pathway through other means.<sup>14</sup> The early identification of the entire pathway from the cell surface to the nucleus and its involvement in cell growth and proliferation made it an excellent candidate for therapeutic intervention in cancer.

#### **1.4. Efforts at Targeting Ras**

The Ras proteins have been extremely difficult to target, and no effective targeted therapy exists. The development of guanine-nucleotide mimics directly targeting the binding site have been deemed unfeasible owing to the high affinity (picomolar) of Ras for both GDP in the inactive state and GTP in the active state, coupled with millimolar concentrations of these nucleotides in cells.<sup>15</sup> Some recent success has been achieved, however, in covalently targeting a mutant form of K-Ras (G12C)<sup>15-16</sup> and in identifying low-affinity (high micromolar) allosteric inhibitors of K-Ras.<sup>17-18</sup> Further development of allosteric inhibitors is needed, however, for them to be viable therapeutic agents.

In lieu of a direct-targeting approach, disruption of the post-translational farnesylation of Ras at its C-terminus, and preventing its subsequent membrane localization, was attempted. The 1990s subsequently witnessed a massive effort by pharmaceutical companies to develop inhibitors of farnesyltransferase (the enzyme responsible for the post-translational modification) based on impressive results in pre-clinical models.<sup>19</sup> This effort was ultimately unfruitful in terms of efficacy in clinical trials as inhibition of farnesyltransferase led to the prenylation of Ras through the alternate mechanism of geranylgeranylation by the enzyme geranylgeranyltransferase. Furthermore, it was believed that the pre-clinical success of farnesyltransferase inhibitors was due to the non-specific inhibition of farnesylation of proteins other than Ras.<sup>14, 19-20</sup>

With little success in directly or indirectly targeting Ras proteins, other methods to target the Ras-signaling pathway have been attempted which have coincided with the concomitant rise of Bcr-Abl inhibitors in the treatment of CML.

### 1.5. Current Targeted Therapy

CML, discussed in detail in **Chapter II**, is one among a very small group of cancers that is driven by a single genetic abnormality. The shortened chromosome observed in CML is caused by a reciprocal translocation t(9;22)(q34;q11) involving the juxtaposition of *Abl1* of chromosome 9 with a part of *Bcr* on chromosome 22.<sup>21</sup> The fusion protein product BCR-Abl, is a kinase that is constitutively activated, leading to uncontrolled cell growth and proliferation.<sup>21-23</sup>

In 2001, the BCR-Abl tyrosine kinase inhibitor Imatinib, was approved for the treatment of CML and a 5-year follow-up displayed a remarkable increase in the overall survival rate from 50% (following cytotoxic chemotherapy) to 89%.<sup>24</sup> The success of Imatinib in converting an invariably fatal disease into a chronic, manageable condition spurred great interest in developing inhibitors of other kinases believed to be involved in a variety of cancers.<sup>25</sup> Most such efforts have been directed toward the development of inhibitors of receptor tyrosine kinases upstream of Ras (EGFR, Her2) and non-receptor kinases downstream from it (BRaf, Mek1/2, and Erk1/2). Several of these drugs are currently in clinical trials while others have been approved for the treatment of certain cancers.

Few kinase inhibitors, however, have shown the dramatic efficacy and safety observed with Imatinib therapy. This is a consequence of the fact that, unlike CML, the majority of tumor types are not ‘addicted’ to a single oncogenic kinase for growth.<sup>25</sup> This does not suggest, however, that kinase inhibitors can only be used to treat ‘addicted’ cancers. The model for the Ras-signaling pathway presented above is a gross oversimplification of the complex signaling that occurs in cell growth and proliferation. This complexity is multiplied by the incredible degree of crosstalk that occurs between pathways, which gives rise to multiple redundant pathways. A second complication that arises in the use of kinase inhibitors is that the off-target inhibition of certain kinases can lead to life-threatening toxic effects and fatalities. Consequently, success in treating malignancies not dependent on a single kinase will depend on targeting multiple, yet

specific, kinases while sparing those that can lead to toxicity. Identifying the appropriate kinases to be targeted in specific cancers remains one of the biggest challenges today, and the development of selective compounds or ‘probes’ will be necessary to delineate the functional role of individual kinases. **Chapter IV** details our efforts in developing covalent inhibitors for underexplored sites of a kinase that could provide uniquely selective compounds for probing the roles of closely related kinases.

A third cause of the failure of kinase inhibitors in the treatment of certain cancers is the development of resistance to treatment. Such resistance is commonly observed in patients receiving Imatinib therapy and renders the drug ineffective. **Chapter II** details our efforts in developing a highly selective Bcr-Abl inhibitor that is capable of inhibiting one of the most common mutations observed in CML. However, as targeted therapy with kinase inhibitors is not a cure for cancer, but rather the conversion to a chronic disease, the problem of resistance is likely to grow in the coming years as the overall survival rate of patients continues to increase. Consequently, the exploration of other viable targets is essential for improvements in targeted therapy. **Chapter III** details our efforts in developing inhibitors for one such target, Grb2, which in addition to being a key component of Ras-signaling, is also known to play a role in CML.

## **1.6. Conclusions**

Despite the fact that our current abilities for the treatment of certain cancers seemed unattainable until only a decade ago, advancements in targeted therapy have not kept up with growing incidences of cancer. While kinase inhibitors have been the most successful forms of targeted cancer chemotherapy, a comprehensive understanding of the biological roles of individual kinases will be necessary for therapies to be effective in a majority of cancers. The development of selective kinase probes and inhibitors, is, therefore, essential, for continued improvement in cancer chemotherapy. For therapies that are currently effective against certain types of cancer, the development of resistance poses a grave risk. Consequently, in addition to developing next-generation inhibitors that can overcome such resistance, the identification and exploration of non-kinase targets will be vital.

## 1.7. References

1. Rous, P., A Sarcoma of the Fowl Transmissible by an Agent Separable from the Tumor Cells. *J Exp Med* **1911**, *13* (4), 397-411.
2. Yeatman, T. J., A renaissance for SRC. *Nat Rev Cancer* **2004**, *4* (6), 470-480.
3. Rubin, H., Quantitative relations between causative virus and cell in the Rous no. 1 chicken sarcoma. *Virology* **1955**, *1* (5), 445-473.
4. Knudson, A. G., Two genetic hits (more or less) to cancer. *Nat Rev Cancer* **2001**, *1* (2), 157-162.
5. Gilman, A., The initial clinical trial of nitrogen mustard. *Am J Surg* **1963**, *105*, 574-578.
6. Chabner, B. A.; Roberts, T. G., Jr., Timeline: Chemotherapy and the war on cancer. *Nat Rev Cancer* **2005**, *5* (1), 65-72.
7. Nowell, P. C.; Hungerford, D. A., Chromosome studies on normal and leukemic human leukocytes. *J Natl Cancer Inst* **1960**, *25*, 85-109.
8. Rudkin, C. T.; Hungerford, D. A.; Nowell, P. C., DNA Contents of Chromosome Ph1 and Chromosome 21 in Human Chronic Granulocytic Leukemia. *Science* **1964**, *144* (3623), 1229-1231.
9. Rowley, J. D., Identificaton of a translocation with quinacrine fluorescence in a patient with acute leukemia. *Ann Genet* **1973**, *16* (2), 109-112.
10. Stehelin, D.; Varmus, H. E.; Bishop, J. M.; Vogt, P. K., DNA related to the transforming gene(s) of avian sarcoma viruses is present in normal avian DNA. *Nature* **1976**, *260* (5547), 170-173.
11. Martin, G. S., Rous sarcoma virus: a function required for the maintenance of the transformed state. *Nature* **1970**, *227* (5262), 1021-1023.
12. Lowenstein, E. J.; Daly, R. J.; Batzer, A. G.; Li, W.; Margolis, B.; Lammers, R.; Ullrich, A.; Skolnik, E. Y.; Bar-Sagi, D.; Schlessinger, J., The SH2 and SH3 domain-containing protein GRB2 links receptor tyrosine kinases to ras signaling. *Cell* **1992**, *70* (3), 431-442.
13. Bos, J. L., ras oncogenes in human cancer: a review. *Cancer Res* **1989**, *49* (17), 4682-4689.
14. Downward, J., Targeting RAS signalling pathways in cancer therapy. *Nat Rev Cancer* **2003**, *3* (1), 11-22.
15. Lim, S. M.; Westover, K. D.; Ficarro, S. B.; Harrison, R. A.; Choi, H. G.; Pacold, M. E.; Carrasco, M.; Hunter, J.; Kim, N. D.; Xie, T.; Sim, T.; Janne, P. A.; Meyerson, M.; Marto, J. A.; Engen, J. R.; Gray, N. S., Therapeutic targeting of oncogenic K-Ras by a covalent catalytic site inhibitor. *Angew Chem Int Ed Engl* **2014**, *53* (1), 199-204.
16. Ostrem, J. M.; Peters, U.; Sos, M. L.; Wells, J. A.; Shokat, K. M., K-Ras(G12C) inhibitors allosterically control GTP affinity and effector interactions. *Nature* **2013**, *503* (7477), 548-551.
17. Sun, Q.; Burke, J. P.; Phan, J.; Burns, M. C.; Olejniczak, E. T.; Waterson, A. G.; Lee, T.; Rossanese, O. W.; Fesik, S. W., Discovery of small molecules that bind to K-Ras and inhibit Sos-mediated activation. *Angew Chem Int Ed Engl* **2012**, *51* (25), 6140-6143.
18. Maurer, T.; Garrenton, L. S.; Oh, A.; Pitts, K.; Anderson, D. J.; Skelton, N. J.; Fauber, B. P.; Pan, B.; Malek, S.; Stokoe, D.; Ludlam, M. J.; Bowman, K. K.; Wu, J.; Giannetti, A. M.; Starovasnik, M. A.; Mellman, I.; Jackson, P. K.; Rudolph, J.; Wang, W.;

- Fang, G., Small-molecule ligands bind to a distinct pocket in Ras and inhibit SOS-mediated nucleotide exchange activity. *Proc Natl Acad Sci U S A* **2012**, *109* (14), 5299-5304.
19. Sebti, S. M.; Hamilton, A. D., Farnesyltransferase and geranylgeranyltransferase I inhibitors in cancer therapy: important mechanistic and bench to bedside issues. *Expert Opin Investig Drugs* **2000**, *9* (12), 2767-2782.
20. Sebti, S. M.; Hamilton, A. D., Farnesyltransferase and geranylgeranyltransferase I inhibitors and cancer therapy: lessons from mechanism and bench-to-bedside translational studies. *Oncogene* **2000**, *19* (56), 6584-6593.
21. Kurzrock, R.; Gutterman, J. U.; Talpaz, M., The Molecular Genetics of Philadelphia Chromosome-Positive Leukemias. *New England Journal of Medicine* **1988**, *319* (15), 990-998.
22. Lugo, T.; Pendergast, A.; Muller, A.; Witte, O., Tyrosine kinase activity and transformation potency of bcr-abl oncogene products. *Science* **1990**, *247* (4946), 1079-1082.
23. Daley, G.; Van Etten, R.; Baltimore, D., Induction of chronic myelogenous leukemia in mice by the P210bcr/abl gene of the Philadelphia chromosome. *Science* **1990**, *247* (4944), 824-830.
24. Druker, B. J.; Guilhot, F.; O'Brien, S. G.; Gathmann, I.; Kantarjian, H.; Gattermann, N.; Deininger, M. W. N.; Silver, R. T.; Goldman, J. M.; Stone, R. M.; Cervantes, F.; Hochhaus, A.; Powell, B. L.; Gabrilove, J. L.; Rousselot, P.; Reiffers, J.; Cornelissen, J. J.; Hughes, T.; Agis, H.; Fischer, T.; Verhoef, G.; Shepherd, J.; Saglio, G.; Gratwohl, A.; Nielsen, J. L.; Radich, J. P.; Simonsson, B.; Taylor, K.; Baccarani, M.; So, C.; Letvak, L.; Larson, R. A., Five-Year Follow-up of Patients Receiving Imatinib for Chronic Myeloid Leukemia. *New England Journal of Medicine* **2006**, *355* (23), 2408-2417.
25. Baselga, J.; Arribas, J., Treating cancer's kinase 'addiction'. *Nat Med* **2004**, *10* (8), 786-787.

## CHAPTER II

### Development of a Selective Inhibitor of Abl Kinase that Targets the T315I Gatekeeper Mutation

#### 2.1. Abstract

Patients with Chronic Myelogenous Leukemia (CML) show a dramatic improvement in 5-year overall survival on treatment with the Bcr-Abl inhibitor, Imatinib. Long term treatment, however, invariably leads to the development of point mutations in the c-Abl kinase domain resulting in Imatinib being rendered ineffective. Second generation inhibitors are effective against all but the single most common point mutation, the T315I ‘gatekeeper’ mutation. While the third generation inhibitor, Ponatinib, can inhibit the gatekeeper mutant c-Abl, it displays severe and life-threatening toxicity possibly due to its promiscuity in inhibiting other kinases. This chapter details our efforts in developing a selective inhibitor of c-Abl with the ability to inhibit the clinically relevant T315I mutant. Based on the prevailing model of selectivity for the c-Abl kinase domain, we developed a library of small molecules targeting the c-Abl kinase domain and identified compound **2.4** with high potency for both the wild type (380 pM) and T315I (550 pM) Abl. The potency was comparable to that of Ponatinib, with a significantly improved spectrum of selectivity. The efficacy of compound **2.4** was demonstrated both biochemically and *in cellulo* in wild type and T315I Bcr-Abl dependent cell lines. Additionally, the development of compound **2.4** led to a more comprehensive understanding of pharmacophores necessary for targeting certain groups of kinases while sparing others.

#### 2.2. Chronic Myelogenous Leukemia and Treatment with Imatinib

A striking example of a cancer caused by a genetic abnormality through chromosomal translocation is that of Chronic Myelogenous Leukemia (CML). The reciprocal translocation t(9;22)(q34;q11) involves juxtaposition of *Abl1* of chromosome 9 with a part of *Bcr* on chromosome 22 giving rise to a shortened chromosome 22, termed the Philadelphia chromosome.<sup>1</sup> The two possible fusion protein products, p185, and p210

BCR-Abl have deregulated tyrosine kinase activity leading to uncontrolled cell growth and proliferation.<sup>1-3</sup> The p210 form of BCR-Abl is observed in over 95% of patients with CML and 20% of patients with acute lymphocytic leukemia (ALL), while the p185 form is seen in 10% of patients with ALL.<sup>4</sup>

CML accounts for about 15% of leukemias in adults and left untreated, is characterized by three distinct clinical phases. The first, a chronic phase lasting three to six years, followed by an accelerated phase lasting 1 to 1.5 years, and finally a blast crisis resulting in the patient's death within 3 to 6 months.<sup>5-7</sup> Prior to 2001, treatment options for patient with CML were limited to conventional chemotherapy, allogeneic stem cell transplantation (for the 20% of patients that were eligible), and interferon- $\alpha$  therapy resulting in a 5-year overall survival rate of 50% when treated in the chronic phase.<sup>7</sup> In 2001, the c-Abl tyrosine kinase inhibitor Imatinib, was approved for treatment of CML and a 5-year follow-up displayed a remarkable increase in overall survival rate to 89%.<sup>8</sup> Patients in the accelerated phase receiving Imatinib, however, demonstrated a significantly lower estimated 4-year survival rate of 53%.<sup>9</sup> Furthermore, long-term treatment often gave rise to Imatinib-resistant CML, necessitating the development of next generation inhibitors.

### **2.3. c-Abl and its Conformations**

c-Abl is a 150 kDa protein, the N-terminal consisting of the SH2, SH3 and kinase domains, and a 90 kDa C-terminal half is unique and consists of DNA binding domains and repeating actin binding domains.<sup>10</sup> Two isoforms of c-Abl have been identified, one of which is myristoylated at the N-terminus (c-Abl 1a), and the other which is 19 residues shorter and non-myristoylated (c-Abl 1b). Amino acid numbering throughout this chapter is based on the 1b isoform. The minimal domains required for tyrosine kinase activity and regulation comprise residues 1 to 531 and include the SH3 domain, SH2 domain, and the catalytic kinase domain.<sup>11</sup>

The catalytic domain has a typical kinase fold<sup>12</sup>, comprised of an N-lobe, which is primarily made up of  $\beta$ -sheets and a C-lobe, which is mostly made up of  $\alpha$ -helices. A deep hydrophobic cleft exists between the two lobes forming the ATP-binding site. Key structural elements illustrated in **Figure 2.1** required for binding to ATP and catalysis include:

- i. A hinge region in the cleft between the lobes forms hydrogen bonds with ATP and most small molecule inhibitors.
- ii. A phosphate-binding loop (P-loop) forms the ceiling of the ATP binding site and clamps down on the phosphates of ATP, enabling catalysis. The glycine-rich nature of the P-loop enables flexibility in the absence of ATP, resulting in different conformations in different kinases.<sup>13</sup>

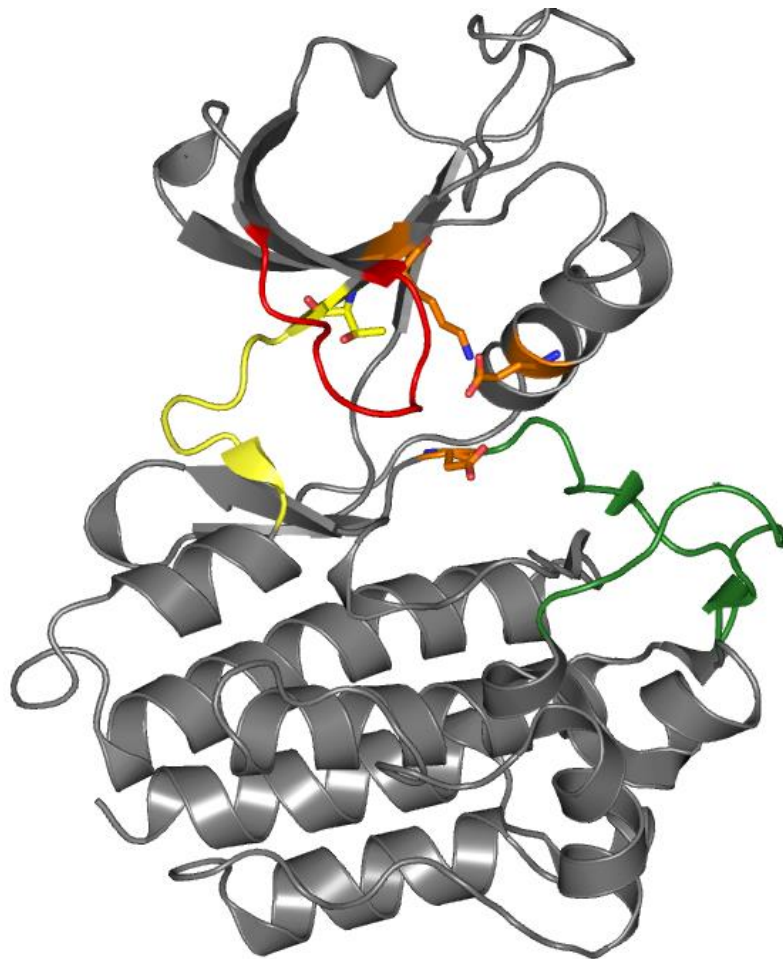


**Figure 2.1.** Key structural features of the kinase domain of c-Abl (PDB 2GQG). A loop between the N- and C-terminal lobes is termed as the hinge region (shown in yellow) and is preceded by the gatekeeper Thr315 residue. A flexible glycine rich P-loop (red) positions ATP for catalysis. An activation loop (green) is responsible for regulation and begins with a DFG motif. Asp381 (of DFG) is positioned in close proximity to Lys271 and Glu286 that collectively form a conserved triad responsible for catalysis (orange).



- iii. An activation loop, containing a conserved DFG-motif (residues 381-383) and a tyrosine (Y393) that serves as a phosphorylation site, plays a role in regulating the enzyme.<sup>13</sup>
- iv. Conserved residues involved in catalysis are Lys271, Asp381 of the DFG motif, and Glu286 on the  $\alpha$ C helix.
- v. An important residue determining access to a back-pocket of the kinase is Thr315 and is also termed the ‘gatekeeper’ residue.

c-Abl binds to ATP-competitive small molecules in three distinct conformations. The first, an active ‘DFG-in’ conformation, mimics the binding mode of ATP, in which Phe382 of the DFG-motif is buried in a hydrophobic pocket, positioning Asp381 for catalysis (**Figure 2.2, left**). Inhibitors that bind to this conformation are known as type-I inhibitors and are restricted to contacts with the hinge region. The second, an inactive ‘DFG-out’ conformation, has a substantial movement of the activation loop, in which Phe382 is flipped outward creating a hydrophobic cavity that can be occupied by (type-II) inhibitors extending from the hinge region (**Figure 2.2, right**). The third, ‘ $\alpha$ C-out’ conformation, is also inactive and is caused by the outward movement and rotation of the  $\alpha$ C-helix, preventing the optimal positioning of Glu286 for catalysis. The  $\alpha$ C-out conformation will not be discussed further in this chapter.

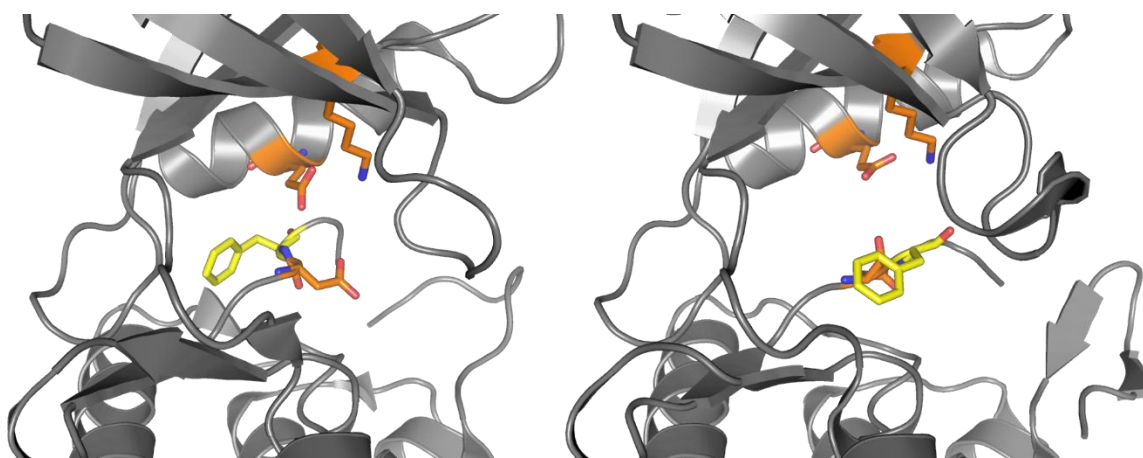


**Figure 2.2.** Active and inactive conformations of c-Abl. *Left* – Active DFG-in conformation with Lys271, Asp381, and Glu286 (orange) positioned for catalysis (PDB 2GQG). *Right* – Inactive DFG-out conformation with Phe382 (yellow) flipped outward creating a new hydrophobic cavity (PDB 1IEP).

The remarkable efficacy and selectivity of Imatinib was initially attributed to its ability to bind to c-Abl in a DFG-out conformation. This conformation was then believed to be accessible by only a few kinases and not by others, notably c-Src, that shares 46% sequence identity with c-Abl.<sup>14-15</sup> This was subsequently proved to be untrue as a crystal structure of c-Src bound to Imatinib, displayed an identical DFG-out conformation.<sup>16</sup> A detailed look at the basis for selectivity toward c-Abl is described in **Section 2.6**. The Imatinib/c-Abl crystal structure (**Figure 2.3, Left**) showed the pyridine and pyrimidine rings positioned in the ATP binding pocket, with the pyridine nitrogen making an H-bond with the backbone of Met318 in the hinge region. The P-loop of c-Abl forms a hydrophobic cage around the pyridine and pyrimidine ring systems. The compound extends past the gatekeeper residue Thr315 through an *ortho*-substituted aniline linker and makes an H-bond with its side chain. Four additional hydrogen bonds are formed between the compound and residues Glu286, Asp381, His361, and Ile360. A majority of contacts are mediated by van der Waals interactions with a total of 1251 Å<sup>2</sup> surface area buried between Imatinib and c-Abl.<sup>14</sup>

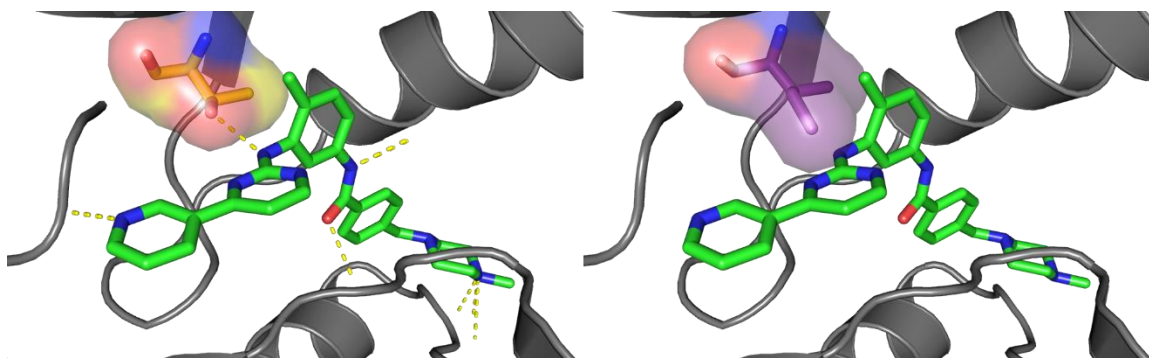


**Figure 2.3.** Binding conformation of Imatinib to c-Abl. *Left* – Imatinib forms H-bonds with the hinge, Thr315, and 4 additional residues on extending past the gatekeeper. *Right* – The T315I mutation leads to loss of an H-bond and steric occlusion of Imatinib.

#### 2.4. Imatinib-Resistant CML and Second Generation Inhibitors

Patients display either an innate resistance or an acquired resistance to Imatinib on prolonged treatment. To date, over 50 point mutations in the kinase domain of c-Abl have been observed that reduce or abrogate binding to Imatinib while retaining catalytic activity. Mutations that render Imatinib ineffective can be of several types - those that possibly prevent kinking of the P-loop, those that sterically occlude small molecules, and those that

de-stabilize the DFG-out conformation.<sup>17</sup> Despite the large number of mutations observed, several of these are relatively rare. A handful of residues; Gly250, Tyr253, Glu255, Thr315, Met351, and Phe359, account for about 70% of all mutated residues.<sup>18</sup> An additional complication involves the fact that two of the more commonly detected mutations, Y253F, and E255K, have a greater oncogenic potential than the native enzyme itself. Consequently, though Imatinib binding to these mutants is reduced by only 5 to 10-fold in biochemical studies<sup>19</sup>, inhibition of cellular proliferation is disproportionately affected.<sup>18</sup> Most mutations are observed in the P-loop of c-Abl, which can accommodate amino acid substitutions without losing catalytic activity, owing to its dynamic nature. The single most common mutation, however, is the T315I gatekeeper mutation<sup>20</sup> which completely eliminates binding to Imatinib (**Figure 2.3, Right**), due to steric hindrance of

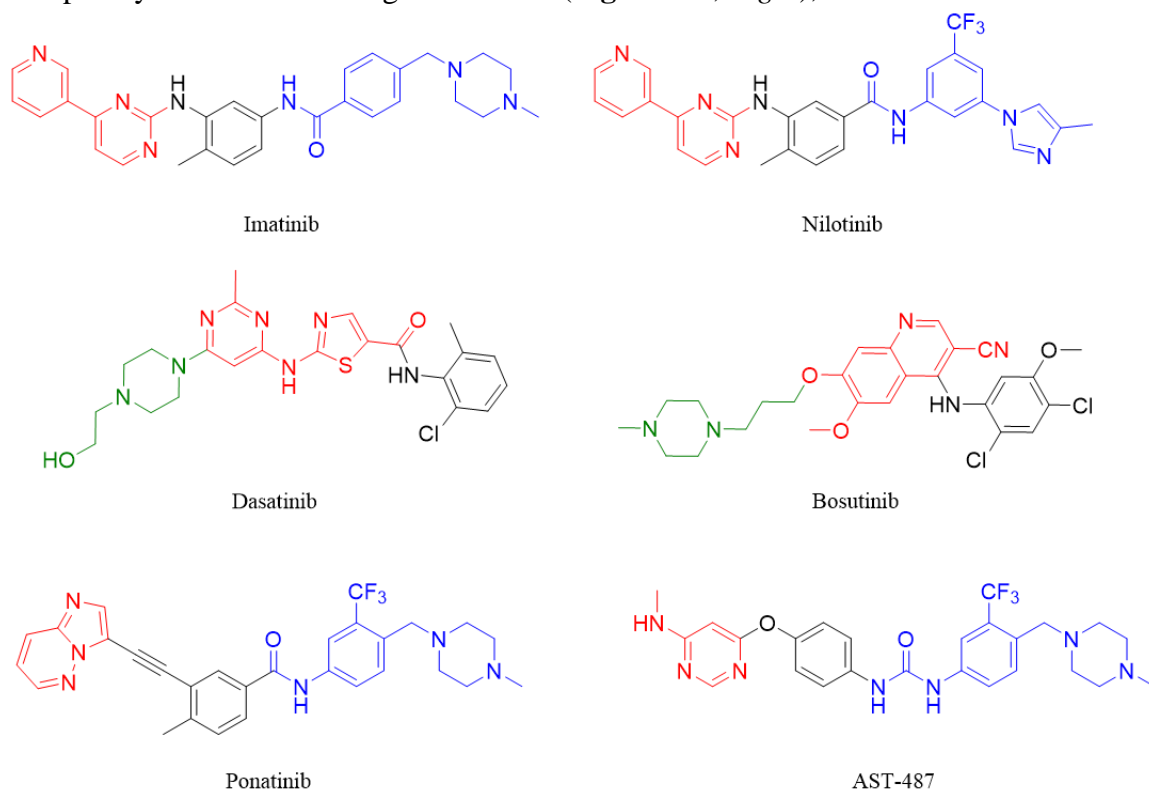


**Figure 2.4.** FDA-approved drugs for the treatment of CML and the RET inhibitor AST-487. Red indicates the portion of the molecule binding to the ATP-binding pocket and makes contacts with the hinge region. Black indicates the portion directly adjacent to the gatekeeper residue and is referred to as the linker group. Blue indicates the portion of type II inhibitors that binds to the cavity created by the outward flip of the DFG motif. Green in Dasatinib and Bosutinib is primarily a solubilizing group.

the bulkier Isoleucine substitution, loss of an H-bond with the side chain of Threonine, and an increased affinity for ATP.

Point mutations leading to Imatinib-resistant CML necessitated the development of second generation inhibitors that could overcome this resistance. Nilotinib, Bosutinib, and Dasatinib are effective at inhibiting most P-loop mutants of c-Abl. The inhibitors are, however, completely ineffective at inhibiting the T315I mutation, possibly due to the same mechanisms as observed for Imatinib.

## 2.5. Ponatinib and c-Abl Inhibitors that Target the T315I Gatekeeper Mutation

All first and second generation inhibitors approved for the treatment of CML form a critical H-bond with the side-chain hydroxyl group of Thr315. Mutation of this residue to Ile315 prevents high-affinity binding, requires a significant rearrangement of the binding conformation and alters the topology of the binding pocket.<sup>21-22</sup>

Three general design elements have now been identified for the development of type II inhibitors that can bypass the gatekeeper mutant c-Abl (**Figure 2.5**). The first, identified empirically, involves incorporating additional H-bond donor and acceptor atoms to increase the number of polar interactions with the hinge region. Consequently, binding is not entirely reliant on the single H-bond formed between the linker aniline and the side chain of Thr315, and a mutation to Ile315 does not significantly reduce affinity. Molecules

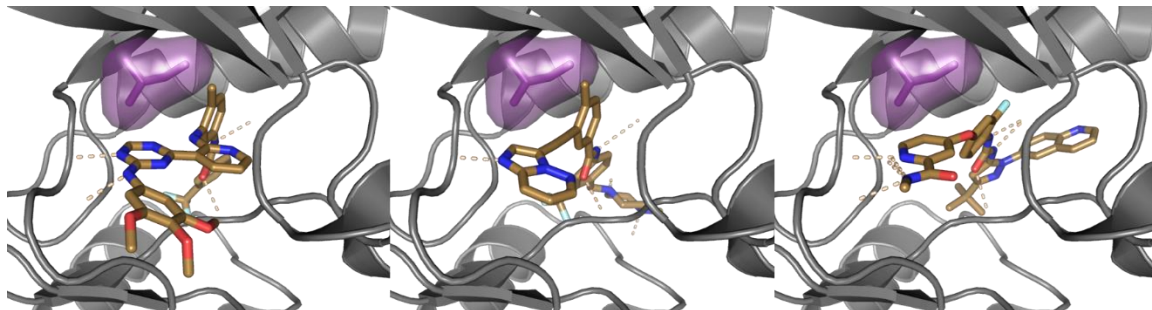


**Figure 2.5.** Design elements for circumventing the T315I mutation. Additional H-bond donor and acceptor atoms in the hinge-binding portion of the molecule, compensates for the loss of an H-bond with the side chain of Thr315. Additionally, a slight rotation of the *ortho*-aniline linker prevents a clash with the bulky isoleucine residue (*Left*). An alkyne linker (*Middle*) and a *para*-substituted phenol (*Right*) are not sterically occluded by a bulky gatekeeper and are not reliant on an H-bond.

incorporating this design element, are, however, very potent inhibitors of Src Family

Kinases (SFKs) and have poor kinome-wide selectivity.<sup>22-23</sup> A possible reason for the promiscuity of these compounds is discussed in **Section 2.6**.

The second strategy involves the use of an alkyne to link the hinge-binding portion of the molecule to the type-II tail. Unlike the larger, *ortho*-substituted aniline linker present in Imatinib and all second generation c-Abl inhibitors, the compact alkyne linker is neither sterically occluded nor reliant on the ability to form an H-bond with the gatekeeper residue. Since then, a number of alkyne and alkene linker-based compounds have been identified to inhibit both wild-type and T315I c-Abl.<sup>21, 24-25</sup> None of these compounds, however, display a spectrum of selectivity similar to Imatinib or Nilotinib. Further development of this class of compounds by ARIAD Pharmaceuticals, led to the approval of Ponatinib for the treatment of Imatinib resistant and refractory CML. In addition to inhibiting wild-type and T315I c-Abl, Ponatinib inhibited almost every other clinically relevant mutant with high potency.<sup>21</sup> Ponatinib's approval was through the FDA's Accelerated Approval pathway, based on data from a single phase II trial of 449 patients, 29% of which harbored a T315I mutation.<sup>26</sup> A consequence of a short follow-up period of 10 months was that primary endpoints were surrogate outcomes such as hematological and cytogenetic response, and not outcomes such as mortality. At the time of approval, 56% of patients with chronic-phase CML showed a major cytogenetic response, and that number climbed to 70% when only considering patients with a T315I mutation.<sup>27</sup> 10 months after approval, however, the FDA temporarily suspended sales of Ponatinib due to mounting evidence of serious and life-threatening toxicity after a longer follow-up period. 24% of participants from the Phase II study experienced myocardial infarction, stroke, limb ischemia, and stenosis of blood vessels. Similarly, a 30-month follow-up of participants from the Phase I study demonstrated vascular events in 48% of patients.<sup>26</sup> Subsequently, the suspension of sales was partially lifted and a black-box warning was issued for the use of Ponatinib, while a larger Phase III trial for approval as a first-line therapy was halted. Though the exact cause of its toxicity has not been determined, it is hypothesized that it may be due to its high promiscuity in potently inhibiting multiple kinases and/or due to an effect related to its scaffold. The kinases involved have not been unambiguously identified, however, evidence suggests that the inhibition of kinases critical for angiogenesis such as VEGFR-1 (FLT1), VEGFR-2 (KDR), and VEGFR-3 (FLT4) could cause cardiotoxicity.<sup>28</sup> Other

important targets that may be involved in cardiotoxicity include HER2, c-KIT, PDGFR $\alpha/\beta$ , and JAK2.<sup>29</sup> With the exception of HER2, Ponatinib inhibits all of the above-listed kinases very potently.<sup>30</sup>

The last design element for developing T315I c-Abl inhibitors includes a *para*-substituted phenol or aniline linker. Such a linker does not make an H-bond with the gatekeeper residue and effectively bypasses the Ile315 mutant. This class contains compounds such as DCC-2036<sup>31</sup>, AST-487<sup>32</sup> (**Figure 2.4**), and Sorafenib<sup>33</sup>, which can inhibit both wild-type and T315I c-Abl, but are currently under clinical investigation for cancers other than CML. AST-487 and Sorafenib are extremely promiscuous pan-kinase inhibitors. DCC-2036, though slightly more selective, inhibits a number of unwanted targets including the SFKs. Incorporation of these design elements into the development of a selective inhibitor of wild-type and T315I c-Abl has been described in **Section 2.7**.

## 2.6. Selectivity for c-Abl over c-Src

Though c-Abl and c-Src do not belong to the same family of kinases, their kinase domains are highly conserved and share 46% sequence identity. With a few exceptions, most inhibitors of c-Abl also inhibit c-Src potently. As a result, c-Src has been used as an initial selectivity filter to screen for compounds that could potentially have a favorable spectrum of selectivity. Imatinib is the most striking such exception, with over 3000-fold difference in selectivity for c-Abl over c-Src. The aforementioned X-ray crystal structure of c-Src bound to Imatinib irrefutably proved that it too could adopt a DFG-out conformation.<sup>16</sup> The low affinity of Imatinib for c-Src was especially puzzling given that the crystal structure revealed it made almost identical contacts to those seen in the Imatinib/c-Abl complex. It was hypothesized that both enzymes must be in an equilibrium between the DFG-in and DFG-out conformations and differed in the probability of occupying a particular conformation. Such a conformation-selection mechanism involved c-Src overcoming a steep entropic penalty to adopt a DFG-out conformation as compared to c-Abl where this conformation was more readily available.<sup>16, 34-36</sup>

This hypothesis too was weakened when analogs of Imatinib with a hydrophilic hinge-binding head group were shown to be equipotent for c-Src and c-Abl.<sup>23</sup> The P-loop of c-Src is extended while that of c-Abl is kinked and forms a hydrophobic shell around Imatinib (**Figure 2.6, top**). Seeliger et al. hypothesized that Imatinib's selectivity for c-Abl

over c-Src could be attributed to the kinked P-loop of c-Abl that makes hydrophobic contacts with the pyridine and pyrimidine rings of Imatinib.<sup>23</sup> The extended P-loop of c-Src offered no such protection from solvent molecules, thus increasing the solvation penalty on binding. Altering Imatinib's hinge binding region to a more polar hydrophilic surface enabled favorable binding to c-Src. Furthermore, it was suggested that Imatinib's sensitivity to P-loop mutants in c-Abl could be explained if such mutants prevented kinking of the P-loop, thus exposing Imatinib to solvent.<sup>23,37</sup> Recent kinetic evidence has confirmed that c-Src does not pay a significant energetic penalty for conformation selection. Instead, it has been suggested that Imatinib binds to the kinases *via* a two-step mechanism (**Figure 2.6, bottom**). The first, involves Imatinib binding to the DFG-out conformation of both c-Src and c-Abl, followed by an induced-fit step that is significantly slower in c-Src as compared to c-Abl.<sup>38-39</sup> Though the nature of the intermediate conformation is unknown, it has been proposed that it may involve an extended P-loop that kinks readily in the case of c-Abl allowing for favorable binding to Imatinib. In the case of c-Src, kinking of the P-loop would be significantly slower accounting for the unfavorable binding to Imatinib.<sup>39</sup>

While being a compelling argument, certain problems lie with the P-loop hypothesis. Lck, a Src Family Kinase (SFK) with an extended P-loop, is a potent target of

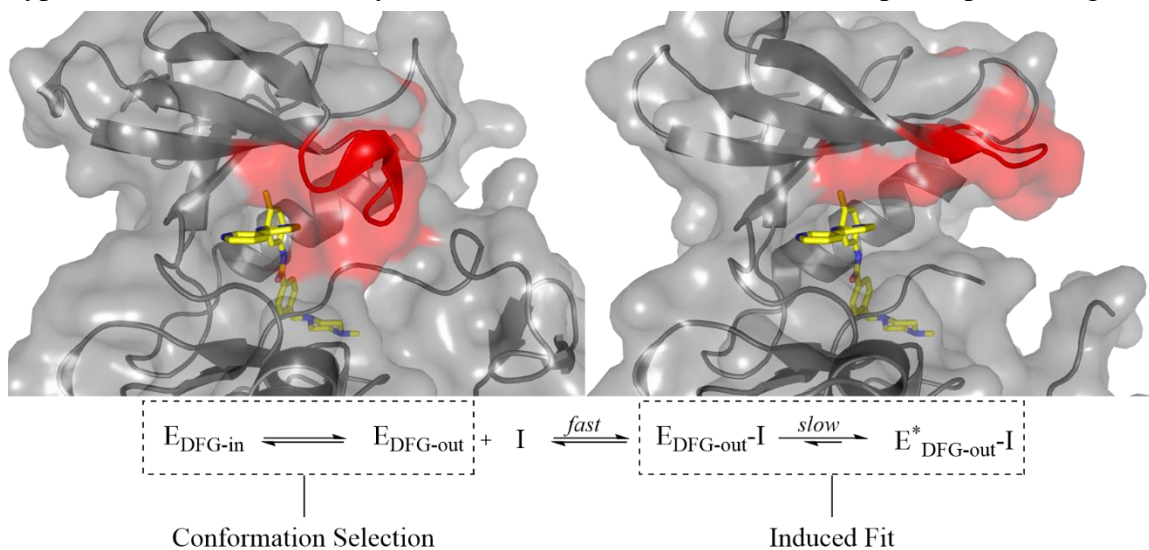


**Figure 2.6.** Determining the selectivity of Imatinib for c-Abl over c-Src. *Top left* – The kinked P-loop of c-Abl forms a hydrophobic shell around Imatinib (PDB 1IEP). *Top Right* – X-ray crystal structure of Imatinib/c-Src complex with an extended P-loop. *Bottom* – A two-step mechanism involving a slow induced fit step.

Imatinib.<sup>19</sup> If selectivity between c-Abl and the SFKs were solely determined by kinking of the P-loop, the potency of Imatinib for Lck should have been substantially reduced. Furthermore, Nilotinib, which bears a hinge-binding head group identical to Imatinib, does not show significant sensitivity to P-loop mutants.<sup>19, 40</sup> Despite these flaws, the P-loop hypothesis does at least partially explain selectivity of Imatinib for c-Abl over c-Src and was the basis for our design of selective inhibitors for c-Abl that could target the T315I gatekeeper mutation.

## 2.7. Development of Selective Inhibitors Bypassing the Gatekeeper Mutation

Inhibitors that have been successful in bypassing the gatekeeper mutation mostly bind c-Abl in a DFG-out conformation. A general strategy for the development of inhibitors that can reliably bind to a given kinase in a DFG-out conformation has been well-established.<sup>41</sup> Necessary moieties include a hinge-binding motif, a hydrophobic linker that binds adjacent to the gatekeeper residue, an amide or urea that can H-bond to the conserved catalytic Asp381 and Glu286 residues, and finally a second hydrophobic moiety that binds to a pocket created by the outward flip of Phe382.

Based on the ability of the non-selective inhibitors, DCC-2036 and AST-487, to inhibit the T315I mutant, we employed a *para*-substituted aminophenol linker to bypass the bulky isoleucine gatekeeper (see **Section 2.5**). Based on the above-mentioned selectivity hypothesis (**Section 2.6**), we reasoned that a hydrophobic hinge-binding moiety could potentially offer selectivity for c-Abl over c-Src. To test this hypothesis, we were interested in:

- a. Altering the hinge-binding motif
  - b. Altering the type-II tail
- 
- a. Altering the hinge-binding motif

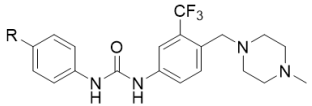
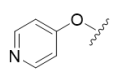
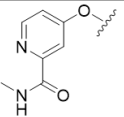
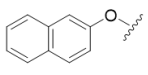
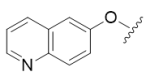
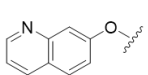
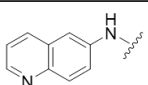
The compound AST-487 (**Figure 2.4**), is a promiscuous kinase inhibitor that binds to the DFG-out conformation of the kinase. Despite its promiscuity, it has the advantage of being a very potent inhibitor of c-Abl ( $K_d = 680$  pM) and the ability to inhibit clinically relevant c-Abl mutants including the T315I gatekeeper mutant with high potency ( $K_d = 2.8$



nM).<sup>19</sup> We hypothesized that replacing the head group of AST-487 with hydrophobic moieties could potentially increase selectivity for c-Abl over c-Src and associated SFKs while retaining potency.

Replacing the 6-aminopyrimidine ring of AST-487 with a slightly more hydrophobic pyridine ring in compound **2.1** and a pyridine carboxamide in compound **2.2** retained potency for c-Abl while providing moderate selectivity over c-Src (see **Table 2.1**). Gratifyingly, in line with our hypothesis, compound **2.3** with a very hydrophobic naphthyl ring entirely lacking a H-bond acceptor atom, displayed a  $K_i$  of 155 nM for c-Abl with a dramatic loss in potency for c-Src with no inhibition below 27  $\mu$ M (the highest concentration of compound tested). Moreover, the pyridine containing compounds (**2.1** and **2.2**) as well as the naphthyl-containing compound **2.3**, maintained potency for T315I c-Abl. While useful in proving that a hydrophobic motif could provide for a dramatic increase

**Table 2.1.**  $K_i$  values of compounds with an altered hinge-binding motif.

					
R	Compound	wt c-Src	wt c-Abl	T315I c-Abl	Y253F c-Abl
	<b>2.1</b>	28 nM	< 1 nM	< 1 nM	< 1 nM
	<b>2.2</b>	36 nM	< 1 nM	< 1 nM	< 1 nM
	<b>2.3</b>	> 27 $\mu$ M	155 nM	119 nM	> 9 $\mu$ M
	<b>2.4</b>	216 nM	< 1 nM	< 1 nM	< 1 nM
	<b>2.5</b>	12 $\mu$ M	2 nM	4 nM	6.2 nM
	<b>2.6</b>	4.5 $\mu$ M	1.7 nM	2.1 nM	50 nM

$K_i$  < 1 nM indicates the compound was too potent to characterize in our assay. Compound **2.4** was characterized in a binding assay and displayed a  $K_d$  of 380 pM for wild-type c-Abl and 550 pM for T315I c-Abl.

in potency for c-Abl over c-Src, compound **2.3** has the drawbacks of significantly lower potency for wild-type c-Abl and sensitivity towards P-loop mutants of c-Abl, such as the Y253F mutant, which showed no inhibition below 9  $\mu\text{M}$ . It did suggest, however, that a balance between a hydrophilic and a very hydrophobic hinge-binding moiety could provide for selectivity over c-Abl over c-Src while maintaining potency and retaining the ability to inhibit P-loop mutants of c-Abl. Consequently, we switched to hydrophobic rings that contained at least one H-bond acceptor atom.

Compounds **2.4** – **2.6** included region-isomers of quinoline ethers and amines, and each of these compounds retained high potency for c-Abl, with compound **2.4** being the most potent. Compound **2.4** was too potent to characterize in our assay (see Experimental for details). Instead,  $K_d$  determination of compound **2.4** through a binding assay, revealed it potently inhibited both wild-type c-Abl (380 pM) and T315I c-Abl (550 pM). Its strong inhibition of Y253F c-Abl and 570-fold loss in potency for c-Src ( $K_i = 216 \text{ nM}$ ), made it an excellent lead compound. Unexpectedly, compounds **2.5** and **2.6** showed an even more dramatic loss of potency for c-Src, with  $K_i$  values of 12  $\mu\text{M}$  and 4.5  $\mu\text{M}$ , respectively. The 5-6 fold loss in potency for wild type c-Abl and sensitivity for the T315I and Y253F mutants precluded the further development of these compounds. Despite an equal number of H-bond donor atoms and overall hydrophobicity as **2.4**, the startling loss in potency against c-Src for compounds **2.5** and **2.6** suggests that desolvation due to kinking of the P-loop is not the sole determinant of selectivity for c-Abl over c-Src.

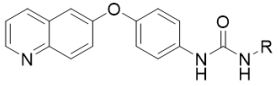
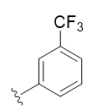
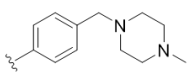
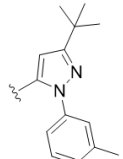
#### b. Altering the type-II tail

With the hinge-binding group in **2.4** providing an adequate balance between potency for c-Abl and selectivity against c-Src, the type-II tail was modified to probe whether either of these attributes could be accentuated (**Table 2.2**)

While removal of the N-methyl piperazine ring in compound **2.7** maintained both potency and selectivity, its poor solubility and pharmacokinetic properties precluded its further use. Removal of the trifluoromethyl group that occupies the hydrophobic pocket created by the outward flip of Phe382 in compound **2.8** led to a substantial loss in potency for c-Abl. Finally, other work in our lab has suggested that a *meta*-tolyl pyrazole containing type-II tail shows an enhancement in kinome-wide selectivity as compared to

trifluoromethylphenylpiperazine tail. Incorporation of the *meta*-tolyl pyrazole tail in compound **3.8**, however, led to a 20-fold loss in potency for c-Abl while maintaining potency for c-Src. Consequently, the original compound **3.4** was selected for further investigation.

**Table 2.2.**  $K_i$  values of compounds with an altered type-II tail

			
R	Compound	wt c-Src	Wt c-Abl
	<b>2.7</b>	1500 nM	4 nM
	<b>2.8</b>	> 9000 nM	311 nM
	<b>2.9</b>	14 nM	230 nM

## 2.8. Kinome Profiling of Compound 2.4

While potency for c-Src over c-Abl served as a useful initial selectivity filter, kinome-wide profiling was necessary to assess the actual selectivity of compound **2.4**. A concentration of 40 nM (100-fold greater than the  $K_d$  of the primary target, c-Abl) was used in a primary screen performed through the KINOMEscan™ profiling service of the DiscoverX Corporation. Kinases, probes immobilized on affinity resin, and compound **2.4** were incubated at room temperature for 1 hour, and the percentage of probe remaining bound to the kinase was measured (see Experimental for details). Thus, the selectivity of compound **2.4** was assessed for 395 non-mutant protein kinases and 61 mutants and atypical kinases.

Compound **2.4** displayed an S(35) selectivity score of 0.084 and an S(10) selectivity score of 0.035. The S(35) score indicates that 8.4% of non-mutant kinases had less than 35% of the probe remaining (**Figure 2.7**). Likewise, the S(10) score indicates that 3.5% of non-mutant kinases had less than 10% of the probe remaining. Additionally, compound **2.4** inhibited all relevant clinical mutations of c-Abl potently.

A direct comparison to drugs approved for the treatment of CML is not possible since published data includes either primary screens at a single concentration of 10  $\mu\text{M}$  (several-fold higher than the  $K_d$  of the intended target) or individual  $K_d$  values for each of

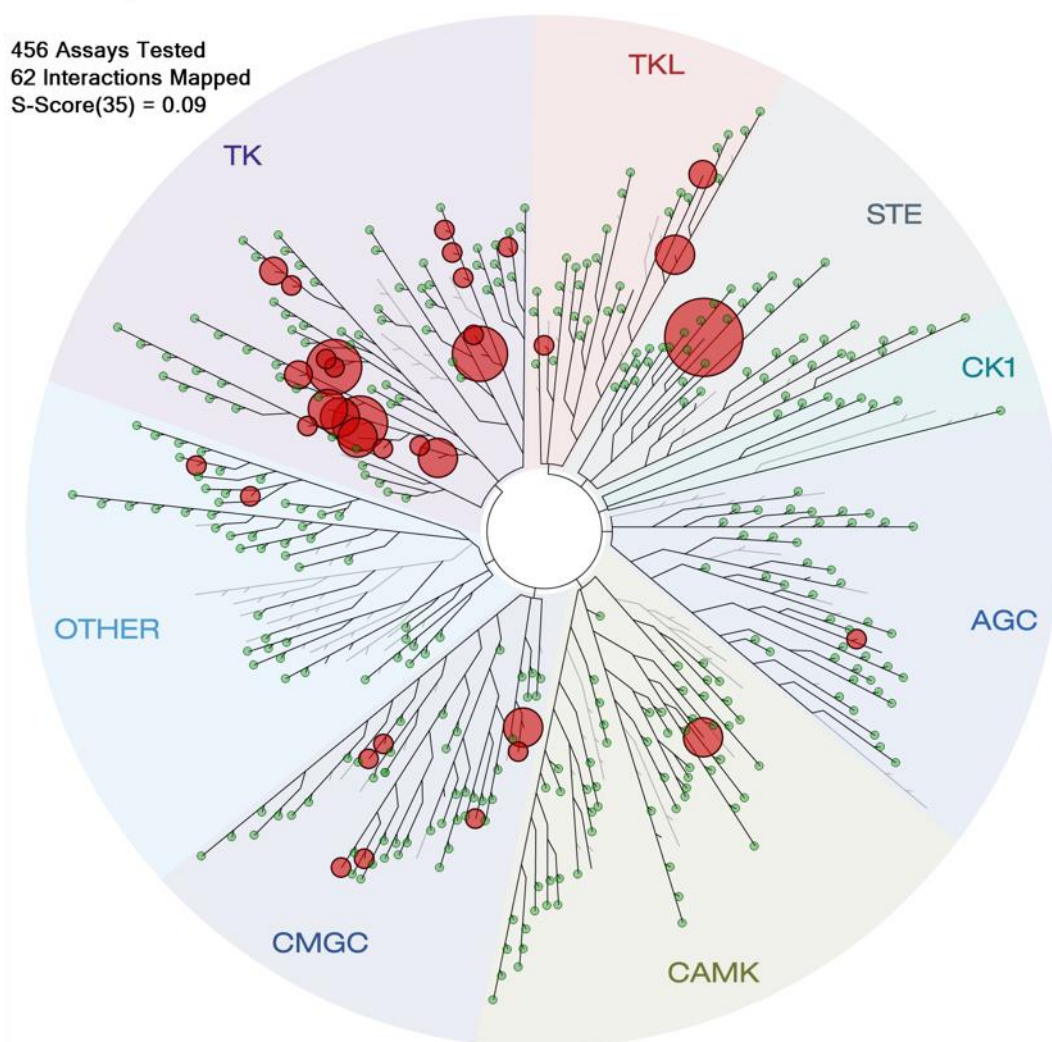


**Figure 2.7.** Selectivity profile of compound **2.4**. The kinome is represented as a phylogenetic tree with each green dot representing an individual kinase. Red spots indicate interactions with compound **2.4**, and the larger the spot, the stronger is the interaction.

the 395 non-mutant kinases. However, some general conclusions can be drawn from comparing the selectivity profile of compound **2.4** to the profiles of approved drugs.

For a valid comparison, it is important to identify the selectivity score that best reflects the kinases inhibited at or below the screening concentration. It is important to note that the percentage of probe remaining is not a direct measure of the  $K_d$  of a small molecule for a particular kinase. For example, compound **2.4**, screened at a concentration of 40 nM shows 54% of probe remains bound to the kinase SIK2; this, however, does not mean that the  $K_d$  of compound **2.4** for SIK2 is 40 nM. Instead, a comparison of the primary screen scores versus the  $K_d$  of small molecules by KINOMEscan™ reveals that a 10% cut-off is more typically reflective of targets with a  $K_d$  at or below the screening concentration (For details, see **Section 2.11 – Correlating Selectivity Scores to  $K_d$  values**).

Applying a cut-off of 10%, compound **2.4** inhibited 14 kinases with a  $K_d$  value likely below 40 nM. In comparison, Imatinib inhibits only 9 kinases with a  $K_d$  values within 100-fold of its intended target (c-Abl). This isn't surprising, considering Imatinib happens to be the second most selective kinase inhibitor that has been approved by the FDA. The selectivity of compound **2.4**, however, is comparable to that of Nilotinib which inhibits 13 kinases potently, and far surpasses the selectivity of Dasatinib, Bosutinib, and AST-487 which inhibit 30, 28, and 56 kinases, respectively. These analyses, though not exact, offer a qualitative representation of the selectivity spectrum of compound **2.4** in comparison to other clinical candidates.

Two general trends emerge in terms of the pharmacophores responsible for targeting certain groups of kinases. A comparison of the targets of compound **2.4** and AST-487 reveals every target of compound **2.4** to be a potent target of AST-487. The opposite, however, is not true. AST-487, which has an identical linker moiety and type-II tail as compound **2.4**, is highly promiscuous indicating that the selectivity of compound **2.4** is entirely derived from its hydrophobic hinge-binding moiety. The hydrophobic quinoline of compound **2.4** was initially used to provide for selectivity for c-Abl over c-Src and other SFKs. However, it seems to have provided for selectivity over at least 30 other targets of AST-487 listed in **Table 2.3**.

**Table 2.3.** 56 kinases inhibited by AST-487 with a  $K_d < 69$  nM. % Control indicates the percentage of probe that remains bound to each kinase after incubation with 40 nM compound **2.4**. High affinity targets of **2.4** are highlighted in red, medium affinity in orange, and those in green have little to no affinity.

Kinase	% Control	Kinase	% Control	Kinase	% Control
STK10	0.05	MAPK12	20	MINK1	72
DDR1	0.45	CDKL3	22	TNIK	75
ABL1	0.85	EPHA8	23	CDKL1	76
FLT3	0.9	BLK	29	MAP2K7	77
KIT	1.5	TIE1	31	HIPK3	78
CDKL2	1.8	ULK3	31	TAOK2	83
ZAK	2.6	PDGFRA	34	TAOK3	83
TEK	3.4	LYN	40	MYO3A	85
MKNK2	3.6	MKNK1	43	TAOK1	88
PDGFRB	3.7	MAPK9	44	HIPK2	89
CSF1R	4.6	CDK13	50	SLK	93
LCK	5	FRK	50	STK35	93
RET	5.4	CHUK	52	TNK1	96
MAP3K7	6	NTRK3	55	FYN	97
CDK11	11	HIPK4	56	CDK18	97
MUSK	11	CDK7	59	CDK14	97
CDK8	13	CDK17	65	CDKL5	100
ABL2	15	MAP4K4	69	CIT	100
DDR2	15	MAPK13	70		

All kinases inhibited by Imatinib are also inhibited by compound **2.4**, suggesting that these kinases may have a better affinity for type-II inhibitors. An analysis of the targets of **2.4** not inhibited by Imatinib, reveals an interesting fact. Of the 23 kinases that are at least weak affinity targets of **2.4**, but not of Imatinib, 19 have a bulky gatekeeper residue in the form of phenylalanine, isoleucine, valine, methionine, or leucine (**Table 2.4**). The exceptions, Zak, EphA8, Blk, and p38 $\alpha$  have the same threonine gatekeeper residue as c-Abl. This suggests that the stark selectivity of Imatinib is at least in part due to the inability to bind to kinases with bulky gatekeeper residues. Consequently, the advantage of compound **2.4** in being able to bypass the gatekeeper residue is also a shortcoming in terms of kinome-wide selectivity. In fact, most of these additional targets are shared by other inhibitors of c-Abl that can inhibit the T315I mutant such as AST-487, DCC-2036, and Sorafenib. This underscores the difficulty in developing selective inhibitors that can also

inhibit clinically relevant kinase mutants as these mutants might share certain commonalities with off-targets.

**Table 2.4.** Targets of **2.4**, but not of Imatinib. Only 4 of the 23 targets have a threonine gatekeeper residue (highlighted in red).

Kinase	% Control	GK Residue
LOK	0.05	I
FLT3	0.9	F
CDKL2	1.8	F
<b>ZAK</b>	<b>2.6</b>	<b>T</b>
TIE2	3.4	I
MKNK2	3.6	F
RET	5.4	V
TAK1	6	V
CDK11	11	M
MUSK	11	F
CDK8	13	F
AURKC	17	L

Kinase	% Control	GK Residue
p38-gamma	20	M
CDKL3	22	F
AXL	23	L
<b>EPHA8</b>	<b>23</b>	<b>T</b>
LRRK2	24	M
TRKB	27	F
<b>BLK</b>	<b>29</b>	<b>T</b>
ULK3	31	M
CLK4	32	F
TRKA	34	F
<b>p38-alpha</b>	<b>35</b>	<b>T</b>

Lastly, Ponatinib has not been profiled using the same assay platform as compound **2.4**. IC<sub>50</sub> values of Ponatinib, however, have been obtained for a panel of 82 kinases. Its IC<sub>50</sub> against c-Abl was found to be 370 pM, and if a cutoff of 37 nM is used, Ponatinib was found to inhibit 43 of the 82 kinases (52%) in the panel.<sup>21</sup> Evaluating the same kinases from within the KINOMEscreen™ profile of compound **2.4**, revealed it to inhibit only 9 of the 82 kinases (11%) on using a percent control cutoff of 10% and 18 kinases (22%) on using a percent control cutoff of 35%. In addition to all nine SFKs, which Ponatinib inhibited potently, its additional off-targets included the receptor tyrosine kinases EphA2-8, EphB1-3, FGFR1-4, and VEGFR1-3. Compound **2.4** was found to be significantly more selective and does not inhibit some of the off-targets that could be related to the cardiotoxicity observed with Ponatinib.

## 2.9. In Cellulo Results

The efficacy of compound **2.4** was evaluated in a number of non-CML and CML related cell lines by Taylor Johnson (**Table 2.5**). Ba/F3 cell line is an immortalized murine bone marrow-derived pro-B-cell line which when transformed with Bcr-Abl becomes entirely dependent on it. Compound **2.4** potently inhibited the growth of both wild-type

and T315I forms of Bcr-Abl transformed Ba/F3 cells. Imatinib demonstrated comparable growth inhibition in wild-type Bcr-Abl transformed Ba/F3 cells but showed no inhibition in those transformed with the gatekeeper mutant. Ba/F3 cells, while very useful in determining the effect of inhibiting a particular kinase in its native state, does not accurately reflect the complexity of inhibiting Bcr-Abl in CML.

Consequently, BV-173, a cell line derived from a patient with Ph<sup>+</sup> Acute Lymphocytic Leukemia, and K562 cells, obtained from a CML patient in blast crisis were used. Both cell lines were potently inhibited by compound **2.4** with low nanomolar growth inhibition values.

Compound **2.4** displayed a GI<sub>50</sub> value of 6 nM and 144 nM against the Imatinib-resistant cell lines, BV-173R and K562R respectively. The BV-173R cell line is predominantly dependent on T315I Bcr-Abl and is thus effectively inhibited by compound **2.4**. The K562R cell line, however, is not dependent on Bcr-Abl mutants, but instead overexpresses the Src Family Kinase, Lyn. Compound **2.4** does not inhibit Lyn potently and consequently shows lower potency in K562R cells. Any attempt at developing an inhibitor that would also potently inhibit Lyn, would likely increase its spectrum of targets and could lead to toxicity. This underscores the importance of combination therapy in the treatment of cancer since mutation of the intended target is not the sole cause of resistance.

Lastly, Ba/F3 parental cells and human mammary epithelial (HME) cells were used as representatives of healthy cells. Compound **2.4** did not significantly inhibit either cell line demonstrating a large therapeutic window in the inhibition of cancer cells versus healthy cells.

**Table 2.5.** *In cellulo* evaluation of compound **2.4**.

Cell Line	GI <sub>50</sub> (nM)
Ba/F3 wt Abl	6
Ba/F3 T315I	29
BV-173	10
BV-173R	6
K562	6
K562R	144
Ba/F3 Parental	3000
HME	2000



## 2.10. Conclusions

The discovery of Imatinib has heralded a new age in the treatment of CML Leukemia and spurred the investigation of kinase inhibitors for the treatment of several other cancers. Over the last two decades, the identification of entire human kinome and advancements in profiling technology have brought about a deeper understanding of the complexity and challenges involved in developing selective inhibitors of a particular protein kinase. Imatinib's success is even more apparent now as it remains the mainstay of CML therapy 15 years after its approval. Despite its development at a time when the entire kinome had not been identified, it remains one of the most selective kinase inhibitors approved to date. It is, however, ineffective in a subset of patients with CML who have an innate or acquired form of resistance to Imatinib.

Attempts at overcoming Imatinib resistance have led to the development of second and third-generation inhibitors. While second generation inhibitors are effective in treating several forms of Imatinib-resistant CML, they are incapable of treating resistance arising from the T315I gatekeeper mutation of Bcr-Abl.

The third generation inhibitor, Ponatinib, can overcome this resistance but has life-threatening toxic effects in a large percentage of patients thereby severely limiting its use. The toxicity of Ponatinib has been attributed to the fact that it inhibits several off-target kinases in addition to Bcr-Abl, some of which might be responsible for its cardiotoxic effects.

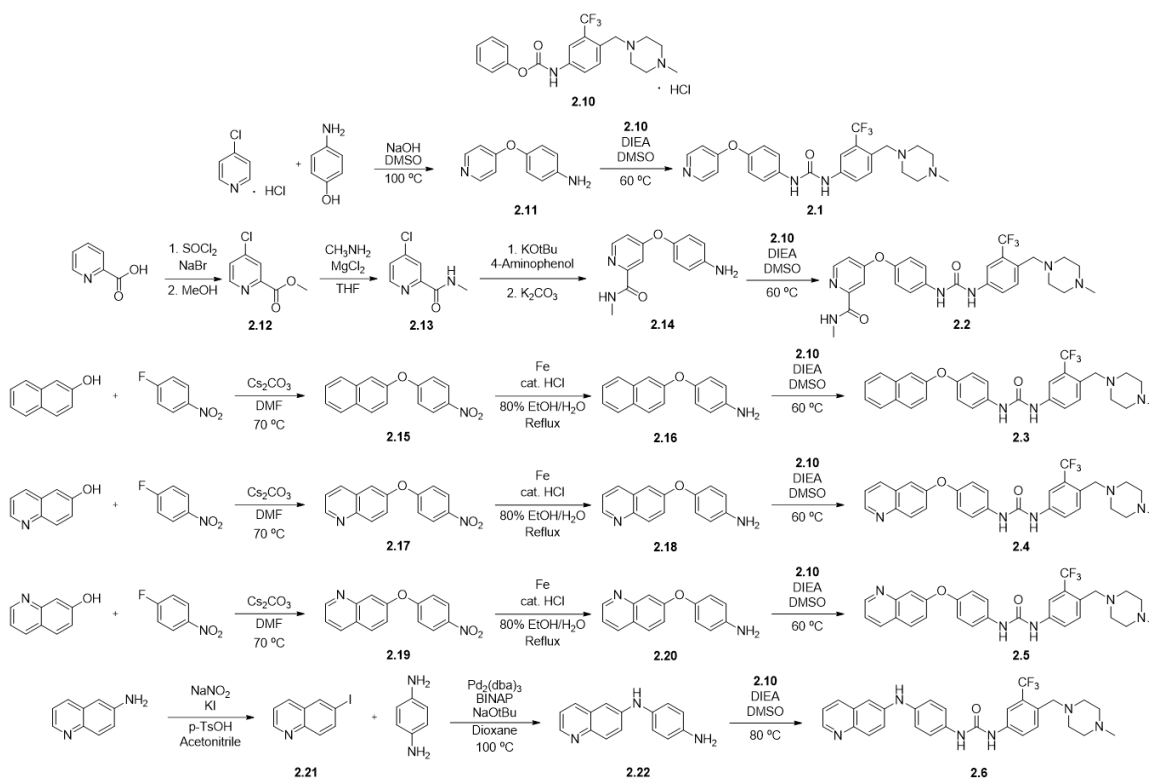
Consequently, this chapter detailed our efforts in developing a selective c-Abl inhibitor that is capable of inhibiting the T315I mutant form of the enzyme. Utilizing a pharmacophore that can inhibit T315I Abl, we developed a library of small molecules based on a hypothesis of obtaining selectivity for c-Abl over c-Src. Our lead molecule, compound **2.4**, inhibited c-Abl and mutant forms of c-Abl very potently while displaying a 570-fold lower potency for the homologous enzyme c-Src. Kinome profiling of the compound **2.4** demonstrated it to be one of the most selective inhibitors of c-Abl, with a spectrum of selectivity similar to Nilotinib and narrower than that of other drugs used in the treatment of CML. The biochemical potency of **2.4** translated to effective inhibition of CML cell lines while its narrow spectrum of selectivity provided for a large therapeutic window using a toxicity model of HME cells.

## 2.11. Materials and Methods

### General Synthetic Methods

Unless otherwise noted, all reagents were obtained via commercial sources and used without further purification. Tetrahydrofuran (THF) and dichloromethane ( $\text{CH}_2\text{Cl}_2$ ) were dried over alumina under a nitrogen atmosphere.  $^1\text{H}$  and  $^{13}\text{C}$  NMR spectra were measured with a Varian MR400, Varian VNMRs 500, or Inova 500 spectrometer. Mass Spectrometry (HRMS) was carried out by the University of Michigan Mass Spectrometry Facility (J. Windak, director).

### Synthetic Protocols



Scheme 2.1. Synthesis of compounds 2.1 – 2.6.

Synthesis of 2.10 – Compound 2.10 was synthesized according to a previously described procedure.

Synthesis of **2.11** – 4-chloropyridine hydrochloride (500 mg, 3.33 mmol), 4-aminophenol (364 mg, 3.33 mmol), and sodium hydroxide (333 mg, 8.33 mmol) were dissolved in DMSO and the solution was heated to 100 °C, overnight. The solution was then cooled to room temperature, poured into an excess of ice-water and extracted with ether (3 x 100 ml). Combined organic extracts were washed with brine, dried over sodium sulfate, and evaporated *in vacuo*. The crude product was purified *via* silica gel chromatography using a Biotage Isolera One system (linear gradient EtOAc → 5% MeOH/EtOAc) to give 53 mg (9% yield) of compound **2.11**. <sup>1</sup>H NMR (500 MHz, Chloroform-*d*) δ 8.44 – 8.38 (m, 2H), 6.89 (d, *J* = 8.5 Hz, 2H), 6.81 – 6.76 (m, 2H), 6.71 (d, *J* = 8.5 Hz, 2H), 3.69 (s, 2H). <sup>13</sup>C NMR (100 MHz, Chloroform-*d*) δ 165.83, 151.38, 145.88, 144.23, 122.13, 116.37, 111.70. HRMS-ESI (*m/z*): [M + H]<sup>+</sup> calcd for C<sub>11</sub>H<sub>10</sub>N<sub>2</sub>O, 187.0866; found 187.0865.

Synthesis of **2.12** – A flame-dried flask was charged with 2-picolinic acid (2 g, 16.2 mmol) and sodium bromide (3.3 g, 32.5 mmol). Thionyl chloride (8.2 ml, 114 mmol) was added carefully to give a green solution which was refluxed overnight. The solution was then cooled to room temperature and the excess thionyl chloride was evaporated *in vacuo*. Methanol (16 ml) was added slowly to the flask and the solution was stirred at room temperature for 30 min. The volatiles were then evaporated *in vacuo*, saturated sodium bicarbonate solution was added to the residue and was extracted with EtOAc (3 x 75 ml). Combined organic extracts were washed with brine, dried over sodium sulfate, and evaporated *in vacuo*. The crude product was purified *via* silica gel chromatography using a Biotage Isolera One system (linear gradient 25% EtOAc/Hexanes → 33% EtOAc/Hexanes) to give 2.1 g (75% yield) of compound **2.12** as a brown solid. <sup>1</sup>H NMR (500 MHz, Chloroform-*d*) δ 8.61 (d, *J* = 5.2 Hz, 1H), 8.10 (t, *J* = 1.5 Hz, 1H), 7.46 (dt, *J* = 5.3, 1.6 Hz, 1H), 3.98 (s, 3H). <sup>13</sup>C NMR (100 MHz, Chloroform-*d*) δ 164.57, 150.57, 149.18, 145.36, 127.08, 125.59, 53.14. HRMS-ESI (*m/z*): [M + H]<sup>+</sup> calcd for C<sub>7</sub>H<sub>6</sub>ClNO<sub>2</sub>, 172.0160; found 172.0157.

Synthesis of **2.13** – Compound **2.12** (1.5 g, 8.74 mmol) and anhydrous magnesium chloride (416 mg, 4.37 mmol) was added to dry THF (5 ml). After 5 min, a 2M methylamine/THF solution (15 ml, 30 mmol) was added dropwise over 10 min. The resultant suspension was

stirred at room temperature for 2h, after which water (17 ml) and 1M HCl (9 ml) were added. The product was extracted with EtOAc (3 x 50 ml) and the combined organic layers were washed with brine, dried over sodium sulfate, and evaporated *in vacuo* to give 1.46 g (98% yield) of compound **2.13** as a yellow oil and was used without further purification. <sup>1</sup>H NMR (500 MHz, Chloroform-*d*) δ 8.40 (d, *J* = 5.3 Hz, 1H), 8.16 (d, *J* = 2.0 Hz, 1H), 7.96 (s, 1H), 7.39 (dd, *J* = 5.3, 2.0 Hz, 1H), 3.00 (d, *J* = 5.1 Hz, 3H). <sup>13</sup>C NMR (100 MHz, Chloroform-*d*) δ 163.73, 151.35, 148.91, 145.76, 126.16, 122.67, 26.15. HRMS-ESI (*m/z*): [M + H]<sup>+</sup> calcd for C<sub>7</sub>H<sub>8</sub>ClN<sub>2</sub>O, 171.0320; found 171.0317.

Synthesis of **2.14** – 4-aminophenol (672 mg, 6.15 mmol) was dissolved in DMF (6 ml) and potassium *tert*-butoxide (697 mg, 6.21 mmol) was added it. The solution was stirred at room temperature for 1 hour after which a solution of compound **2.12** (1 g, 5.86 mmol) in DMF (3 ml) was added to it. Potassium carbonate (405 mg, 2.93 mmol) was added to the combined solution, which was then heated to 80 °C, overnight. The mixture was cooled to room temperature, diluted with about 100 ml water and extracted with EtOAc (3 x 50 ml). Combined organic extracts were washed with brine, dried over sodium sulfate, and evaporated *in vacuo*. The crude product was purified *via* silica gel chromatography using a Biotage Isolera One system (linear gradient 50% EtOAc/Hexanes → 80% EtOAc/Hexanes) to give 820 mg (57% yield) of compound **2.14**. <sup>1</sup>H NMR (500 MHz, Chloroform-*d*) δ 8.29 (d, *J* = 5.6 Hz, 1H), 8.06 – 8.00 (m, 1H), 7.64 (d, *J* = 2.5 Hz, 1H), 6.90 – 6.80 (m, 3H), 6.66 (d, *J* = 8.7 Hz, 2H), 3.77 (bs, 2H), 2.96 (d, *J* = 5.1 Hz, 3H). <sup>13</sup>C NMR (100 MHz, Chloroform-*d*) δ 167.10, 164.68, 152.04, 149.47, 145.34, 144.45, 121.81, 121.70, 116.32, 116.25, 113.65, 109.76, 26.08. HRMS-ESI (*m/z*): [M + H]<sup>+</sup> calcd for C<sub>13</sub>H<sub>13</sub>N<sub>3</sub>O<sub>2</sub>, 244.1081; found 244.1081. [M + Na]<sup>+</sup> calcd for C<sub>13</sub>H<sub>13</sub>N<sub>3</sub>O<sub>2</sub>, 266.0900; found 266.0900.

General procedure for S<sub>N</sub>Ar coupling of compounds **2.15**, **2.17**, and **2.19**:

In a dry flask, the appropriate naphthol or quinolol (1 Eq), 4-fluoronitrobenzene (1.01 Eq), and cesium carbonate (1.01 Eq) were dissolved in DMF (0.2 M) and heated to 70 °C. The reaction was monitored by TLC (in 70% EtOAc/Hex) and was typically complete in 2 hours. The solution was cooled to room temperature, poured into water (10x the amount of

DMF) and extracted with EtOAc (3x). The combined organics layers were washed with 10% K<sub>2</sub>CO<sub>3</sub> solution, brine, dried over sodium sulfate, and evaporated *in vacuo*. The crude product was used without further purification or purified *via* silica gel chromatography using a Biotage Isolera One system.

2-(4'-nitrophenoxy)naphthalene (**2.15**) –  $\beta$ -naphthol (250 mg, 1.73 mmol) was used in this reaction and the crude product obtained (444 mg, 97% yield) was used without further purification.

6-(4'-nitrophenoxy)quinoline (**2.17**) – 6-hydroxyquinoline (726 mg, 5 mmol) was used in this reaction and the crude product obtained was purified *via* silica gel chromatography using a Biotage Isolera One system (linear gradient Hexanes  $\rightarrow$  50% EtOAc/Hexanes) to give 1159 mg (87% yield) of compound **2.17** as a yellow solid. <sup>1</sup>H NMR (500 MHz, Chloroform-*d*)  $\delta$  8.90 (dd, *J* = 4.2, 1.6 Hz, 1H), 8.21 (d, *J* = 9.1 Hz, 2H), 8.16 (d, *J* = 9.0 Hz, 1H), 8.09 (d, *J* = 8.4 Hz, 1H), 7.50 – 7.39 (m, 3H), 7.08 (d, *J* = 9.0 Hz, 2H). <sup>13</sup>C NMR (100 MHz, Chloroform-*d*)  $\delta$  162.69, 152.74, 150.15, 145.9, 143.07, 135.40, 132.18, 129.02, 126.00, 123.59, 121.88, 117.67, 116.21. HRMS-ESI (*m/z*): [M + H]<sup>+</sup> calcd for C<sub>15</sub>H<sub>10</sub>N<sub>2</sub>O<sub>3</sub>, 267.0764; found 267.0765.

7-(4'-nitrophenoxy)quinoline (**2.19**) – 7-hydroxyquinoline (82 mg, 0.56 mmol) was used in this reaction and the crude product obtained was purified *via* silica gel chromatography using a Biotage Isolera One system (linear gradient 20% EtOAc/Hexanes  $\rightarrow$  40% EtOAc/Hexanes) to give 90 mg (60% yield) of compound **2.19** as a light yellow solid. <sup>1</sup>H NMR (500 MHz, Chloroform-*d*)  $\delta$  8.94 (dd, *J* = 4.3, 1.6 Hz, 1H), 8.29 – 8.23 (m, 2H), 8.21 (dd, *J* = 8.3, 1.6 Hz, 1H), 7.91 (d, *J* = 8.8 Hz, 1H), 7.73 (d, *J* = 2.4 Hz, 1H), 7.43 (dd, *J* = 8.3, 4.3 Hz, 1H), 7.36 (dd, *J* = 8.9, 2.4 Hz, 1H), 7.19 – 7.13 (m, 2H). <sup>13</sup>C NMR (100 MHz, Chloroform-*d*)  $\delta$  162.25, 155.79, 151.41, 149.22, 143.29, 135.87, 130.09, 126.01, 125.74,

120.78, 120.73, 118.19, 117.72. HRMS-ESI ( $m/z$ ):  $[M + H]^+$  calcd for  $C_{15}H_{10}N_2O_3$ , 267.0764; found 267.0763.

General procedure for iron reduction of the nitro group to give **2.16**, **2.18**, and **2.20**:

1 Eq of compound **2.15**, **2.17**, or **2.19** was suspended in 80% (v/v) EtOH/water (0.2 M) followed by the addition of Iron (5 Eq) and 1-2 drops of concentrated HCl. The suspension was refluxed and the reaction monitored by TLC (in 70% EtOAc/Hex). The reaction was typically complete in 1.5 h, after which the mixture was filtered over celite, and washed with EtOAc. The volatiles were evaporated *in vacuo*, 10%  $K_2CO_3$  was added and the mixture was extracted with EtOAc (3x). The combined organic layers were washed with 10%  $K_2CO_3$ , brine, dried over sodium sulfate, and evaporated *in vacuo*. The crude product was used without further purification or purified *via* silica gel chromatography using a Biotage Isolera One system.

4-(naphthalen-2-yloxy)aniline (**2.16**) – Compound **2.15** (445 mg, 1.68 mmol) was used in this reaction and the crude product was purified *via* silica gel chromatography using a Biotage Isolera One system (linear gradient Hexanes  $\rightarrow$  30% EtOAc/Hexanes) to give 249 mg (63% yield) of compound **2.16** as a brown solid.  $^1H$  NMR (500 MHz, Chloroform-*d*)  $\delta$  7.81 (d,  $J = 8.6$  Hz, 2H), 7.67 (d,  $J = 8.2$  Hz, 1H), 7.48 – 7.40 (m, 1H), 7.38 (td,  $J = 7.3, 6.7, 1.2$  Hz, 1H), 7.27 (dd,  $J = 9.0, 2.5$  Hz, 1H), 7.18 (d,  $J = 2.4$  Hz, 1H), 7.00 – 6.93 (m, 2H), 6.77 – 6.70 (m, 2H).  $^{13}C$  NMR (100 MHz, Chloroform-*d*)  $\delta$  156.84, 148.47, 142.84, 134.32, 129.60, 129.58, 127.63, 126.92, 126.36, 124.15, 121.31, 119.19, 116.27, 111.63. HRMS-ESI ( $m/z$ ):  $[M + H]^+$  calcd for  $C_{16}H_{13}NO$ , 236.1070; found 236.1068.

4-(quinolin-6-yloxy)aniline (**2.18**) – Compound **2.17** (1000 mg, 3.756) was used in this reaction to give 876 mg (98% yield) of **2.18** that was used without further purification.  $^1H$  NMR (500 MHz, Chloroform-*d*)  $\delta$  8.78 (dd,  $J = 4.2, 1.5$  Hz, 1H), 8.04 (d,  $J = 9.2$  Hz, 1H), 7.94 (dd,  $J = 8.3, 1.6$  Hz, 1H), 7.47 (dd,  $J = 9.2, 2.7$  Hz, 1H), 7.35 – 7.29 (m, 1H), 7.06 (d,  $J = 2.7$  Hz, 1H), 6.97 – 6.91 (m, 2H), 6.75 – 6.69 (m, 2H), 3.68 (s, 2H).  $^{13}C$  NMR (126 MHz, Chloroform-*d*)  $\delta$  188.00, 157.28, 148.57, 147.83, 144.75, 143.33, 134.99, 131.11,

129.10, 122.52, 121.62, 121.40, 116.32, 110.51, 67.25. HRMS-ESI ( $m/z$ ):  $[M + H]^+$  calcd for  $C_{15}H_{12}N_2O$ , 237.1022; found 237.1021.

4-(quinolin-7-yloxy)aniline (**2.20**) – Compound **2.19** (95 mg, 0.36 mmol) was used in this reaction to give 77 mg (91% yield) of **2.20** that was used without further purification.  $^1H$  NMR (500 MHz, Chloroform- $d$ )  $\delta$  8.82 (d,  $J = 4.2$  Hz, 1H), 8.10 (d,  $J = 8.2$  Hz, 1H), 7.76 (d,  $J = 8.9$  Hz, 1H), 7.39 (d,  $J = 2.4$  Hz, 1H), 7.34 (dd,  $J = 8.9, 2.4$  Hz, 1H), 7.31 – 7.21 (m, 1H), 6.97 (d,  $J = 8.3$  Hz, 2H), 6.73 (d,  $J = 8.2$  Hz, 2H), 3.60 (s, 2H).  $^{13}C$  NMR (100 MHz, Chloroform- $d$ )  $\delta$  160.39, 150.72, 149.50, 147.35, 143.48, 135.67, 129.08, 124.06, 121.81, 119.70, 119.32, 116.30, 112.31. HRMS-ESI ( $m/z$ ):  $[M + H]^+$  calcd for  $C_{15}H_{12}N_2O$ , 237.1022; found 237.1022.

Synthesis of **2.21** – *para*-toluenesulfonic acid (1.48 g, 7.8 mmol) and 6-aminoquinoline (325 mg, 2.6 mmol) were dissolved in acetonitrile (10 ml), and the solution was cooled in an ice-bath. A solution of sodium nitrite (359 mg, 5.2 mmol) and potassium iodide (1.1 g, 6.5 mmol) in 1.5 ml water was prepared and added dropwise to the acetonitrile solution (highly exothermic reaction). The resultant suspension was allowed to warm to room temperature and stirred overnight. 50 ml water was added and the pH adjusted to 9 using sodium bicarbonate. Sodium thiosulfate (2M, 5.2 ml) was then added and the suspension filtered to give a solid precipitate. The precipitate was dissolved in EtOAc, washed with sat. sodium bicarbonate, brine, dried over sodium sulfate, and evaporated *in vacuo*. The orange-red solid obtained (284 mg, 43% yield) was used without further purification. HRMS-ESI ( $m/z$ ):  $[M + H]^+$  calcd for  $C_9H_6IN$ , 255.9618; found 255.9616.

Synthesis of **2.22** – compound **2.21** (77 mg, 0.3 mmol), phenylenediamine (97 mg, 0.9 mmol),  $Pd_2(dba)_3$  (28 mg, 0.03 mmol), BINAP (37 mg, 0.06 mmol), and sodium *tert*-butoxide (86 mg, 0.9 mmol) were added to a flame-dried vial charged with a stirrer. The vial was evacuated and back-filled with  $N_2$  (3x) and 3 ml Dioxane (0.1 M) was added. The vial was sealed and heated to 101 °C for 12 h. The solution was cooled to room temperature, poured into water and extracted with EtOAc (3x). The combined organic layers were washed with sat. sodium bicarbonate, brine, dried over sodium sulfate, and evaporated *in*

*vacuo*. The crude product was purified *via* silica gel chromatography using a Biotage Isolera One system (linear gradient 0.1% TEA/39.9% EtOAc/Hexanes → 0.1% TEA/99.9% EtOAc) to give 40 mg (57% yield) of compound **2.22**. HRMS-ESI ( $m/z$ ):  $[M + H]^+$  calcd for  $C_{15}H_{13}N_3$ , 236.1182; found 236.1180.

General Procedure for formation of the urea to give final products **2.1** – **2.6**:

The appropriate aniline-containing compound (1 Eq) and **2.10** (1 Eq) were added to DMSO (0.1 M) followed by the addition of DIEA (1.08 Eq). The resultant slurry was heated at 60°C and the reaction was monitored by TLC. The reaction was typically complete in 2 h, after which the resultant solution was cooled to room temperature and purified directly using reverse-phase (C18) column chromatography on a Biotage Isolera One system (linear gradient 30% MeCN/H<sub>2</sub>O → 90% MeCN/H<sub>2</sub>O).

Compound **2.1** – The reaction was performed using compound **2.11** (11 mg, 58 μmol) and gave 16 mg (57% yield) of compound **2.1** as a white solid. <sup>1</sup>H NMR (500 MHz, Chloroform-*d*) δ 8.49 – 8.43 (m, 2H), 7.78 (s, 1H), 7.73 (s, 1H), 7.67 (m, 1H), 7.62 – 7.54 (m, 2H), 7.45 – 7.38 (m, 2H), 7.05 – 6.99 (m, 2H), 6.86 – 6.80 (m, 2H), 3.57 (s, 2H), 2.44 (s, 8H), 2.29 (s, 3H). HRMS-ESI ( $m/z$ ):  $[M + H]^+$  calcd for  $C_{25}H_{26}F_3N_5O_2$ , 486.2111; found 486.2112.

Compound **2.2** – The reaction was performed using compound **2.14** (14 mg, 58 μmol) and gave 18 mg (57% yield) of compound **2.2** as a white solid. <sup>1</sup>H NMR (500 MHz, Chloroform-*d*) δ 8.44 (d,  $J = 5.6$  Hz, 1H), 8.37 – 8.30 (m, 2H), 8.20 (s, 1H), 7.69 – 7.60 (m, 3H), 7.59 (dd,  $J = 19.9, 2.2$  Hz, 2H), 7.39 – 7.33 (m, 2H), 7.13 (dd,  $J = 5.6, 2.5$  Hz, 1H), 6.99 – 6.94 (m, 2H), 3.59 – 3.55 (m, 2H), 3.05 (d,  $J = 5.1$  Hz, 3H), 2.48 (s, 3H), 2.43 (s, 2H), 2.30 (d,  $J = 1.3$  Hz, 4H). HRMS-ESI ( $m/z$ ):  $[M + H]^+$  calcd for  $C_{27}H_{29}F_3N_6O_3$ , 543.2326; found 543.2321.

Compound **2.3** – The reaction was performed using compound **2.16** (24 mg, 0.1 mmol) and gave 28 mg (53% yield) of compound **2.3** as a white solid. <sup>1</sup>H NMR (500 MHz, DMSO-*d*<sub>6</sub>) δ 9.01 (s, 1H), 8.82 (s, 1H), 7.99 – 7.87 (m, 3H), 7.79 (d,  $J = 8.1$  Hz, 1H), 7.65 – 7.38

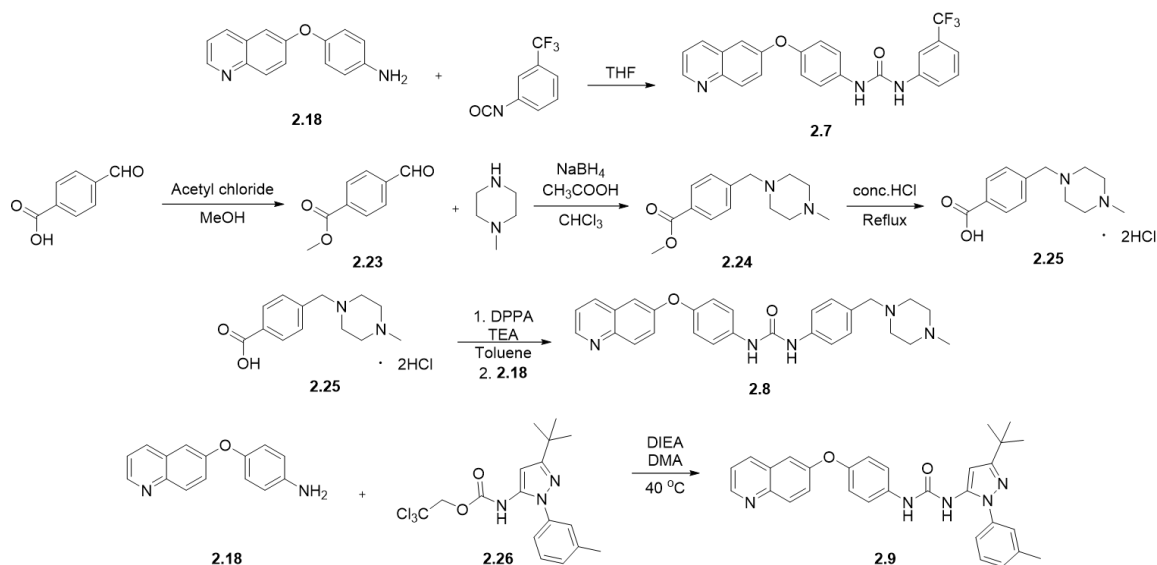


(m, 7H), 7.28 (dd,  $J = 4.8, 2.3$  Hz, 2H), 7.07 (d,  $J = 8.9$  Hz, 2H), 3.52 (s, 2H), 2.36 (s, 9H), 2.16 (s, 3H). HRMS-ESI ( $m/z$ ):  $[M + H]^+$  calcd for  $C_{30}H_{29}F_3N_4O_2$ , 535.2315; found 535.2315.

Compound **2.4** – The reaction was performed using compound **2.18** (59 mg, 0.25 mmol) and gave a 20% yield of compound **2.4** as a white solid.  $^1H$  NMR (500 MHz, Chloroform- $d$ )  $\delta$  8.84 (dd,  $J = 4.2, 1.7$  Hz, 1H), 8.07 (d,  $J = 9.1$  Hz, 1H), 8.00 (dd,  $J = 8.3, 1.6$  Hz, 1H), 7.75 (s, 1H), 7.68 – 7.60 (m, 2H), 7.60 – 7.52 (m, 2H), 7.44 (dd,  $J = 9.2, 2.7$  Hz, 1H), 7.43 – 7.31 (m, 3H), 7.18 (d,  $J = 2.7$  Hz, 1H), 7.06 – 6.98 (m, 2H), 3.55 (s, 2H), 2.45 (s, 7H), 2.28 (s, 3H). HRMS-ESI ( $m/z$ ):  $[M + H]^+$  calcd for  $C_{29}H_{28}F_3N_5O_2$ , 536.2268; found 536.2268.

Compound **2.5** – The reaction was performed using compound **2.20** (24 mg, 0.1 mmol) and gave 20 mg (34% yield) of compound **2.5** as a white solid.  $^1H$  NMR (500 MHz, DMSO- $d_6$ )  $\delta$  9.05 (s, 1H), 8.88 (s, 1H), 8.82 (dd,  $J = 4.2, 1.7$  Hz, 1H), 8.34 (dd,  $J = 8.3, 1.7$  Hz, 1H), 8.04 – 7.95 (m, 2H), 7.62 (d,  $J = 8.5$  Hz, 1H), 7.61 – 7.53 (m, 3H), 7.42 (ddd,  $J = 13.1, 8.6, 3.4$  Hz, 2H), 7.14 (d,  $J = 8.9$  Hz, 2H), 3.53 (s, 2H), 2.37 (s, 8H), 2.15 (s, 3H). HRMS-ESI ( $m/z$ ):  $[M + H]^+$  calcd for  $C_{29}H_{28}F_3N_5O_2$ , 536.2268; found 536.2271.

Compound **2.6** – The reaction was performed using compound **2.22** (20 mg, 85  $\mu$ mol) and gave 10.2 mg (22% yield) of compound **2.6** as a white solid. HRMS-ESI ( $m/z$ ):  $[M + H]^+$  calcd for  $C_{29}H_{29}F_3N_6O$ , 535.2428; found 535.2429.



**Scheme 2.2.** Synthesis of compounds **2.7** – **2.9**.

Synthesis of **2.7** – Compound **2.18** (50 mg, 0.21 mmol) was dissolved in THF (2 ml) and 3-trifluoromethylphenyl isocyanate (31  $\mu$ L, 0.22 mmol) was added to it to give a fine slurry. Triethylamine (31  $\mu$ L, 0.22 mmol) was then added and the solution was refluxed overnight. EtOAc was added to the flask and the organic layer was washed with 10%  $\text{K}_2\text{CO}_3$ , brine, dried over sodium sulfate, and evaporated *in vacuo*. The crude product was purified *via* reverse phase HPLC (linear gradient 30% MeCN/ $\text{H}_2\text{O}$   $\rightarrow$  90% MeCN/ $\text{H}_2\text{O}$ ) to give 17 mg (18% yield) of compound **2.7** as a white solid.  $^1\text{H}$  NMR (500 MHz, Chloroform-*d*)  $\delta$  8.80 (dd,  $J = 4.3, 1.7$  Hz, 1H), 8.06 (d,  $J = 9.1$  Hz, 1H), 7.97 (ddd,  $J = 8.2, 1.8, 0.8$  Hz, 1H), 7.49 (dd,  $J = 9.2, 2.8$  Hz, 1H), 7.34 (dd,  $J = 8.3, 4.2$  Hz, 1H), 7.08 (d,  $J = 2.7$  Hz, 1H), 7.01 – 6.93 (m, 2H), 6.79 – 6.72 (m, 2H).  $^{19}\text{F}$  NMR (376 MHz, Chloroform-*d*)  $\delta$  -63.02. HRMS-ESI ( $m/z$ ):  $[\text{M} + \text{H}]^+$  calcd for  $\text{C}_{23}\text{H}_{16}\text{F}_3\text{N}_3\text{O}_2$ , 424.1267; found 424.1267.

Synthesis of **2.23** – 4-formylbenzoic acid (1.5 g, 10 mmol) was dissolved in anhydrous methanol (30 ml) and the solution was cooled in an ice-bath. Acetyl chloride (7.1 ml, 100 mmol) was added dropwise and the reaction was allowed to warm to room temperature and stirred overnight. The volatiles were evaporated *in vacuo*, the residue dissolved in EtOAc (200 ml) and washed with 1N NaOH (5 x 50 ml), brine (3 x 50 ml), dried over sodium

sulfate, and evaporated *in vacuo*. 1.6 g (97% yield) of crude product was obtained and was carried forward without further purification.

Synthesis of **2.24** – Sodium borohydride (746 mg, 19.7 mmol) was added to chloroform (8 ml) and cooled in an ice-bath. Acetic acid (5.2 ml, 91 mmol) was then added and the reaction was stirred for 1.5 h on ice. A solution of **2.23** (1.6 g, 9.76 mmol) and N-methylpiperazine (1 ml, 9.3 mmol) in chloroform (2 ml) was then added to it and stirring was continued on ice for 1 h and at room temperature for 12 h. 5 ml water was then added to it and the pH adjusted to 9 using 10% sodium carbonate. The aqueous mixture was extracted with DCM (2x). The combined organic layers were washed with water, brine, dried over sodium sulfate, and evaporated *in vacuo*. The crude product obtained (2.3 g, 100% yield) was carried forward without further purification.

Synthesis of **2.25** – Compound **2.24** (2.3 g, 9.26 mmol) was added to conc. HCl (16 ml) and the solution refluxed for 5 h. The resultant suspension was cooled to 45 °C and filtered. The filter cake was washed with isopropanol and dried to give 1.55 g (54% yield) of compound **2.25** as a yellow-white crystalline solid. HRMS-ESI (*m/z*): [M + H]<sup>+</sup> calcd for C<sub>13</sub>H<sub>18</sub>N<sub>2</sub>O<sub>2</sub>, 235.1441; found 235.1441.

Synthesis of **2.8** – Compound **2.25** (52 mg, 0.17 mmol), diphenylphosphoryl azide (38 μL, 0.17 mmol) and triethylamine (118 μL, 0.85 mmol) were added to Toluene (1 ml) and refluxed for 1 h. Compound **2.18** (20 mg, 0.08 mmol) was then added and the refluxed continued for 2 h. The reaction was cooled to room temperature, toluene was evaporated *in vacuo*, and the crude product was purified directly purified *via* reverse phase HPLC (linear gradient 5% MeCN/H<sub>2</sub>O → 90% MeCN/H<sub>2</sub>O). 9.6 mg (24% yield) of compound **2.28** was obtained as a white solid. HRMS-ESI (*m/z*): [M + H]<sup>+</sup> calcd for C<sub>28</sub>H<sub>29</sub>N<sub>5</sub>O<sub>2</sub>, 468.2394; found 468.2392.

Compound **2.26** was synthesized by Kristin Ko.

Synthesis of **2.9** – Compounds **2.18** (47 mg, 0.2 mmol), **2.26** (162 mg, 0.4 mmol), and DIEA (143  $\mu$ L, 0.8 mmol) were added to DMA (2 ml) and stirred at 40 °C for 3 h. The reaction mixture was cooled to room temperature, poured into 10% K<sub>2</sub>CO<sub>3</sub>, and extracted with EtOAc (3x). The combined organic layers were washed with brine, dried over sodium sulfate, and evaporated *in vacuo*. The crude product was purified using reverse-phase (C18) column chromatography on a Biotage Isolera One system (linear gradient 40% MeCN/H<sub>2</sub>O → 100% MeCN) to give 64 mg (65% yield) of compound **2.9** as a white solid. <sup>1</sup>H NMR (500 MHz, Chloroform-*d*)  $\delta$  8.80 (dd, *J* = 4.3, 1.7 Hz, 1H), 8.07 (d, *J* = 9.1 Hz, 1H), 7.99 (ddd, *J* = 8.4, 1.7, 0.8 Hz, 1H), 7.46 (dd, *J* = 9.2, 2.8 Hz, 1H), 7.37 (dd, *J* = 8.3, 4.2 Hz, 1H), 7.34 – 7.23 (m, 4H), 7.26 – 7.15 (m, 2H), 7.15 – 7.07 (m, 2H), 7.08 – 7.00 (m, 2H), 6.61 (s, 1H), 6.41 (s, 1H), 2.34 (s, 3H), 1.37 (s, 9H). HRMS-ESI (*m/z*): [M + H]<sup>+</sup> calcd for C<sub>30</sub>H<sub>29</sub>N<sub>5</sub>O<sub>2</sub>, 492.2394; found 492.2392.

#### *Spectral Data*

Spectral data for all compounds in this chapter are shown in **Appendix A**.

#### *General Biochemical Methods*

Black, opaque-bottom 96 well plates were used for fluorescence assays and were purchased from Nunc. c-Src, c-Abl, T315I Abl, and Y253F Abl were expressed in *E. coli* by Christel Fox and Frank Kwarczynski using previously published procedures.<sup>42</sup> c-Abl numbering is based on the 1b isoform. Data was obtained using a Biotek Synergy 4 plate reader. Curve fitting was performed using GraphPad Prism 4 software.

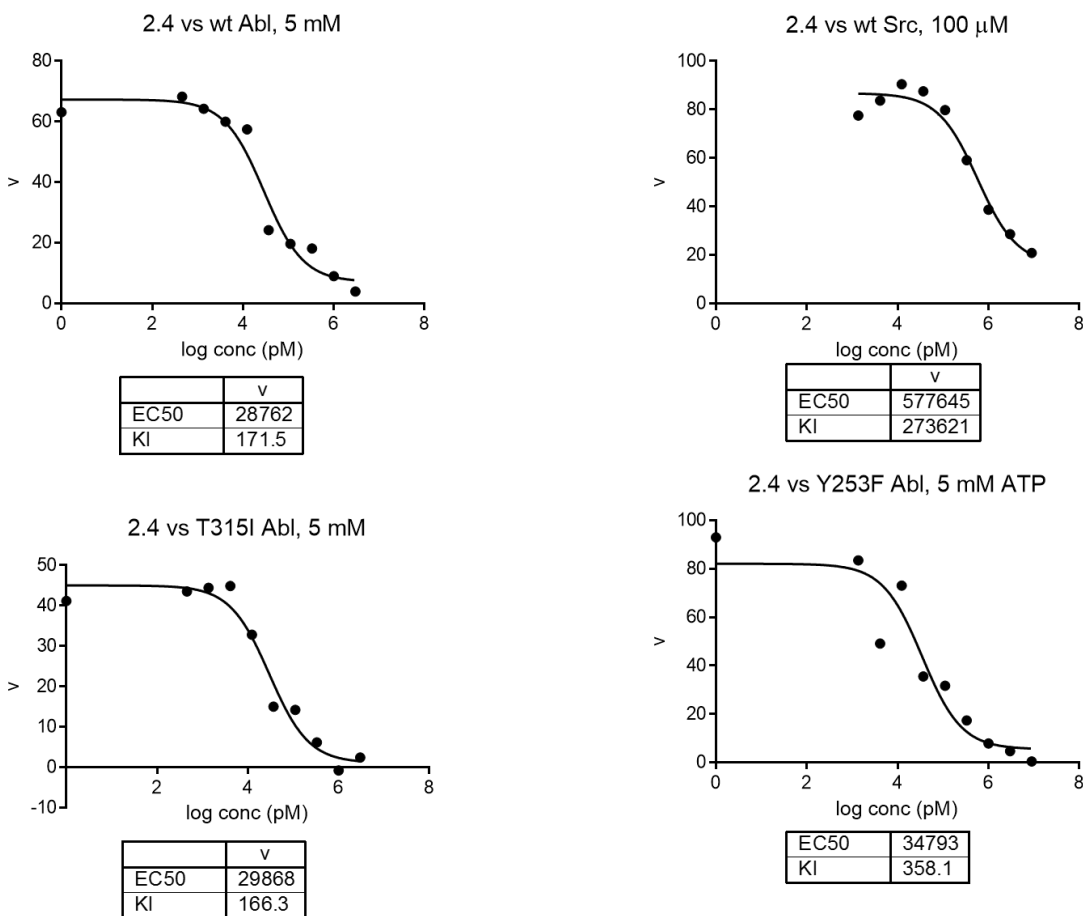
#### *Determination of Inhibitor IC<sub>50</sub>*

A previously reported continuous fluorescence assay was used to determine inhibitor IC<sub>50</sub> values.<sup>43</sup> Reaction volumes of 100  $\mu$ L were used in 96-well plates. 85  $\mu$ L of enzyme in buffer mix was added to each well followed by 2.5  $\mu$ L of the appropriate inhibitor dilution (typically 360, 120, 40, 13.33, 4.44, 1.48, 0.49, 0.164, and 0.055 Mm in DMSO) and 2.5  $\mu$ L of a substrate peptide solution (typically 1.8 mM in DMSO for the c-Src substrate and 2.4 mM in DMSO for the substrate of c-Abl and its mutants). The reaction was initiated with 10  $\mu$ L of ATP (50 mM or 1 mM in water), and reaction progress was immediately monitored at 405 nm (ex. 340 nm) for 10 min. Each well had a final

concentration of 30 nM c-Src or c-Abl, 45  $\mu$ M c-Src substrate or 60  $\mu$ M c-Abl substrate, 100  $\mu$ M or 5 mM ATP, 100  $\mu$ M  $\text{Na}_3\text{VO}_4$ , 100 mM Tris buffer (pH 8), 10 mM  $\text{MgCl}_2$ , and 0.01% Triton X-100.

The initial-rate data collected was used for determination  $K_i$  values. For  $K_i$  determination, the kinetic values were obtained directly from nonlinear regression of substrate-velocity curves in the presence of various concentrations of the inhibitor. The equation  $Y = \text{Bottom} + (\text{Top} - \text{Bottom}) / (1 + 10^{\text{X} - \text{LogEC50}})$ ,  $X = \log(\text{concentration})$  and  $Y = \text{binding}$ ; was used in the nonlinear regression. The  $K_i$  value was determined using  $\geq 3$  independent experiments. The mean  $K_i$  value is reported in this chapter and the mean, standard deviation, and a representative curve for each inhibitor is reported in **Appendix A**.

#### Representative curves for compound 2.4



Average  $K_i = 216 \pm 60$  nM (wt Src), Titrate enzyme ( $\text{IC}_{50} \sim 30$  nM) for wt, T315I, and Y253F Abl

### Correlating Selectivity Score to $K_d$ values

A plot of the selectivity score observed in a primary screen versus the  $K_d$  values for each individual target aids in choosing the selectivity score which best represents targets inhibited at or below the screening concentration. **Figure 2.8** shows that for a compound screened at 1  $\mu\text{M}$ , an S(35) score includes targets with a  $K_d$  greater than 10-fold the screening concentration. An S(10) score, however, mostly includes targets with a  $K_d$  equal or below the screening concentration of 1  $\mu\text{M}$

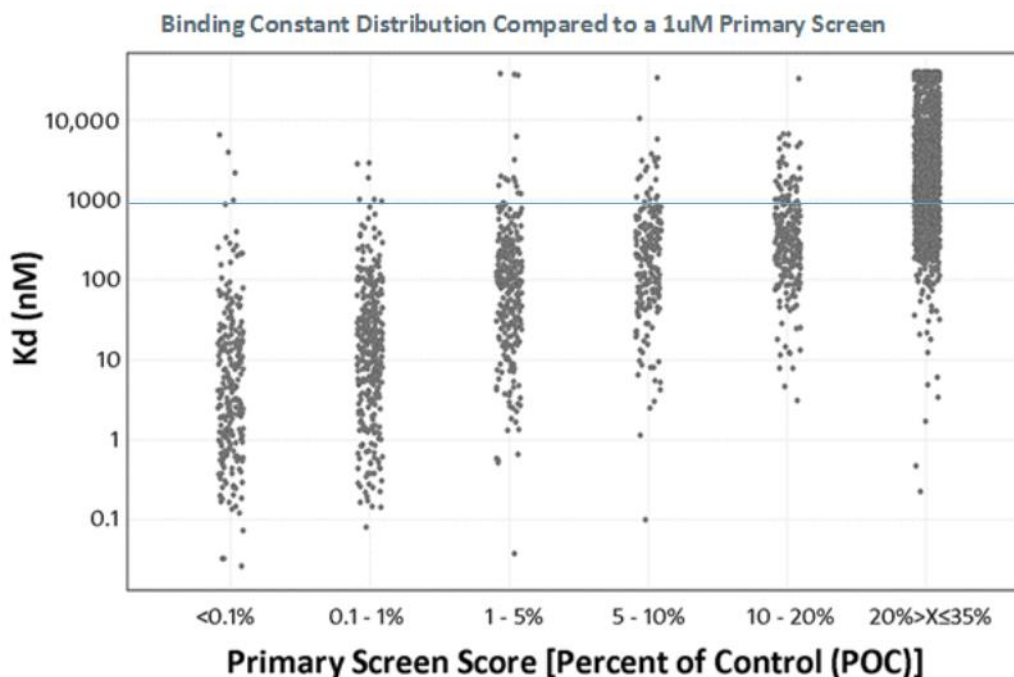


**Figure 2.8.** A plot of the primary screen score versus  $K_d$  values for individual targets. The blue marks targets with a  $K_d$  value of 1  $\mu\text{M}$ . An S(10) only includes targets with a  $K_d$  value below the screening concentration of 1  $\mu\text{M}$ .

## 2.12. References

1. Kurzrock, R.; Gutterman, J. U.; Talpaz, M., The Molecular Genetics of Philadelphia Chromosome–Positive Leukemias. *New England Journal of Medicine* **1988**, *319* (15), 990-998.
2. Lugo, T.; Pendergast, A.; Muller, A.; Witte, O., Tyrosine kinase activity and transformation potency of bcr-abl oncogene products. *Science* **1990**, *247* (4946), 1079-1082.
3. Daley, G.; Van Etten, R.; Baltimore, D., Induction of chronic myelogenous leukemia in mice by the P210bcr/abl gene of the Philadelphia chromosome. *Science* **1990**, *247* (4944), 824-830.
4. Druker, B. J.; Sawyers, C. L.; Kantarjian, H.; Resta, D. J.; Reese, S. F.; Ford, J. M.; Capdeville, R.; Talpaz, M., Activity of a specific inhibitor of the BCR-ABL tyrosine kinase in the blast crisis of chronic myeloid leukemia and acute lymphoblastic leukemia with the Philadelphia chromosome. *New England Journal of Medicine* **2001**, *344* (14), 1038-1042.
5. Sawyers, C. L., Chronic Myeloid Leukemia. *New England Journal of Medicine* **1999**, *340* (17), 1330-1340.
6. Kantarjian, H. M.; Deisseroth, A.; Kurzrock, R.; Estrov, Z.; Talpaz, M., Chronic myelogenous leukemia: a concise update. *Blood* **1993**, *82* (3), 691-703.
7. Faderl, S.; Kantarjian, H. M.; Talpaz, M., Chronic myelogenous leukemia: update on biology and treatment. *Oncology (Williston Park, NY)* **1999**, *13* (2), 169-180; discussion 181, 184.
8. Druker, B. J.; Guilhot, F.; O'Brien, S. G.; Gathmann, I.; Kantarjian, H.; Gattermann, N.; Deininger, M. W. N.; Silver, R. T.; Goldman, J. M.; Stone, R. M.; Cervantes, F.; Hochhaus, A.; Powell, B. L.; Gahrilove, J. L.; Rousselot, P.; Reiffers, J.; Cornelissen, J. J.; Hughes, T.; Agis, H.; Fischer, T.; Verhoef, G.; Shepherd, J.; Saglio, G.; Gratwohl, A.; Nielsen, J. L.; Radich, J. P.; Simonsson, B.; Taylor, K.; Baccarani, M.; So, C.; Letvak, L.; Larson, R. A., Five-Year Follow-up of Patients Receiving Imatinib for Chronic Myeloid Leukemia. *New England Journal of Medicine* **2006**, *355* (23), 2408-2417.
9. Kantarjian, H.; Talpaz, M.; O'Brien, S.; Giles, F.; Faderl, S.; Verstovsek, S.; Garcia-Manero, G.; Shan, J.; Rios, M. B.; Champlin, R.; de Lima, M.; Cortes, J., Survival benefit with imatinib mesylate therapy in patients with accelerated-phase chronic myelogenous leukemia--comparison with historic experience. *Cancer* **2005**, *103* (10), 2099-2108.
10. Van Etten, R. A., Cycling, stressed-out and nervous: cellular functions of c-Abl. *Trends Cell Biol* **1999**, *9* (5), 179-186.
11. Pluk, H.; Dorey, K.; Superti-Furga, G., Autoinhibition of c-Abl. *Cell* **2002**, *108* (2), 247-259.
12. Knighton, D. R.; Zheng, J. H.; Ten Eyck, L. F.; Ashford, V. A.; Xuong, N. H.; Taylor, S. S.; Sowadski, J. M., Crystal structure of the catalytic subunit of cyclic adenosine monophosphate-dependent protein kinase. *Science* **1991**, *253* (5018), 407-414.
13. Huse, M.; Kuriyan, J., The conformational plasticity of protein kinases. *Cell* **2002**, *109* (3), 275-282.
14. Nagar, B.; Bornmann, W. G.; Pellicena, P.; Schindler, T.; Veach, D. R.; Miller, W. T.; Clarkson, B.; Kuriyan, J., Crystal structures of the kinase domain of c-Abl in complex with the small molecule inhibitors PD173955 and imatinib (STI-571). *Cancer Res* **2002**, *62* (15), 4236-4243.

15. Schindler, T.; Bornmann, W.; Pellicena, P.; Miller, W. T.; Clarkson, B.; Kuriyan, J., Structural mechanism for STI-571 inhibition of abelson tyrosine kinase. *Science* **2000**, 289 (5486), 1938-1942.
16. Seeliger, M. A.; Nagar, B.; Frank, F.; Cao, X.; Henderson, M. N.; Kuriyan, J., c-Src Binds to the Cancer Drug Imatinib with an Inactive Abl/c-Kit Conformation and a Distributed Thermodynamic Penalty. *Structure* **2007**, 15 (3), 299-311.
17. O'Hare, T.; Eide, C. A.; Deininger, M. W., Bcr-Abl kinase domain mutations, drug resistance, and the road to a cure for chronic myeloid leukemia. *Blood* **2007**, 110 (7), 2242-2249.
18. Weisberg, E.; Manley, P. W.; Cowan-Jacob, S. W.; Hochhaus, A.; Griffin, J. D., Second generation inhibitors of BCR-ABL for the treatment of imatinib-resistant chronic myeloid leukaemia. *Nat Rev Cancer* **2007**, 7 (5), 345-356.
19. Davis, M. I.; Hunt, J. P.; Herrgard, S.; Ciceri, P.; Wodicka, L. M.; Pallares, G.; Hocker, M.; Treiber, D. K.; Zarrinkar, P. P., Comprehensive analysis of kinase inhibitor selectivity. *Nat Biotechnol* **2011**, 29 (11), 1046-1051.
20. O'Hare, T.; Eide, C. A.; Deininger, M. W., Bcr-Abl kinase domain mutations and the unsettled problem of Bcr-AblT315I: looking into the future of controlling drug resistance in chronic myeloid leukemia. *Clin Lymphoma Myeloma* **2007**, 7 Suppl 3, S120-130.
21. O'Hare, T.; Shakespeare, W. C.; Zhu, X.; Eide, C. A.; Rivera, V. M.; Wang, F.; Adrian, L. T.; Zhou, T.; Huang, W. S.; Xu, Q.; Metcalf, C. A., 3rd; Tyner, J. W.; Loriaux, M. M.; Corbin, A. S.; Wardwell, S.; Ning, Y.; Keats, J. A.; Wang, Y.; Sundaramoorthi, R.; Thomas, M.; Zhou, D.; Snodgrass, J.; Commodore, L.; Sawyer, T. K.; Dalgarno, D. C.; Deininger, M. W.; Druker, B. J.; Clackson, T., AP24534, a pan-BCR-ABL inhibitor for chronic myeloid leukemia, potently inhibits the T315I mutant and overcomes mutation-based resistance. *Cancer Cell* **2009**, 16 (5), 401-412.
22. Choi, H. G.; Ren, P.; Adrian, F.; Sun, F.; Lee, H. S.; Wang, X.; Ding, Q.; Zhang, G.; Xie, Y.; Zhang, J.; Liu, Y.; Tuntland, T.; Warmuth, M.; Manley, P. W.; Mestan, J.; Gray, N. S.; Sim, T., A type-II kinase inhibitor capable of inhibiting the T315I "gatekeeper" mutant of Bcr-Abl. *J Med Chem* **2010**, 53 (15), 5439-5448.
23. Seeliger, M. A.; Ranjitkar, P.; Kasap, C.; Shan, Y.; Shaw, D. E.; Shah, N. P.; Kuriyan, J.; Maly, D. J., Equally potent inhibition of c-Src and Abl by compounds that recognize inactive kinase conformations. *Cancer Res* **2009**, 69 (6), 2384-2392.
24. Deng, X.; Lim, S. M.; Zhang, J.; Gray, N. S., Broad spectrum alkynyl inhibitors of T315I Bcr-Abl. *Bioorg Med Chem Lett* **2010**, 20 (14), 4196-4200.
25. Huang, W. S.; Zhu, X.; Wang, Y.; Azam, M.; Wen, D.; Sundaramoorthi, R.; Thomas, R. M.; Liu, S.; Banda, G.; Lentini, S. P.; Das, S.; Xu, Q.; Keats, J.; Wang, F.; Wardwell, S.; Ning, Y.; Snodgrass, J. T.; Broudy, M. I.; Russian, K.; Daley, G. Q.; Iulucci, J.; Dalgarno, D. C.; Clackson, T.; Sawyer, T. K.; Shakespeare, W. C., 9-(Arenethenyl)purines as dual Src/Abl kinase inhibitors targeting the inactive conformation: design, synthesis, and biological evaluation. *J Med Chem* **2009**, 52 (15), 4743-4756.
26. Prasad, V.; Mailankody, S., The accelerated approval of oncologic drugs: lessons from ponatinib. *JAMA* **2014**, 311 (4), 353-354.



27. Cortes, J. E.; Kim, D. W.; Pinilla-Ibarz, J.; le Coutre, P.; Paquette, R.; Chuah, C.; Nicolini, F. E.; Apperley, J. F.; Khoury, H. J.; Talpaz, M.; DiPersio, J.; DeAngelo, D. J.; Abruzzese, E.; Rea, D.; Baccharani, M.; Muller, M. C.; Gambacorti-Passerini, C.; Wong, S.; Lustgarten, S.; Rivera, V. M.; Clackson, T.; Turner, C. D.; Haluska, F. G.; Guilhot, F.; Deininger, M. W.; Hochhaus, A.; Hughes, T.; Goldman, J. M.; Shah, N. P.; Kantarjian, H.; Investigators, P., A phase 2 trial of ponatinib in Philadelphia chromosome-positive leukemias. *N Engl J Med* **2013**, *369* (19), 1783-1796.
28. Cheng, H.; Force, T., Why do kinase inhibitors cause cardiotoxicity and what can be done about it? *Prog Cardiovasc Dis* **2010**, *53* (2), 114-120.
29. Force, T.; Krause, D. S.; Van Etten, R. A., Molecular mechanisms of cardiotoxicity of tyrosine kinase inhibition. *Nat Rev Cancer* **2007**, *7* (5), 332-344.
30. FDA Iclusig (ponatinib) Drug Approval Package. [http://www.accessdata.fda.gov/drugsatfda\\_docs/nda/2012/203469Orig1s000TOC.cfm](http://www.accessdata.fda.gov/drugsatfda_docs/nda/2012/203469Orig1s000TOC.cfm) (accessed March 30, 2015).
31. Eide, C. A.; Adrian, L. T.; Tyner, J. W.; Mac Partlin, M.; Anderson, D. J.; Wise, S. C.; Smith, B. D.; Petillo, P. A.; Flynn, D. L.; Deininger, M. W.; O'Hare, T.; Druker, B. J., The ABL switch control inhibitor DCC-2036 is active against the chronic myeloid leukemia mutant BCR-ABL T315I and exhibits a narrow resistance profile. *Cancer Res* **2011**, *71* (9), 3189-3195.
32. Akeno-Stuart, N.; Croyle, M.; Knauf, J. A.; Malaguarnera, R.; Vitagliano, D.; Santoro, M.; Stephan, C.; Grosios, K.; Wartmann, M.; Cozens, R.; Caravatti, G.; Fabbro, D.; Lane, H. A.; Fagin, J. A., The RET kinase inhibitor NVP-AST487 blocks growth and calcitonin gene expression through distinct mechanisms in medullary thyroid cancer cells. *Cancer Res* **2007**, *67* (14), 6956-6964.
33. Wilhelm, S.; Carter, C.; Lynch, M.; Lowinger, T.; Dumas, J.; Smith, R. A.; Schwartz, B.; Simantov, R.; Kelley, S., Discovery and development of sorafenib: a multikinase inhibitor for treating cancer. *Nat Rev Drug Discov* **2006**, *5* (10), 835-844.
34. Lin, Y. L.; Roux, B., Computational analysis of the binding specificity of Gleevec to Abl, c-Kit, Lck, and c-Src tyrosine kinases. *J Am Chem Soc* **2013**, *135* (39), 14741-14753.
35. Lin, Y. L.; Meng, Y.; Jiang, W.; Roux, B., Explaining why Gleevec is a specific and potent inhibitor of Abl kinase. *Proc Natl Acad Sci U S A* **2013**, *110* (5), 1664-1669.
36. Lovera, S.; Sutto, L.; Boubeva, R.; Scapozza, L.; Dolker, N.; Gervasio, F. L., The different flexibility of c-Src and c-Abl kinases regulates the accessibility of a druggable inactive conformation. *J Am Chem Soc* **2012**, *134* (5), 2496-2499.
37. Hari, S. B.; Perera, B. G.; Ranjitkar, P.; Seeliger, M. A.; Maly, D. J., Conformation-selective inhibitors reveal differences in the activation and phosphate-binding loops of the tyrosine kinases Abl and Src. *ACS Chem Biol* **2013**, *8* (12), 2734-2743.
38. Agafonov, R. V.; Wilson, C.; Otten, R.; Buosi, V.; Kern, D., Energetic dissection of Gleevec's selectivity toward human tyrosine kinases. *Nat Struct Mol Biol* **2014**, *21* (10), 848-853.
39. Wilson, C.; Agafonov, R. V.; Hoemberger, M.; Kutter, S.; Zorba, A.; Halpin, J.; Buosi, V.; Otten, R.; Waterman, D.; Theobald, D. L.; Kern, D., Kinase dynamics. Using ancient protein kinases to unravel a modern cancer drug's mechanism. *Science* **2015**, *347* (6224), 882-886.

40. Weisberg, E.; Manley, P. W.; Breitenstein, W.; Brugger, J.; Cowan-Jacob, S. W.; Ray, A.; Huntly, B.; Fabbro, D.; Fendrich, G.; Hall-Meyers, E.; Kung, A. L.; Mestan, J.; Daley, G. Q.; Callahan, L.; Catley, L.; Cavazza, C.; Azam, M.; Neuberg, D.; Wright, R. D.; Gilliland, D. G.; Griffin, J. D., Characterization of AMN107, a selective inhibitor of native and mutant Bcr-Abl. *Cancer Cell* **2005**, *7* (2), 129-141.
41. Okram, B.; Nagle, A.; Adrian, F. J.; Lee, C.; Ren, P.; Wang, X.; Sim, T.; Xie, Y.; Wang, X.; Xia, G.; Spraggon, G.; Warmuth, M.; Liu, Y.; Gray, N. S., A general strategy for creating "inactive-conformation" abl inhibitors. *Chem Biol* **2006**, *13* (7), 779-786.
42. Seeliger, M. A.; Young, M.; Henderson, M. N.; Pellicena, P.; King, D. S.; Falick, A. M.; Kuriyan, J., High yield bacterial expression of active c-Abl and c-Src tyrosine kinases. *Protein Science* **2005**, *14* (12), 3135-3139.
43. Wang, Q.; Cahill, S. M.; Blumenstein, M.; Lawrence, D. S., Self-Reporting Fluorescent Substrates of Protein Tyrosine Kinases. *Journal of the American Chemical Society* **2006**, *128* (6), 1808-1809.

## CHAPTER III

### Development of Cyclic Peptides as Inhibitors of Grb2 SH2

#### 3.1. Abstract

Growth factor receptor bound protein 2 (Grb2) is an adaptor protein linking extracellular signals to intracellular signaling cascades critical for cell growth. Its key role in Ras-signaling has made it an attractive target for targeted therapy in cancer. Current inhibitors of Grb2, however, suffer from poor cellular efficacy, which is likely a consequence of most such inhibitors being primarily based on a single scaffold.

This chapter details a comprehensive effort in developing potent inhibitors of the SH2 domain of Grb2 based on the motif of its endogenous binding partner. We hypothesized that utilizing conformational constraint for inhibitor development could lead to compounds with increased potency due to a lowered entropic cost of binding. Furthermore, we believed constraint through macrolactamization to be an effective method in increasing cell permeability and efficacy in whole cells.

Using the consensus sequence for Grb2 SH2 binding, a series of phosphotyrosine-containing cyclic peptides with increasing macrocycle size were synthesized. An optimal 26-membered macrocycle, **3.5**, identified through a fluorescence polarization assay was then modified by replacing the phosphotyrosine motif with a variety of mimetics. A phosphatase-stable analog, compound **3.10**, was found to be the most potent of these mimetics and was analyzed biophysically and *in cellulo*. Surface plasmon resonance and Isothermal titration calorimetry revealed **3.10** to have a markedly increased potency compared to its linear analogs. This increase in potency was driven entirely by a lowered entropic cost of binding to the protein, thereby, validating our hypothesis. Analysis of the kinetics of binding revealed compound **3.10** to have a slower dissociation rate than its linear counterpart, adding insight into the role of conformational restriction in altering the residence time of a ligand. Furthermore, compound **3.10** was shown to possess *in cellulo* activity in K562 cells while its linear analog did not, suggesting that the global

conformational restriction could indeed aid in the promotion of intramolecular H-bonds, thereby increasing cell permeability and cellular efficacy. Our effort in understanding the thermodynamics and kinetics of ligand-binding to Grb2 SH2 has set the stage for the further development of efficacious inhibitors, thereby, realizing the opportunity of targeting Grb2 in the treatment of cancer.

### 3.2. Role of Grb2 in Cell Signaling

In 1992, Lowenstein et al. identified the missing link connecting EGF stimulation of cells with their phenotypically observed response of growth.<sup>1</sup> Grb2 was identified from a phage display library as an adaptor protein, linking EGFR to the Ras signaling cascade, thereby completing the delineation of one of the most important signaling pathways

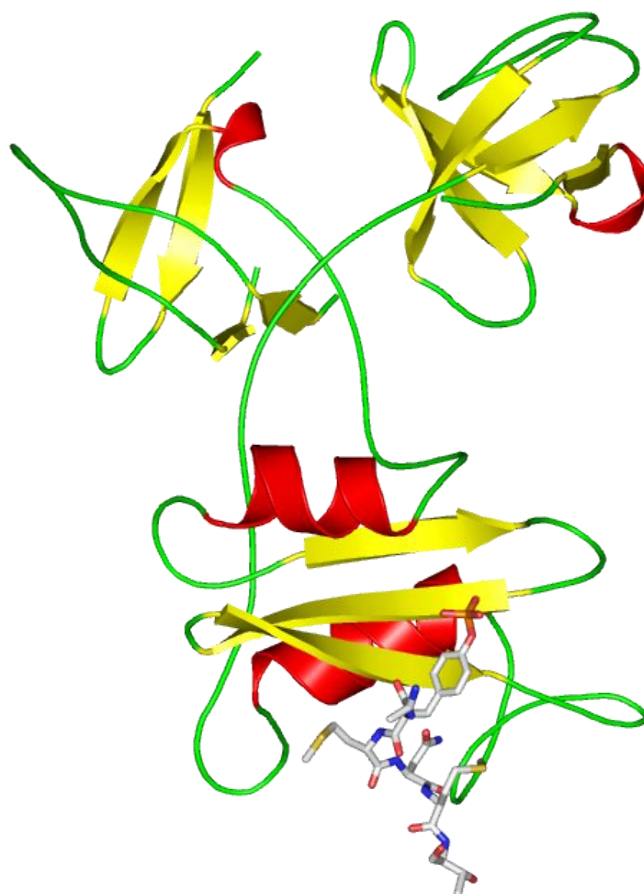


**Figure 3.1.** Grb2 is comprised of one SH2 domain flanked by two SH3 domains. The SH2 domain binds a peptide with a pYXNX motif in a  $\beta$ -turn

involved in cell growth. This discovery led to the rapid characterization of Grb2, and it was observed to be a 25 kDa protein comprised of one SH2 domain flanked by N-terminal and C-terminal SH3 domains (**Figure 3.1**). The SH2 domain consists of a central antiparallel  $\beta$ -sheet flanked by two helices and specifically binds peptides with a pYXNX motif in a  $\beta$ -turn. The SH3 domains, which share 34% sequence identity and are primarily composed of  $\beta$ -sheets, both bind to peptides with a polyproline type II (PPII) helix with differing selectivity.<sup>2</sup>

A substantial amount of cytosolic Grb2 is associated with the PPII helix of the Son of Sevenless (Sos) protein via its SH3 domains. Upon EGF stimulation and receptor phosphorylation, the Grb2-Sos complex binds *via* the Grb2 SH2 domain either directly or indirectly to EGFR. Direct binding is achieved through the pY1068 or pY1086 residue of EGFR, while indirect binding is mediated *via* a tyrosine phosphorylated protein, Shc, which itself binds to pY1148 of EGFR.<sup>3</sup> This results in membrane localization of Sos, which functions as a guanine nucleotide exchange factor (GEF), and loads membrane-bound Ras with GTP thus activating it, leading to the propagation of the activating signal downstream.<sup>1, 4-5</sup>

While the role of Grb2 within the above-mentioned pathway is the most extensively characterized, later discoveries have expanded its functional role to several other pathways. Grb2 SH2 can bind to several other RTKs such as Her-2, Her-3, PDGFR, c-Met and FGFR-2,<sup>6</sup> and to other phosphorylated proteins such as  $\beta$ 4 integrin, IRS-1<sup>7</sup>, BCR-Abl and FAK either directly or indirectly through linker proteins such as Shc and SHP-2. Furthermore, in addition to Sos, many other effector molecules, such as the GEFs (C3G, VAV), receptors (CD28), adaptor proteins (Cbl, Slp-76), phosphotyrosine phosphatases (SHP2) and serine/threonine kinases (PAK1, MEKK1) can bind to the SH3 domains of Grb2.<sup>7</sup> The astounding number of binding partners of both the SH2 and SH3 domains of Grb2 provide for an incredible degree of cross-talk between various signaling pathways, which may be highly dependent on temporal and spatial factors as well as differential concentrations in diverse cell types.

### 3.3. Grb2 as a Therapeutic Target in Cancer

Due to its critical role in several signaling pathways, Grb2 is considered a putative therapeutic target in several cancers. The fusion protein, Bcr-Abl, discussed in detail in Chapter II binds to the Grb2 SH2 domain through a phosphorylated tyrosine residue (Y177) in the Bcr region and implicates Ras signaling in CML. A Y177F mutant is unable to transform primary bone marrow cultures underscoring the role of Grb2 in CML progression.<sup>8</sup> While the FDA-approved inhibitors and compound **2.4** are very successful at inhibiting Bcr-Abl *in cellulo* and in the clinic, resistance eventually develops rendering these molecules ineffective. In addition to the innate forms of resistance, such as through the T315I mutation (discussed in Chapter II), long-term sequential therapy gives rise to acquired resistance through the emergence of double-mutants which render all CML drugs ineffective.<sup>9-10</sup> Combination therapy with ‘drug cocktails’ comprising of a Bcr-Abl inhibitor and Grb2 inhibitor could be advantageous in preventing or slowing the emergence of drug-induced resistance.

Furthermore, Grb2 is overexpressed in several breast cancer cell lines and tissue samples.<sup>11-12</sup> The most marked overexpression is observed in the MCF-7, MDA-MB-361, and MDA-MB-453 cell lines in comparison to human mammary epithelial (HME) cells and the majority of breast cancer cell lines.<sup>11</sup> Within the context of breast cancer, the major role of Grb2 is related to cell adhesion, motility, and invasion rather than growth and proliferation.<sup>13</sup> This suggests that Grb2 is a putative target for the inhibition of tumor metastasis in invasive breast cancer.

Antisense oligonucleotides have demonstrated the efficacy of silencing Grb2 in Ph<sup>+</sup> leukemia cells<sup>14</sup> and in breast cancer cells expressing high levels of Her2 (MDA-MB-453 and SKBr3)<sup>15</sup> paving the way for intervention using small molecules and peptides.

### 3.4. Current Inhibitors of Grb2

The SH2 domain of Grb2 binds phosphotyrosine-containing peptides in a  $\beta$  turn with micromolar potencies.<sup>16</sup> About 50% of the binding energy is proposed to originate from the phosphotyrosine residue while the residues C-terminal to it control specificity among SH2 domains.<sup>17-18</sup> The SH3 domain forms weak interactions over a relatively flat and hydrophobic surface with a polyproline type-II helix-containing binding partner.<sup>19-20</sup> The high-affinity handle of a phosphotyrosine residue and the specificity that can be

achieved has made the SH2 domain a more attractive target for inhibitor development than the SH3 domain.

Despite the relative ‘druggability’ of the SH2 domain, inhibitor development has primarily focused on a few scaffolds with limited success. The first, disclosed by Novartis, consists of a 1-aminocyclohexanecarboxylic acid at the pY+1 position to stabilize a  $\beta$  turn and a C-terminus 3-naphthalen-1-yl-propyl group.<sup>21-22</sup> Burke and co-workers have extensively modified each segment of the Novartis scaffold from the point of view of increasing potency through functional group modifications and imposing conformational constraints as well as to increase stability towards phosphatases (**Figure 3.2**).<sup>23-27</sup> Despite the large number of analogs that have been synthesized only a few modifications have shown an improvement in potency and the most effective compounds retain the characteristics of the original Novartis scaffold.<sup>28</sup> Moreover, compounds with low nanomolar affinity for Grb2 SH2, show a significant reduction in potency *in cellulo*, presumably due to poor cell permeability. The compounds that do show activity, typically do so under non-standard conditions such as daily dosing for extended periods of time and under serum-starved conditions.<sup>29-31</sup>

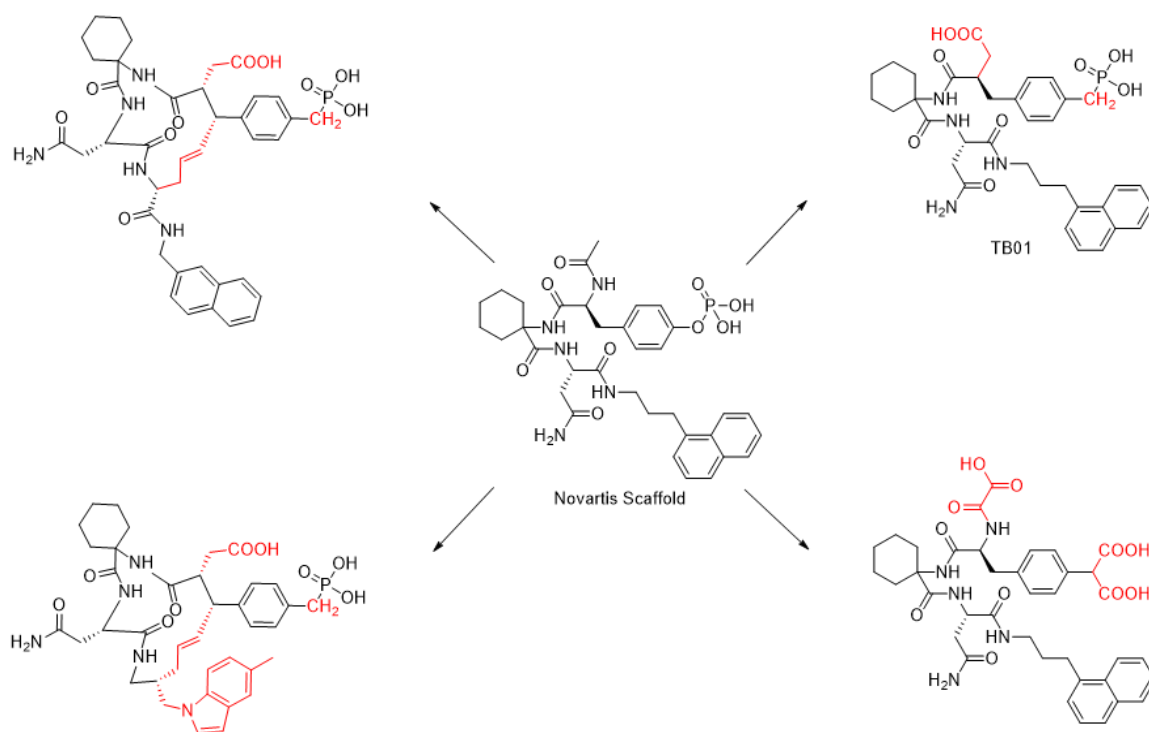


**Figure 3.2.** Novartis scaffold and the analogs synthesized by Burke and coworkers.

The second scaffold to be explored, termed G1, was obtained from a disulfide-cyclized phage library.<sup>32</sup> G1, and its thioether analog, G1TE, which have potencies in the range of 10 to 25  $\mu\text{M}$ , are noteworthy in that they lack a phosphotyrosine residue. While these analogs themselves show no activity *in cellulo* the finding that non-phosphorylated compounds could inhibit Grb2 SH2 spurred interest in the further development of this scaffold. Optimization and modification of the scaffold, however, did not significantly increase potency and the initial promise of circumventing the poor permeability associated with di-anionic inhibitors was not realized. A few analogs with low nanomolar potencies rely on a phosphotyrosine mimic and are di-anionic in nature.<sup>33-34</sup>

Lastly, a class of compounds, relatively underexplored for its *in cellulo* potential is that of conformationally restricted peptides based on the consensus binding sequence of Grb2 SH2 (**Figure 3.3**). Conformational constraint applied locally to the phosphotyrosine residue has typically led to a significant loss in potency.<sup>35</sup> While global constraint through macrocyclization has shown to increase potency and has been studied from a thermodynamic standpoint,<sup>36</sup> a systematic study of the effect of macrocycle size on potency and *in cellulo* efficacy is lacking.<sup>36-38</sup> Consequently, we sought to employ conformational restriction as a means to develop potent inhibitors of Grb2 SH2 and to assess these inhibitors using biophysical methods and *in cellulo*.

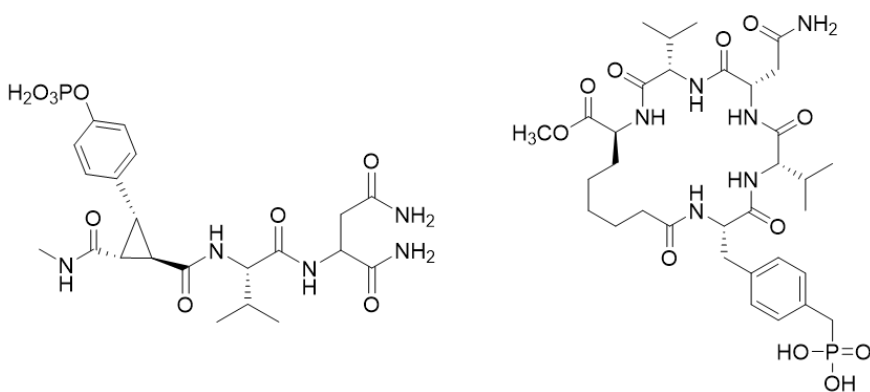


**Figure 3.3.** Examples of local (left) and global (right) conformational constraint in the development of Grb2 SH2



### 3.5. Utilizing Conformational Constraint in the Development of Grb2 SH2 Inhibitors

Conformational constraint, when applied correctly, has long been believed to increase the potency of a ligand. The rationale, rooted in the thermodynamics of a protein-

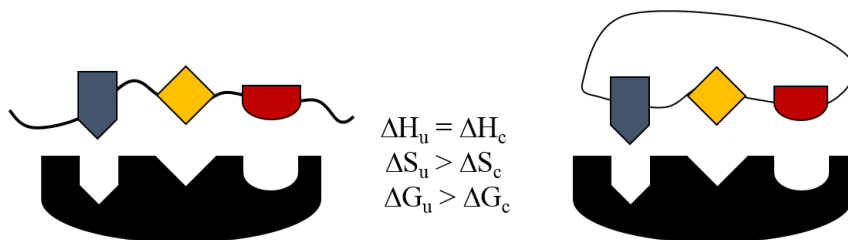


**Figure 3.4.** The thermodynamic rationale of ligand pre-organization. The subscript *u* indicates an unconstrained ligand and *c* indicates a constrained ligand.

ligand interaction, is that pre-organizing a ligand and restricting its degrees of freedom would lead to a smaller entropic change on binding to the protein (**Figure 3.4**).<sup>36, 39</sup> Provided that the constrained and unconstrained ligands are able to make optimal interactions with the protein ( $\Delta H$  for the pair of ligands is the same), a lower entropic cost for the constrained ligand would be reflected in a lower free energy of binding.

Several distinct examples of improved potency using conformational constraint have been observed over the last decade.<sup>40-41</sup> We reasoned that conformational restriction through peptide macrocyclization was ideally suited for the development of inhibitors of the Grb2 SH2 domain. In addition to the advantage of increased potency, macrocyclization offers an avenue for achieving selectivity for Grb2 SH2. Of the 120 SH2 domains encoded in the human genome, the vast majority bind a phosphotyrosine-containing peptide in an extended conformation.<sup>42</sup> Cyclic peptides would be unable to adopt an extended conformation and would be preferred by Grb2 SH2, which binds peptides in a  $\beta$ -turn conformation. Furthermore, cyclization could promote the formation of intramolecular H-bonds which could aid in increasing the permeability of these inhibitors.

### 3.6. Macrocycle Optimization

Our synthetic strategy, based on that described by the Hruby group,<sup>43</sup> involved the use of an  $\alpha$ -Fmoc  $\epsilon$ -Alloc protected Lysine at the N-terminus and a Fmoc  $\beta$ -allyl protected Aspartic acid at the C-terminus. Both amino acids were compatible with and orthogonal to

Fmoc SPPS and precluded the need for unnatural amino acids as are often required for peptide stapling. Deprotection of the allyl/alloc protecting groups was carried out using tetrakis(triphenylphosphine)palladium(0) and *N,N*-dimethylbarbituric acid and cyclization was carried out on-resin, prior to cleavage, using standard coupling conditions.

Macrocycles of increasing length were synthesized as shown in **Table 3.1**. Glycine residues were incorporated with increasing macrocycle size to allow added flexibility to accommodate optimal interactions with the protein surface. Biochemical inhibition was measured by using a fluorescence polarization assay. Increasing the size of the macrocycle from 17 atoms (compound **3.1**) to 26 atoms (compound **3.5**) led to a dramatic increase in potency. Further increasing the size of the macrocycle or altering the position of the glycine residue (compounds **3.6** – **3.9**), resulted in a plateau or slight decrease in potency. This could be rationalized by the fact that an increase in size would be required to make appropriate contacts with the so-called hot spots at the protein surface. After a point, however, any increase in macrocycle size would result in a loss of effective pre-organization, and any increase in enthalpy would be compensated by a greater entropic penalty paid for binding to the protein.

**Table 3.1.** Summary of IC<sub>50</sub> values of macrocycles of increasing size

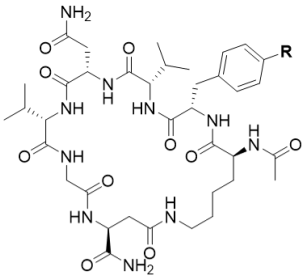
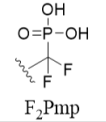
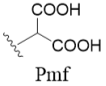
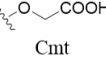
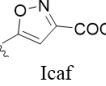
Compound	Sequence	Atoms in Macrocycle	IC <sub>50</sub> (μM)
<b>3.1</b>	Ac-K-pY-V-D-NH <sub>2</sub>	17	>100
<b>3.2</b>	Ac-K-pY-V-N-D-NH <sub>2</sub>	20	64
<b>3.3</b>	Ac-K-pY-V-N-V-D-NH <sub>2</sub>	23	5.3
<b>3.4</b>	Ac-K-pY-V-N-V-E-NH <sub>2</sub>	24	2.8
<b>3.5</b>	Ac-K-pY-V-N-V-G-D-NH <sub>2</sub>	26	0.7
<b>3.6</b>	Ac-K-G-pY-V-N-V-D-NH <sub>2</sub>	26	2
<b>3.7</b>	Ac-K-G-G-pY-V-N-V-D-NH <sub>2</sub>	29	1.4
<b>3.8</b>	Ac-K-G-pY-V-N-V-G-D-NH <sub>2</sub>	29	2.7
<b>3.9</b>	Ac-K-pY-V-N-V-G-G-D-NH <sub>2</sub>	29	2.6

### 3.7. Use of Phosphotyrosine Mimetics

Compound **3.5** with 26 atoms and an  $i \rightarrow i+6$  linkage was the most potent with an  $IC_{50}$  of 0.7  $\mu\text{M}$ . We next sought to replace the phosphotyrosine residue with a non-hydrolysable phosphotyrosine (pY) mimetic to enable the use of this compound *in cellulo*.

Burke and coworkers have successfully used di-anionic residues such as phosphonomethyl phenylalanine (Pmp) and *p*-malonyl phenylalanine (Pmf) as pY mimetics for SH2 domains,<sup>31, 44-45</sup> and difluorophosphonomethyl phenylalanine (F<sub>2</sub>Pmp) as a pY mimetic for phosphatases.<sup>46</sup> Of these mimetics, compound **3.10**, with Pmp showed

**Table 3.2.**  $IC_{50}$  values of compounds with phosphotyrosine mimetics

Compound	R	$IC_{50}$ ( $\mu\text{M}$ )
<b>3.10</b>	 Pmp	0.54
<b>3.11</b>	 F <sub>2</sub> Pmp	0.96
<b>3.12</b>	 Pmf	193
<b>3.13</b>	 Cmt	>100
<b>3.14</b>	 Icaf	>100

the greatest potency with an IC<sub>50</sub> of 540 nM (**Table 3.2**). This slight increase in potency is in agreement with a similar replacement on the Novartis scaffold.<sup>47</sup>

In contrast to a previous report which showed a 2 to 8-fold loss in potency on substituting Pmp with Pmf,<sup>31</sup> we observed a 350-fold reduction in potency for the same replacement (compound **3.12**) suggesting that the use of this mimetic may be scaffold-specific.

Yao and coworkers have shown that an isoxazolecarboxylic acid-containing compound could inhibit the STAT3 SH2 domain. Though the affinity of their compound was low, only a small loss in potency was observed when compared to a similar phosphotyrosine-containing compound.<sup>48</sup> Consequently, we attempted replacing the phosphate group with mono-anionic mimetics that would result in the reduction of the net charge of the molecule and could aid in improving cell permeability. The replacement with mimetics such as carboxymethyltyrosine (Cmt) in compound **3.13** and *p*-(isoxazolecarboxylic acid)phenylalanine (Icaf) in compound **3.14**, however, resulted in poor to no inhibition. This result underscores the difficulty in developing mono-anionic inhibitors of Grb2 SH2 and that phosphotyrosine mimetics are not equally effective across SH2 domains since these domains are not necessarily optimized for ligand binding.<sup>16</sup>

### 3.8. Surface Plasmon Resonance Studies

While a fluorescence polarization assay is useful for ranking compounds based on their IC<sub>50</sub> values, its ability to determine accurate  $K_i$  values for inhibitors is limited by the  $K_d$  of the probe. To determine whether cyclization did actually provide the hypothesized increase in potency and to obtain accurate  $K_d$  values, the linear and cyclic Pmp analogs, compounds **3.10** and **3.15**, were tested against immobilized Grb2 SH2 using surface plasmon resonance (SPR).

Both compounds showed rapid association rates, attaining equilibrium in under a minute. Compound **3.10** (**Figure 3.5**) showed a slightly larger  $k_a$  of  $2.70 \times 10^5 \text{ M}^{-1}\text{s}^{-1}$ , approximately 2-fold greater than that of compound **3.15** (**Figure 3.6**). Compound **3.10** does, however, have a markedly slower off-rate ( $0.0562 \text{ s}^{-1}$ ) as compared to its linear counterpart ( $0.638 \text{ s}^{-1}$ ). In a set of similar ligands, a slower off-rate is typically observed in one if a conformational change is required for dissociation. This 11-fold faster off-rate for

compound **3.15** could arise from its increased flexibility allowing a conformational change to occur rapidly during dissociation.

Satisfactorily, the slower off-rate for compound **3.10** is translated into a 20-fold enhancement in potency ( $K_d = 207$  nM as compared to  $4.3\mu\text{M}$  for **3.15**). The  $K_d$  values obtained from the kinetic analysis were validated using an equilibrium analysis, and the curves are shown in **Appendix B**.

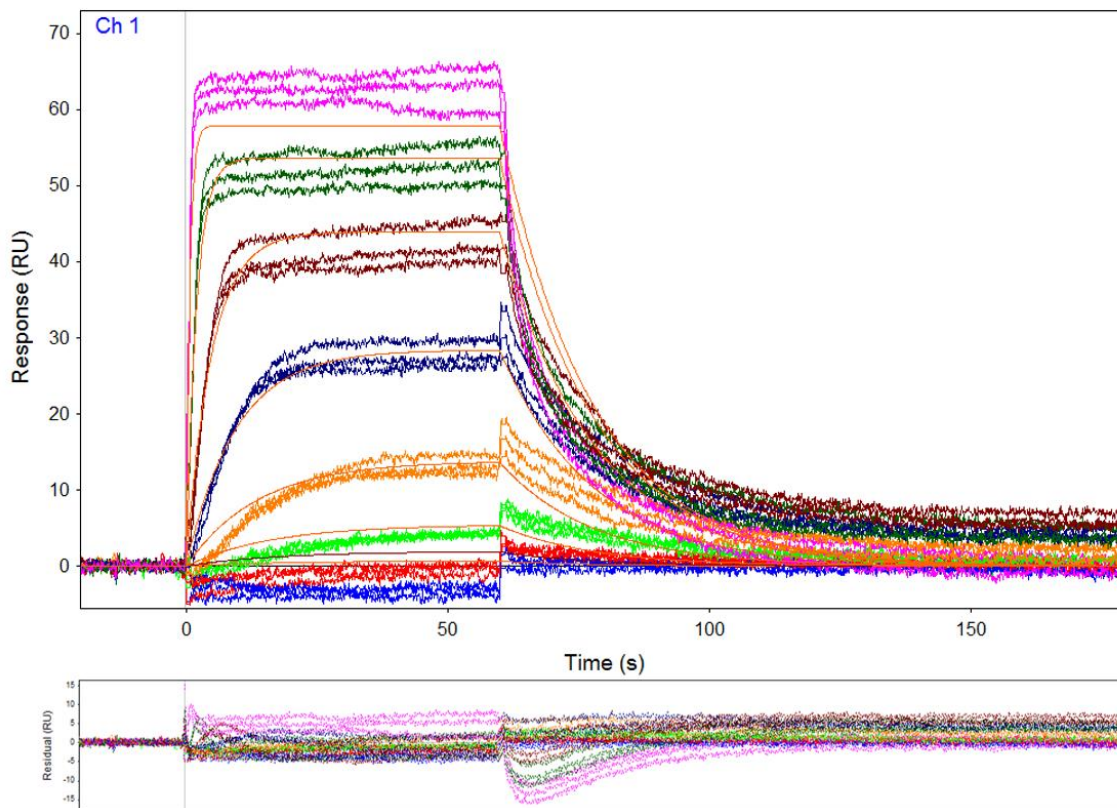
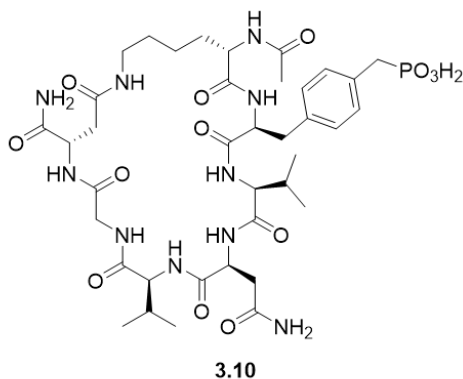


**Figure 3.5.** SPR kinetic data for cyclic peptide **3.10**.  $K_D = 207.7 \pm 0.7$  nM,  $k_a$  ( $\text{M}^{-1}\text{s}^{-1}$ ) =  $2.70 \times 10^5$ ,  $k_d$  ( $\text{s}^{-1}$ ) = 0.0562,  $R_{\text{max}} = 60.33$ , Res SD = 3.43 RU

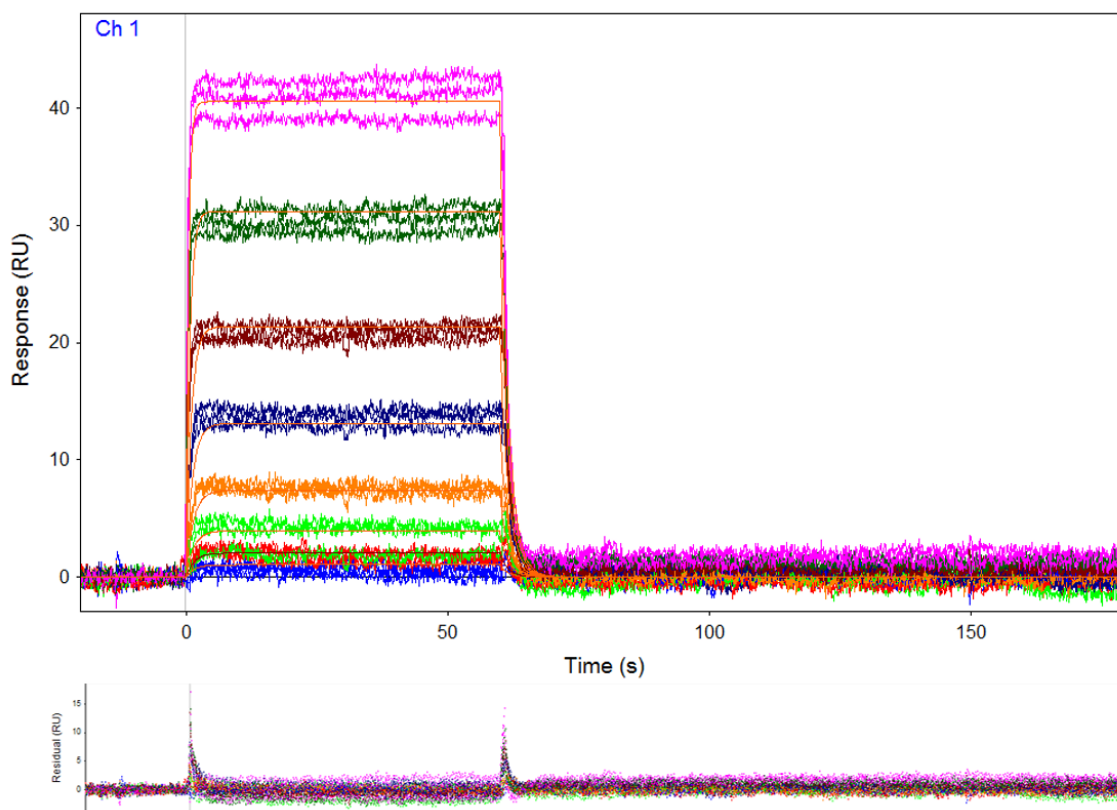
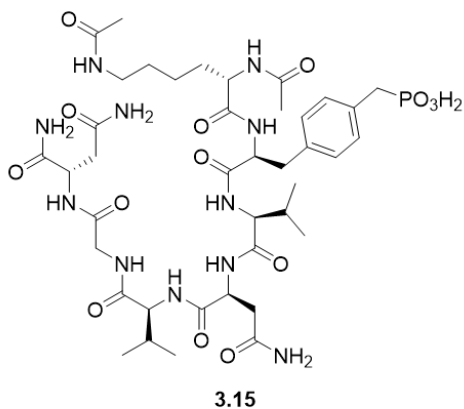


**Figure 3.6.** SPR kinetic data for linear peptide **3.15**.  $K_D = 4.274 \pm 0.009 \mu\text{M}$ ,  $k_a (\text{M}^{-1}\text{s}^{-1}) = 1.493 \times 10^5$ ,  $k_d (\text{s}^{-1}) = 0.638$ ,  $R_{\text{max}} = 57.92$ ,  $\text{Res SD} = 1.087 \text{ RU}$

### 3.9. Isothermal Titration Calorimetry

Martin and co-workers have argued that conformational constraint doesn't necessarily lead to a lowered entropic cost on binding and that the observed enhancement in potency could, in fact, be due to a lower enthalpic component. Using isothermal titration calorimetry (ITC) they have compared a series of constrained and unconstrained analogs to delineate the energetic components on binding to Grb2 SH2. Their argument, counter to

conventional wisdom suggests that conformational constraint could lead to more favorable binding interactions as compared to the unconstrained analog, which in turn would *increase* the entropic penalty paid upon binding.<sup>36, 39, 49</sup>

To demonstrate the increased potency of compound **3.10** was indeed due to a lowered entropic cost, we sought to measure the energetic components of the binding

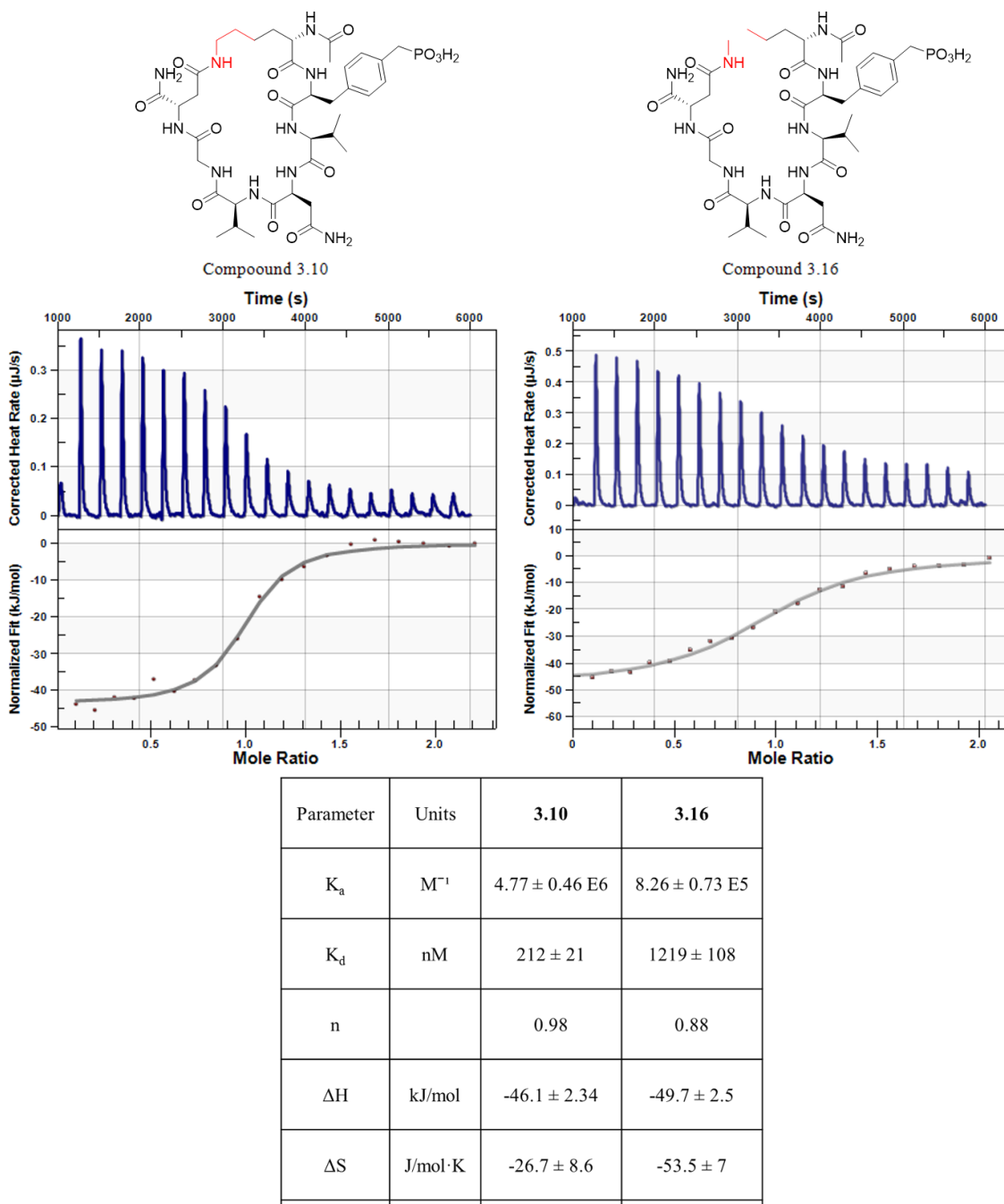


**Figure 3.7.** ITC comparison of cyclic and linear peptides.

interaction. For the enthalpic and entropic values of two ligands to be directly comparable, it is essential that the molecular weights of the ligands are as close to each other as possible. Consequently, we synthesized compound **3.16** which retained the same functional groups as **3.10** and differed in molecular weight by 1 Da.

As seen in **Figure 3.7**, the  $K_d$  value of compound **3.10** obtained is almost identical to, and in good agreement with, the value obtained from kinetic analysis using SPR. Moreover, the change in enthalpy on binding for each compound is within error of each other, and the observed enhancement in potency is solely driven by a more favorable entropic term. These data suggest that cyclization does indeed lower the entropic cost associated with binding and underscores the importance of optimizing the size of the macrocycle to achieve a maximum enhancement in potency.

### 3.10. Inhibition of Cancer Cell Growth

As described in **Section 3.3**, Grb2 plays a role in growth and proliferation of tumor cells in CML. Consequently, to assess the efficacy of cyclic and linear compounds **3.10** and **3.15** on cell growth, they were tested in the Bcr-Abl dependent K562 cell line.

Compound **3.10** showed a  $GI_{50}$  of 19  $\mu\text{M}$  after 72 hours of exposure, while its linear analog, compound **3.15**, showed no inhibition below 100  $\mu\text{M}$ . Furthermore, the low nanomolar inhibitor TB01 (see **Figure 3.2**) has been tested in K562 cells by Burke and coworkers with an observed  $GI_{50}$  of 39  $\mu\text{M}$ .<sup>28</sup> A ratio of the cellular to biochemical  $IC_{50}$ s can offer a measure of the permeability of a compound. Compound **3.10** with a ratio of 100 does significantly better than TB01, which has a ratio of about 5000.<sup>28, 50</sup> This improved cellular efficacy of **3.10** compared to compounds **3.15** and TB01 can be attributed to its biochemical potency coupled with an increase in cell permeability due to the promotion of intramolecular H-bond formation.

### 3.11. Conclusions

Despite the crucial role of Grb2 in cellular growth signaling cascades, relatively few SH2 domain-targeting scaffolds have been examined. Through the systematic development of conformationally constrained cyclic peptides, we have identified a novel scaffold for the inhibition of Grb2 SH2. A detailed analysis of the kinetic and thermodynamic parameters of binding of compound **3.10** indicates a significant



enhancement in potency compared to its linear counterpart. This enhancement in potency is entirely driven by a lower entropic cost upon binding and results in a slower dissociation rate upon binding. Furthermore, a significant improvement in cellular permeability is achieved validating our hypothesis that conformational restriction could be an attractive means for developing cell-permeable inhibitors of Grb2 SH2.

### 3.12. Materials and Methods

#### *General Synthetic Methods*

Unless otherwise noted, all reagents were obtained via commercial sources and used without further purification. Tetrahydrofuran (THF) and dichloromethane (CH<sub>2</sub>Cl<sub>2</sub>) were dried over alumina under a nitrogen atmosphere. <sup>1</sup>H and <sup>13</sup>C NMR spectra were measured with a Varian MR400, Varian VNMRs 500, or Inova 500 spectrometer. Mass Spectrometry (HRMS) was carried out by the University of Michigan Mass Spectrometry Facility (J. Windak, director). A detailed protocol for the synthesis of cyclic peptides and characterization data is provided in **Appendix B**.

#### *General Biochemical Methods*

Black, opaque-bottom, half-area 96 well plates were used for fluorescence polarization assays and were purchased from Nunc. Grb2 SH2 was expressed in *E. coli* and purified as a monomer by Christel Fox using previously published procedures. Data was obtained using a Biotek Synergy 4 plate reader. Curve fitting was performed using GraphPad Prism 4 software.

#### *K<sub>d</sub> Determination of the Probe used in Fluorescence Polarization Assays*

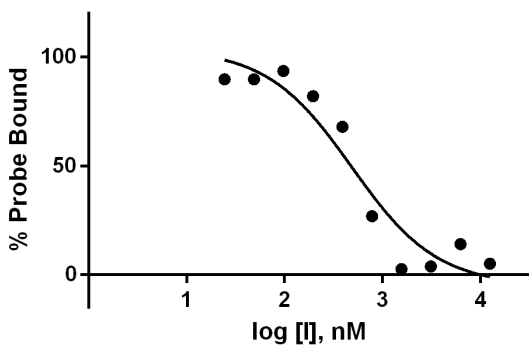
In a Costar® 96-well black plate, 55 µL water was added to each well, followed by 5 µL of probe (1 µM in DMSO). 40 µL of the appropriate dilution of Grb2 SH2 in 2.5x buffer (50 mM Na<sub>2</sub>HPO<sub>4</sub>/NaH<sub>2</sub>PO<sub>4</sub>, 250 mM NaCl, 0.125% Tween-20) was then added and the plate incubated on ice for 45 min. Each well contained a final concentration of 50 nM probe; 12, 6, 3, 1.5, 0.75, 0.375, 0.187, 0.09, 0.46, 0.023, 0.011 or 0 µM Grb2 SH2 in 20 mM Na<sub>2</sub>HPO<sub>4</sub>/NaH<sub>2</sub>PO<sub>4</sub> [pH 7.4], 100 mM NaCl, 0.05% Tween-20, 5% DMSO. The plate was then placed into a Biotek® Synergy 4 spectrophotometric plate reader and fluorescence polarization was measured with excitation at 485 nm (bandwidth = 20 nm)

and emission at 528 nm (bandwidth = 20 nm). The millipolarization (mP) value was converted to % Bound using the equation:  $\% \text{ Bound} = (\text{mPx} - \text{mPL}) * 100 / (\text{mPH} - \text{mPL})$  where mPx is the polarization value for concentration x, mPL is the lowest polarization value for the no-protein control where the probe is completely unbound and mPH is the highest polarization value where the probe is completely bound. The equation  $Y = \text{Bmax} * X / (\text{Kd} + X)$  was used in the nonlinear regression and an average Kd of three independent runs was obtained.

#### *Procedure for the Determination of IC<sub>50</sub> Values of Inhibitors*

Competition assays were carried out in a Costar® 96-well black plate with a final volume of 100 µL. To each well was added 45 µL water, 2.5 µL of the appropriate dilution of inhibitor in DMSO, 2.5 µL of probe (1 µM) and 50 µL Grb2 SH2 (3 µM) in buffer 2X (or only buffer 2x without Grb2 SH2 for the no-protein control) and the plate incubated on ice for 45 min. Each well contained a final concentration of 25 nM probe; 1.5 µM Grb2 SH2; 100, 50, 25, 12.5, 6, 3, 1.5, 0.78, 0.39, 0.19 or 0 µM inhibitor; in 20 mM Na<sub>2</sub>HPO<sub>4</sub>/NaH<sub>2</sub>PO<sub>4</sub> [pH 7.4], 100 mM NaCl, 0.05% Tween-20, 5% DMSO. The plate was then placed into a Biotek® Synergy 4 spectrophotometric plate reader and fluorescence polarization was measured with excitation at 485 nm (bandwidth = 20 nm) and emission at 528 nm (bandwidth = 20 nm). The millipolarization (mP) value was converted to % Probe Bound using the equation:  $\% \text{ Probe Bound} = (\text{mPx} - \text{mPL}) * 100 / (\text{mPH} - \text{mPL})$  where mPx is the polarization value for inhibitor concentration x, mPL is the lowest polarization value for the no-protein control where the probe is completely unbound and mPH is the highest polarization value for the no-inhibitor control where the probe is >90% bound. The equation  $Y = \text{Bottom} + (\text{Top} - \text{Bottom}) / (1 + 10^{-(X - \text{LogIC}_{50})})$  was used in the nonlinear regression. The IC<sub>50</sub> value was determined using ≥ 3 independent experiments. Average IC<sub>50</sub> values, standard deviations, and representative curves for each compound is included in **Appendix B**.

### Representative IC<sub>50</sub> curve for compound **3.10**



EC50	487.0
------	-------

Average IC<sub>50</sub> = 0.54 ± 0.04 μM

### *Surface Plasmon Resonance*

The surface plasmon resonance experiments were performed using a SensiQ® Pioneer instrument on a COOH5 chip (high density, hydrogel-based, three-dimensional carboxylated surface) containing 3 channels in series.

Grb2 SH2 (10 kDa) was immobilized on channel 1 (CH 1), and Bovine Serum Albumin (BSA) was immobilized on channel 2 (CH 2) using standard amine coupling chemistry with a running buffer of 20 mM HEPES, pH 7.4, 100 mM NaCl.

400 mM 3-(N,N-dimethylamino)propyl-N-ethylcarbodiimide (EDC) and 100 mM N-hydroxysuccinimide (NHS) was mixed in a 1:1 proportion and injected using the ‘fast inject’ option over CH 3-2 for 7 min at a flow rate of 25 μL/min. 50 μg/ml BSA in 10 mM Acetate, pH 4.5, was injected using ‘fast inject’ over CH 3-2 at 10 μL/min to give a density of 3500 RU and served as the reference surface. 1M Ethanolamine, pH 8.5, was injected for 4 min at a flow rate of 25 μL/min over CH 3-2 to cap any activated esters.

400 mM EDC and 100 mM NHS, mixed in a 1:1 proportion was then injected using ‘fast inject’ over CH 1 for 7 min at 25μL/min followed by an injection of 48 μg/ml Grb2 SH2 in 10 mM Acetate, pH 5, over CH 1 at 10 μL/min to give a density matching that of the reference BSA surface. 1 M Ethanolamine, pH 8.5, was injected for 4 min at a flow rate of 25 μL/min over CH 1 to cap any activated esters.

After immobilization, the buffer was switched to 50 mM HEPES, pH 7.4, 150 mM NaCl, 0.05% Tween 20, 5% DMSO and primed 5X followed by equilibration at a flow rate of 75  $\mu\text{L}/\text{min}$  for at least 30 min. Serial dilutions of analytes were prepared manually (typically 5  $\mu\text{M}$  high concentration and 7 subsequent 2 or 3-fold dilutions) in a buffer that was carefully matched to the running buffer. The analyte was injected over the two flow cells at a flow rate of 75  $\mu\text{L}/\text{min}$  and at a temperature of 25  $^{\circ}\text{C}$ . The analyte-ligand complex was allowed to associate for 60 seconds and dissociate for 90 seconds (compound **3.15**) or 120 seconds (compound **3.10**). **3.15** dissociated back to baseline within the dissociation time stated above and did not require regeneration. A 12 second injection of 1M Ethanolamine, pH 8.5, at a flow rate of 75  $\mu\text{L}/\text{min}$  was used to regenerate the surface after the 120 second dissociation time of **3.10**. Each assay was preceded by priming the system, 5 buffer blanks, and 8 DMSO standards. Additionally 1 buffer blank was injected after every 4 injections of the analyte. Each analyte was tested in triplicate (from low to high concentration) with a data collection rate of 10 Hz. The data were fit to 1:1 interaction model using global data analysis with the Qdat<sup>TM</sup> analysis software package from SensiQ<sup>®</sup>. The  $K_d$  values obtained from kinetic parameters matched those obtained from an equilibrium analysis and the curves for it are presented in **Appendix B**.

#### *Isothermal Titration Calorimetry*

ITC experiments were performed in duplicate using a Nano-ITC equilibrated at 25  $^{\circ}\text{C}$ . Between experiments involving the same ligand, the sample cell was thoroughly rinsed with water followed by the final HEPES dialysis buffer. The injection apparatus was cleaned sequentially with water and methanol and dried. The sample cell was cleaned with a 0.01% SDS solution between experiments involving different ligands. Typically, after an initial injection of 0.2  $\mu\text{L}$ , 19 x 20  $\mu\text{L}$  injections of ligand were made into the sample cell. Raw data were integrated, background heats for injecting ligand into buffer were subtracted, and binding parameters were measured using the NanoAnalyze<sup>TM</sup> software.  $K_a$  and  $\Delta H^{\circ}$ .  $\Delta G^{\circ}$  was calculated indirectly from  $K_a$  by applying the modified Arrhenius equation,  $\Delta G^{\circ} = -RT\ln K_a$ .  $\Delta S^{\circ}$  was calculated by applying the Gibbs relationship  $\Delta G^{\circ} = \Delta H^{\circ} - T\Delta S^{\circ}$ .

### 3.13. References

1. Lowenstein, E. J.; Daly, R. J.; Batzer, A. G.; Li, W.; Margolis, B.; Lammers, R.; Ullrich, A.; Skolnik, E. Y.; Bar-Sagi, D.; Schlessinger, J., The SH2 and SH3 domain-containing protein GRB2 links receptor tyrosine kinases to ras signaling. *Cell* **1992**, *70* (3), 431-442.
2. Maignan, S.; Guilloteau, J. P.; Fromage, N.; Arnoux, B.; Becquart, J.; Ducruix, A., Crystal structure of the mammalian Grb2 adaptor. *Science* **1995**, *268* (5208), 291-293.
3. Okutani, T.; Okabayashi, Y.; Kido, Y.; Sugimoto, Y.; Sakaguchi, K.; Matuoka, K.; Takenawa, T.; Kasuga, M., Grb2/Ash binds directly to tyrosines 1068 and 1086 and indirectly to tyrosine 1148 of activated human epidermal growth factor receptors in intact cells. *J Biol Chem* **1994**, *269* (49), 31310-31314.
4. Egan, S. E.; Giddings, B. W.; Brooks, M. W.; Buday, L.; Sizeland, A. M.; Weinberg, R. A., Association of Sos Ras exchange protein with Grb2 is implicated in tyrosine kinase signal transduction and transformation. *Nature* **1993**, *363* (6424), 45-51.
5. Rozakis-Adcock, M.; Fernley, R.; Wade, J.; Pawson, T.; Bowtell, D., The SH2 and SH3 domains of mammalian Grb2 couple the EGF receptor to the Ras activator mSos1. *Nature* **1993**, *363* (6424), 83-85.
6. Buday, L.; Downward, J., Epidermal growth factor regulates p21ras through the formation of a complex of receptor, Grb2 adapter protein, and Sos nucleotide exchange factor. *Cell* **1993**, *73* (3), 611-620.
7. Skolnik, E. Y.; Lee, C. H.; Batzer, A.; Vicentini, L. M.; Zhou, M.; Daly, R.; Myers, M. J., Jr.; Backer, J. M.; Ullrich, A.; White, M. F.; et al., The SH2/SH3 domain-containing protein GRB2 interacts with tyrosine-phosphorylated IRS1 and Shc: implications for insulin control of ras signalling. *EMBO J* **1993**, *12* (5), 1929-1936.
8. Pendergast, A. M.; Quilliam, L. A.; Cripe, L. D.; Bassing, C. H.; Dai, Z.; Li, N.; Batzer, A.; Rabun, K. M.; Der, C. J.; Schlessinger, J.; et al., BCR-ABL-induced oncogenesis is mediated by direct interaction with the SH2 domain of the GRB-2 adaptor protein. *Cell* **1993**, *75* (1), 175-185.
9. Shah, N. P.; Skaggs, B. J.; Branford, S.; Hughes, T. P.; Nicoll, J. M.; Paquette, R. L.; Sawyers, C. L., Sequential ABL kinase inhibitor therapy selects for compound drug-resistant BCR-ABL mutations with altered oncogenic potency. *J Clin Invest* **2007**, *117* (9), 2562-2569.
10. Gibbons, D. L.; Pricl, S.; Posocco, P.; Laurini, E.; Fermeglia, M.; Sun, H.; Talpaz, M.; Donato, N.; Quintas-Cardama, A., Molecular dynamics reveal BCR-ABL1 polymutants as a unique mechanism of resistance to PAN-BCR-ABL1 kinase inhibitor therapy. *Proc Natl Acad Sci U S A* **2014**, *111* (9), 3550-3555.
11. Daly, R. J.; Binder, M. D.; Sutherland, R. L., Overexpression of the Grb2 gene in human breast cancer cell lines. *Oncogene* **1994**, *9* (9), 2723-2727.
12. Verbeek, B. S.; Adriaansen-Slot, S. S.; Rijksen, G.; Vroom, T. M., Grb2 overexpression in nuclei and cytoplasm of human breast cells: a histochemical and biochemical study of normal and neoplastic mammary tissue specimens. *J Pathol* **1997**, *183* (2), 195-203.
13. Giubellino, A.; Burke, T. R., Jr.; Bottaro, D. P., Grb2 signaling in cell motility and cancer. *Expert Opin Ther Targets* **2008**, *12* (8), 1021-1033.

14. Tari, A. M.; Arlinghaus, R.; Lopez-Berestein, G., Inhibition of Grb2 and Crkl proteins results in growth inhibition of Philadelphia chromosome positive leukemic cells. *Biochem Biophys Res Commun* **1997**, *235* (2), 383-388.
15. Tari, A. M.; Hung, M. C.; Li, K.; Lopez-Berestein, G., Growth inhibition of breast cancer cells by Grb2 downregulation is correlated with inactivation of mitogen-activated protein kinase in EGFR, but not in ErbB2, cells. *Oncogene* **1999**, *18* (6), 1325-1332.
16. Kaneko, T.; Huang, H.; Cao, X.; Li, X.; Li, C.; Voss, C.; Sidhu, S. S.; Li, S. S., Superbinder SH2 domains act as antagonists of cell signaling. *Sci Signal* **2012**, *5* (243), ra68.
17. Huang, H.; Li, L.; Wu, C.; Schibli, D.; Colwill, K.; Ma, S.; Li, C.; Roy, P.; Ho, K.; Songyang, Z.; Pawson, T.; Gao, Y.; Li, S. S., Defining the specificity space of the human SRC homology 2 domain. *Mol Cell Proteomics* **2008**, *7* (4), 768-784.
18. Songyang, Z.; Cantley, L. C., Recognition and specificity in protein tyrosine kinase-mediated signalling. *Trends Biochem Sci* **1995**, *20* (11), 470-475.
19. Kay, B. K.; Williamson, M. P.; Sudol, M., The importance of being proline: the interaction of proline-rich motifs in signaling proteins with their cognate domains. *FASEB J* **2000**, *14* (2), 231-241.
20. Viguera, A. R.; Arrondo, J. L.; Musacchio, A.; Saraste, M.; Serrano, L., Characterization of the interaction of natural proline-rich peptides with five different SH3 domains. *Biochemistry* **1994**, *33* (36), 10925-10933.
21. Gay, B.; Suarez, S.; Caravatti, G.; Furet, P.; Meyer, T.; Schoepfer, J., Selective GRB2 SH2 inhibitors as anti-Ras therapy. *Int J Cancer* **1999**, *83* (2), 235-241.
22. Furet, P.; Gay, B.; Caravatti, G.; Garcia-Echeverria, C.; Rahuel, J.; Schoepfer, J.; Fretz, H., Structure-based design and synthesis of high affinity tripeptide ligands of the Grb2-SH2 domain. *J Med Chem* **1998**, *41* (18), 3442-3449.
23. Gao, Y.; Wu, L.; Luo, J. H.; Guo, R.; Yang, D.; Zhang, Z. Y.; Burke, T. R., Jr., Examination of novel non-phosphorus-containing phosphotyrosyl mimetics against protein-tyrosine phosphatase-1B and demonstration of differential affinities toward Grb2 SH2 domains. *Bioorg Med Chem Lett* **2000**, *10* (9), 923-927.
24. Burke, T. R., Jr.; Yao, Z. J.; Gao, Y.; Wu, J. X.; Zhu, X.; Luo, J. H.; Guo, R.; Yang, D., N-terminal carboxyl and tetrazole-containing amides as adjuvants to Grb2 SH2 domain ligand binding. *Bioorg Med Chem* **2001**, *9* (6), 1439-1445.
25. Gao, Y.; Voigt, J.; Wu, J. X.; Yang, D.; Burke, T. R., Jr., Macrocyclization in the design of a conformationally constrained Grb2 SH2 domain inhibitor. *Bioorg Med Chem Lett* **2001**, *11* (14), 1889-1892.
26. Shi, Z. D.; Lee, K.; Liu, H.; Zhang, M.; Roberts, L. R.; Worthy, K. M.; Fivash, M. J.; Fisher, R. J.; Yang, D.; Burke, T. R., Jr., A novel macrocyclic tetrapeptide mimetic that exhibits low-picomolar Grb2 SH2 domain-binding affinity. *Biochem Biophys Res Commun* **2003**, *310* (2), 378-383.
27. Burke, T. R., Development of Grb2 SH2 Domain Signaling Antagonists: A Potential New Class of Antiproliferative Agents. *Int J Pept Res Ther* **2006**, *12* (1), 33-48.
28. Zhang, M.; Luo, Z.; Liu, H.; Croce, C. M.; Burke, T. R., Jr.; Bottaro, D. P., Synergistic anti-leukemic activity of imatinib in combination with a small molecule Grb2 SH2 domain binding antagonist. *Leukemia* **2014**, *28* (4), 948-951.

29. Soriano, J. V.; Liu, N.; Gao, Y.; Yao, Z. J.; Ishibashi, T.; Underhill, C.; Burke, T. R., Jr.; Bottaro, D. P., Inhibition of angiogenesis by growth factor receptor bound protein 2-Src homology 2 domain bound antagonists. *Mol Cancer Ther* **2004**, *3* (10), 1289-1299.
30. Wei, C. Q.; Gao, Y.; Lee, K.; Guo, R.; Li, B.; Zhang, M.; Yang, D.; Burke, T. R., Jr., Macrocyclization in the design of Grb2 SH2 domain-binding ligands exhibiting high potency in whole-cell systems. *J Med Chem* **2003**, *46* (2), 244-254.
31. Gao, Y.; Luo, J.; Yao, Z. J.; Guo, R.; Zou, H.; Kelley, J.; Voigt, J. H.; Yang, D.; Burke, T. R., Jr., Inhibition of Grb2 SH2 domain binding by non-phosphate-containing ligands. 2. 4-(2-Malonyl)phenylalanine as a potent phosphotyrosyl mimetic. *J Med Chem* **2000**, *43* (5), 911-920.
32. Oligino, L.; Lung, F. D.; Sastry, L.; Bigelow, J.; Cao, T.; Curran, M.; Burke, T. R., Jr.; Wang, S.; Krag, D.; Roller, P. P.; King, C. R., Nonphosphorylated peptide ligands for the Grb2 Src homology 2 domain. *J Biol Chem* **1997**, *272* (46), 29046-29052.
33. Li, P.; Zhang, M.; Peach, M. L.; Zhang, X.; Liu, H.; Nicklaus, M.; Yang, D.; Roller, P. P., Structural basis for a non-phosphorus-containing cyclic peptide binding to Grb2-SH2 domain with high affinity. *Biochem Biophys Res Commun* **2003**, *307* (4), 1038-1044.
34. Li, P.; Zhang, M.; Long, Y. Q.; Peach, M. L.; Liu, H.; Yang, D.; Nicklaus, M.; Roller, P. P., Potent Grb2-SH2 domain antagonists not relying on phosphotyrosine mimics. *Bioorg Med Chem Lett* **2003**, *13* (13), 2173-2177.
35. Shi, Y.; Zhu, C. Z.; Martin, S. F.; Ren, P., Probing the effect of conformational constraint on phosphorylated ligand binding to an SH2 domain using polarizable force field simulations. *J Phys Chem B* **2012**, *116* (5), 1716-1727.
36. Delorbe, J. E.; Clements, J. H.; Whiddon, B. B.; Martin, S. F., Thermodynamic and Structural Effects of Macrocyclization as a Constraining Method in Protein-Ligand Interactions. *ACS Med Chem Lett* **2010**, *1* (8), 448-452.
37. Dekker, F. J.; de Mol, N. J.; Fischer, M. J.; Kemmink, J.; Liskamp, R. M., Cyclic phosphopeptides for interference with Grb2 SH2 domain signal transduction prepared by ring-closing metathesis and phosphorylation. *Org Biomol Chem* **2003**, *1* (19), 3297-3303.
38. Ettmayer, P.; France, D.; Gounarides, J.; Jarosinski, M.; Martin, M. S.; Rondeau, J. M.; Sabio, M.; Topiol, S.; Weidmann, B.; Zurini, M.; Bair, K. W., Structural and conformational requirements for high-affinity binding to the SH2 domain of Grb2(1). *J Med Chem* **1999**, *42* (6), 971-980.
39. DeLorbe, J. E.; Clements, J. H.; Teresk, M. G.; Benfield, A. P.; Plake, H. R.; Millsbaugh, L. E.; Martin, S. F., Thermodynamic and structural effects of conformational constraints in protein-ligand interactions. Entropic paradox associated with ligand preorganization. *J Am Chem Soc* **2009**, *131* (46), 16758-16770.
40. Harrison, R. S.; Shepherd, N. E.; Hoang, H. N.; Ruiz-Gomez, G.; Hill, T. A.; Driver, R. W.; Desai, V. S.; Young, P. R.; Abbenante, G.; Fairlie, D. P., Downsizing human, bacterial, and viral proteins to short water-stable alpha helices that maintain biological potency. *Proc Natl Acad Sci U S A* **2010**, *107* (26), 11686-11691.
41. Udugamasooriya, G.; Saro, D.; Spaller, M. R., Bridged peptide macrocycles as ligands for PDZ domain proteins. *Org Lett* **2005**, *7* (7), 1203-1206.
42. Kaneko, T.; Huang, H.; Zhao, B.; Li, L.; Liu, H.; Voss, C. K.; Wu, C.; Schiller, M. R.; Li, S. S., Loops govern SH2 domain specificity by controlling access to binding pockets. *Sci Signal* **2010**, *3* (120), ra34.

43. Grieco, P.; Gitu, P. M.; Hruby, V. J., Preparation of 'side-chain-to-side-chain' cyclic peptides by Allyl and Alloc strategy: potential for library synthesis. *J Pept Res* **2001**, *57* (3), 250-256.
44. Burke, T. R., Jr.; Smyth, M. S.; Otaka, A.; Nomizu, M.; Roller, P. P.; Wolf, G.; Case, R.; Shoelson, S. E., Nonhydrolyzable phosphotyrosyl mimetics for the preparation of phosphatase-resistant SH2 domain inhibitors. *Biochemistry* **1994**, *33* (21), 6490-6494.
45. Li, P.; Zhang, M.; Peach, M. L.; Liu, H.; Yang, D.; Roller, P. P., Concise and enantioselective synthesis of Fmoc-Pmp(But)2-OH and design of potent Pmp-containing Grb2-SH2 domain antagonists. *Org Lett* **2003**, *5* (17), 3095-3098.
46. Burke, T. R., Jr., Design and synthesis of phosphonodifluoromethyl phenylalanine (F2Pmp): a useful phosphotyrosyl mimetic. *Curr Top Med Chem* **2006**, *6* (14), 1465-1471.
47. Yao, Z. J.; King, C. R.; Cao, T.; Kelley, J.; Milne, G. W.; Voigt, J. H.; Burke, T. R., Jr., Potent inhibition of Grb2 SH2 domain binding by non-phosphate-containing ligands. *J Med Chem* **1999**, *42* (1), 25-35.
48. Ge, J.; Wu, H.; Yao, S. Q., An unnatural amino acid that mimics phosphotyrosine. *Chem Commun (Camb)* **2010**, *46* (17), 2980-2982.
49. Clements, J. H.; DeLorbe, J. E.; Benfield, A. P.; Martin, S. F., Binding of flexible and constrained ligands to the Grb2 SH2 domain: structural effects of ligand preorganization. *Acta Crystallogr D Biol Crystallogr* **2010**, *66* (Pt 10), 1101-1115.
50. Wei, C. Q.; Li, B.; Guo, R.; Yang, D.; Burke, T. R., Jr., Development of a phosphatase-stable phosphotyrosyl mimetic suitably protected for the synthesis of high-affinity Grb2 SH2 domain-binding ligands. *Bioorg Med Chem Lett* **2002**, *12* (19), 2781-2784.



## CHAPTER IV

### Development of Substrate-Competitive Irreversible Inhibitors of Akt1

#### 4.1. Abstract

Targeting the substrate-binding site of a protein kinase offers many advantages over targeting the ATP-binding site, most significantly obtaining a higher degree of selectivity. The nature of the substrate-binding site typically requires the development of peptidic inhibitors that lack potency and suffer from poor cell permeability and stability. In this study, the challenges of developing small molecule inhibitors of the substrate-binding site, have been overcome by covalently inhibiting the target Akt1 kinase. A library of 110 fragments with electrophiles appended to them was screened against Akt1 yielding 8 hits with greater than 75% inhibition at a single screening concentration of 100  $\mu\text{M}$ . Follow-up dose-response curves confirmed 1 hit with an  $\text{IC}_{50}$  value of 9  $\mu\text{M}$ . Limited modifications of the hit resulted in compound **4.4** with an  $\text{IC}_{50}$  of 4.4  $\mu\text{M}$ . Docking studies have enabled a proposed binding mode for the molecule and set the stage for the further development of a selective substrate-competitive irreversible inhibitor of Akt1.

#### 4.2. Inhibitors Targeting the ATP-Binding Site of Kinases

518 protein kinases encoded in the human genome collectively catalyze the transfer of the  $\gamma$ -phosphate of ATP to a serine, threonine or tyrosine residue of substrate proteins or peptides. The result is the phosphorylation of up to one-third of intracellular proteins or 20,000 distinct phosphoproteins, with a remarkable degree of specificity for their substrates.<sup>1-2</sup>

Despite the high degree of complexity required for an individual protein kinase to phosphorylate only a particular substrate, all 518 protein kinases share a remarkably similar overall architecture, termed the kinase fold.<sup>3</sup> This fold is comprised of an N-lobe primarily comprised of  $\beta$ -sheets and a C-lobe made up of  $\alpha$ -helices. The common substrate for all protein kinases is ATP, which binds to a deep hydrophobic cleft formed between the N-lobe and C-lobe with high nanomolar to low micromolar potencies.<sup>4</sup> The ability of all

members of this large superfamily of proteins to bind to ATP, stems from a highly conserved ATP-binding pocket, making exquisitely selective inhibitor development challenging.

All current FDA-approved kinase inhibitors target the ATP-binding site of kinases. The spectrum of selectivity displayed by these inhibitors ranges from inhibiting 2% to over 90% of the kinome. No FDA-approved kinase inhibitor or inhibitor in clinical development that targets the ATP-binding site has demonstrated efficacy against a single kinase only.<sup>5</sup> Off-target kinase inhibition can have several undesirable consequences. The primary concern is toxicity that can impact patient compliance, and in certain cases, be life-threatening as described in the case of Ponatinib in Chapter II. Furthermore, studies by our lab, and by others, have demonstrated that inhibition of kinases that have an anti-oncogenic role could lead to increased tumor growth. c-Abl, which in its fused Bcr-Abl form is the molecular cause of Chronic Myelogenous Leukemia (CML), is anti-oncogenic in the case of breast cancer.<sup>6</sup> Most c-Src inhibitors currently in development for treating breast cancer also inhibit c-Abl with high potency and this inhibition may be counterproductive. Similarly, the off-target inhibition of wild-type Raf can lead to dimerization and paradoxical activation of downstream pathways leading to increased cell growth and proliferation.<sup>7-8</sup>

Pan-kinase inhibitors, may not be necessarily disadvantageous from a drug development standpoint, where targeting multiple kinases involved in tumorigenesis may be preferred over targeting a single kinase. Only a select group of cancers such as CML and Gastrointestinal Stromal Tumors (GIST) are driven by a single oncogenic kinase (Bcr-Abl and c-Kit, respectively). The vast majority of cancers, particularly those with high mortality rates, can escape inhibition of a single kinase through mutations in the active site of the targeted kinase, activation of surrogate kinases that can take over the activity of the targeted kinase, and the activation of multiple, redundant kinase signaling pathways. In such cases, developing inhibitors targeting multiple kinases or using cocktails of highly selective inhibitors would be preferable.<sup>9</sup> Nevertheless, identifying the appropriate kinases to be targeted for a particular cancer remains challenging and can only be achieved through the development of inhibitors with a narrow spectrum of selectivity.

Developing chemical probes to study the biological function of a particular protein kinase is particularly challenging when targeting the ATP-binding site. Even when ‘drug-like’ properties and pharmacokinetics of a small molecule are disregarded, selectivity is difficult to achieve within any particular family of protein kinases due to a high degree of sequence similarity between family members. KB-4-102, an ATP-competitive probe developed in our lab, is one of the most selective c-Src inhibitors reported to date inhibiting only 8 of 96 kinases tested.<sup>6</sup> It does, however, inhibit 3 (Lck, Fgr, Yes) of the 6 Src Family Kinases (SFKs) it was tested against with a  $K_d$  value within 10-fold of that observed for c-Src. Consequently, its use as a probe to delineate the biological function of individual SFKs is limited.

### 4.3. Inhibitors Targeting the Substrate-Binding Site of Kinases

The specificity of a protein kinase for its substrate is achieved through multiple mechanisms including differing peptide-binding sites, sub-cellular localization, and recruitment *via* additional domains of the protein kinase. The lack of conservation within the peptide-binding site offers an avenue for the development of selective inhibitors for a protein kinase. For example, Lck and c-Src mentioned above, share over 85% sequence identity within the ATP-binding site, but about a 60% sequence identity with the peptide binding site, enabling the development of inhibitors that can selectively target c-Src over Lck. Using this approach, a bi-substrate probe developed in our lab was observed to inhibit only 2 (c-Src and c-Yes) of 213 kinases tested eliminating any affinity for Lck and Fgr.<sup>10</sup>

Despite the potential for selectivity that can be gained through targeting the substrate-binding site of a kinase, over 99% of reported kinase inhibitors target the ATP-binding site. This asymmetry can be attributed to the fact that while ATP binds to a deep, well-defined, hydrophobic pocket within the kinase, a peptide or protein substrate typically binds to a shallow, open, and extended surface (**Figure 4.1**). The tractable nature of the ATP-binding site enabled the rapid development of adenosine analogs and identification of adenosine-like heterocyclic hits through high-throughput screening libraries. In comparison, the nature of the peptide-substrate binding site dictates inhibitors targeting it have a large surface area enabling them to make multiple contacts with so-called hot-spots within the binding site.<sup>11</sup> Additionally a lack of structural data – fewer than 15 kinases have

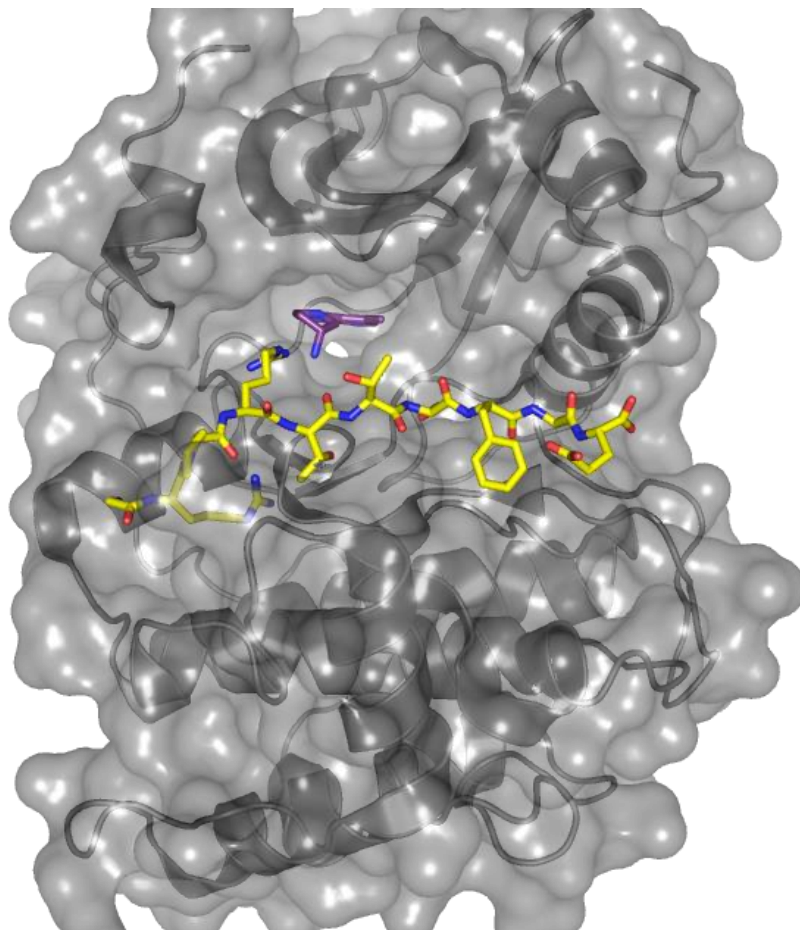


**Figure 4.1.** Surface representation of Akt1 (PDB 3MV5). An ATP-competitive inhibitor (purple) is bound in a deep hydrophobic pocket and a peptide substrate (yellow) is bound over a shallow extended interface.

been crystallized with a ligand bound to the peptide-binding site - has compounded the difficulty of developing substrate-competitive inhibitors.<sup>12</sup>

Consequently, inhibitors developed to target the substrate-binding site are typically linear peptides based on the known biological substrate, which suffer from the disadvantages of poor cell-permeability and stability, resulting in low *in cellulo* efficacy. Small molecule substrate-competitive inhibitors, which could circumvent the problems of permeability and stability, are challenging to develop due to the abovementioned nature of the substrate-binding site. When successful, small molecule substrate-competitive inhibitors can have several advantages over their ATP-competitive counterparts. In addition to the aforementioned selectivity disadvantage, ATP-competitive inhibitors

contend with high intracellular levels of ATP in the millimolar range. As a result, biochemical potency usually does not correlate well with *in cellulo* potency. Substrate-competitive inhibitors, on the other hand must contend with low micromolar levels of endogenous substrate resulting in a higher degree of correlation between biochemical and cellular efficacy. For example, SCI, a small molecule substrate-competitive c-Src inhibitor, developed in our lab, demonstrated a 3 to 20-fold selectivity for c-Src over all other SFKs and showed a cellular to biochemical efficacy ratio of 1. This was a marked improvement over an ATP-competitive c-Src inhibitor, PP2, which despite its higher potency, lacked any selectivity among SFKs and displayed a cellular to biochemical efficacy ratio of 44.<sup>4</sup>

#### **4.4. Covalent Inhibitors of Protein Kinases**

Recently, there has been a resurgence in the use of covalent inhibitors to target protein kinases. Once avoided for their purported off-target effects ascribed to their intrinsic reactivity, covalent kinase inhibitors such as Afatinib and Ibrutinib, have demonstrated good efficacy with minimal toxicity.

Covalent inhibition offers an additional selectivity filter for targeting protein kinases. Work by Frank Kwarcinski in our lab, has demonstrated that a reversible inhibitor based on a promiscuous scaffold can be converted to a selective inhibitor by strategically appending an electrophile that could react with a non-conserved cysteine on the desired enzyme.<sup>13</sup> While most such efforts have been directed towards the development of ATP-competitive inhibitors, covalent inhibition is uniquely suited for the development of substrate-competitive inhibitors. In addition to being able to leverage selectivity by targeting a non-conserved cysteine, covalently targeting the substrate-binding site could circumvent the problem of low affinity associated with substrate-competitive inhibitors. Since covalent inhibition is irreversible and time-dependent, a low affinity inhibitor could elicit the same response *in cellulo* as a high-affinity reversible ATP-competitive inhibitor.

Few kinases are observed to have a cysteine in their activation loop, which upon activation, is immediately proximal to the substrate-binding site of the kinase. One of these kinases, Akt1, has been previously targeted at the Cys310 residue of the activation loop with toxic quinone-containing antibiotics<sup>14-15</sup> and peptidomimetic inhibitors.<sup>16-17</sup> Given the importance of Akt1 in cancer cell-signaling (described in **Section 4.5**), we sought to

develop covalent substrate-competitive inhibitors using a fragment-based lead discovery (FBLD) approach.

#### 4.5. Akt1 as a Therapeutic Target in Cancer

The Akt kinases are a sub-family of the AGC family of kinases, and consist of 3 isoforms – Akt1 (PKB $\alpha$ ), Akt2 (PKB $\beta$ ), and Akt3 (PKB $\gamma$ ). All 3 isoforms have an N-terminal Pleckstrin Homology (PH) domain, a central catalytic serine/threonine kinase domain, and a C-terminal regulatory domain.<sup>18</sup> The Akt kinases form an integral part of the phosphoinositide 3-kinase (PI3K) signaling pathway, which in turn is connected to, yet distinct from, growth factor signaling pathways.

Growth factor stimulation of cells leads to the activation of growth factor receptors, membrane localization of adaptor proteins, and the activation of Ras by the exchange of GDP with GTP. Details of Ras activation through growth factor stimulation have been discussed in **Chapters I and III**. The PI3Ks are heterodimers of regulatory and catalytic subunits. On receptor activation, the regulatory subunit of PI3K can bind directly to phosphotyrosine residues on receptors or to adaptor proteins, while the catalytic subunit can bind directly to Ras. Consequently, the plasma membrane lipid, phosphatidylinositol-4,5-bisphosphate is phosphorylated to phosphatidylinositol-3,4,5-trisphosphate (PI(3,4,5)P<sub>3</sub>), by the kinase activity of PI3K.<sup>19</sup>

The Akt kinases are recruited to the membrane through the association of their PH domain with PI(3,4,5)P<sub>3</sub>. Membrane localization results in the phosphorylation and activation of Akt and is negatively regulated by the phosphatase PTEN. Activated Akt kinases have been known to phosphorylate more than 50 downstream substrates involved in a variety of cellular processes, including proliferation, survival, motility, angiogenesis, and glucose homeostasis.<sup>20</sup> Mutational loss of PTEN activity leading to constitutively activated Akt kinases have been observed in a variety of human malignancies.<sup>21-22</sup>

While there may be a large degree of overlap between the substrates of Akt kinases, the different isoforms are not believed to be redundant as certain substrates are known to be specifically phosphorylated by a particular isoform.<sup>20</sup> Akt3, which is restricted to neuronal tissue and the testes,<sup>20</sup> probably has the greatest variability in substrates owing to its tissue-specific expression. Consistent with this hypothesis, knockout of Akt3 in mice, resulted in a 20% decrease in brain size but had no role in the maintenance of carbohydrate

metabolism.<sup>23</sup> The individual roles of Akt1 and Akt2, however, have been difficult to delineate and while many cancer types have shown a dependence on both these isoforms, certain evidence suggests that they may have opposing roles in tumorigenesis within the context of particular breast cancers.<sup>24</sup>

A lack of isoform-specific inhibitors has compounded the problem of delineating the role of different isoforms. Current strategies generally rely on the use of ATP-competitive small molecules such as MKK-2206 or GSK690693 which are pan-Akt inhibitors or on gene knockouts which can result in the activation of redundant pathways. Of the three isoforms, only Akt1 has a cysteine residue in the activation loop adjacent to the substrate binding site. The development of a covalent substrate-competitive inhibitor of Akt1 could enable isoform-specificity and could be useful as a tool for the exploration of the therapeutic potential of targeting Akt kinases in cancer.

#### **4.6. Fragment Screening of an Electrophile Library**

FBLD is now widely used in both academia and industry. Over 30 current clinical candidates, including a few approved drugs, have been identified and developed through fragment-based methods.<sup>25</sup> The approach entails screening a relatively small library, members of which are typically less than 300 Da in molecular weight, against the target of interest. The small size of the fragments, generally enables the identification of weak hits with affinity values in the high micromolar to millimolar range. The low affinity hits can then be combined or grown to yield stronger hits. The fragment universe in terms of chemical space is many orders of magnitude smaller than that of molecules with a molecular weight greater than 300 Da. Thus, a library, substantially smaller than that used in traditional high throughput screening (HTS) efforts, can sample a larger proportion of chemical space resulting in a higher hit rate.<sup>26</sup> This method is particularly well suited for the identification of substrate-competitive inhibitors which would require a greater sampling of chemical diversity for the successful development of potent inhibitors.

Our target of interest, Akt1, was screened against a 110-member library of electrophilic-containing fragments using a Z'-LYTE™ activity assay and enabled the identification of covalent substrate-competitive fragments.

### *Z'-LYTE™ Activity Assay*

Fragment screening is typically accomplished through biophysical methods such as NMR and SPR. While these are powerful tools to identify weak affinity binders, they do not necessarily identify compounds that can inhibit the activity of the protein of interest. Monitoring the activity of an enzyme in the presence of fragments provides for the direct identification of inhibitors of the enzyme. In the case of kinases, activity assays can lead to the identification of both ATP-competitive as well as substrate-competitive inhibitors. This problem is particularly exacerbated in the case of HTS where the flat, heterocyclic composition of library members leads to a biased identification of ATP-competitive inhibitors.<sup>12</sup> We believed that screening our library with an ATP concentration (75  $\mu$ M) equal to that of its  $K_m$  against Akt1, coupled with the lack of a cysteine residue in the hinge binding region, would be sufficient to bias our effort to the identification of substrate-competitive inhibitors.

The commercially available Z'-LYTE™ kinase assay kit was used to screen our fragment library. The Z'-LYTE™ kinase assay is a coupled assay system, and consists of an optimized Akt1 substrate peptide which bears a coumarin-based fluorophore on one end and a fluorescein-based fluorophore on the other, which together form a FRET pair. In the primary reaction, Akt1 catalyzes the phosphorylation of a serine residue on the fluorophore-labelled substrate peptide. In the secondary reaction, the addition of a site-specific protease, cleaves the non-phosphorylated peptides, resulting in a disruption of FRET between the coumarin and fluorescein moieties. Uncleaved, phosphorylated peptides maintain their FRET signal. Fully active, uninhibited Akt1 would result in a high proportion of phosphorylated peptide with a high FRET signal. Inhibition of Akt1, would result in a higher proportion of cleaved peptides, thereby suppressing the FRET signal. A ratiometric method is used to calculate percent activity of the enzyme on inhibition.

### *Fragment Library*

A commercially available fragment library obtained from InFarmatik Inc. was used in the screen. Structures of library members are provided in **Appendix C**. The average molecular weight of the library members was 235 Da that comprised of aliphatic and aromatic anilines capped to give an acrylamide electrophile, which could be used to screen for covalent inhibitors.



### Screening Results

The library was screened at a single concentration of 100  $\mu\text{M}$ , and percent inhibition of Akt1 activity was measured after a 1 hour incubation period (**Figure 4.2**). The Z-factor, a measure of the statistical quality of an assay, was 0.62, indicating that the assay was robust with a large dynamic range and small data variability.<sup>27</sup> A mean inhibition value of 16% was obtained with a standard deviation of  $\pm 25\%$ . A cut-off value of 66% (2 standard deviations from the mean) yielded a 9% hit rate.

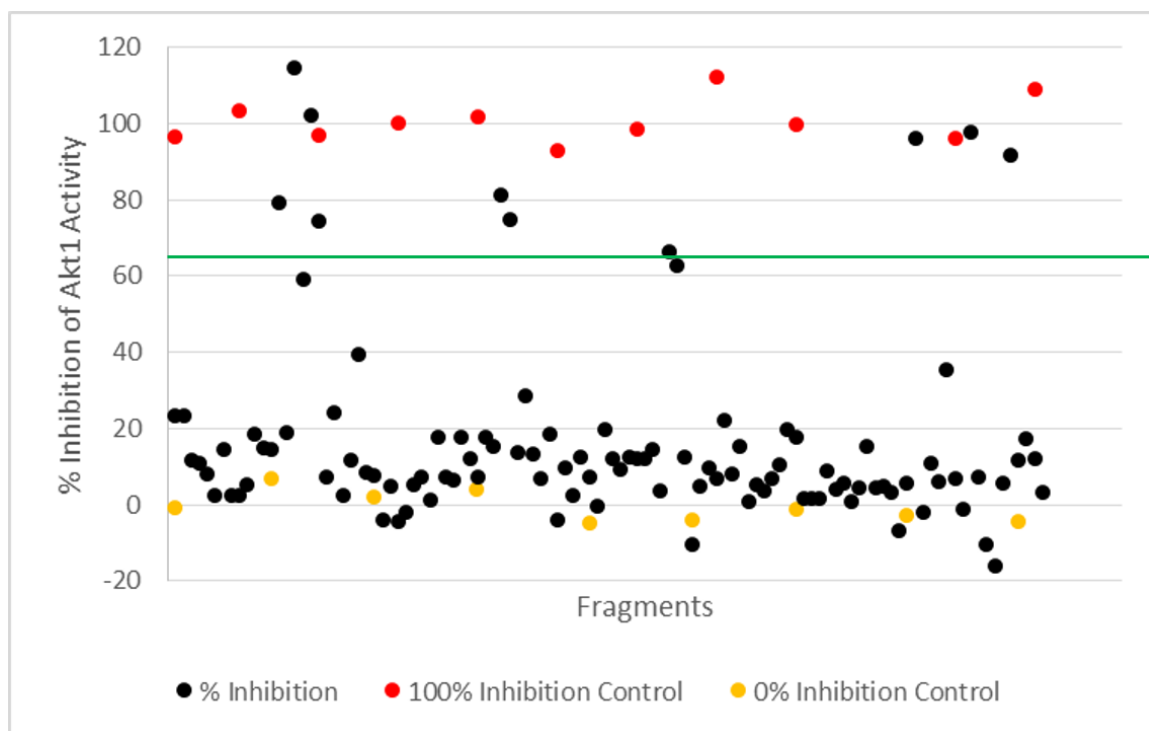


**Figure 4.2.** Fragment screening results of Akt1. The green line indicates the 66% cut-off value used to determine positive hits.

The top 10 hits obtained are shown in **Figure 4.3**. The hits obtained had certain conserved scaffolds such as indoles, furans, pyrrolidine, and cyclopentyl groups, suggesting that combining fragments would be feasible. Full dose-response curves were obtained to confirm the 10 hits and to identify inhibitors with low micromolar potencies. Only 2 compounds, EL-1119 and EL-1061, were confirmed as inhibitors of Akt1 with  $\text{IC}_{50}$  values of 9  $\mu\text{M}$  and 76  $\mu\text{M}$  respectively. Re-synthesis and re-testing of EL-1119 (subsequently labelled compound **4.1**) provided an  $\text{IC}_{50}$  value of  $9.7 \pm 3.7 \mu\text{M}$  in line with the original value obtained from a follow-up of the fragment screen. A close analog of

compound **4.1** containing a *meta*-aniline was appended with an electrophile to give compound **4.2**, but displayed a loss in potency with an  $IC_{50}$  of  $48 \pm 2\mu M$ .

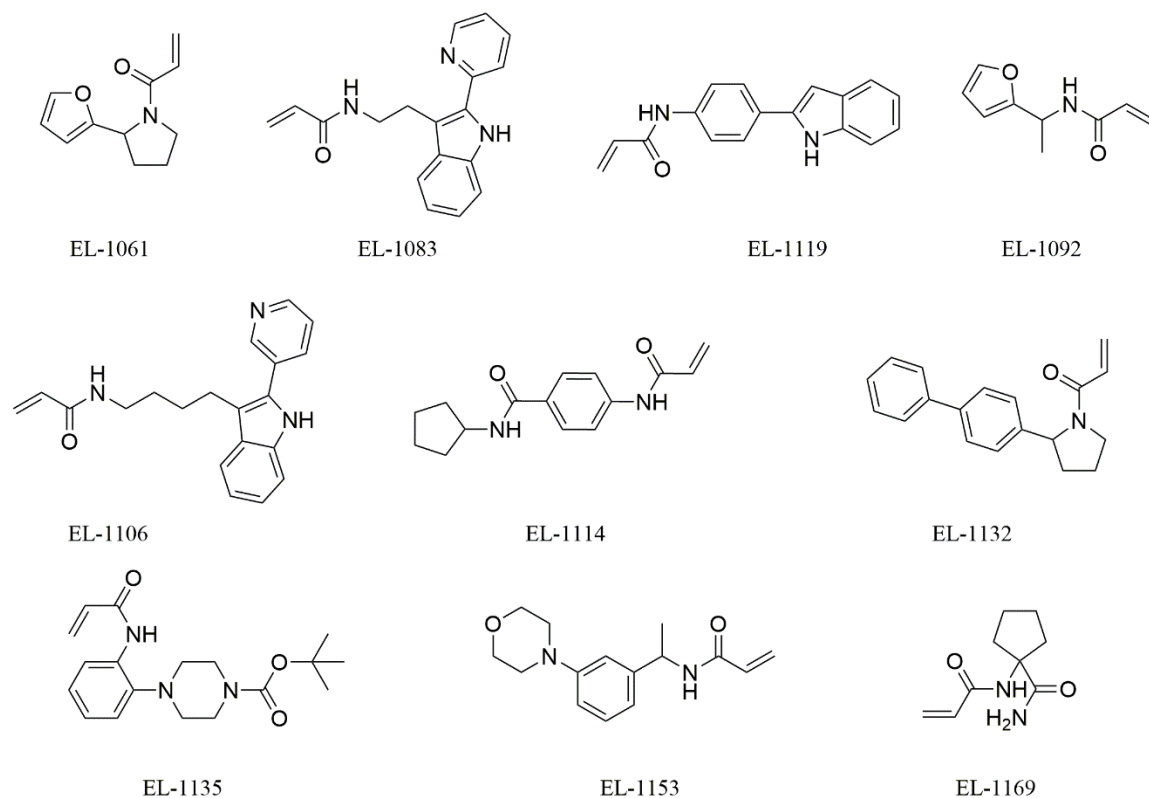


**Figure 4.3.** Top 10 hits obtained from the fragment screen

#### 4.7. Modification of the Electrophile

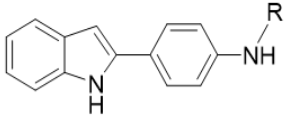
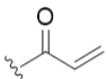
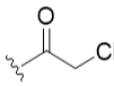
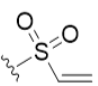
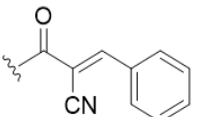
Varying the electrophilic group can have large differences on potency either due to the innate reactivity of the electrophile or due to spatial positioning of the electrophile relative to the nucleophilic cysteine on the enzyme. Two additional electrophiles, an  $\alpha$ -chloroacetamide and a vinylsulfonamide were appended in place of the acrylamide of compound **4.1**, to give compounds **4.3** and **4.4**, respectively.

The Taunton group has demonstrated the ability of  $\beta$ -aryl- $\alpha$ -cyanoacrylamide based electrophiles to reversibly and covalently bind to cysteine nucleophiles.<sup>28</sup> The reversibility of the reaction is thought to arise from the increased acidity of the  $\alpha$ -proton which can be easily de-protonated at physiological pH leading to dissociation of the cysteine adduct. While reversible covalent inhibitors do not necessarily present any biological advantage

over irreversible inhibitors, the synthetic route used to make them offers an opportunity for the late-stage introduction of chemically diverse moieties at the  $\beta$ -aryl position. To explore if diversification at the  $\beta$ -aryl position was feasible, a  $\beta$ -phenyl- $\alpha$ -cyanoacrylamide moiety was appended on to the starting fragment to give compound **4.5**.

As shown in **Table 4.1**, the  $\alpha$ -chloroacetamide containing compound **4.3** showed about a 10-fold loss in potency suggesting that the distance between the electrophilic carbon and reactive cysteine is a key determinant of potency. Compound **4.4** with a vinyl sulfonamide electrophile was found to have the greatest potency with an  $IC_{50}$  value of 4.4  $\mu$ M (a slight improvement compared to the acrylamide containing **4.1**). Lastly, the reversible covalent analog, compound **4.5**, had an  $IC_{50}$  value greater than 100  $\mu$ M suggesting that the binding site does not permit bulky groups at the  $\beta$  position of the electrophile.

**Table 4.1.**  $IC_{50}$  values obtained on varying the electrophile.

		
R =	Compound	$IC_{50}$ ( $\mu$ M)
	<b>4.1</b>	$9.7 \pm 3.7$
	<b>4.3</b>	$83 \pm 6$
	<b>4.4</b>	$4.4 \pm 0.3$
	<b>4.5</b>	$274 \pm 45$

#### 4.8. Proposed Binding Mode

In the absence of a crystal structure, to gain insight into the binding mode of the fragment, compound **4.1** was docked into the substrate site of Akt1 using an online docking server, CovalentDock Cloud. This program is built on top of the source code of the widely used Autodock, with the ability to estimate the free energy change on covalent linkage formation.<sup>29</sup> The proposed binding mode is as shown in **Figure 4.4** with a covalent bond formed with Cys310 of Akt1, and the phenylindole ring oriented away from the peptide binding site. Its close proximity to the phenylalanine of the overlaid GSK3 $\beta$  peptide could enable further growth of the fragment.

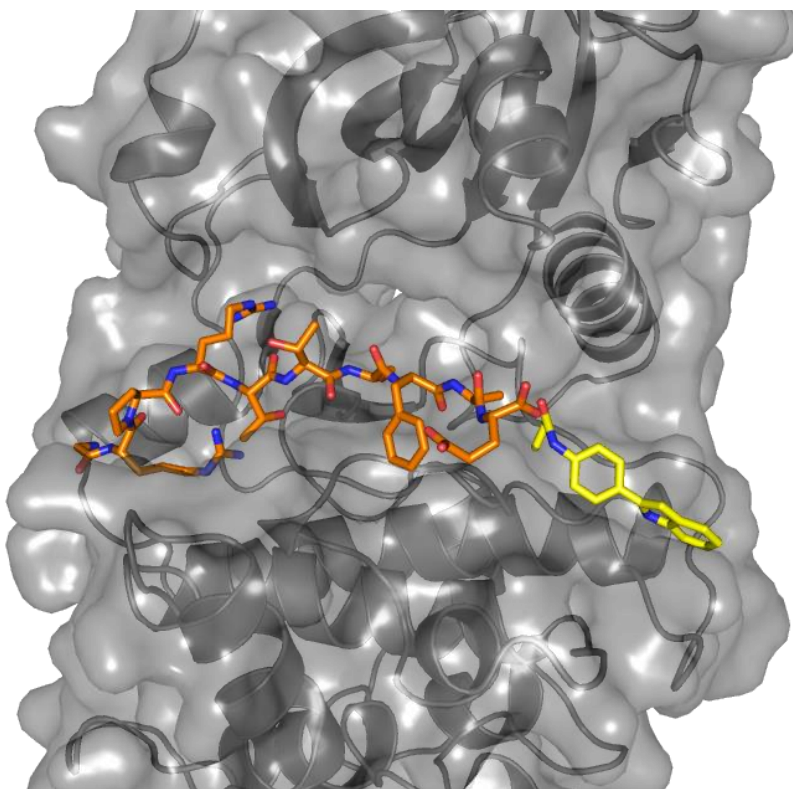


**Figure 4.4.** Proposed binding mode of compound **4.1** to Akt1

#### 4.9. Conclusions

Substrate-competitive inhibitors of protein kinases can present certain advantages over ATP-competitive inhibitors such as greater selectivity and the requirement to compete against lower levels of endogenous substrate. These type of inhibitors, however, remain drastically underexplored due to their lack of potency, screening tools, and structural information available. Covalently targeting the substrate binding site offers an attractive solution for countering issues related to poor potency of inhibitors as these show a time

dependent inactivation of the enzyme. A fragment screen of electrophile-containing fragments against the serine/threonine kinase Akt1 enabled the identification of compound **4.1** with low micromolar potency. Further modification of the electrophile led to the identification of compound **4.4** with a vinyl sulfonamide electrophile and a slight improvement in potency over **4.1**. The lack of a cysteine residue in the activation loop of Akt2 and Akt3, could make compound **4.4** uniquely suited for discerning the functional role of Akt1 within the PI3K signaling pathway.

#### **4.10. Materials and Methods**

##### *General Synthetic Methods*

Unless otherwise noted, all reagents were obtained via commercial sources and used without further purification. Dichloromethane (DCM) was dried over alumina under a nitrogen atmosphere.  $^1\text{H}$  and  $^{13}\text{C}$  NMR spectra were measured with a Varian MR400, Varian VNMRS 500, or Inova 500 spectrometer. Mass Spectrometry (HRMS) was carried out by the University of Michigan Mass Spectrometry Facility (J. Windak, director).



white solid.  $^1\text{H}$  NMR (500 MHz,  $\text{DMSO-}d_6$ )  $\delta$  11.46 – 11.42 (m, 1H), 10.25 (s, 1H), 7.81 (d,  $J = 8.4$  Hz, 2H), 7.75 (d,  $J = 8.4$  Hz, 2H), 7.49 (d,  $J = 7.9$  Hz, 1H), 7.36 (d,  $J = 8.1$  Hz, 1H), 7.09 – 7.02 (m, 1H), 6.96 (t,  $J = 7.4$  Hz, 1H), 6.81 (d,  $J = 2.1$  Hz, 1H), 6.45 (dd,  $J = 16.9, 10.1$  Hz, 1H), 6.27 (dd,  $J = 16.9, 1.9$  Hz, 1H), 5.76 (dd,  $J = 10.1, 1.9$  Hz, 1H).  $^{13}\text{C}$  NMR (126 MHz,  $\text{DMSO-}d_6$ )  $\delta$  163.57, 138.74, 137.97, 137.47, 132.25, 129.16, 127.92, 127.44, 125.91, 121.76, 120.27, 120.03, 119.75, 111.60, 98.46. HRMS-ESI ( $m/z$ ):  $[\text{M} + \text{H}]^+$  calcd for  $\text{C}_{17}\text{H}_{14}\text{N}_2\text{O}$ , 263.1179; found x.x.

Synthesis of **4.2** - 3-(1H-indol-2-yl)aniline (50 mg, 0.24 mmol) and triethylamine (35.2  $\mu\text{L}$ , 0.252 mmol) were added to DCM (2.5 ml) and the solution was cooled in an ice-water bath. Acryloyl chloride (35.2  $\mu\text{L}$ , 0.252 mmol) was then added and the reaction was monitored by TLC (50% EtOAc/Hex). Complete conversion to product was observed after 3 h at which point 0.5 ml methanol was added to quench excess acryloyl chloride. The solvents were removed *in vacuo* and the crude product was purified using reverse-phase (C18) column chromatography on a Biotage Isolera One system (linear gradient 30% MeCN/ $\text{H}_2\text{O}$   $\rightarrow$  100% MeCN) to give 17.5 mg (28% yield) of compound **4.2** as a cream-white solid.  $^1\text{H}$  NMR (500 MHz,  $\text{DMSO-}d_6$ )  $\delta$  11.54 (s, 1H), 10.26 (s, 1H), 8.19 (d,  $J = 1.9$  Hz, 1H), 7.55 (t,  $J = 8.2$  Hz, 3H), 7.42 (t,  $J = 8.8$  Hz, 2H), 7.10 (t,  $J = 7.5$  Hz, 1H), 7.00 (t,  $J = 7.4$  Hz, 1H), 6.80 (d,  $J = 2.0$  Hz, 1H), 6.49 (dd,  $J = 16.9, 10.1$  Hz, 1H), 6.31 (dd,  $J = 17.0, 1.9$  Hz, 1H), 5.80 (dd,  $J = 10.1, 1.9$  Hz, 1H).  $^{13}\text{C}$  NMR (126 MHz,  $\text{DMSO-}d_6$ )  $\delta$  163.72, 139.93, 138.05, 137.62, 133.27, 132.30, 129.81, 128.99, 127.53, 122.07, 120.84, 120.54, 119.84, 119.17, 116.78, 111.86, 99.17. HRMS-ESI ( $m/z$ ):  $[\text{M} + \text{H}]^+$  calcd for  $\text{C}_{17}\text{H}_{14}\text{N}_2\text{O}$ , 263.1179; found 263.1176.

Synthesis of **4.3** - 4-(1H-indol-2-yl)aniline (150 mg, 0.72 mmol) and triethylamine (120.6  $\mu\text{L}$ , 0.864 mmol) were added to acetonitrile (7.2 ml) and the solution was cooled in an ice-water bath. Chloroacetyl chloride (68.7  $\mu\text{L}$ , 0.864 mmol) was then added and the reaction was monitored by TLC (50% EtOAc/Hex). Complete conversion to product was observed after 1.5 h at which point 70 ml water was added to give a suspension. The mixture was stirred for 10 min, filtered, and the residue dried. The crude residue was purified using reverse-phase (C18) column chromatography on a Biotage Isolera One system (linear

gradient 30% MeCN/H<sub>2</sub>O → 100% MeCN) to give 39.7 mg (19% yield) of compound **4.3** as an orange-brown solid. <sup>1</sup>H NMR (500 MHz, DMSO-*d*<sub>6</sub>) δ 11.46 (s, 1H), 10.41 (s, 1H), 7.82 (d, *J* = 8.1 Hz, 2H), 7.68 (d, *J* = 8.3 Hz, 2H), 7.49 (d, *J* = 7.8 Hz, 1H), 7.38 (d, *J* = 8.1 Hz, 1H), 7.07 (t, *J* = 7.5 Hz, 1H), 6.97 (t, *J* = 7.4 Hz, 1H), 6.81 (s, 1H), 4.28 (s, 2H). <sup>13</sup>C NMR (126 MHz, DMSO-*d*<sub>6</sub>) δ 165.08, 138.17, 137.84, 137.49, 129.15, 128.29, 125.97, 121.82, 120.32, 120.08, 119.78, 111.62, 98.59, 44.07. HRMS-ESI (*m/z*): [M + H]<sup>+</sup> calcd for C<sub>16</sub>H<sub>13</sub>ClN<sub>2</sub>O, 285.0789; found 285.0787.

Synthesis of **4.4** - 4-(1H-indol-2-yl)aniline (80 mg, 0.384 mmol) and triethylamine (64.2 μL, 0.46 mmol) were added to acetonitrile (3.8 ml) and the solution was cooled in an ice-water bath. 2-chloro-1-ethanesulfonyl chloride (48 μL, 0.46 mmol) was then added and the reaction was monitored by TLC (50% EtOAc/Hex). Complete conversion to product was observed after 1.5 h. The volatile components were removed *in vacuo* and the residue was purified using reverse-phase (C18) column chromatography on a Biotage Isolera One system (linear gradient 40% MeCN/H<sub>2</sub>O → 80% MeCN/H<sub>2</sub>O) to give 31 mg (27% yield) of compound **4.4** as an off-white solid. <sup>1</sup>H NMR (500 MHz, DMSO-*d*<sub>6</sub>) δ 11.47 – 11.42 (m, 1H), 10.13 (s, 1H), 7.82 – 7.75 (m, 2H), 7.50 (dt, *J* = 8.0, 0.9 Hz, 1H), 7.37 (dq, *J* = 8.1, 1.0 Hz, 1H), 7.25 – 7.19 (m, 2H), 7.07 (ddd, *J* = 8.2, 7.0, 1.2 Hz, 1H), 6.98 (ddd, *J* = 7.9, 7.0, 1.1 Hz, 1H), 6.87 – 6.78 (m, 2H), 6.15 (d, *J* = 16.4 Hz, 1H), 6.06 (d, *J* = 9.9 Hz, 1H). <sup>13</sup>C NMR (126 MHz, DMSO-*d*<sub>6</sub>) δ 137.71, 137.65, 137.47, 136.79, 129.11, 128.19, 128.05, 126.28, 121.80, 120.39, 120.29, 119.76, 111.61, 98.57. HRMS-ESI (*m/z*): [M + H]<sup>+</sup> calcd for C<sub>16</sub>H<sub>14</sub>N<sub>2</sub>O<sub>2</sub>S, 299.0849; found 299.0848.

Synthesis of **4.6** - 4-(1H-indol-2-yl)aniline (100 mg, 0.48 mmol) was dissolved in DMF and cooled in an ice-water bath. Cyanoacetic acid (49 mg, 0.576 mmol), N-methylmorpholine (127 μL, 1.15 mmol) and EDC.HCl (110.4 mg, 0.576 mmol) were then added to the solution and the reaction was monitored by TLC (50% EtOAc/Hex). After 3h, the reaction was diluted with 20 ml water and extracted with EtOAc (3x). The combined organic layers were washed with sat. NaHCO<sub>3</sub>, brine, dried over sodium sulfate, and evaporated *in vacuo*. The crude product was purified using reverse-phase (C18) column chromatography on a Biotage Isolera One system (linear gradient 30% MeCN/H<sub>2</sub>O →



100% MeCN) to give 48 mg (36% yield) of compound **4.6**.  $^1\text{H}$  NMR (401 MHz, DMSO- $d_6$ )  $\delta$  11.43 (d,  $J = 2.1$  Hz, 1H), 10.38 (s, 1H), 7.83 – 7.76 (m, 2H), 7.63 – 7.54 (m, 2H), 7.47 (d,  $J = 7.8$  Hz, 1H), 7.42 – 7.31 (m, 1H), 7.04 (ddd,  $J = 8.2, 7.0, 1.2$  Hz, 1H), 6.99 – 6.90 (m, 1H), 6.79 (d,  $J = 2.1$  Hz, 1H), 3.90 (s, 2H).  $^{13}\text{C}$  NMR (100 MHz, DMSO- $d_6$ )  $\delta$  161.46, 138.04, 137.78, 137.46, 129.10, 128.29, 125.98, 121.81, 120.29, 119.91, 119.76, 116.33, 111.60, 98.57, 27.23. HRMS-ESI ( $m/z$ ):  $[\text{M} + \text{H}]^+$  calcd for  $\text{C}_{17}\text{H}_{13}\text{N}_3\text{O}$ , 276.1131; found 276.1130.

Synthesis of **4.5** – Compound **4.6** (40 mg, 0.145 mmol), benzaldehyde (14.7  $\mu\text{L}$ , 0.144 mmol), and piperidine (14.2  $\mu\text{L}$ , 0.144 mmol) were added to isopropanol and the solution was heated at 60 °C and monitored by TLC (70% EtOAc/Hex). Complete conversion to product was observed after 2 h and the reaction mixture was cooled to room temperature and purified directly using reverse-phase (C18) column chromatography on a Biotage Isolera One system (linear gradient 50% MeCN/ $\text{H}_2\text{O}$   $\rightarrow$  100% MeCN) to give compound **4.5** as an orange solid.  $^1\text{H}$  NMR (500 MHz, DMSO- $d_6$ )  $\delta$  11.53 – 11.48 (m, 1H), 10.54 (s, 1H), 8.32 (s, 1H), 8.04 – 7.98 (m, 2H), 7.91 – 7.84 (m, 2H), 7.81 – 7.75 (m, 2H), 7.67 – 7.57 (m, 3H), 7.52 (d,  $J = 7.8$  Hz, 1H), 7.39 (dq,  $J = 8.3, 0.9$  Hz, 1H), 7.09 (ddd,  $J = 8.2, 7.1, 1.2$  Hz, 1H), 6.99 (ddd,  $J = 8.0, 7.0, 1.1$  Hz, 1H), 6.87 (dd,  $J = 2.2, 0.9$  Hz, 1H).  $^{13}\text{C}$  NMR (100 MHz, DMSO- $d_6$ )  $\delta$  160.92, 151.33, 137.90, 137.75, 137.50, 132.97, 132.33, 130.51, 129.75, 129.11, 128.72, 125.80, 121.89, 121.22, 120.35, 119.80, 116.63, 111.64, 107.70, 98.77. HRMS-ESI ( $m/z$ ):  $[\text{M} + \text{H}]^+$  calcd for  $\text{C}_{24}\text{H}_{17}\text{N}_3\text{O}$ , 364.1444; found 364.1444.

### *Spectral Data*

$^1\text{H}$  and  $^{13}\text{C}$  NMR Spectra for all compounds synthesized in this chapter are shown in **Appendix C**.

### *General Biochemical Methods*

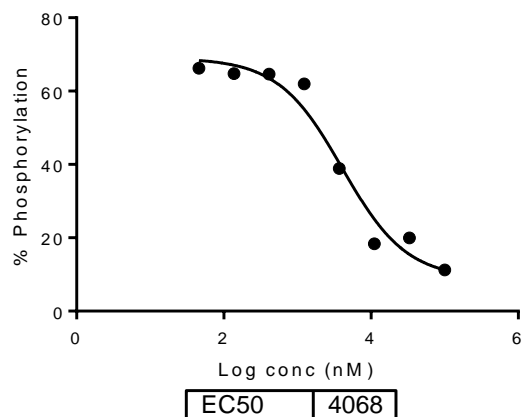
Full length Akt1 was purchased from Life Technologies<sup>TM</sup> and used according to the manufacturer's instructions. The fragment library was obtained from InFarmatik Inc., and stored as 50 mM stock solutions in DMSO at -80 °C. The Z'-LYTE<sup>TM</sup> activity assay kit was purchased from Life Technologies<sup>TM</sup> and used according to the protocol provided.

Black, low-volume Corning 384-well plates were used for the TR-FRET assay and data was obtained using a Biotek Synergy 4 plate reader. Curve fitting was performed using GraphPad Prism 4 software.

#### *Fragment Screening Protocol and Determination of IC<sub>50</sub>*

All reagents were diluted in 1.33X kinase buffer. Reaction volumes of 10  $\mu$ L were used in 384-well plates. Briefly, 2.5  $\mu$ L of the fragment stock solution (10 mM in DMSO) was added to each well followed by the addition of 5  $\mu$ L of a 2X Akt1 (20.3 nM)/peptide (4  $\mu$ M) mixture. The reactions were initiated with 2.5  $\mu$ L 4X ATP (300  $\mu$ M), mixed and incubated in the dark at room temperature for 1h. Each well had a final concentration of 10 nM Akt1, 2  $\mu$ M substrate peptide, 100  $\mu$ M inhibitor, 75  $\mu$ M ATP in 1X kinase buffer (50 mM HEPES pH 7.5, 0.01% BRIJ-35, 10 mM MgCl<sub>2</sub>, 1 mM EGTA). 5  $\mu$ L of development reagent was then added and the assay mixture was mixed and further incubated in the dark for 1 h. The reaction was terminated by the addition of a stop reagent and the FRET signal was measured using an excitation wavelength of 400 nm and emission wavelengths of 445 nm and 520 nm. The appropriate positive and negative controls were used according to the protocol provided. The emission ratio at the two wavelengths was used to calculate the percent phosphorylation. The equation  $\% \text{ Phosphorylation} = (\text{Emission Ratio} \times F_{100\%}) - C_{100\%} / (C_{0\%} - C_{100\%}) + [\text{Emission Ratio} \times (F_{100\%} - F_{0\%})]$  was used where  $C_{100\%}$  is the average coumarin emission signal of the 100% phosphorylation control,  $C_{0\%}$  is the average coumarin emission signal of the 0% phosphorylation signal,  $F_{100\%}$  is the average fluorescein emission signal of the 100% phosphorylation control, and  $F_{0\%}$  is the average fluorescein emission signal of the 0% phosphorylation control. For IC<sub>50</sub> values determination, 3-fold dilutions of compounds (typically 100, 33.3, 11.1, 3.7, 1.23, 0.41, 0.137, and 0.045  $\mu$ M) were used. The structures of the fragments in the library and all representative IC<sub>50</sub> curves are reported in **Appendix C**.

#### Representative IC<sub>50</sub> curve for compound 4.4



Avg IC<sub>50</sub> = 4.4 ± 0.3 μM

#### 4.11. References

1. Manning, G.; Whyte, D. B.; Martinez, R.; Hunter, T.; Sudarsanam, S., The protein kinase complement of the human genome. *Science* **2002**, *298* (5600), 1912-1934.
2. Johnson, S. A.; Hunter, T., Kinomics: methods for deciphering the kinome. *Nat Methods* **2005**, *2* (1), 17-25.
3. Knighton, D. R.; Zheng, J. H.; Ten Eyck, L. F.; Ashford, V. A.; Xuong, N. H.; Taylor, S. S.; Sowadski, J. M., Crystal structure of the catalytic subunit of cyclic adenosine monophosphate-dependent protein kinase. *Science* **1991**, *253* (5018), 407-414.
4. Breen, M. E.; Steffey, M. E.; Lachacz, E. J.; Kwarcinski, F. E.; Fox, C. C.; Soellner, M. B., Substrate activity screening with kinases: discovery of small-molecule substrate-competitive c-Src inhibitors. *Angew Chem Int Ed Engl* **2014**, *53* (27), 7010-7013.
5. Davis, M. I.; Hunt, J. P.; Herrgard, S.; Ciceri, P.; Wodicka, L. M.; Pallares, G.; Hocker, M.; Treiber, D. K.; Zarrinkar, P. P., Comprehensive analysis of kinase inhibitor selectivity. *Nat Biotechnol* **2011**, *29* (11), 1046-1051.
6. Brandvold, K. R.; Steffey, M. E.; Fox, C. C.; Soellner, M. B., Development of a highly selective c-Src kinase inhibitor. *ACS Chem Biol* **2012**, *7* (8), 1393-1398.
7. Carnahan, J.; Beltran, P. J.; Babij, C.; Le, Q.; Rose, M. J.; Vonderfecht, S.; Kim, J. L.; Smith, A. L.; Nagapudi, K.; Broome, M. A.; Fernando, M.; Kha, H.; Belmontes, B.; Radinsky, R.; Kendall, R.; Burgess, T. L., Selective and potent Raf inhibitors paradoxically stimulate normal cell proliferation and tumor growth. *Mol Cancer Ther* **2010**, *9* (8), 2399-2410.
8. Poulikakos, P. I.; Zhang, C.; Bollag, G.; Shokat, K. M.; Rosen, N., RAF inhibitors transactivate RAF dimers and ERK signalling in cells with wild-type BRAF. *Nature* **2010**, *464* (7287), 427-430.
9. Knight, Z. A.; Lin, H.; Shokat, K. M., Targeting the cancer kinome through polypharmacology. *Nat Rev Cancer* **2010**, *10* (2), 130-137.
10. Brandvold, K. R.; Santos, S. M.; Breen, M. E.; Lachacz, E. J.; Steffey, M. E.; Soellner, M. B., Exquisitely Specific Bisubstrate Inhibitors of c-Src Kinase. *ACS Chem Biol* **2015**.

11. Hajduk, P. J.; Huth, J. R.; Fesik, S. W., Druggability indices for protein targets derived from NMR-based screening data. *J Med Chem* **2005**, *48* (7), 2518-2525.
12. Breen, M. E.; Soellner, M. B., Small molecule substrate phosphorylation site inhibitors of protein kinases: approaches and challenges. *ACS Chem Biol* **2015**, *10* (1), 175-189.
13. Kwarcinski, F. E.; Fox, C. C.; Steffey, M. E.; Soellner, M. B., Irreversible inhibitors of c-Src kinase that target a nonconserved cysteine. *ACS Chem Biol* **2012**, *7* (11), 1910-1917.
14. Salaski, E. J.; Krishnamurthy, G.; Ding, W. D.; Yu, K.; Insaf, S. S.; Eid, C.; Shim, J.; Levin, J. I.; Tabei, K.; Toral-Barza, L.; Zhang, W. G.; McDonald, L. A.; Honores, E.; Hanna, C.; Yamashita, A.; Johnson, B.; Li, Z.; Laakso, L.; Powell, D.; Mansour, T. S., Pyranonaphthoquinone lactones: a new class of AKT selective kinase inhibitors alkylate a regulatory loop cysteine. *J Med Chem* **2009**, *52* (8), 2181-2184.
15. Toral-Barza, L.; Zhang, W. G.; Huang, X.; McDonald, L. A.; Salaski, E. J.; Barbieri, L. R.; Ding, W. D.; Krishnamurthy, G.; Hu, Y. B.; Lucas, J.; Bernan, V. S.; Cai, P.; Levin, J. I.; Mansour, T. S.; Gibbons, J. J.; Abraham, R. T.; Yu, K., Discovery of lactoquinomycin and related pyranonaphthoquinones as potent and allosteric inhibitors of AKT/PKB: mechanistic involvement of AKT catalytic activation loop cysteines. *Mol Cancer Ther* **2007**, *6* (11), 3028-3038.
16. Anjum, R.; Pae, E.; Blenis, J.; Ballif, B. A., TPCK inhibits AGC kinases by direct activation loop adduction at phenylalanine-directed cysteine residues. *FEBS Lett* **2012**, *586* (19), 3471-3476.
17. Nguyen, T.; Coover, R. A.; Verghese, J.; Moran, R. G.; Ellis, K. C., Phenylalanine-Based Inactivator of AKT Kinase: Design, Synthesis, and Biological Evaluation. *ACS Med Chem Lett* **2014**, *5* (5), 462-467.
18. Coffey, P. J.; Woodgett, J. R., Molecular cloning and characterisation of a novel putative protein-serine kinase related to the cAMP-dependent and protein kinase C families. *Eur J Biochem* **1991**, *201* (2), 475-481.
19. Cantley, L. C., The phosphoinositide 3-kinase pathway. *Science* **2002**, *296* (5573), 1655-1657.
20. Davies, M. A., Regulation, role, and targeting of Akt in cancer. *J Clin Oncol* **2011**, *29* (35), 4715-4717.
21. Vivanco, I.; Sawyers, C. L., The phosphatidylinositol 3-Kinase AKT pathway in human cancer. *Nat Rev Cancer* **2002**, *2* (7), 489-501.
22. Cantley, L. C.; Neel, B. G., New insights into tumor suppression: PTEN suppresses tumor formation by restraining the phosphoinositide 3-kinase/AKT pathway. *Proc Natl Acad Sci U S A* **1999**, *96* (8), 4240-4245.
23. Easton, R. M.; Cho, H.; Roovers, K.; Shineman, D. W.; Mizrahi, M.; Forman, M. S.; Lee, V. M.; Szabolcs, M.; de Jong, R.; Oltersdorf, T.; Ludwig, T.; Efstratiadis, A.; Birnbaum, M. J., Role for Akt3/protein kinase Bgamma in attainment of normal brain size. *Mol Cell Biol* **2005**, *25* (5), 1869-1878.
24. Irie, H. Y.; Pearline, R. V.; Grueneberg, D.; Hsia, M.; Ravichandran, P.; Kothari, N.; Natesan, S.; Brugge, J. S., Distinct roles of Akt1 and Akt2 in regulating cell migration and epithelial-mesenchymal transition. *J Cell Biol* **2005**, *171* (6), 1023-1034.

25. Erlanson, D. Fragments in the clinic: 2015 edition. <http://practicalfragments.blogspot.com/2015/01/fragments-in-clinic-2015-edition.html> (accessed 30 March, 2015).
26. Hajduk, P. J.; Greer, J., A decade of fragment-based drug design: strategic advances and lessons learned. *Nat Rev Drug Discov* **2007**, *6* (3), 211-219.
27. Zhang, J. H.; Chung, T. D.; Oldenburg, K. R., A Simple Statistical Parameter for Use in Evaluation and Validation of High Throughput Screening Assays. *J Biomol Screen* **1999**, *4* (2), 67-73.
28. Serafimova, I. M.; Pufall, M. A.; Krishnan, S.; Duda, K.; Cohen, M. S.; Maglathlin, R. L.; McFarland, J. M.; Miller, R. M.; Frodin, M.; Taunton, J., Reversible targeting of noncatalytic cysteines with chemically tuned electrophiles. *Nat Chem Biol* **2012**, *8* (5), 471-476.
29. Ouyang, X.; Zhou, S.; Su, C. T.; Ge, Z.; Li, R.; Kwoh, C. K., CovalentDock: automated covalent docking with parameterized covalent linkage energy estimation and molecular geometry constraints. *J Comput Chem* **2013**, *34* (4), 326-336.

## CHAPTER V

### Conclusions and Future Directions

#### 5.1 Abstract

Studies presented in this dissertation have focused on developing inhibitors of phospho-signaling proteins involved in cancer pathogenesis. Each chapter has conclusions detailing the lessons learned during the development of inhibitors for a particular protein in question. This chapter puts into focus these lessons at a macroscopic level and investigates whether they could be applicable elsewhere. Furthermore, it provides a roadmap that could be exploited for the development of inhibitors of other de-regulated proteins involved in cancer.

#### 5.2 Development of a Selective Inhibitor of Abl Kinase

The success of Imatinib in the treatment of CML spurred intensive research into the development of inhibitors of other kinases involved in the progression of certain cancers. Despite over a decade of research in the field, few inhibitors have proved to be as selective as Imatinib despite advances in kinase profiling technology<sup>1</sup> and a more complete understanding of the conformational plasticity of kinases.<sup>2</sup> While second and third generation inhibitors of Bcr-Abl have led to improvements in efficacy and the ability to target Imatinib-resistant CML, none of these inhibitors have a spectrum of selectivity better than or even comparable to that of Imatinib. Consequently, substantial effort has been put into understanding the reasons for the selectivity of Imatinib. The predominant model of selectivity, put forth by the Maly group<sup>3</sup>, and expanded upon by the Kern group<sup>4-5</sup>, hypothesizes that the kinked P-loop of c-Abl offers protection to Imatinib against solvent molecules. This hydrophobic shell around Imatinib prevents its solvation and increases its potency for c-Abl. Closely related kinases such as c-Src do not have a kinked P-loop resulting in an energetic penalty for solvation resulting in lower potency. This hypothesis has been substantiated, at least in part, by the development of hydrophilic inhibitors that are equipotent for c-Abl and c-Src, and through mutational and kinetic analysis of the two

enzymes.<sup>3-4</sup> No current approved drug or inhibitor in development, however, has exploited this hypothesis for the development of selective inhibitors of c-Abl.

We sought to validate the above-stated hypothesis and utilize it to develop selective inhibitors of c-Abl. Our studies have detailed the development of a series of DFG-out inhibitors with hinge-binding groups ranging from hydrophilic to highly hydrophobic. The hydrophilic hinge-binding groups led to lower levels of selectivity when comparing c-Src and c-Abl. Compound **2.3**, which bears a very hydrophobic naphthyl group, was found to be moderately potent against c-Abl ( $K_i = 155$  nM) but completely eliminated potency for c-Src ( $K_i > 27$   $\mu$ M). The fact that a hinge-region group without an H-bond donor or acceptor atom could retain potency for c-Abl validated the hypothesis that a kinked P-loop must be an important determinant for potency and selectivity for c-Abl. The addition of a single N-atom in compound **2.4**, led to a 400-fold increase in potency for c-Abl ( $K_d = 380$  pM). While compound **2.4** did lead to an increase in potency for c-Src ( $K_i = 216$  nM) too, the 570-fold difference in potency for c-Abl versus c-Src, was comparable to that of Imatinib. Furthermore, compound **2.4** unlike **2.3**, had the ability to inhibit the Y253F P-loop mutant of c-Abl resulting in it being chosen as the lead compound for further profiling and cell assays. A kinome-wide profile of compound **2.4** revealed it to be the most selective c-Abl inhibitor capable of inhibiting the T315I gatekeeper mutation known to date. Cell assays demonstrated it to be a very potent inhibitor of a variety of cell lines with minimal toxicity to healthy cells. Further *in vivo* studies of compound **2.4** are necessary and underway for establishing the utility of compound **2.4** in the treatment of CML.

### **5.3 Optimizing Entropic Gains for Developing Inhibitors of Specific Kinases**

Inhibitors are typically developed for enthalpic gains through optimization of H-bond donor and acceptor atoms. Our results indicate that counter to conventional wisdom, optimizing entropic gains by increasing the hydrophobicity of a compound seems to be a superior strategy for developing potent and selective inhibitors of c-Abl. The 400-fold increase in potency for c-Abl of **2.4** versus **2.3** corresponds to a free energy change of about -15 kJ, caused solely due to the introduction of a single N-atom. Further studies utilizing Isothermal titration calorimetry (ITC) could allow the delineation of the enthalpic and entropic components of this decrease in overall free energy. Furthermore, the molar heat

capacity change calculated through ITC could aid in the understanding of the de-solvation of each of these compounds on binding to c-Abl.

A general strategy to optimize entropic gains of a compounds has been underexplored in the development of kinase inhibitors. Such a strategy could be very useful in the development of inhibitors of other kinases with a kinked P-loop. Only 6 other kinases – Ack1, AurA, c-Met, FGFR1, MAP4K4, and p38 - have been observed to have a kinked P-loop in their X-ray crystal structures.<sup>6</sup> These kinases could be particularly well-suited for targeting with inhibitors comprising of a hydrophobic hinge-binding group. Despite crystallographic evidence being limited to these 6 kinases, it does not suggest that all other kinases have an extended P-loop. Indeed, even in the case of c-Abl, an analysis of available X-ray crystal structures showed that only 9 of 25 complexes displayed a kinked P-loop.<sup>6</sup> Comparing the results of profiling of compound **2.4** with AST-487 shows that only 3 kinases, AurC, Ax1, and LRRK2 are targets of **2.4** but not of AST-487. Given that the only significant difference between the two compounds is that **2.4** has a hydrophobic hinge binding group, it could well suggest that these kinases can potentially adopt a kinked P-loop and the strategy described above could be complementary for developing inhibitors of these kinases.

#### **5.4 N-Scan of the Core Scaffold Yields Substantial Differences in Selectivity**

Within the quinoline series of compounds, the position of the quinoline N-atom (in compound **2.5**) and replacement of the connecting O-atom with an NH-group (in compound **2.6**) leads to a dramatic loss in potency for c-Src. X-ray crystallography could be useful in determining the exact binding mode of each of these compounds and could aid in the understanding of the vast differences in selectivity. Such single-atom changes have been seldom explored in kinase inhibitors and could lead to a wide variability in selectivity while utilizing the same scaffold.

The Y253F mutant of c-Abl is believed to be resistant to Imatinib due to a partial opening of the P-loop.<sup>3</sup> Compound **2.6** shows a 10-fold loss in potency for Y253F c-Abl suggesting that its potency for c-Abl is strongly determined by the formation of a hydrophobic shell around it. It is, however, expected to bind to Lck potently like most other c-Abl inhibitors, despite the extended P-loop of Lck. A bulky group appended onto the



quinoline moiety of compound **2.6** (**Figure 5.1**) could cause a steric clash with the kinked P-loop of c-Abl, thereby preventing binding. An opening up of its P-loop to accommodate such a moiety would also result in a lower potency as is observed for compound **2.6**. However, such a bulky group could be accommodated within the extended P-loop of Lck, thus providing an avenue for developing a selective inhibitor of Lck that does not bind c-Abl or any Src-family kinase.

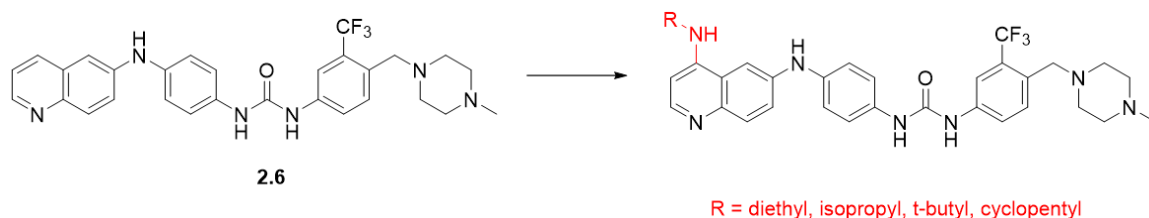


**Figure 5.1.** Potential development of Lck-selective inhibitors

### 5.5 Leveraging the Selectivity of 2.4 for Developing Irreversible Inhibitors

Comparing the selectivity profile of Imatinib to compound **2.4** in **Table 2.4**, it becomes apparent that most of the additional targets of the latter compound are due to its ability to bypass bulky gatekeeper residues. Thus, the advantage of being able to inhibit all clinically relevant mutants of c-Abl, is a slight disadvantage in terms of selectivity. Despite, a slight expansion in potent targets, compound **2.4** remains a highly selective compound kinome-wide. Consequently, its selectivity and potency can be potentially leveraged to develop the core scaffold into a potent inhibitor of one of its off-targets.

A multiple sequence alignment of the 33 high and low affinity targets of compound **2.4** reveals the distribution of residues which interact with the compound (**Figure 5.2**). The sterile kinase Lok is the only target containing a cysteine residue (corresponding to I293 in c-Abl) within the hydrophobic back-pocket of the kinase and Axl contains one just outside this pocket (corresponding to V289 in c-Abl). Modifying the type-II tail of compound **2.4** with a Michael acceptor such as an acrylamide could provide potent irreversible inhibitor of Lok and Axl. Such a strategy could not be used on currently available c-Abl scaffolds

as both these kinases possess non-threonine gatekeeper residues making selective targeting problematic.

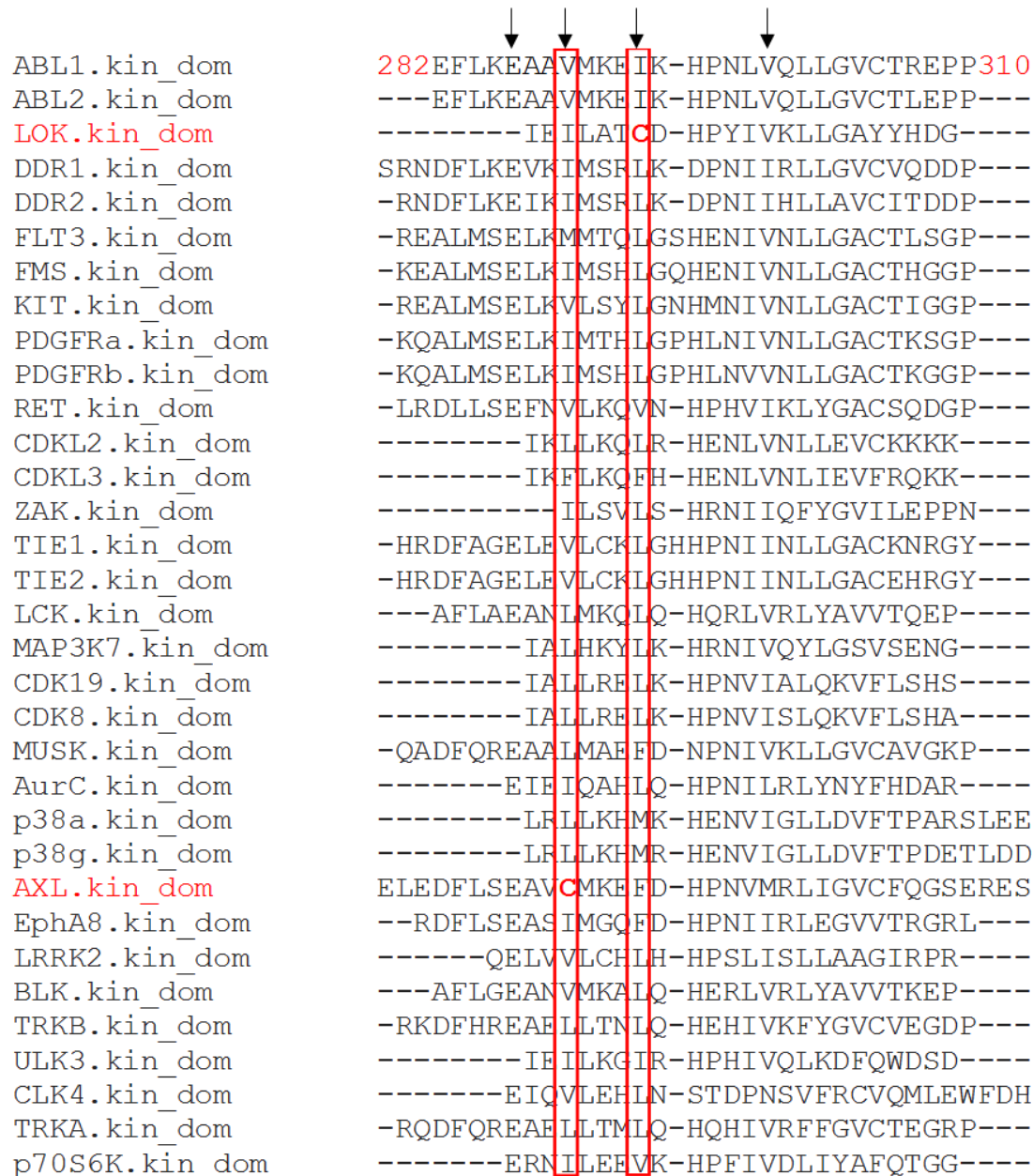


**Figure 5.2.** Multiple sequence alignment of the targets of compound **2.4**. Black arrows indicate sites of interaction with the inhibitor. The red boxes displays the distribution of residues corresponding to V289 and I293 in c-Abl.

## 5.6 Utilizing Conformational Constraint to Stabilize Turns Other than $\alpha$ -Helices

Conformational constraint has, in recent years, been used with great success for stabilizing peptides binding to a protein target in an  $\alpha$ -helical conformation. Such  $\alpha$ -helices are stabilized specifically through an  $i \rightarrow i+4$  or an  $i \rightarrow i+7$  peptide staple.<sup>7</sup> Stabilization of alternate secondary structures such as a  $\beta$  or  $\gamma$ -turn, however, has been seldom explored outside the use of unnatural amino acids to stabilize such turns. In our studies, we sought to examine the effects of macrolactamization on the binding of the consensus sequence peptide pYVNV to the SH2 domain on the adaptor protein Grb2. Through a systematic enlargement of the macrocycle we were able to obtain the optimal macrocycle size for binding to Grb2 SH2. Our lead compound **3.5**, with an  $i \rightarrow i+6$  lactam bond had an  $IC_{50}$  value of 700 nM in a fluorescence polarization assay. Replacement of the phosphotyrosine residue with a non-hydrolyzable phosphonomethyl phenylalanine in compound **3.10** led to a potent inhibitor with a  $K_d$  value of 212 nM and a  $GI_{50}$  of 19  $\mu$ M in K562 cells.

The potency of compound **3.10** is believed to be derived from lowering the entropic penalty of binding to the protein. Martin and co-workers have examined the effect of local and global conformational constraint on the binding of peptides to a number of different proteins including Grb2.<sup>8-10</sup> Extensive analysis of the enthalpic and entropic components of binding through isothermal titration calorimetry led them to the conclusion that conformational constraint does not always lower the entropic penalty of binding. They believed that constraining a peptide could lower the enthalpy of binding, which paradoxically, could increase the entropic cost of binding termed as enthalpy-entropy compensation. According to the laws of thermodynamics, however, provided that enthalpies of a constrained and unconstrained peptide are identical, conformational constraint must lower the entropic cost of binding. We believed that the effect observed by Martin and co-workers was due to the fact that they used a non-optimal macrocycle. Thus, we sought to investigate the enthalpic and entropic components of our optimized lead compound **3.10**. An ITC comparison of **3.10** with its unconstrained analog **3.16** unambiguously demonstrated that the change in enthalpies of the two compounds were identical and the increase in potency for compound **3.10** was solely driven through a lowered entropic penalty of binding.

Additionally, surface plasmon resonance studies demonstrated that the constrained and linear analogs had nearly equal  $k_{\text{on}}$  rates, but compound **3.10** had a significantly slower  $k_{\text{off}}$  suggesting that conformational constraint could be utilized to increase the residence time of a ligand.

An often overlooked advantage of peptide cyclization is that it increases stability of the compound toward cellular proteases. Incubation of the cyclic peptide **3.10** and linear peptide **3.16** with a protease such as elastase, which cuts at the C-terminal end of valine and glycine residues, could offer insight into the stability of the cyclic variant in comparison to its linear counterpart.

### **5.7 Utilizing Cyclic Peptides to Identify Inhibitors of Other SH2 Domains**

The Grb2 SH2 domain is only one of 18 SH2 domain that has a preference for an Asparagine residue in the pY+2 position. Other SH2 domains with such a preference include GRAP, GADS, GRB7/10/14, Fer/Fes, and Tensin 1/2. An Asn at pY+2 residue, however, does not guarantee binding in a  $\beta$ -turn conformation and could instead involve binding in an extended conformation.<sup>11-12</sup> Even within those SH2 domains that bind to their peptide partner with a  $\beta$ -turn, they do so through a variety of mechanisms. In the case of Grb2, GRAP, and GADS, a  $\beta$ -turn is enforced by Trp residue on the EF1 loop of the protein surface (nomenclature based on the structure of the Src SH2 domain). The Grb7 family of SH2 domains lack a Trp residue at EF1. They do, however, have a longer EF loop, the backbone of which blocks the extension of the phosphotyrosine containing peptide. Lastly, the Fes SH2 has a Thr residue on the BG loop which effectively enforces a  $\beta$ -turn similar to that enforced by Trp in Grb2.<sup>11-12</sup> The different mechanisms of enforcing a  $\beta$ -turn suggest that cyclic peptides of different sizes would be needed to inhibit each of these domains. Our library of cyclic peptides could be utilized for optimizing the macrocycle size, and further development of the optimized macrocycles could yield potent inhibitors for each of these SH2 domains. Based on our studies with the SH2 domain of Grb2, such optimized peptides would be predicted to have a lower entropic cost of binding and thus a higher potency compared to their linear analogs.

## 5.8 N-Methylation to Increase Permeability of Cyclic Peptides

Our studies were primarily directed towards using biophysical methods to develop potent inhibitors of Grb2 SH2. While our lead compound showed efficacy in a CML cell line, further development would be needed for the practical use of this peptide in cell assays. N-methylation of the backbone amide bonds is known to be an effective strategy for increasing hydrophobicity of a cyclic peptide. Additionally, N-methylation enforces the formation of intramolecular H-bonds which in turn could further increase cell permeability. The conventional means for the development of N-methylated cyclic peptides is a systematic and iterative process in which each of the amide bonds is methylated and cell permeability is determined.<sup>13</sup> Such a process is extremely cumbersome and could require the synthesis and testing of a large number of N-methyl variants of compound **3.10**.

It has been known for a decade that the temperature dependence of the chemical shift of an amide proton (as determined by variable temperature TOCSY NMR) is indicative of the hydrogen bonding of such a proton.<sup>14</sup> Cierpack et al. determined that amide protons in a protein with a chemical shift temperature coefficient ( $\Delta\delta/\Delta T$ ) of  $<-4.6$  ppb/K are typically water-exposed, while those that are  $\geq -4.6$  ppb/K are involved in intramolecular H-bonds.<sup>14</sup> A recent report demonstrated the utility of this information in the development of N-methylated cyclic peptides.<sup>15</sup> Amides with a chemical shift temperature coefficient of  $<-4.6$  ppb/K were methylated leading to N-methylated cyclic peptides with a substantial increase in cell permeability and bioavailability.<sup>15</sup> Such a process could be utilized for N-methylation of compound **3.10** and could be useful in increasing the cell permeability of the compound through a minimally iterative process.

## 5.9 Substrate Competitive Irreversible Inhibitors of Akt1

Our studies involved developing irreversible inhibitors of Akt1 that bind to the substrate binding site of the enzyme. These inhibitors were identified through a fragment screen and optimized by changing the electrophile. The most potent inhibitor **4.4** with an  $IC_{50}$  value of 4.4  $\mu M$  could be useful in a cellular context despite its micromolar potency due to its irreversible nature and through competition with low levels of endogenous substrate. Akt1 is not the only kinase containing a surface-exposed cysteine residue near the substrate binding pocket. Other kinases such as AurC, CAMK4, and MELK

contain a similarly placed cysteine residue and the methods described in this dissertation could be generally applicable to any of these kinases.<sup>16</sup>

The assay described in the development of compound **4.4** is an end-point assay and cannot be used to measure initial rates of binding thus precluding the availability of valuable kinetic data. A continuous fluorescence quenching assay for Akt1 as described by Imperiali group<sup>17</sup> could circumvent this problem and could be used to measure time dependent IC<sub>50</sub> values of compounds **4.1-4.5** and could thus be used to measure the rate of inactivation ( $k_{\text{inact}}$ ) of each of these compounds.

## **5.10 Conclusions**

In almost half a decade since the ‘war on cancer’ was declared, substantial progress has been made in developing safe and effective therapies for specific cancers. The research leading up to these developments has led to an increased understanding of the molecular causes and incredible complexity of signaling pathways involved in cancer. This understanding has been coupled with the realization that the treatment of different cancers would require targeted therapy towards a variety of proteins involved in oncogenesis. The studies presented in this dissertation have highlighted the difficulties and challenges in developing inhibitors of phospho-signaling proteins involved in cancer. Each of the proteins have been targeted through different methodologies involving a variety of rationales as dictated by the nature of the binding site. In addition to a rationale for developing potent inhibitors for c-Abl, Grb2, and Akt1, the work presented in this dissertation provides a primer could be generally applicable for developing inhibitors of several other kinases and SH2-domain containing proteins.

## 5.11 References

1. Davis, M. I.; Hunt, J. P.; Herrgard, S.; Ciceri, P.; Wodicka, L. M.; Pallares, G.; Hocker, M.; Treiber, D. K.; Zarrinkar, P. P., Comprehensive analysis of kinase inhibitor selectivity. *Nat Biotechnol* **2011**, *29* (11), 1046-1051.
2. Huse, M.; Kuriyan, J., The conformational plasticity of protein kinases. *Cell* **2002**, *109* (3), 275-282.
3. Seeliger, M. A.; Ranjitkar, P.; Kasap, C.; Shan, Y.; Shaw, D. E.; Shah, N. P.; Kuriyan, J.; Maly, D. J., Equally potent inhibition of c-Src and Abl by compounds that recognize inactive kinase conformations. *Cancer Res* **2009**, *69* (6), 2384-2392.
4. Agafonov, R. V.; Wilson, C.; Otten, R.; Buosi, V.; Kern, D., Energetic dissection of Gleevec's selectivity toward human tyrosine kinases. *Nat Struct Mol Biol* **2014**, *21* (10), 848-853.
5. Wilson, C.; Agafonov, R. V.; Hoemberger, M.; Kutter, S.; Zorba, A.; Halpin, J.; Buosi, V.; Otten, R.; Waterman, D.; Theobald, D. L.; Kern, D., Kinase dynamics. Using ancient protein kinases to unravel a modern cancer drug's mechanism. *Science* **2015**, *347* (6224), 882-886.
6. Guimaraes, C. R.; Rai, B. K.; Munchhof, M. J.; Liu, S.; Wang, J.; Bhattacharya, S. K.; Buckbinder, L., Understanding the impact of the P-loop conformation on kinase selectivity. *J Chem Inf Model* **2011**, *51* (6), 1199-1204.
7. Lau, Y. H.; de Andrade, P.; Wu, Y.; Spring, D. R., Peptide stapling techniques based on different macrocyclisation chemistries. *Chem Soc Rev* **2015**, *44* (1), 91-102.
8. DeLorbe, J. E.; Clements, J. H.; Teresk, M. G.; Benfield, A. P.; Plake, H. R.; Millsbaugh, L. E.; Martin, S. F., Thermodynamic and structural effects of conformational constraints in protein-ligand interactions. Entropic paradox associated with ligand preorganization. *J Am Chem Soc* **2009**, *131* (46), 16758-16770.
9. Delorbe, J. E.; Clements, J. H.; Whiddon, B. B.; Martin, S. F., Thermodynamic and Structural Effects of Macrocyclization as a Constraining Method in Protein-Ligand Interactions. *ACS Med Chem Lett* **2010**, *1* (8), 448-452.
10. Clements, J. H.; DeLorbe, J. E.; Benfield, A. P.; Martin, S. F., Binding of flexible and constrained ligands to the Grb2 SH2 domain: structural effects of ligand preorganization. *Acta Crystallogr D Biol Crystallogr* **2010**, *66* (Pt 10), 1101-1115.
11. Huang, H.; Li, L.; Wu, C.; Schibli, D.; Colwill, K.; Ma, S.; Li, C.; Roy, P.; Ho, K.; Songyang, Z.; Pawson, T.; Gao, Y.; Li, S. S., Defining the specificity space of the human SRC homology 2 domain. *Mol Cell Proteomics* **2008**, *7* (4), 768-784.
12. Kaneko, T.; Huang, H.; Zhao, B.; Li, L.; Liu, H.; Voss, C. K.; Wu, C.; Schiller, M. R.; Li, S. S., Loops govern SH2 domain specificity by controlling access to binding pockets. *Sci Signal* **2010**, *3* (120), ra34.
13. Chatterjee, J.; Laufer, B.; Kessler, H., Synthesis of N-methylated cyclic peptides. *Nat Protoc* **2012**, *7* (3), 432-444.
14. Cierpicki, T.; Otlewski, J., Amide proton temperature coefficients as hydrogen bond indicators in proteins. *J Biomol NMR* **2001**, *21* (3), 249-261.
15. Wang, C. K.; Northfield, S. E.; Colless, B.; Chaousis, S.; Hamernig, I.; Lohman, R. J.; Nielsen, D. S.; Schroeder, C. I.; Liras, S.; Price, D. A.; Fairlie, D. P.; Craik, D. J., Rational design and synthesis of an orally bioavailable peptide guided by NMR amide temperature coefficients. *Proc Natl Acad Sci U S A* **2014**, *111* (49), 17504-17509.

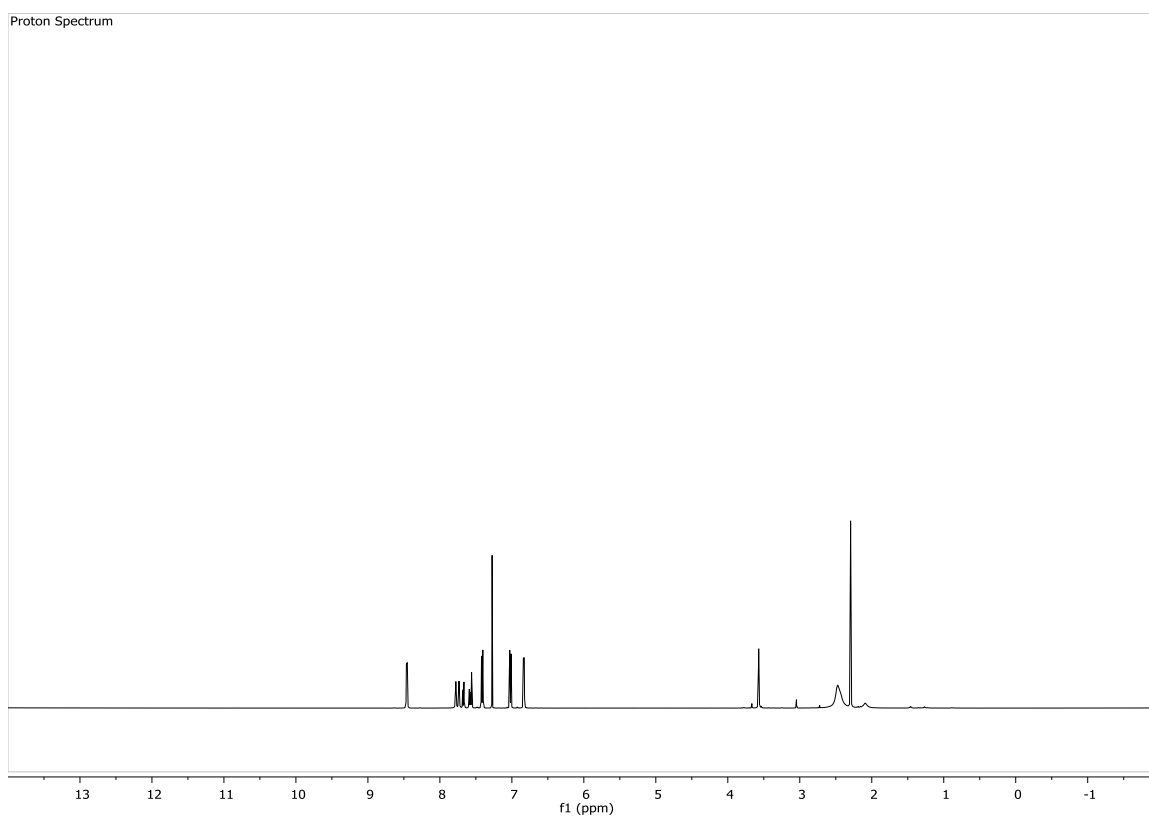
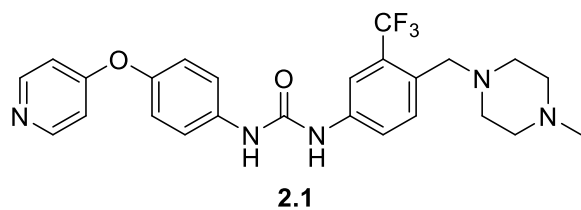
16. Nguyen, T.; Coover, R. A.; Verghese, J.; Moran, R. G.; Ellis, K. C., Phenylalanine-Based Inactivator of AKT Kinase: Design, Synthesis, and Biological Evaluation. *ACS Med Chem Lett* **2014**, *5* (5), 462-467.
17. Lukovic, E.; Gonzalez-Vera, J. A.; Imperiali, B., Recognition-domain focused chemosensors: versatile and efficient reporters of protein kinase activity. *J Am Chem Soc* **2008**, *130* (38), 12821-12827.

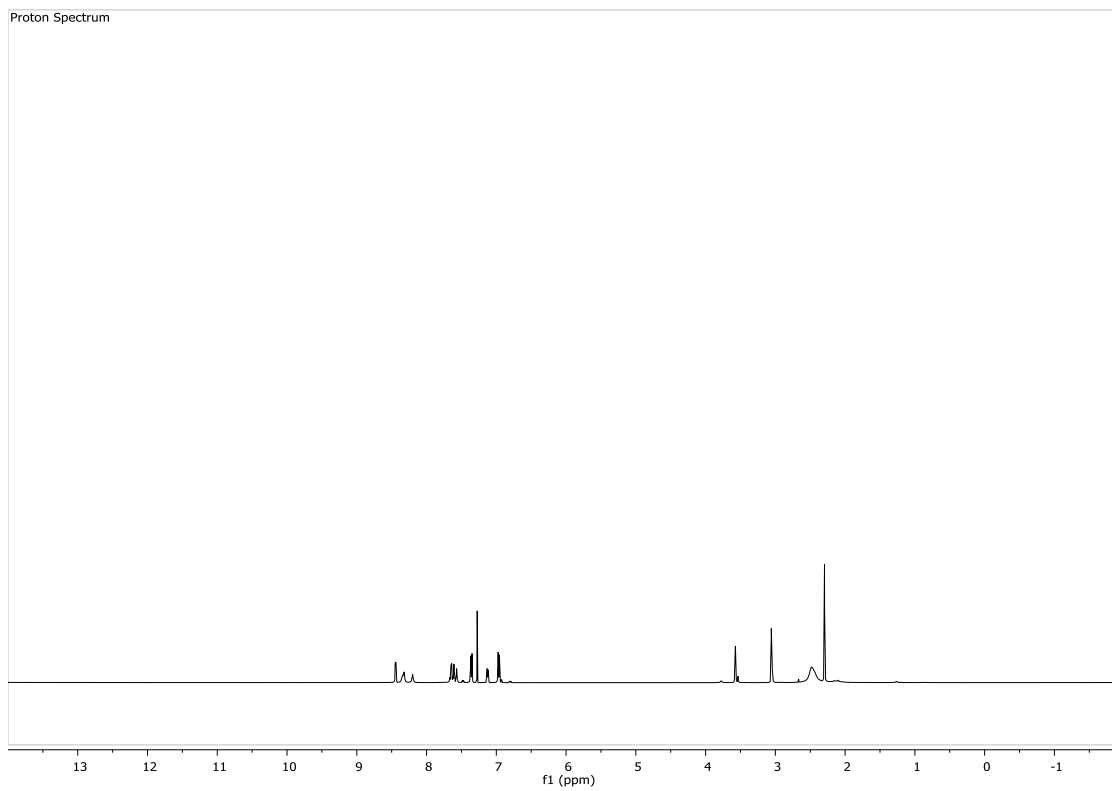
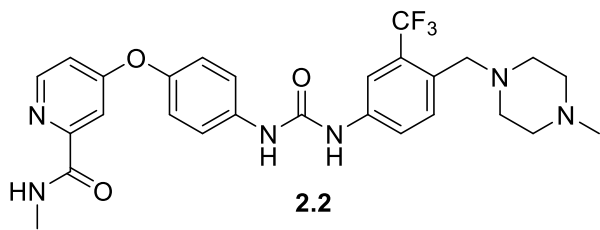


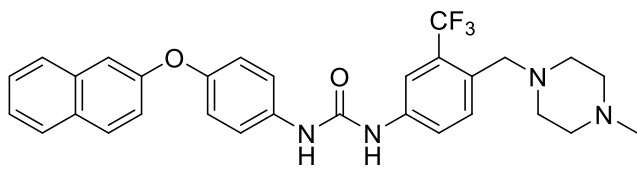
## **APPENDIX A**

### **Analytical Data and Supplemental Information for Chapter II**

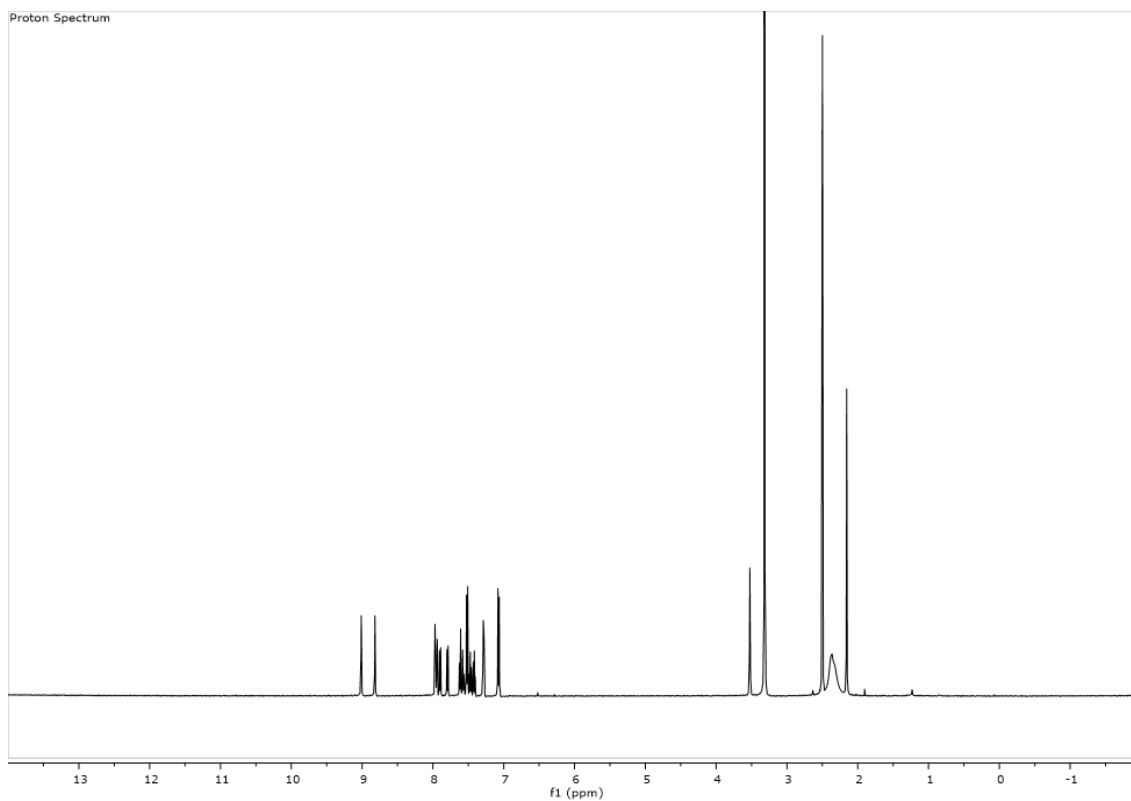
## A.1. Spectral Data for Compounds 2.1-2.25

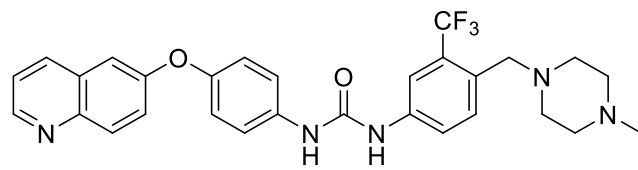




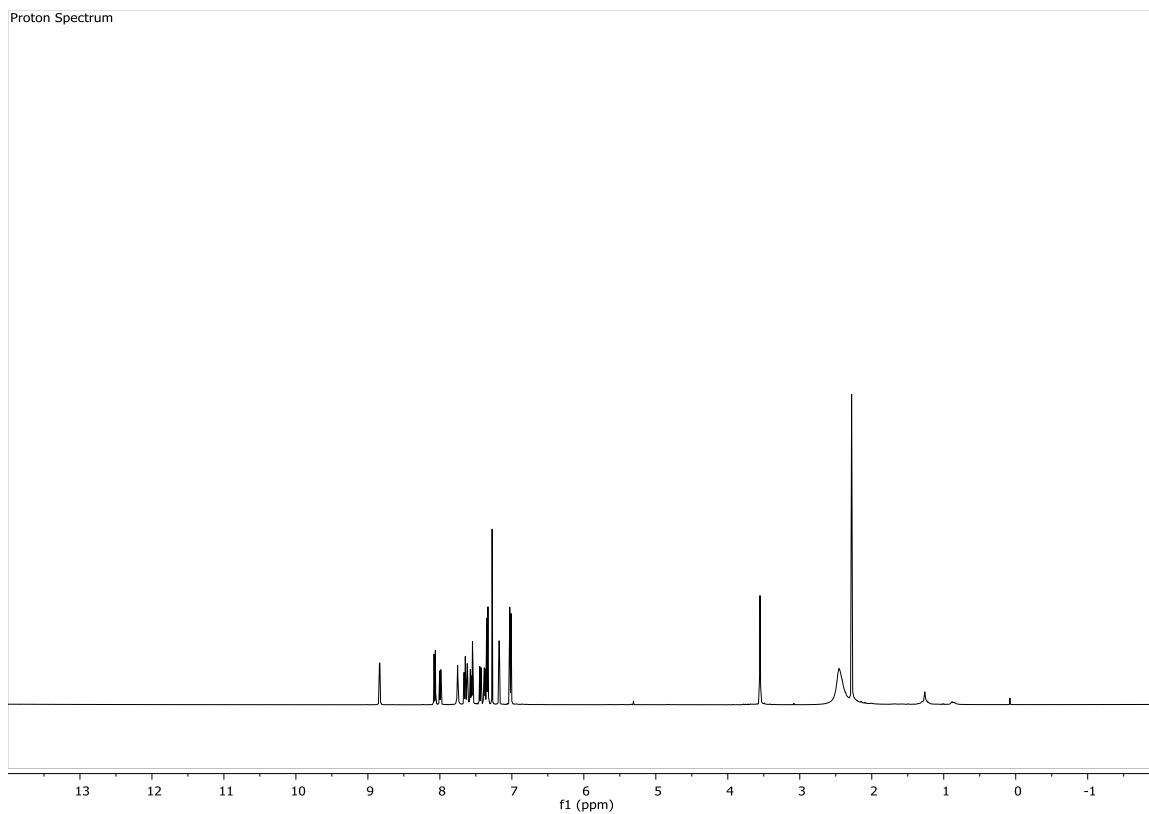


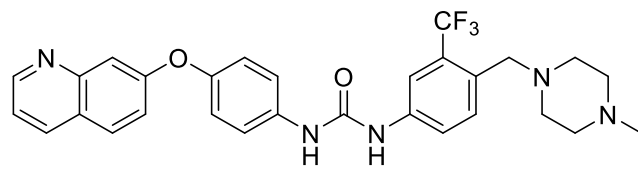
2.3



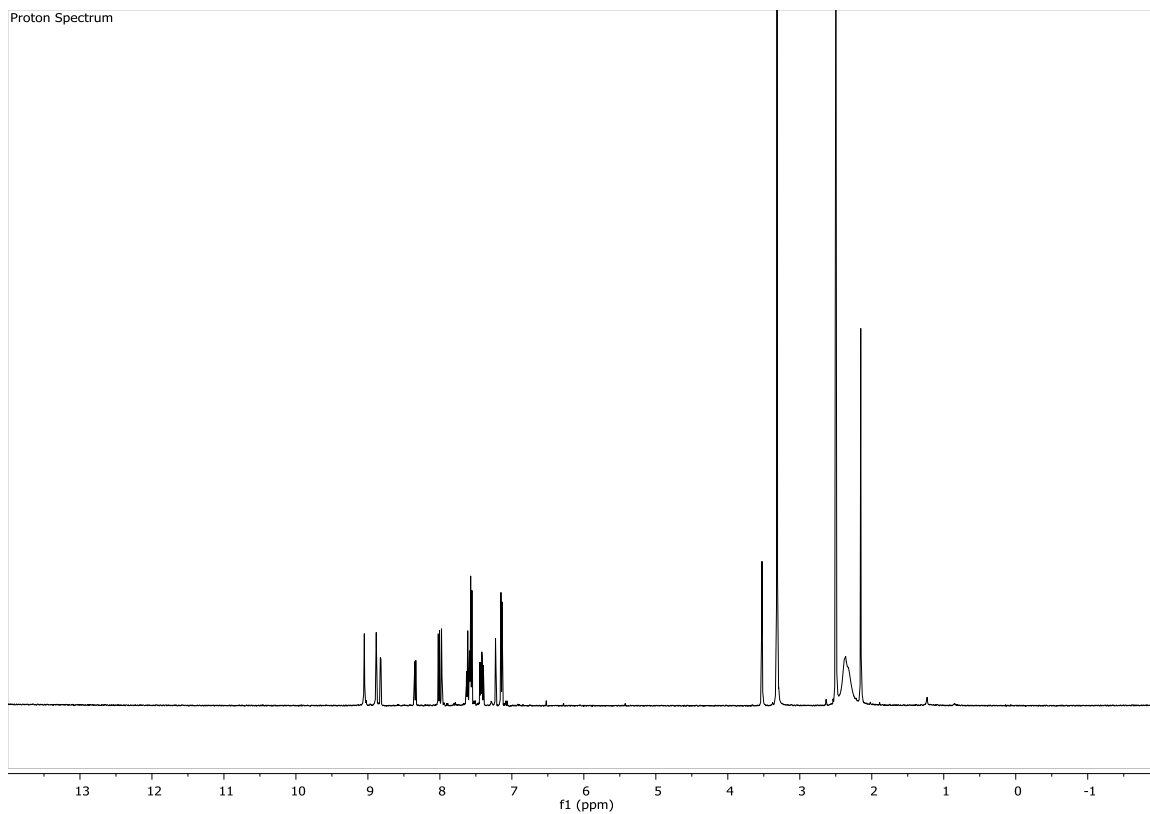


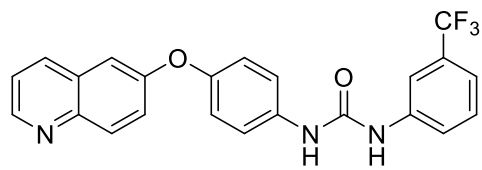
2.4



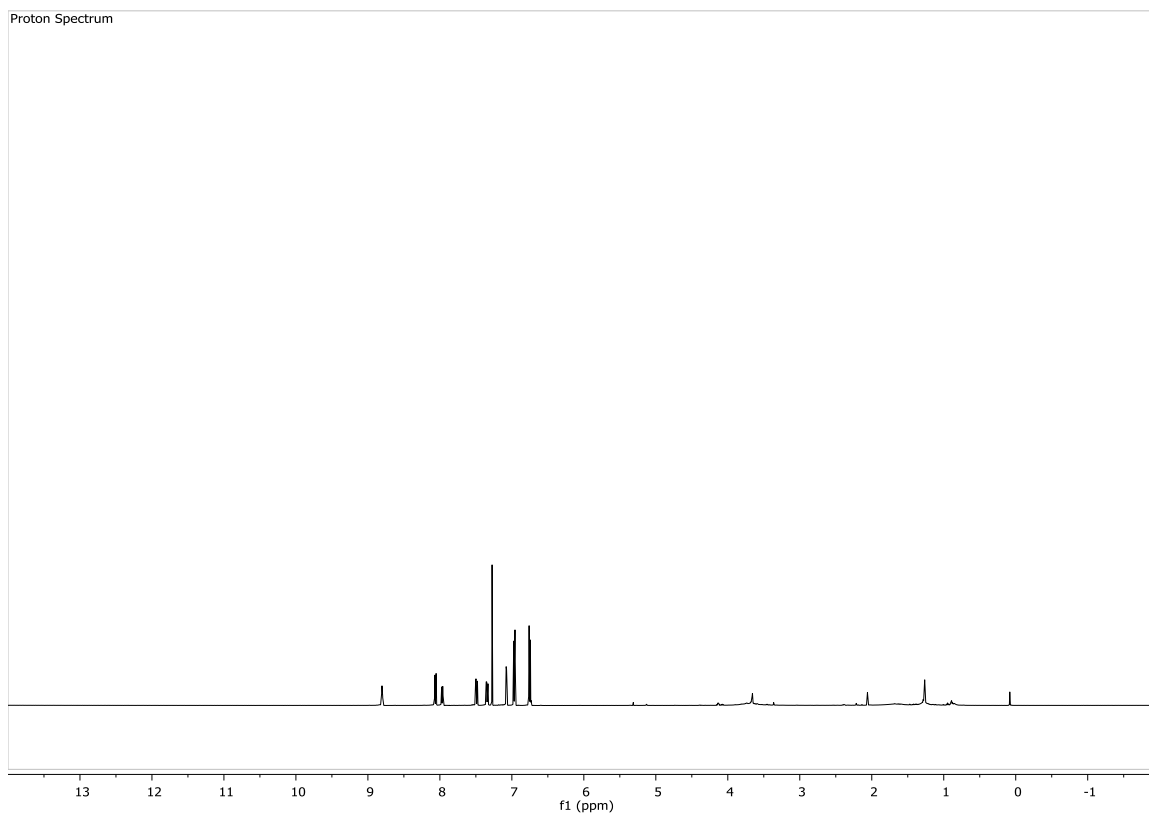


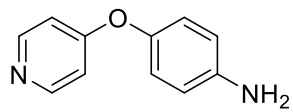
2.5



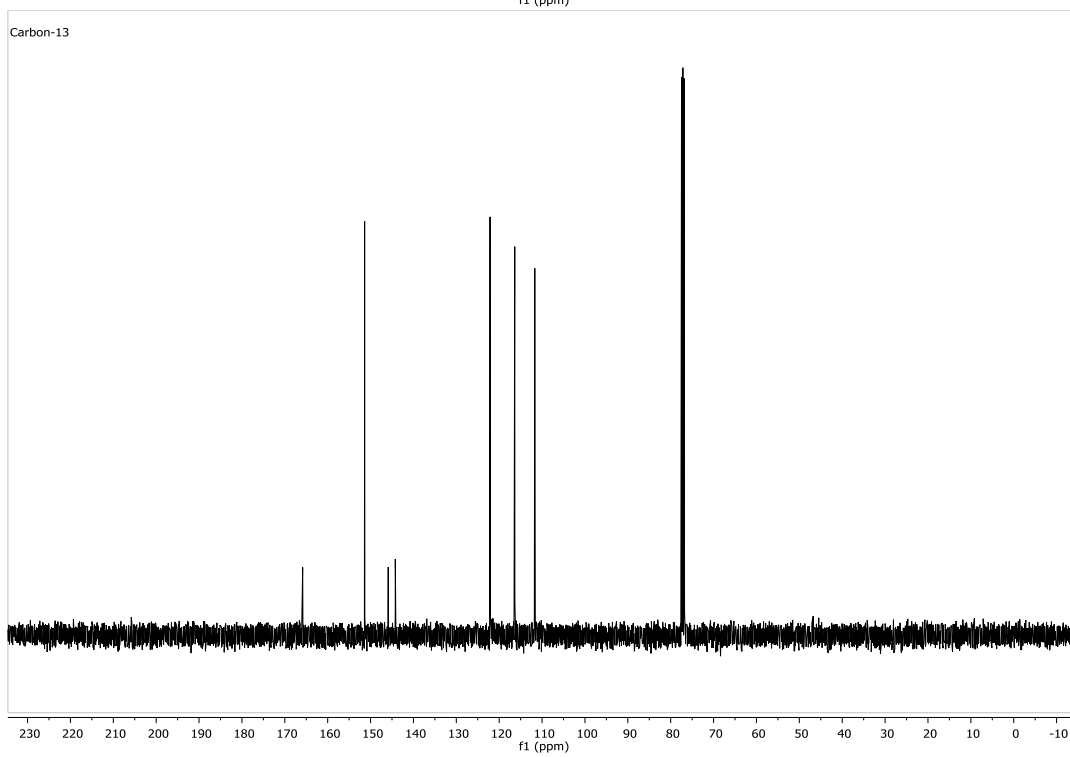
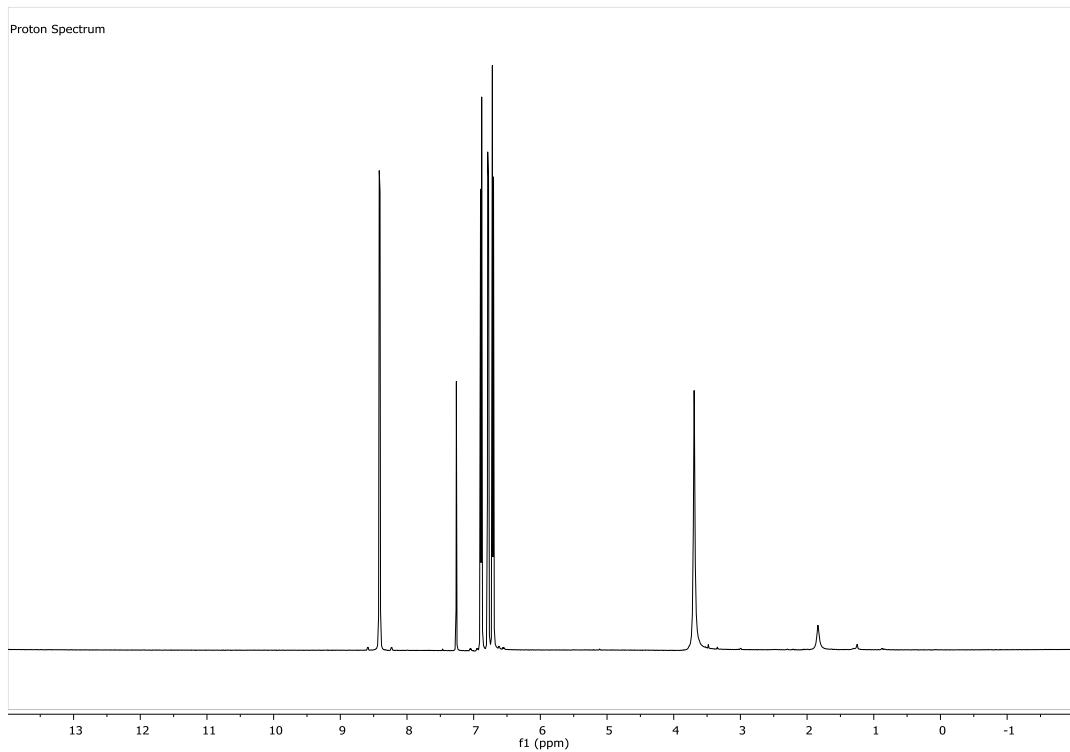


2.7

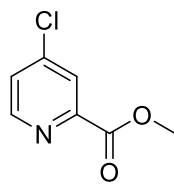




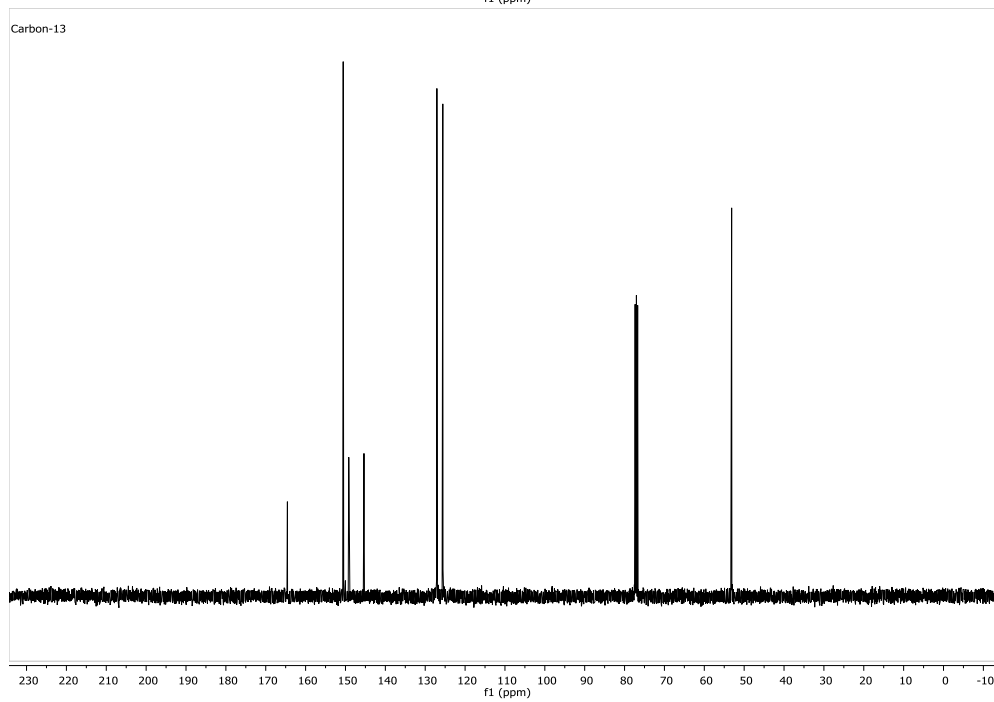
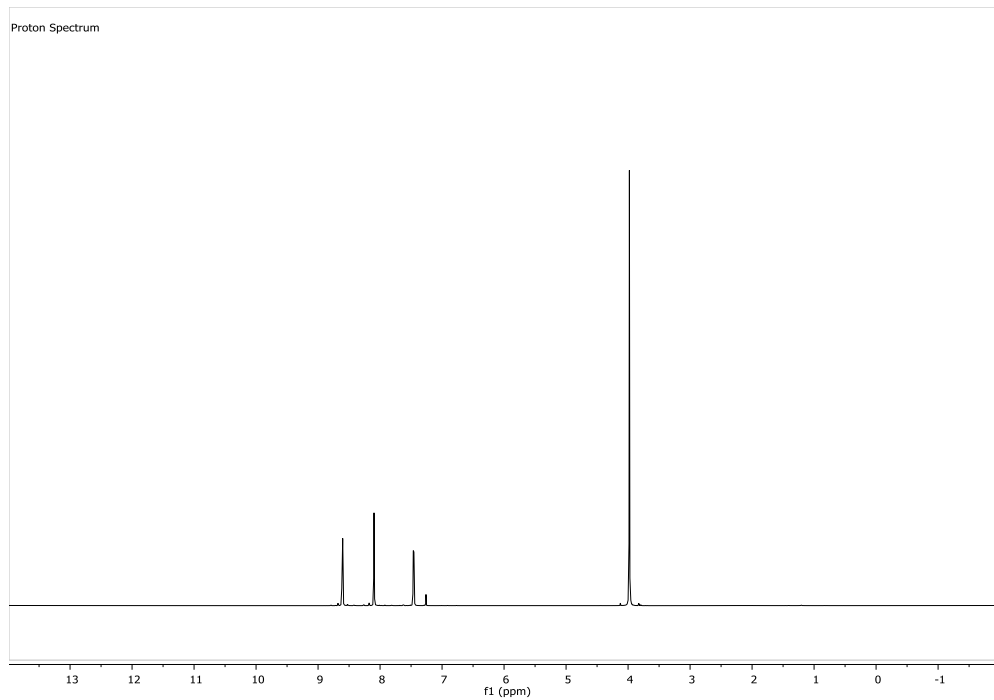
2.11

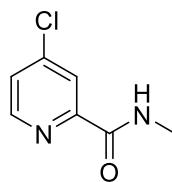




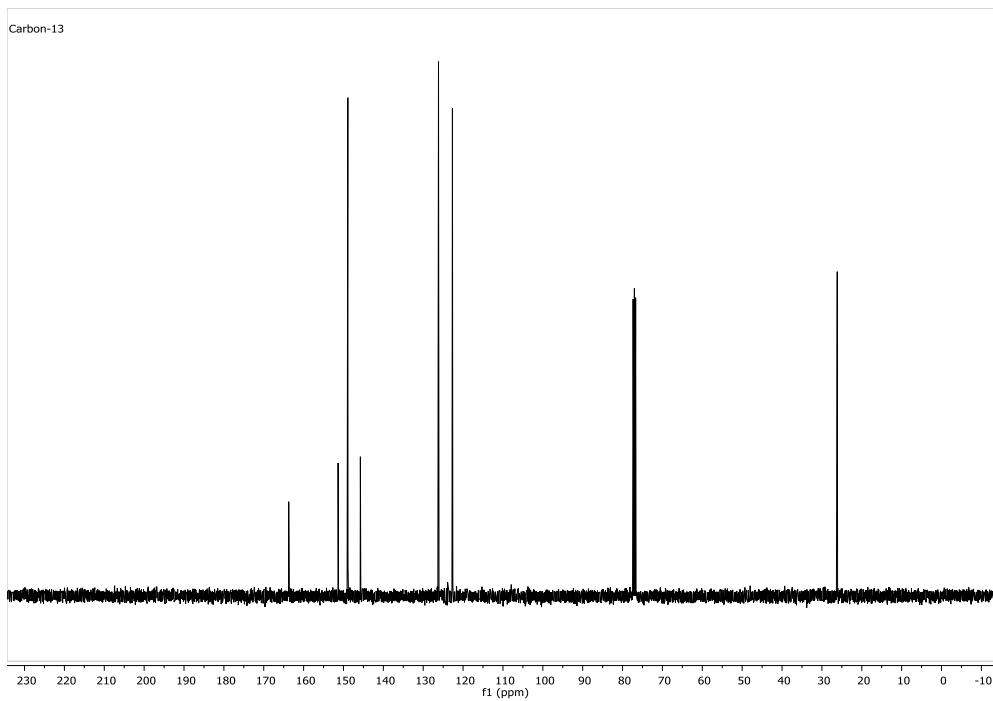
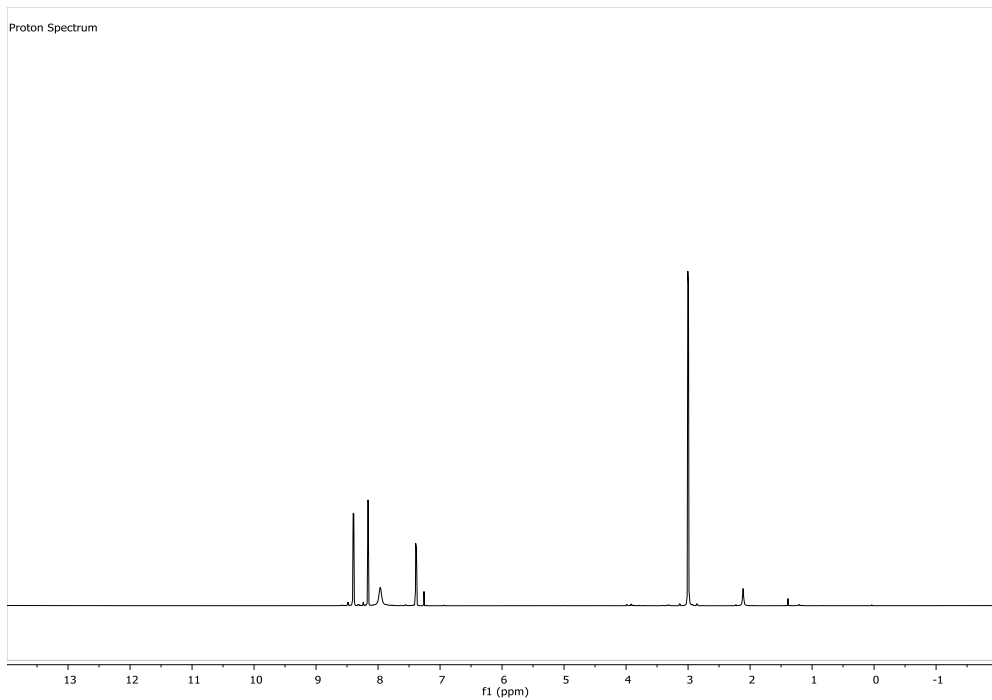


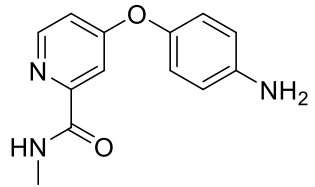
2.12



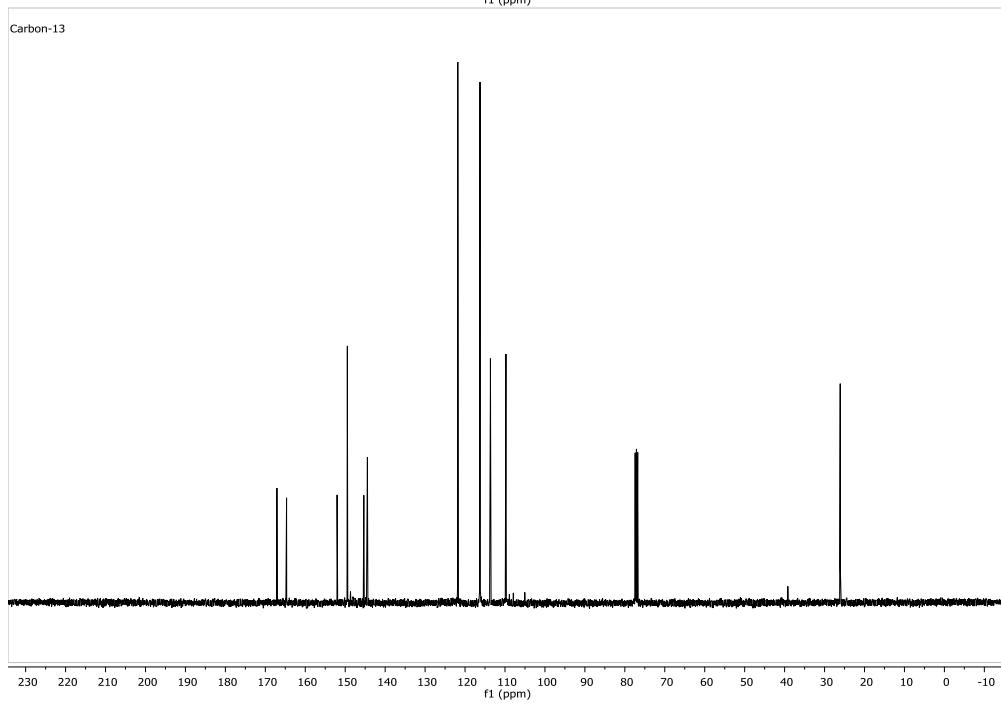
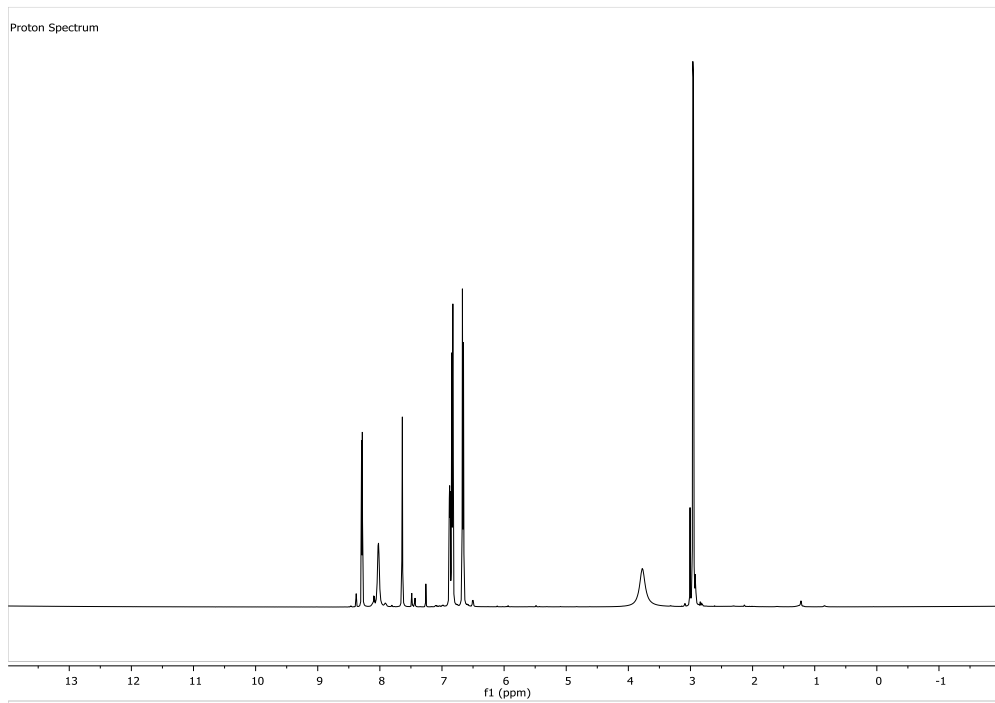


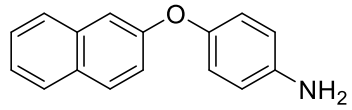
2.13



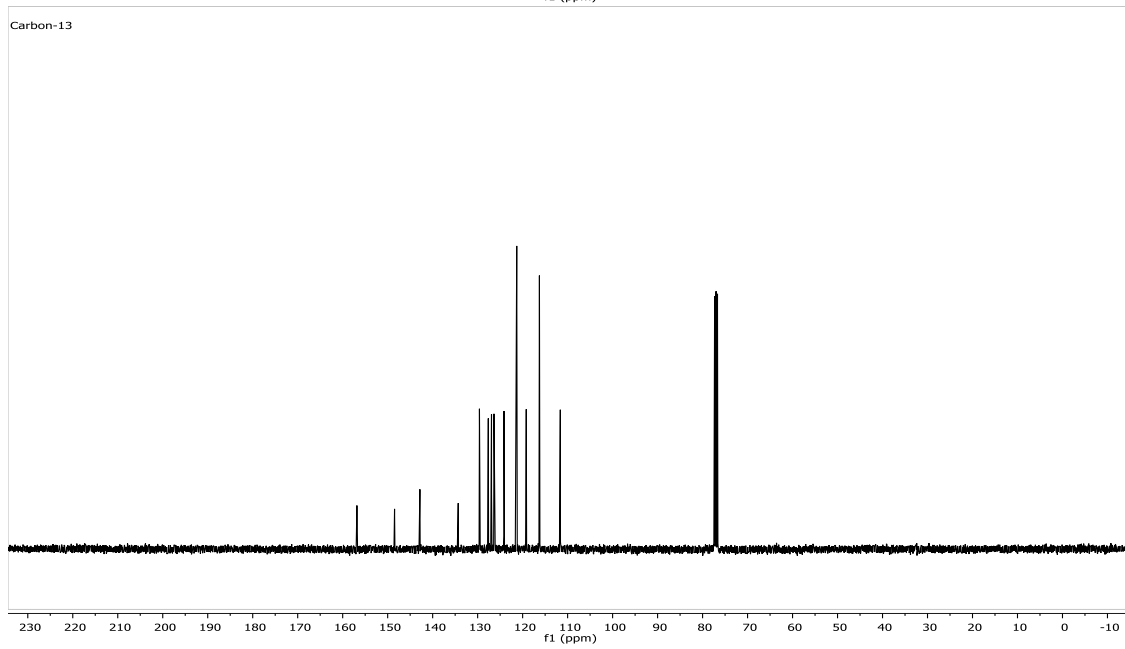
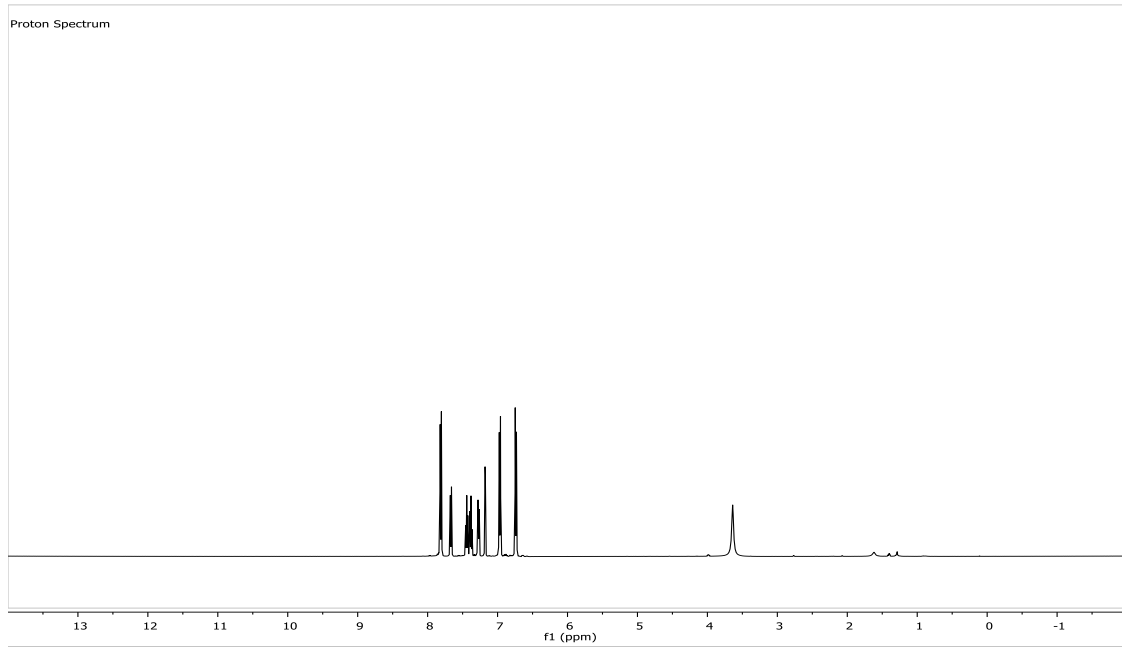


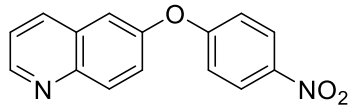
2.14





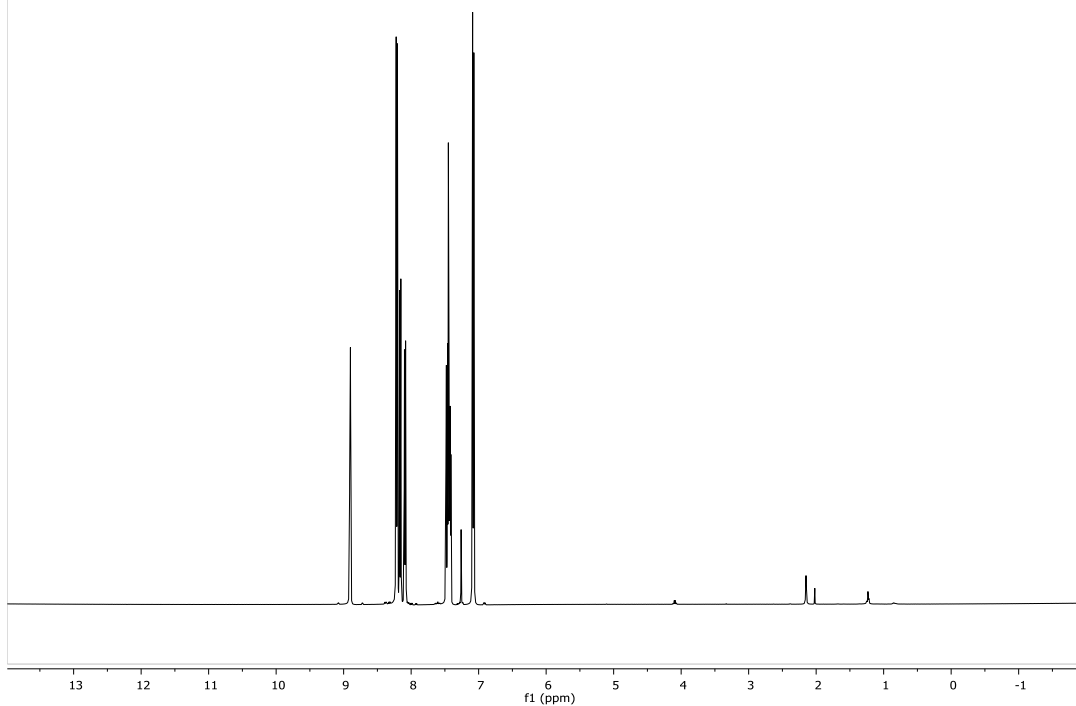
2.16



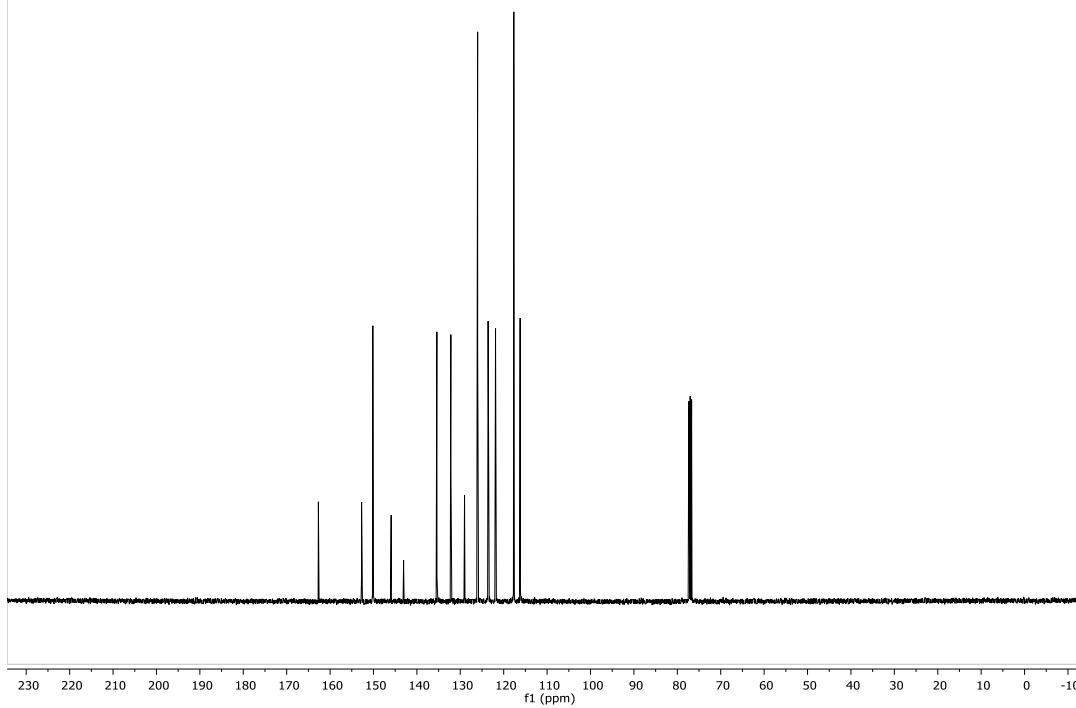


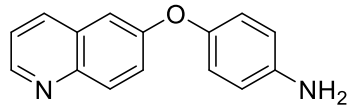
2.17

Proton Spectrum

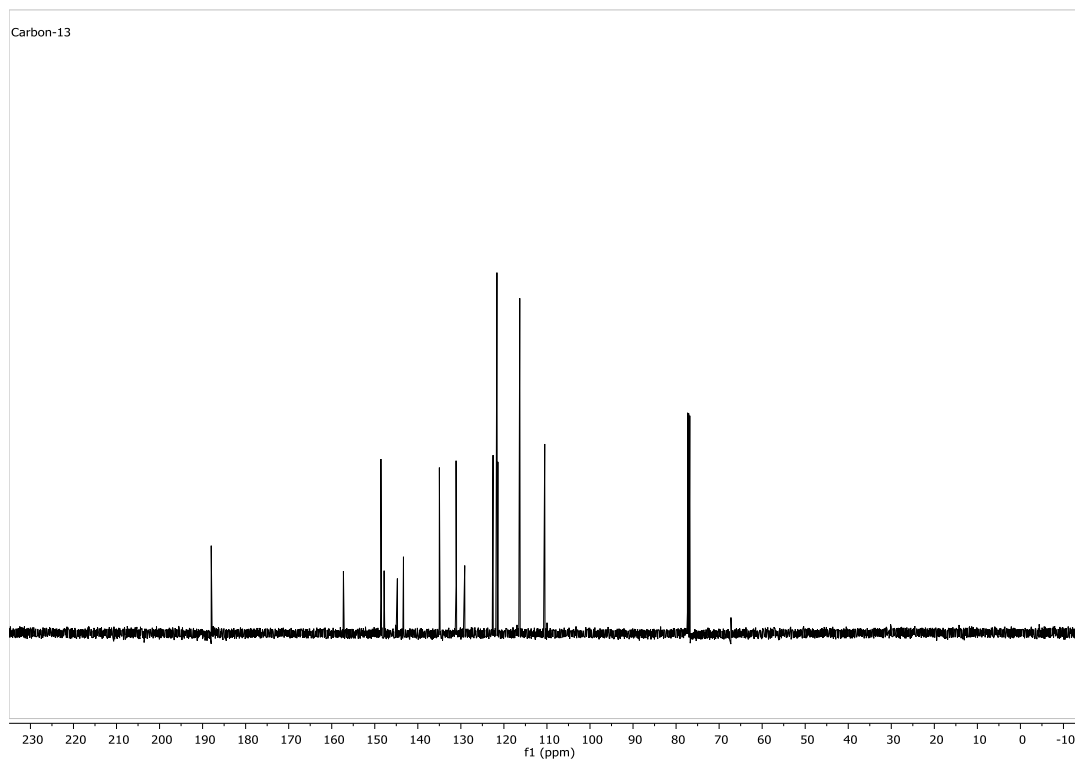
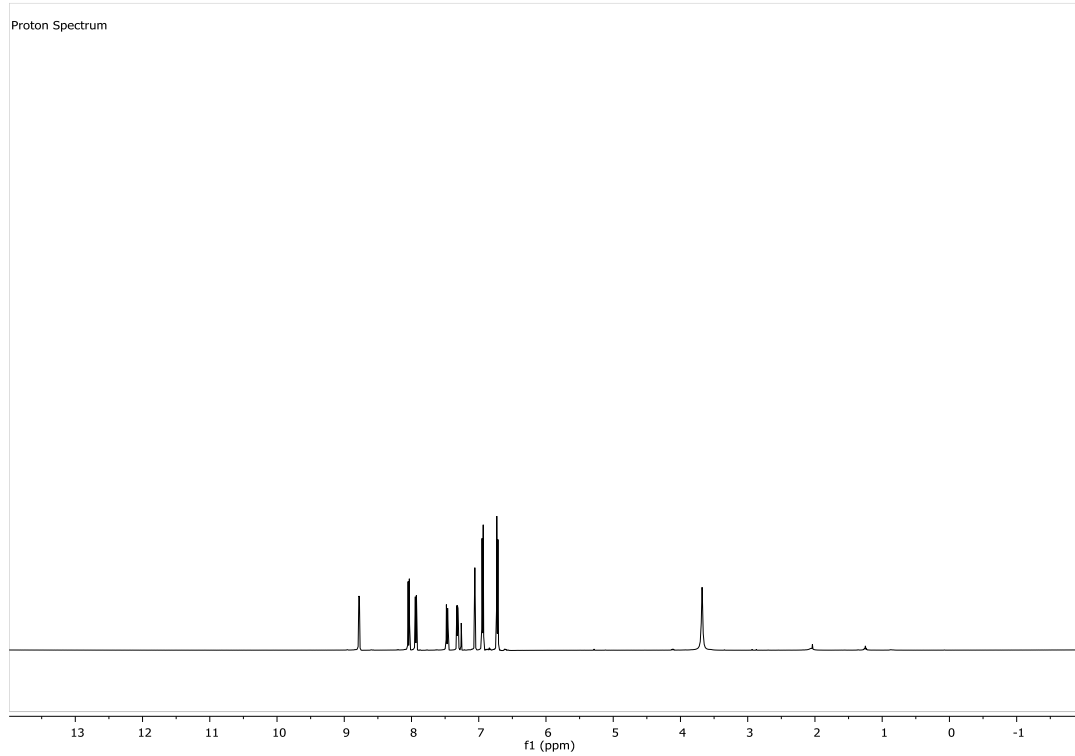


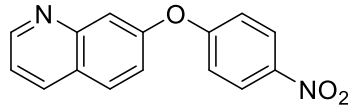
Carbon-13



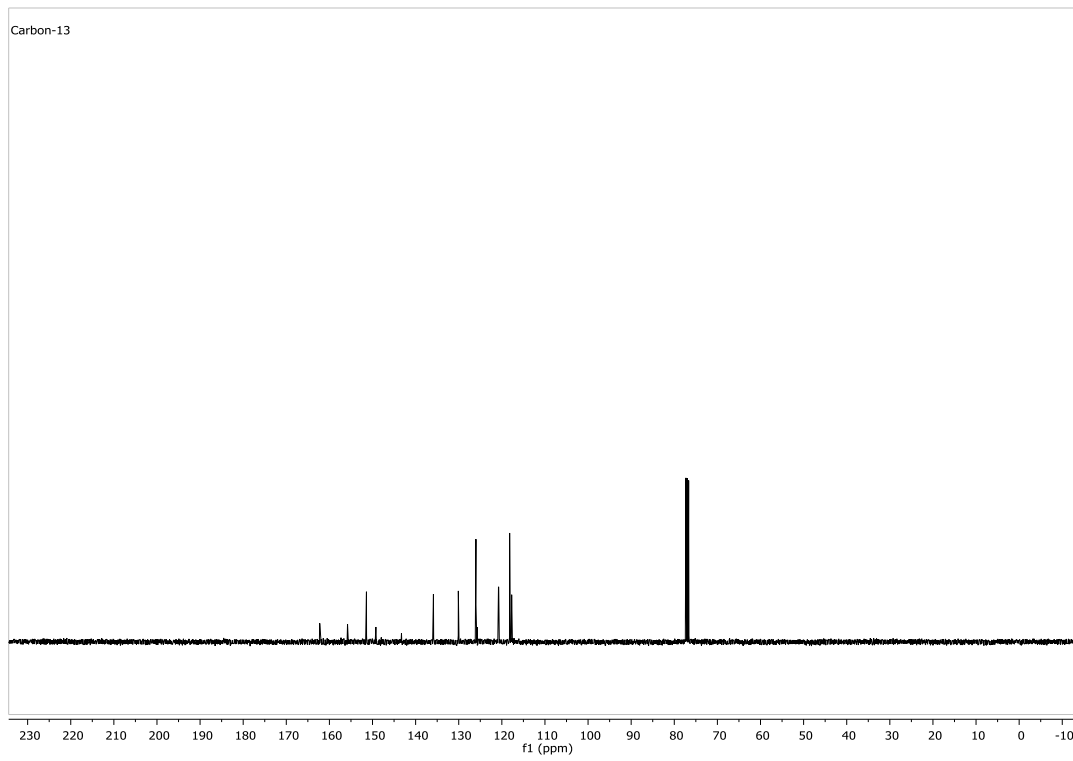
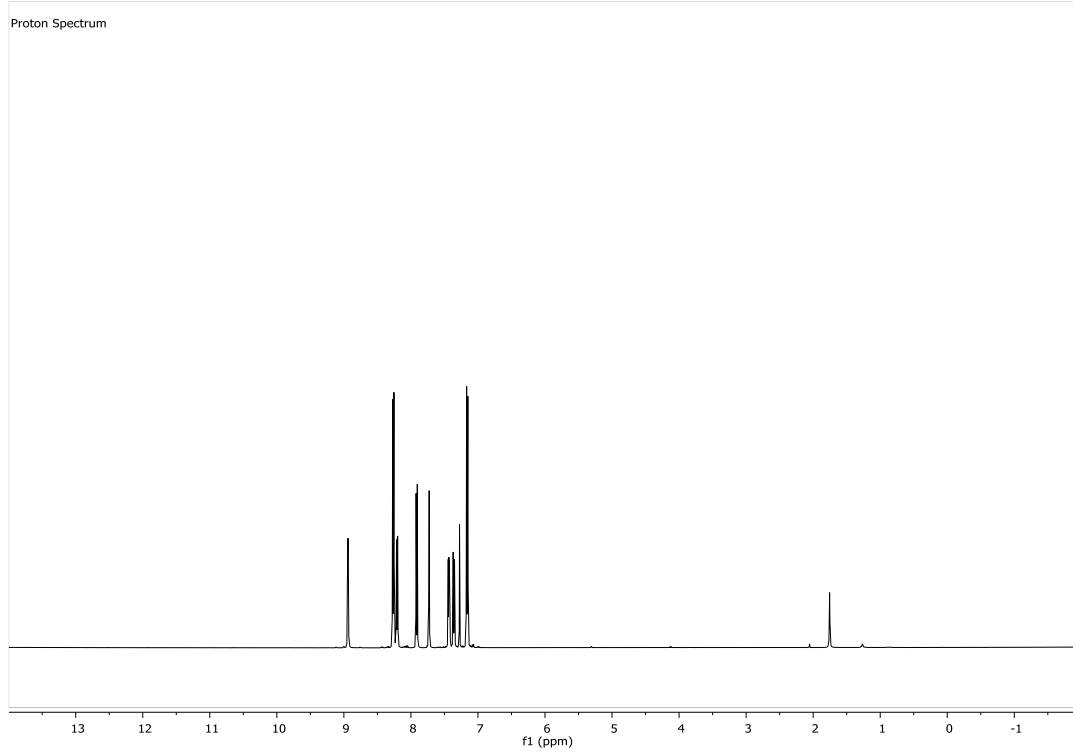


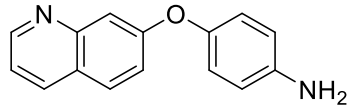
2.18



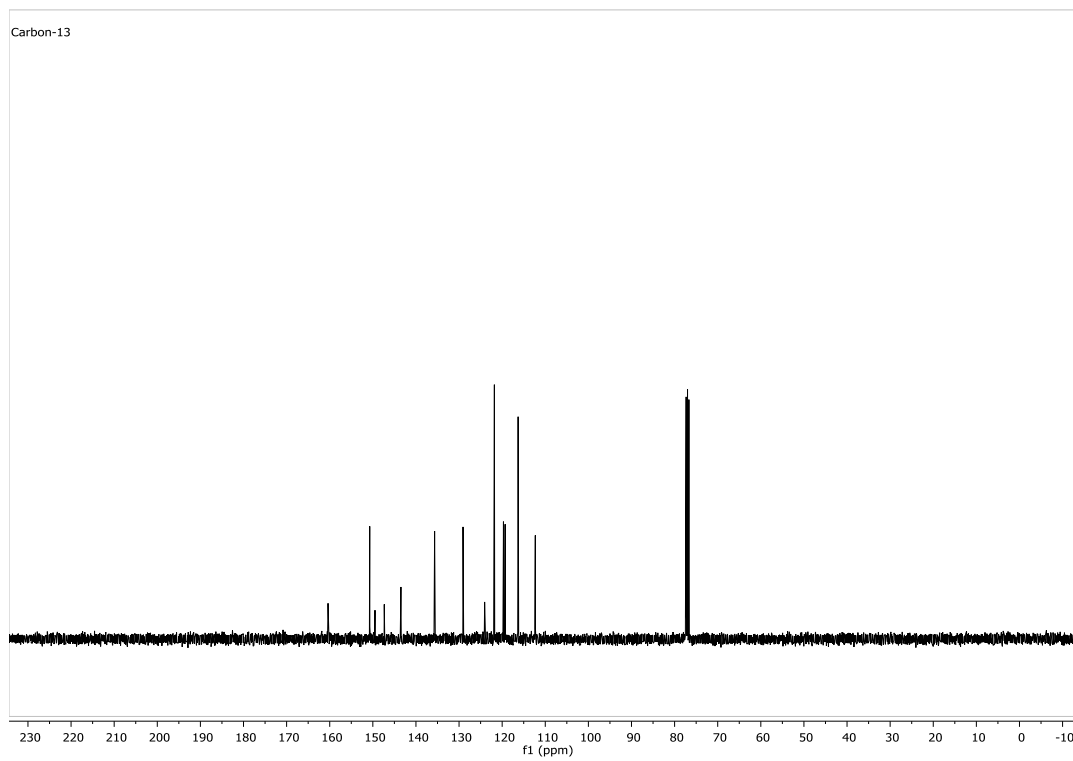
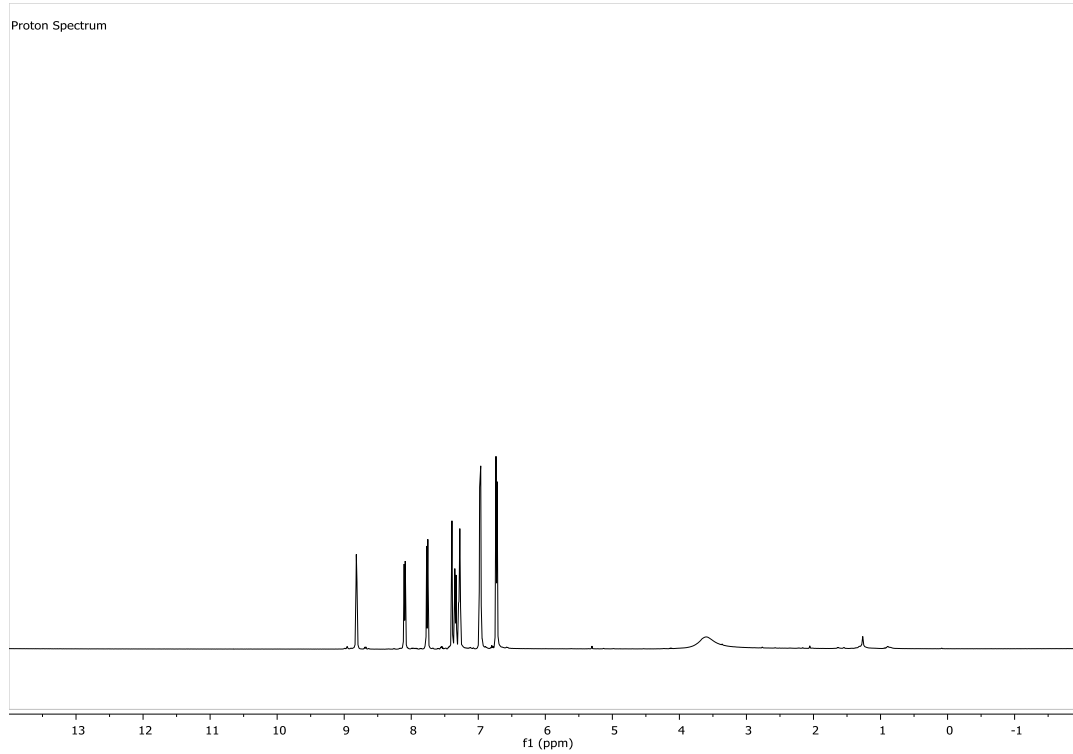


2.19





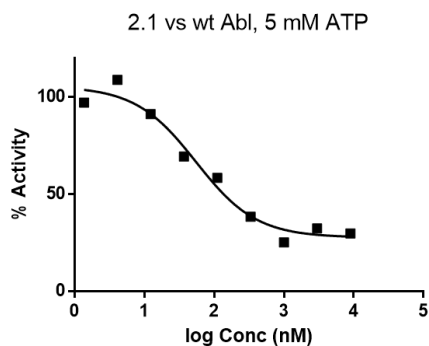
2.20



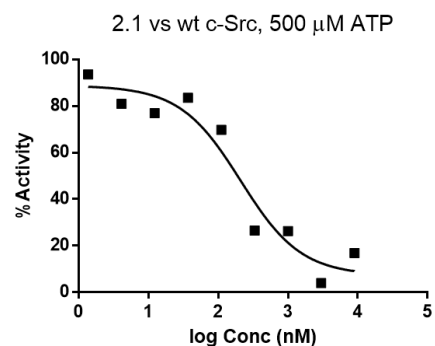


## A.2 Analytical Data for Determination of $K_i$ Values

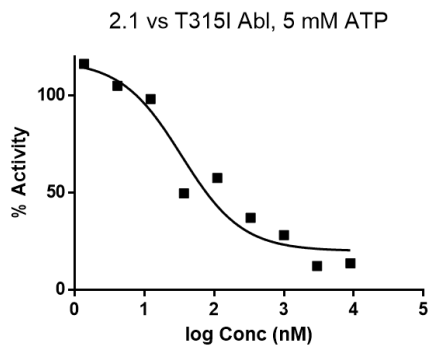
### Compound 2.1



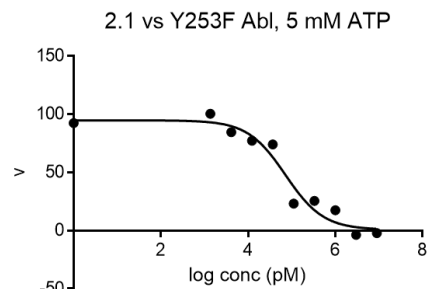
	2.1
EC50	54.94
KI	0.3277



	2.1
EC50	209.6
KI	34.36



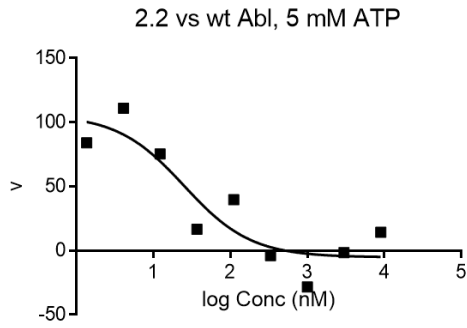
	2.1
EC50	34.15
KI	0.2037



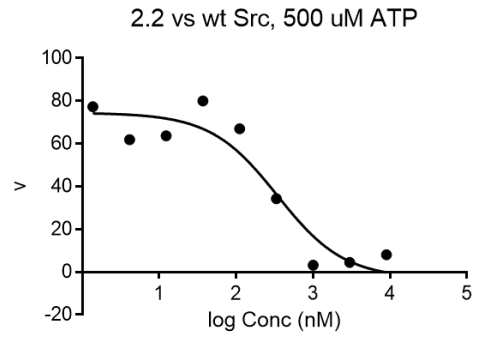
	2.1
EC50	72251
KI	743.7

Average  $K_i = 28.4 \pm 10$  nM (wt Src), Titrates enzyme ( $IC_{50} \sim 30$  nM) for wt, T315I, and Y253F Abl

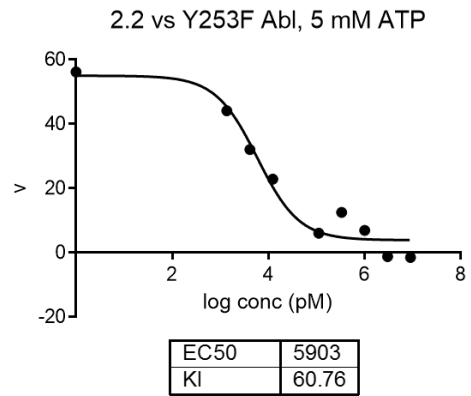
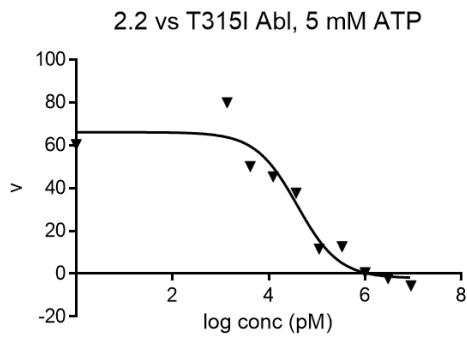
## Compound 2.2



	2.2
EC50	25.25
KI	0.1506

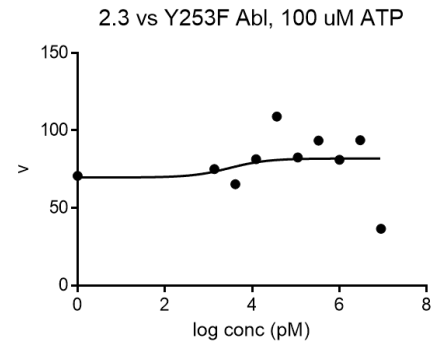
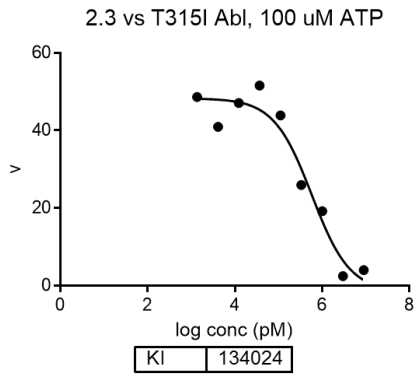
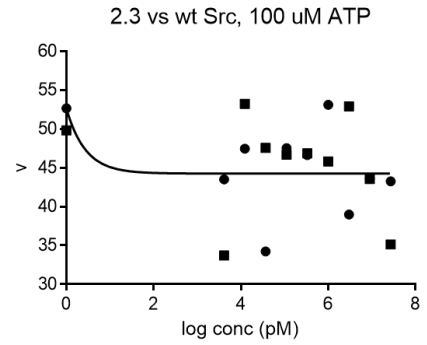
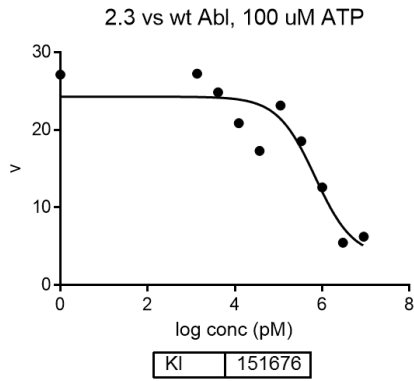


	2.2
EC50	344.4
KI	56.44



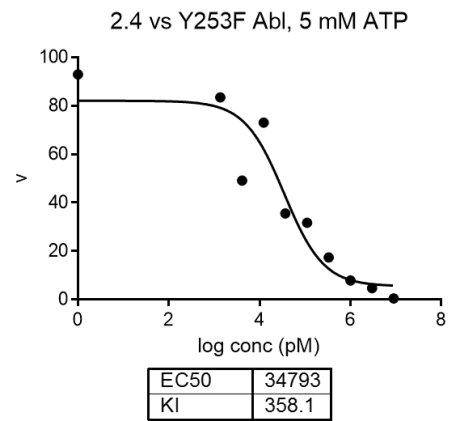
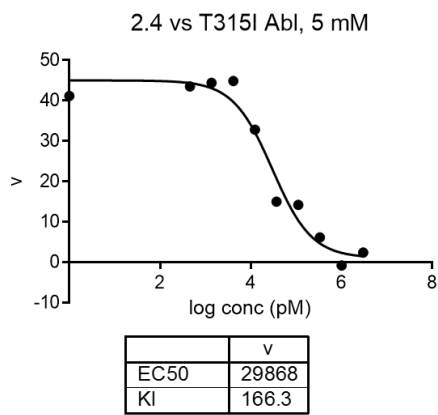
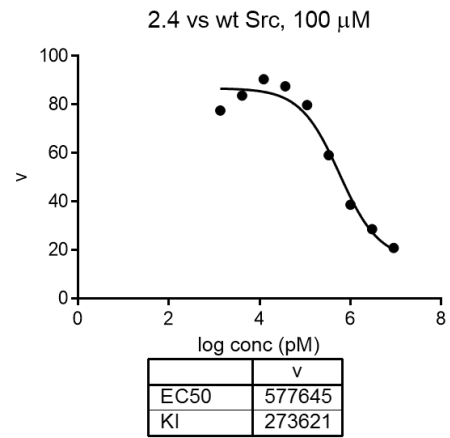
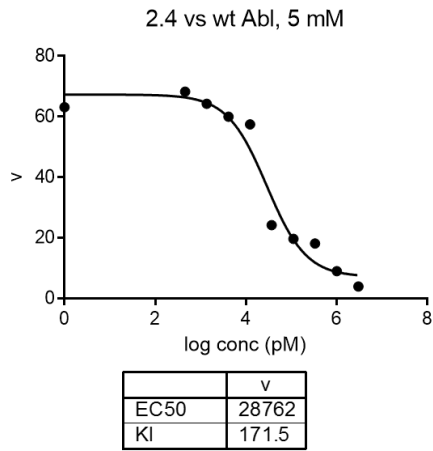
Average  $K_i = 36.3 \pm 19$  nM (wt Src), Titrates enzyme ( $IC_{50} \sim 30$  nM) for wt, T315I, and Y253F Abl

## Compound 2.3



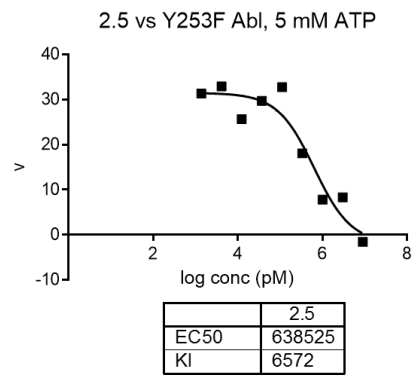
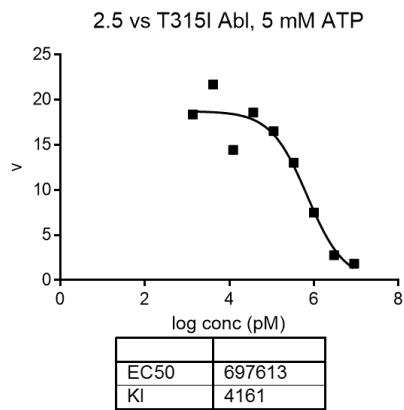
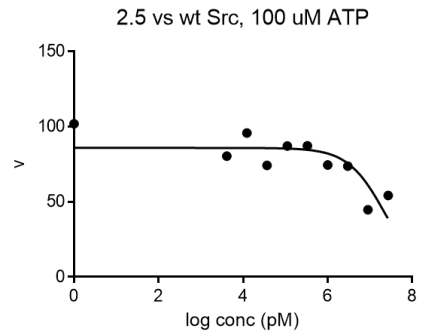
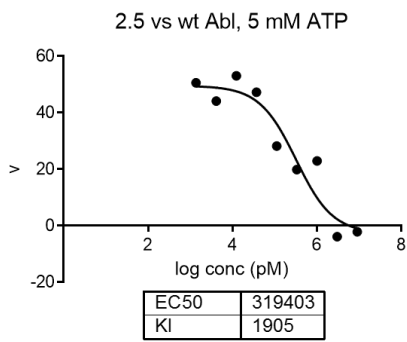
Average  $K_i = 155 \pm 5$  nM (wt Abl),  $119 \pm 62$  nM (T315I Abl), No inhibition  $< 9$   $\mu$ M (Y253F Abl),  $< 27$   $\mu$ M (wt Src)

## Compound 2.4



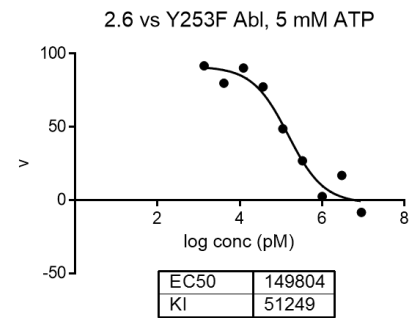
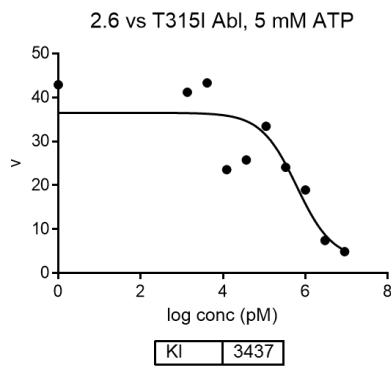
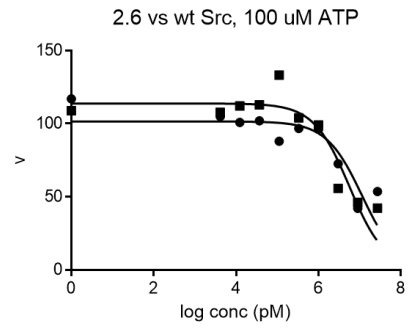
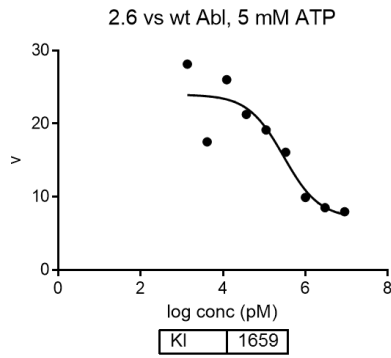
Average  $K_i > 12$  nM (wt Src), Titrates enzyme ( $IC_{50} \sim 30$  nM) for wt, T315I, and Y253F Abl

## Compound 2.5



Average  $K_i = 2 \pm 0.2$  nM (wt Abl),  $4.3 \pm 0.3$  nM (T315I Abl),  $6.1 \pm 0.5$  nM (Y253F Abl),  $12.5 \pm 0.3$   $\mu$ M (wt Src).

## Compound 2.6



Average  $K_i$  =  $1.66 \pm 0.02$  nM (wt Abl),  $2.1 \pm 1.3$  nM (T315I Abl),  $50 \pm 1.7$  nM (Y253F Abl),  $4.2 \pm 2$   $\mu$ M (wt Src).

### A.3 KinomeScan™ Data for Compound 2.4

DiscoverX Gene Symbol	Entrez Gene Symbol	Percent Control	Compound Concentration (nM)
AAK1	AAK1	100	40
ABL1(E255K)-phosphorylated	ABL1	30	40
ABL1(F317I)-nonphosphorylated	ABL1	0	40
ABL1(F317I)-phosphorylated	ABL1	16	40
ABL1(F317L)-nonphosphorylated	ABL1	0.3	40
ABL1(F317L)-phosphorylated	ABL1	14	40
ABL1(H396P)-nonphosphorylated	ABL1	0.45	40
ABL1(H396P)-phosphorylated	ABL1	19	40
ABL1(M351T)-phosphorylated	ABL1	15	40
ABL1(Q252H)-nonphosphorylated	ABL1	2	40
ABL1(Q252H)-phosphorylated	ABL1	31	40
ABL1(T315I)-nonphosphorylated	ABL1	0.2	40
ABL1(T315I)-phosphorylated	ABL1	4.6	40
ABL1(Y253F)-phosphorylated	ABL1	30	40
ABL1-nonphosphorylated	ABL1	0.85	40
ABL1-phosphorylated	ABL1	12	40
ABL2	ABL2	15	40
ACVR1	ACVR1	100	40
ACVR1B	ACVR1B	79	40
ACVR2A	ACVR2A	95	40
ACVR2B	ACVR2B	89	40
ACVRL1	ACVRL1	100	40
ADCK3	CABC1	96	40
ADCK4	ADCK4	85	40
AKT1	AKT1	100	40
AKT2	AKT2	91	40
AKT3	AKT3	98	40
ALK	ALK	76	40
ALK(C1156Y)	ALK	100	40
ALK(L1196M)	ALK	91	40
AMPK-alpha1	PRKAA1	75	40
AMPK-alpha2	PRKAA2	88	40
ANKK1	ANKK1	75	40
ARK5	NUAK1	91	40
ASK1	MAP3K5	85	40
ASK2	MAP3K6	100	40

AURKA	AURKA	92	40
AURKB	AURKB	56	40
AURKC	AURKC	17	40
AXL	AXL	23	40
BIKE	BMP2K	86	40
BLK	BLK	29	40
BMPR1A	BMPR1A	94	40
BMPR1B	BMPR1B	100	40
BMPR2	BMPR2	94	40
BMX	BMX	94	40
BRAF	BRAF	75	40
BRAF(V600E)	BRAF	58	40
BRK	PTK6	100	40
BRSK1	BRSK1	98	40
BRSK2	BRSK2	98	40
BTK	BTK	84	40
BUB1	BUB1	93	40
CAMK1	CAMK1	93	40
CAMK1D	CAMK1D	90	40
CAMK1G	CAMK1G	100	40
CAMK2A	CAMK2A	100	40
CAMK2B	CAMK2B	100	40
CAMK2D	CAMK2D	100	40
CAMK2G	CAMK2G	100	40
CAMK4	CAMK4	100	40
CAMKK1	CAMKK1	100	40
CAMKK2	CAMKK2	100	40
CASK	CASK	100	40
CDC2L1	CDK11B	80	40
CDC2L2	CDC2L2	94	40
CDC2L5	CDK13	50	40
CDK11	CDK19	11	40
CDK2	CDK2	81	40
CDK3	CDK3	100	40
CDK4-cyclinD1	CDK4	95	40
CDK4-cyclinD3	CDK4	100	40
CDK5	CDK5	94	40
CDK7	CDK7	59	40
CDK8	CDK8	13	40
CDK9	CDK9	89	40
CDKL1	CDKL1	76	40



CDKL2	CDKL2	1.8	40
CDKL3	CDKL3	22	40
CDKL5	CDKL5	100	40
CHEK1	CHEK1	100	40
CHEK2	CHEK2	87	40
CIT	CIT	100	40
CLK1	CLK1	40	40
CLK2	CLK2	100	40
CLK3	CLK3	87	40
CLK4	CLK4	32	40
CSF1R	CSF1R	4.6	40
CSF1R-autoinhibited	CSF1R	85	40
CSK	CSK	95	40
CSNK1A1	CSNK1A1	98	40
CSNK1A1L	CSNK1A1L	100	40
CSNK1D	CSNK1D	95	40
CSNK1E	CSNK1E	91	40
CSNK1G1	CSNK1G1	100	40
CSNK1G2	CSNK1G2	100	40
CSNK1G3	CSNK1G3	84	40
CSNK2A1	CSNK2A1	90	40
CSNK2A2	CSNK2A2	84	40
CTK	MATK	57	40
DAPK1	DAPK1	100	40
DAPK2	DAPK2	97	40
DAPK3	DAPK3	100	40
DCAMKL1	DCLK1	88	40
DCAMKL2	DCLK2	96	40
DCAMKL3	DCLK3	100	40
DDR1	DDR1	0.45	40
DDR2	DDR2	15	40
DLK	MAP3K12	97	40
DMPK	DMPK	74	40
DMPK2	CDC42BPG	100	40
DRAK1	STK17A	100	40
DRAK2	STK17B	97	40
DYRK1A	DYRK1A	100	40
DYRK1B	DYRK1B	57	40
DYRK2	DYRK2	90	40
EGFR	EGFR	65	40
EGFR(E746-A750del)	EGFR	82	40

EGFR(G719C)	EGFR	89	40
EGFR(G719S)	EGFR	86	40
EGFR(L747-E749del, A750P)	EGFR	60	40
EGFR(L747-S752del, P753S)	EGFR	65	40
EGFR(L747-T751del,Sins)	EGFR	92	40
EGFR(L858R)	EGFR	70	40
EGFR(L858R,T790M)	EGFR	96	40
EGFR(L861Q)	EGFR	82	40
EGFR(S752-I759del)	EGFR	83	40
EGFR(T790M)	EGFR	71	40
EIF2AK1	EIF2AK1	92	40
EPHA1	EPHA1	100	40
EPHA2	EPHA2	71	40
EPHA3	EPHA3	62	40
EPHA4	EPHA4	80	40
EPHA5	EPHA5	95	40
EPHA6	EPHA6	81	40
EPHA7	EPHA7	100	40
EPHA8	EPHA8	23	40
EPHB1	EPHB1	94	40
EPHB2	EPHB2	87	40
EPHB3	EPHB3	100	40
EPHB4	EPHB4	98	40
EPHB6	EPHB6	92	40
ERBB2	ERBB2	73	40
ERBB3	ERBB3	96	40
ERBB4	ERBB4	100	40
ERK1	MAPK3	100	40
ERK2	MAPK1	93	40
ERK3	MAPK6	96	40
ERK4	MAPK4	79	40
ERK5	MAPK7	79	40
ERK8	MAPK15	70	40
ERN1	ERN1	97	40
FAK	PTK2	91	40
FER	FER	100	40
FES	FES	99	40
FGFR1	FGFR1	86	40
FGFR2	FGFR2	90	40
FGFR3	FGFR3	96	40
FGFR3(G697C)	FGFR3	100	40

FGFR4	FGFR4	95	40
FGR	FGR	91	40
FLT1	FLT1	38	40
FLT3	FLT3	0.9	40
FLT3(D835H)	FLT3	14	40
FLT3(D835Y)	FLT3	15	40
FLT3(ITD)	FLT3	8	40
FLT3(K663Q)	FLT3	1.4	40
FLT3(N841I)	FLT3	0.2	40
FLT3(R834Q)	FLT3	5.6	40
FLT3-autoinhibited	FLT3	100	40
FLT4	FLT4	53	40
FRK	FRK	50	40
FYN	FYN	97	40
GAK	GAK	100	40
GCN2(Kin.Dom.2,S808G)	EIF2AK4	75	40
GRK1	GRK1	100	40
GRK4	GRK4	100	40
GRK7	GRK7	95	40
GSK3A	GSK3A	91	40
GSK3B	GSK3B	74	40
HASPIN	GSG2	96	40
HCK	HCK	44	40
HIPK1	HIPK1	94	40
HIPK2	HIPK2	89	40
HIPK3	HIPK3	78	40
HIPK4	HIPK4	56	40
HPK1	MAP4K1	61	40
HUNK	HUNK	88	40
ICK	ICK	100	40
IGF1R	IGF1R	100	40
IKK-alpha	CHUK	52	40
IKK-beta	IKBKB	57	40
IKK-epsilon	IKBKE	93	40
INSR	INSR	64	40
INSRR	INSRR	100	40
IRAK1	IRAK1	88	40
IRAK3	IRAK3	99	40
IRAK4	IRAK4	99	40
ITK	ITK	98	40
JAK1(JH1domain-catalytic)	JAK1	67	40

JAK1(JH2domain-pseudokinase)	JAK1	100	40
JAK2(JH1domain-catalytic)	JAK2	88	40
JAK3(JH1domain-catalytic)	JAK3	54	40
JNK1	MAPK8	86	40
JNK2	MAPK9	44	40
JNK3	MAPK10	92	40
KIT	KIT	1.5	40
KIT(A829P)	KIT	15	40
KIT(D816H)	KIT	75	40
KIT(D816V)	KIT	81	40
KIT(L576P)	KIT	1.5	40
KIT(V559D)	KIT	0.55	40
KIT(V559D,T670I)	KIT	5.5	40
KIT(V559D,V654A)	KIT	11	40
KIT-autoinhibited	KIT	100	40
LATS1	LATS1	97	40
LATS2	LATS2	91	40
LCK	LCK	5	40
LIMK1	LIMK1	100	40
LIMK2	LIMK2	100	40
LKB1	STK11	100	40
LOK	STK10	0.05	40
LRRK2	LRRK2	24	40
LRRK2(G2019S)	LRRK2	54	40
LTK	LTK	75	40
LYN	LYN	40	40
LZK	MAP3K13	100	40
MAK	MAK	85	40
MAP3K1	MAP3K1	82	40
MAP3K15	MAP3K15	92	40
MAP3K2	MAP3K2	100	40
MAP3K3	MAP3K3	100	40
MAP3K4	MAP3K4	100	40
MAP4K2	MAP4K2	93	40
MAP4K3	MAP4K3	97	40
MAP4K4	MAP4K4	69	40
MAP4K5	MAP4K5	86	40
MAPKAPK2	MAPKAPK2	100	40
MAPKAPK5	MAPKAPK5	100	40
MARK1	MARK1	100	40
MARK2	MARK2	83	40

MARK3	MARK3	100	40
MARK4	MARK4	92	40
MAST1	MAST1	72	40
MEK1	MAP2K1	100	40
MEK2	MAP2K2	100	40
MEK3	MAP2K3	92	40
MEK4	MAP2K4	100	40
MEK5	MAP2K5	100	40
MEK6	MAP2K6	100	40
MELK	MELK	61	40
MERTK	MERTK	41	40
MET	MET	100	40
MET(M1250T)	MET	84	40
MET(Y1235D)	MET	79	40
MINK	MINK1	72	40
MKK7	MAP2K7	77	40
MKNK1	MKNK1	43	40
MKNK2	MKNK2	3.6	40
MLCK	MYLK3	100	40
MLK1	MAP3K9	100	40
MLK2	MAP3K10	100	40
MLK3	MAP3K11	100	40
MRCKA	CDC42BPA	94	40
MRCKB	CDC42BPB	89	40
MST1	STK4	78	40
MST1R	MST1R	91	40
MST2	STK3	69	40
MST3	STK24	100	40
MST4	MST4	95	40
MTOR	MTOR	95	40
MUSK	MUSK	11	40
MYLK	MYLK	100	40
MYLK2	MYLK2	73	40
MYLK4	MYLK4	81	40
MYO3A	MYO3A	85	40
MYO3B	MYO3B	74	40
NDR1	STK38	78	40
NDR2	STK38L	100	40
NEK1	NEK1	92	40
NEK10	NEK10	97	40
NEK11	NEK11	94	40

NEK2	NEK2	100	40
NEK3	NEK3	100	40
NEK4	NEK4	92	40
NEK5	NEK5	100	40
NEK6	NEK6	85	40
NEK7	NEK7	100	40
NEK9	NEK9	100	40
NIK	MAP3K14	89	40
NIM1	MGC42105	95	40
NLK	NLK	75	40
OSR1	OXS1	70	40
p38-alpha	MAPK14	35	40
p38-beta	MAPK11	89	40
p38-delta	MAPK13	70	40
p38-gamma	MAPK12	20	40
PAK1	PAK1	97	40
PAK2	PAK2	100	40
PAK3	PAK3	36	40
PAK4	PAK4	100	40
PAK6	PAK6	100	40
PAK7	PAK7	96	40
PCTK1	CDK16	99	40
PCTK2	CDK17	65	40
PCTK3	CDK18	97	40
PDGFRA	PDGFRA	34	40
PDGFRB	PDGFRB	3.7	40
PDPK1	PDPK1	100	40
PFCDPK1(P.falciparum)	CDPK1	50	40
PFPK5(P.falciparum)	MAL13P1.279	100	40
PFTAIRE2	CDK15	95	40
PFTK1	CDK14	97	40
PHKG1	PHKG1	90	40
PHKG2	PHKG2	100	40
PIK3C2B	PIK3C2B	89	40
PIK3C2G	PIK3C2G	69	40
PIK3CA	PIK3CA	87	40
PIK3CA(C420R)	PIK3CA	65	40
PIK3CA(E542K)	PIK3CA	97	40
PIK3CA(E545A)	PIK3CA	70	40
PIK3CA(E545K)	PIK3CA	91	40
PIK3CA(H1047L)	PIK3CA	88	40

PIK3CA(H1047Y)	PIK3CA	58	40
PIK3CA(I800L)	PIK3CA	89	40
PIK3CA(M1043I)	PIK3CA	60	40
PIK3CA(Q546K)	PIK3CA	78	40
PIK3CB	PIK3CB	100	40
PIK3CD	PIK3CD	77	40
PIK3CG	PIK3CG	92	40
PIK4CB	PI4KB	100	40
PIM1	PIM1	100	40
PIM2	PIM2	95	40
PIM3	PIM3	100	40
PIP5K1A	PIP5K1A	100	40
PIP5K1C	PIP5K1C	100	40
PIP5K2B	PIP4K2B	94	40
PIP5K2C	PIP4K2C	100	40
PKAC-alpha	PRKACA	100	40
PKAC-beta	PRKACB	69	40
PKMYT1	PKMYT1	85	40
PKN1	PKN1	95	40
PKN2	PKN2	100	40
PKNB(M.tuberculosis)	pknB	71	40
PLK1	PLK1	98	40
PLK2	PLK2	94	40
PLK3	PLK3	94	40
PLK4	PLK4	88	40
PRKCD	PRKCD	98	40
PRKCE	PRKCE	100	40
PRKCH	PRKCH	100	40
PRKCI	PRKCI	89	40
PRKCQ	PRKCQ	95	40
PRKD1	PRKD1	100	40
PRKD2	PRKD2	73	40
PRKD3	PRKD3	100	40
PRKG1	PRKG1	68	40
PRKG2	PRKG2	92	40
PRKR	EIF2AK2	100	40
PRKX	PRKX	75	40
PRP4	PRPF4B	67	40
PYK2	PTK2B	100	40
QSK	KIAA0999	100	40
RAF1	RAF1	83	40

RET	RET	5.4	40
RET(M918T)	RET	6.2	40
RET(V804L)	RET	18	40
RET(V804M)	RET	9	40
RIOK1	RIOK1	100	40
RIOK2	RIOK2	96	40
RIOK3	RIOK3	93	40
RIPK1	RIPK1	96	40
RIPK2	RIPK2	90	40
RIPK4	RIPK4	100	40
RIPK5	DSTYK	96	40
ROCK1	ROCK1	94	40
ROCK2	ROCK2	80	40
ROS1	ROS1	100	40
RPS6KA4(Kin.Dom.1-N-terminal)	RPS6KA4	79	40
RPS6KA4(Kin.Dom.2-C-terminal)	RPS6KA4	100	40
RPS6KA5(Kin.Dom.1-N-terminal)	RPS6KA5	100	40
RPS6KA5(Kin.Dom.2-C-terminal)	RPS6KA5	100	40
RSK1(Kin.Dom.1-N-terminal)	RPS6KA1	76	40
RSK1(Kin.Dom.2-C-terminal)	RPS6KA1	100	40
RSK2(Kin.Dom.1-N-terminal)	RPS6KA3	100	40
RSK2(Kin.Dom.2-C-terminal)	RPS6KA3	100	40
RSK3(Kin.Dom.1-N-terminal)	RPS6KA2	97	40
RSK3(Kin.Dom.2-C-terminal)	RPS6KA2	100	40
RSK4(Kin.Dom.1-N-terminal)	RPS6KA6	100	40
RSK4(Kin.Dom.2-C-terminal)	RPS6KA6	95	40
S6K1	RPS6KB1	33	40
SBK1	SBK1	62	40
SGK	SGK1	75	40
SgK110	SgK110	100	40
SGK2	SGK2	77	40
SGK3	SGK3	100	40
SIK	SIK1	98	40
SIK2	SIK2	54	40
SLK	SLK	93	40
SNARK	NUAK2	96	40
SNRK	SNRK	91	40
SRC	SRC	100	40
SRMS	SRMS	89	40
SRPK1	SRPK1	64	40
SRPK2	SRPK2	100	40



SRPK3	SRPK3	97	40
STK16	STK16	98	40
STK33	STK33	66	40
STK35	STK35	93	40
STK36	STK36	85	40
STK39	STK39	90	40
SYK	SYK	100	40
TAK1	MAP3K7	6	40
TAOK1	TAOK1	88	40
TAOK2	TAOK2	83	40
TAOK3	TAOK3	83	40
TBK1	TBK1	92	40
TEC	TEC	95	40
TESK1	TESK1	100	40
TGFBR1	TGFBR1	96	40
TGFBR2	TGFBR2	100	40
TIE1	TIE1	31	40
TIE2	TEK	3.4	40
TLK1	TLK1	100	40
TLK2	TLK2	100	40
TNIK	TNIK	75	40
TNK1	TNK1	96	40
TNK2	TNK2	100	40
TNNI3K	TNNI3K	94	40
TRKA	NTRK1	34	40
TRKB	NTRK2	27	40
TRKC	NTRK3	55	40
TRPM6	TRPM6	100	40
TSSK1B	TSSK1B	92	40
TTK	TTK	61	40
TXK	TXK	90	40
TYK2(JH1domain-catalytic)	TYK2	89	40
TYK2(JH2domain-pseudokinase)	TYK2	100	40
TYRO3	TYRO3	100	40
ULK1	ULK1	61	40
ULK2	ULK2	91	40
ULK3	ULK3	31	40
VEGFR2	KDR	57	40
VRK2	VRK2	90	40
WEE1	WEE1	89	40
WEE2	WEE2	100	40

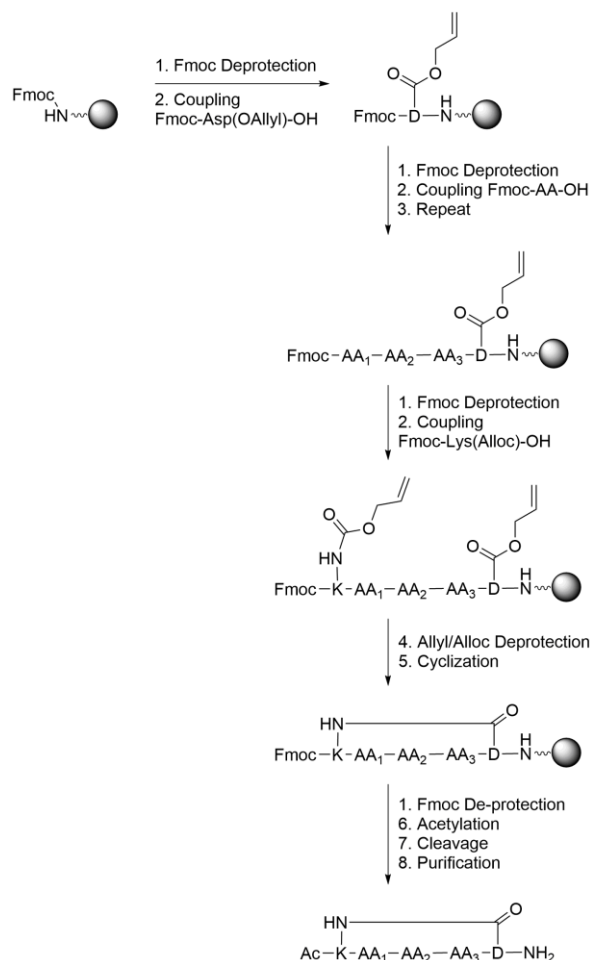
WNK1	WNK1	95	40
WNK3	WNK3	95	40
YANK1	STK32A	82	40
YANK2	STK32B	100	40
YANK3	STK32C	96	40
YES	YES1	100	40
YSK1	STK25	98	40
YSK4	YSK4	96	40
ZAK	ZAK	2.6	40
ZAP70	ZAP70	100	40

## **APPENDIX B**

### **Analytical Data and Supplemental Information for Chapter III**

## B.1. Peptide Synthesis and Characterization

All peptides were synthesized on a 0.1 mmol scale manually, using standard Fmoc-SPPS chemistry on a Rink Amide 'Low Loading' resin. The resin was swelled for 30 min in NMP prior to the first deprotection step. All steps were monitored using the Kaiser test and repeated if necessary.



### *Fmoc Deprotection*

Fmoc deprotection was carried out using 20% (v/v) piperidine in NMP (7 ml) for at least 10 min at room temperature. The deprotection solution was subsequently drained and the resin washed with NMP (4x) before moving on to the next step.

### *Coupling:*

A solution of Fmoc amino acid (0.5 mmol), HBTU (190 mg, 0.5 mmol), and DIEA (0.2 ml, 1.15 mmol) in NMP (4 ml) was added to the resin and mixed for at least 20 min at

rt. Upon completion the resin was washed with NMP (4x). For the coupling of Fmoc-Lys(Alloc)-OH, Fmoc-Asp(OAllyl)-OH and non-natural amino acids, 0.4 mmol of the corresponding amino acid was used and the coupling carried out for at least 1h at room temperature.

#### *Repeat*

The above sequence of Fmoc deprotection and coupling was repeated until the desired amino acids had been assembled on resin.

#### *Allyl/Alloc Deprotection*

A solution of Pd(PPh<sub>3</sub>)<sub>4</sub> (11.5 mg, 0.01 mmol), N,N-dimethyl barbituric acid (62 mg, 0.4 mmol) in 7 ml DCM was added to the resin and mixed for 2 h at room temperature. The solution was drained and the resin washed with DCM (4x) and the step repeated.

#### *Cyclization*

A solution of PyBOP (208 mg, 0.4 mmol), DIEA (0.2 ml, 1.15 mmol) in 8 ml NMP was added to the resin and mixed for at least 1 h at rt. Longer peptides typically required >2 h for cyclization. The solution was drained and the resin washed with NMP (4x).

#### *Acetylation*

A solution of 'Cap Mix A' (10% acetic anhydride, 10% pyridine, 80% THF) was added to the resin and mixed for 20 min at rt. The solution was drained and the resin washed with NMP (4x) and DCM (4x).

#### *Cleavage*

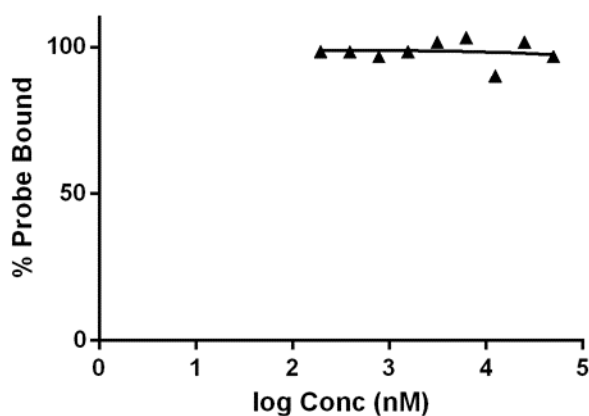
The peptides were cleaved off the resin by incubating with a 4 ml solution of TFA/Water/Triisopropylsilane (95/2.5/2.5 vol ratio) for at least 1 h at room temperature with occasional stirring. The solution containing cleaved peptide was drained and evaporated *in vacuo*. Peptides containing protected phosphonates or difluorophosphonates were stirred in a solution of bromotrimethylsilane (0.5 ml) in Acetonitrile (1.5 ml) for 2 h and the volatiles evaporated *in vacuo*.

### Purification

Crude peptides were dissolved in DMSO (2 ml) for HPLC purification with a Waters® Xbridge Prep C18 column (19 x 250 mm). All peptides were purified using a linear gradient of Acetonitrile (5 to 95%) in Water with both solvents containing 0.1% (v/v) TFA at a rate of 1%/min. Fractions containing the desired product were combined and lyophilized.

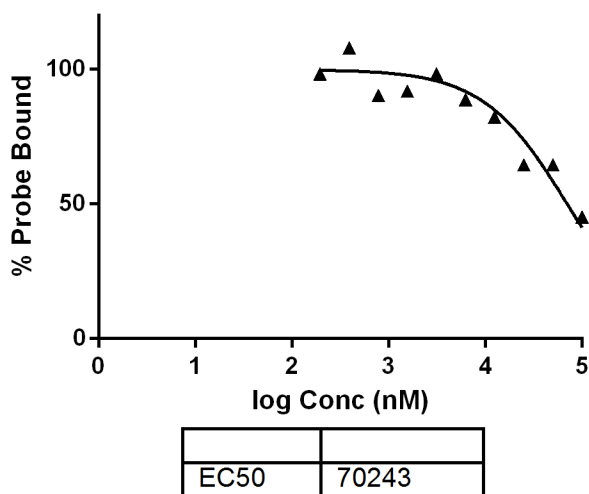
### B.2. Analytical Data for Determination of IC<sub>50</sub> Values

#### Compound 3.1



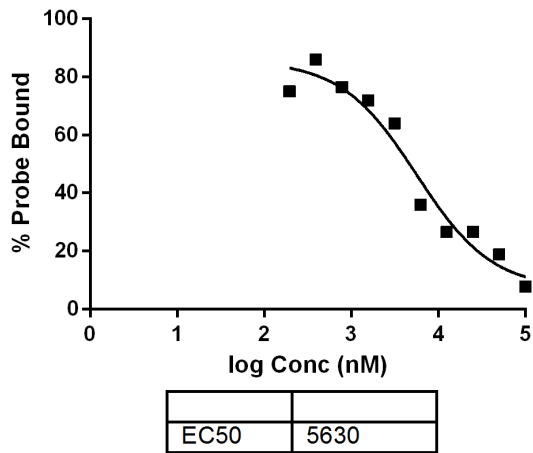
No inhibition >100  $\mu$ M

#### Compound 3.2



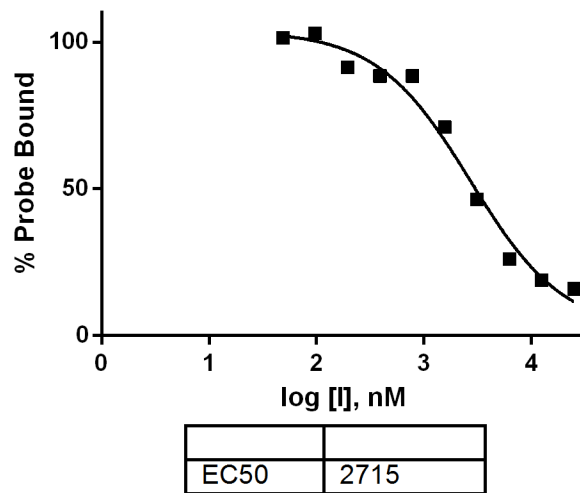
Average IC<sub>50</sub> = 64  $\pm$  12  $\mu$ M

### Compound 3.3



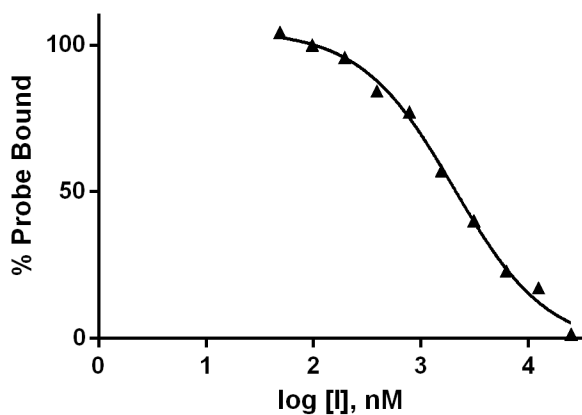
Average  $IC_{50} = 5.3 \pm 1.2 \mu M$

### Compound 3.4



Average  $IC_{50} = 2.8 \pm 0.4 \mu M$

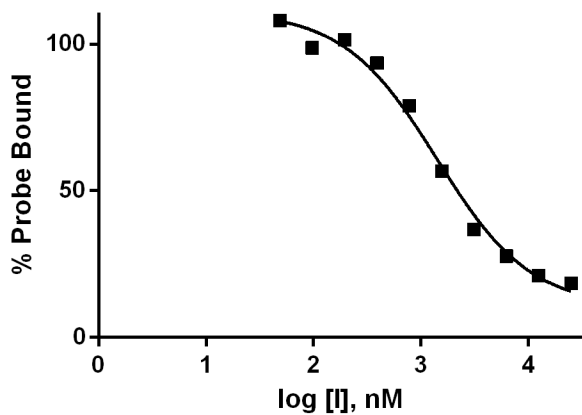
### Compound 3.6



EC50	2036
------	------

Average  $IC_{50} = 1.99 \pm 0.4 \mu M$

### Compound 3.7

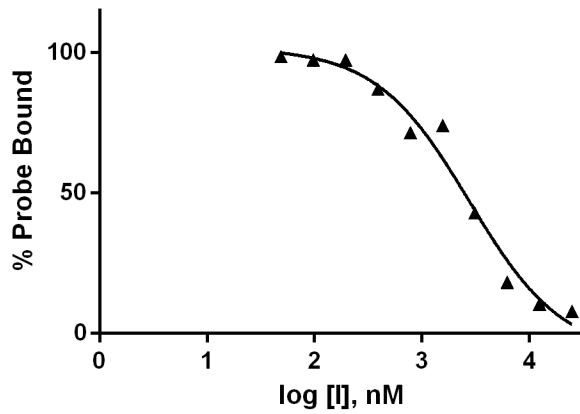


EC50	1416
------	------

Average  $IC_{50} = 1.4 \pm 0.15 \mu M$



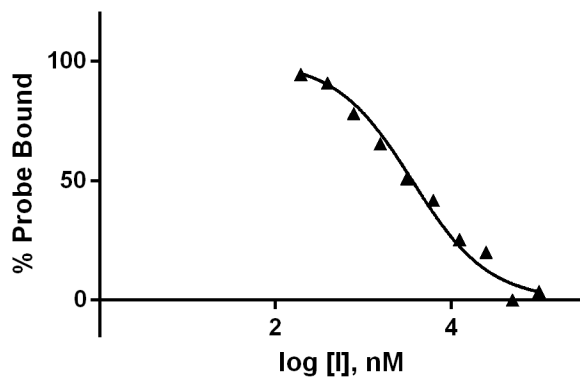
Compound 3.8



EC50	2770

Average  $IC_{50} = 2.7 \pm 0.5 \mu\text{M}$

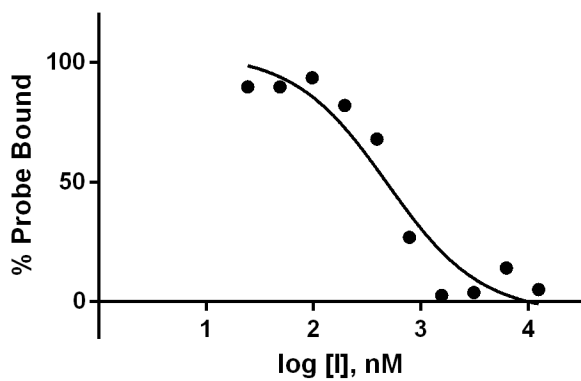
Compound 3.9



EC50	3611

Average  $IC_{50} = 2.6 \pm 0.7 \mu\text{M}$

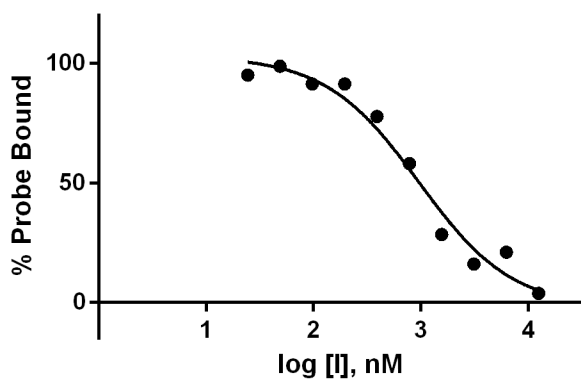
### Compound 3.10



EC50	487.0
------	-------

Average  $IC_{50} = 0.54 \pm 0.04 \mu M$

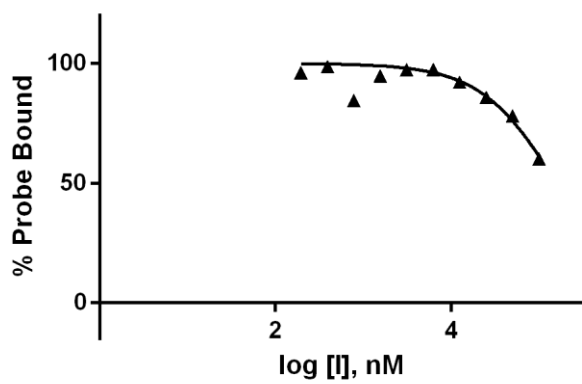
### Compound 3.11



EC50	958.9
------	-------

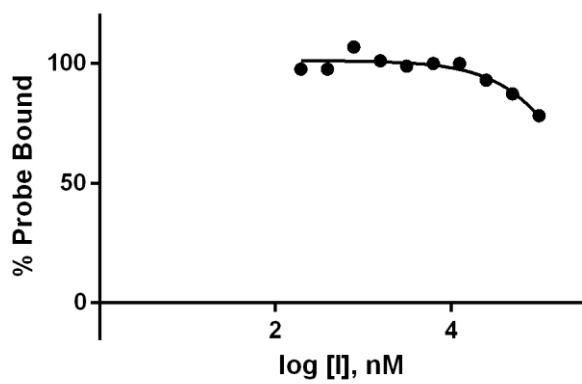
Average  $IC_{50} = 0.9 \pm 0.1 \mu M$

Compound 3.12



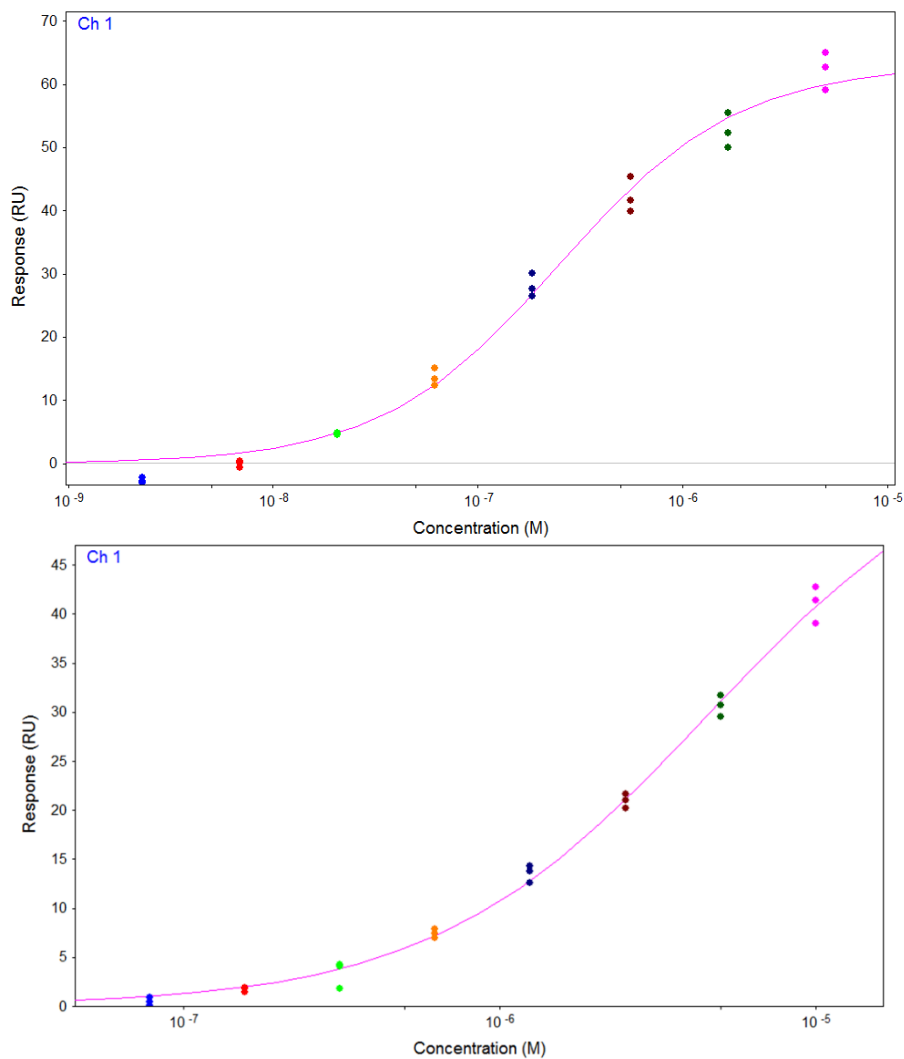
Average  $IC_{50} = 193 \pm 6 \mu M$

Compound 3.13



No inhibition  $>100 \mu M$

### B.3. $K_d$ Determination Using Equilibrium Analysis on SPR

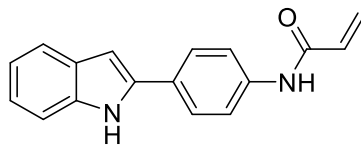


Top – Compound **3.10**  $K_d = 250$  nM, Bottom – Compound **3.15**  $K_d = 4.53$   $\mu$ M

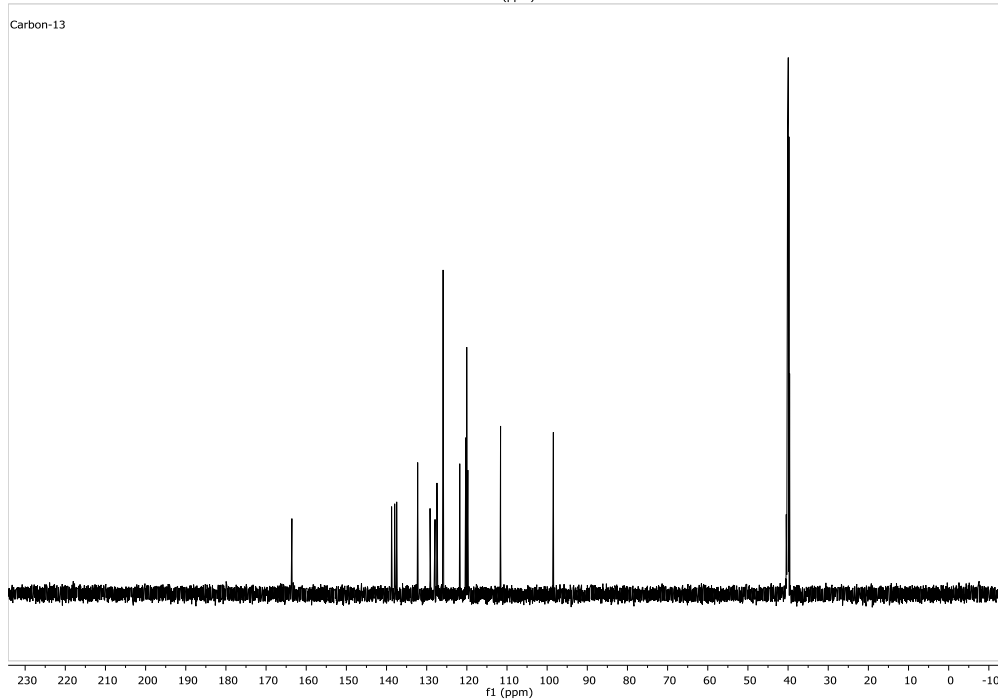
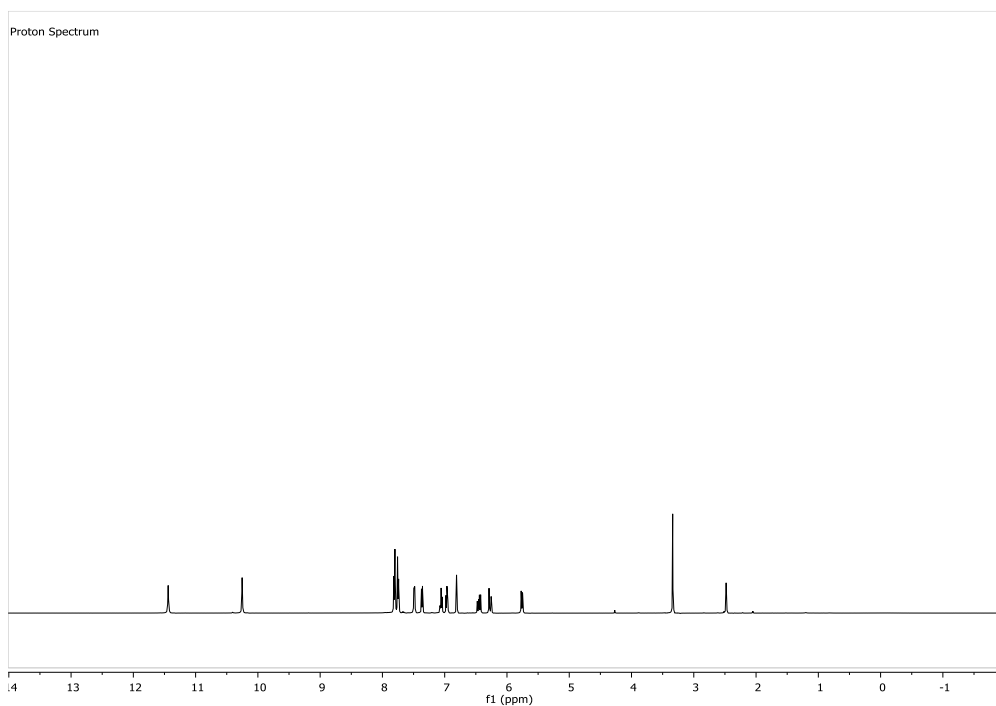
## **APPENDIX C**

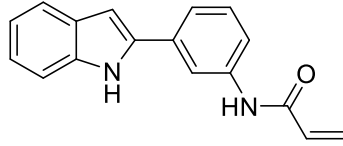
### **Analytical Data and Supplemental Information for Chapter IV**

### C.1. Spectral Data for Compounds 4.1 – 4.6

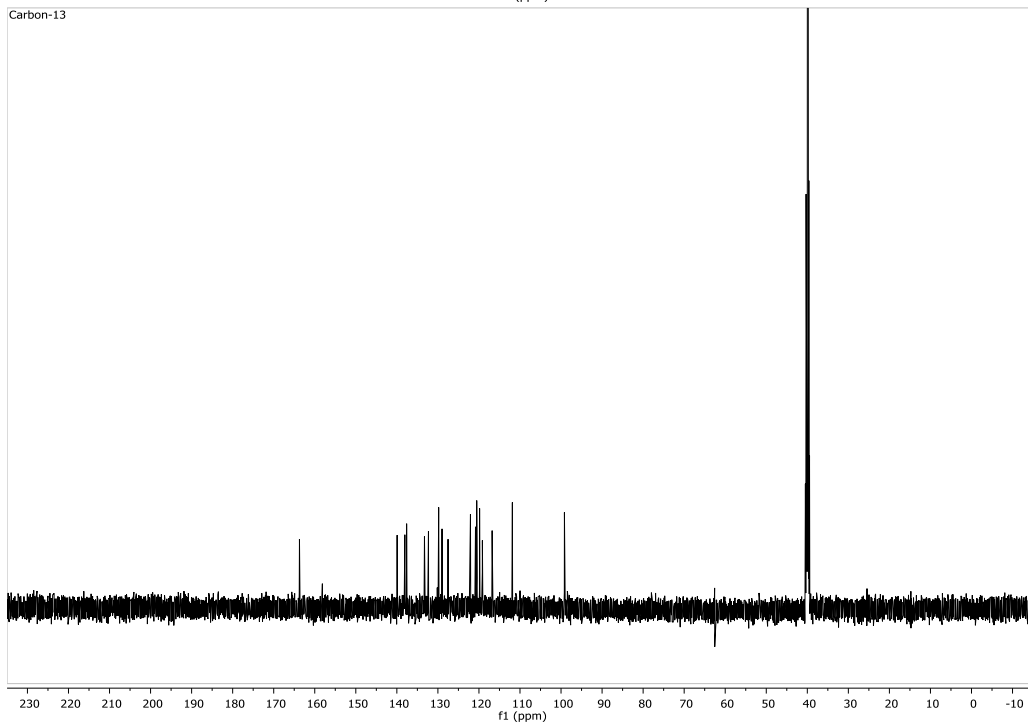
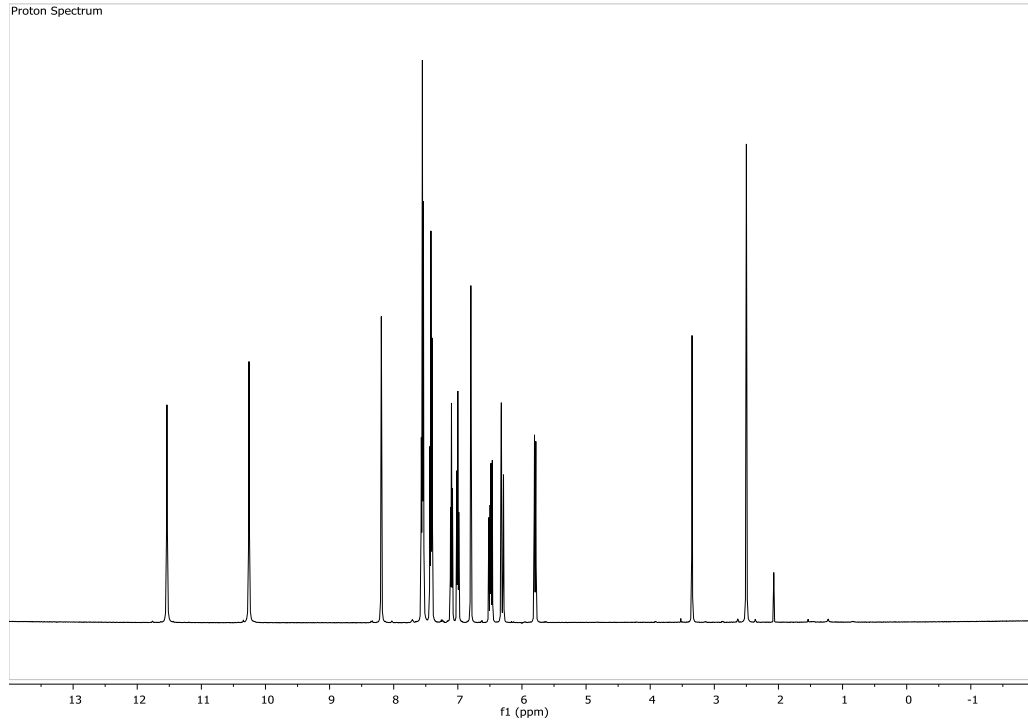


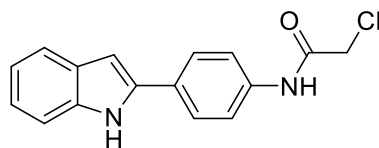
**4.1**



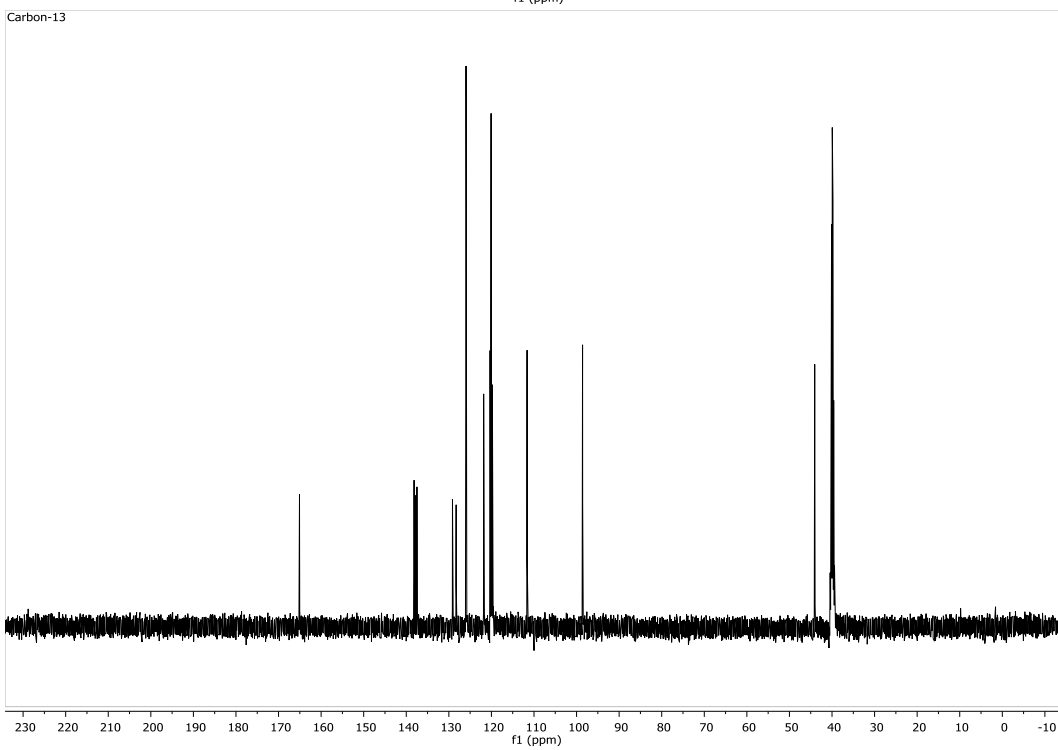
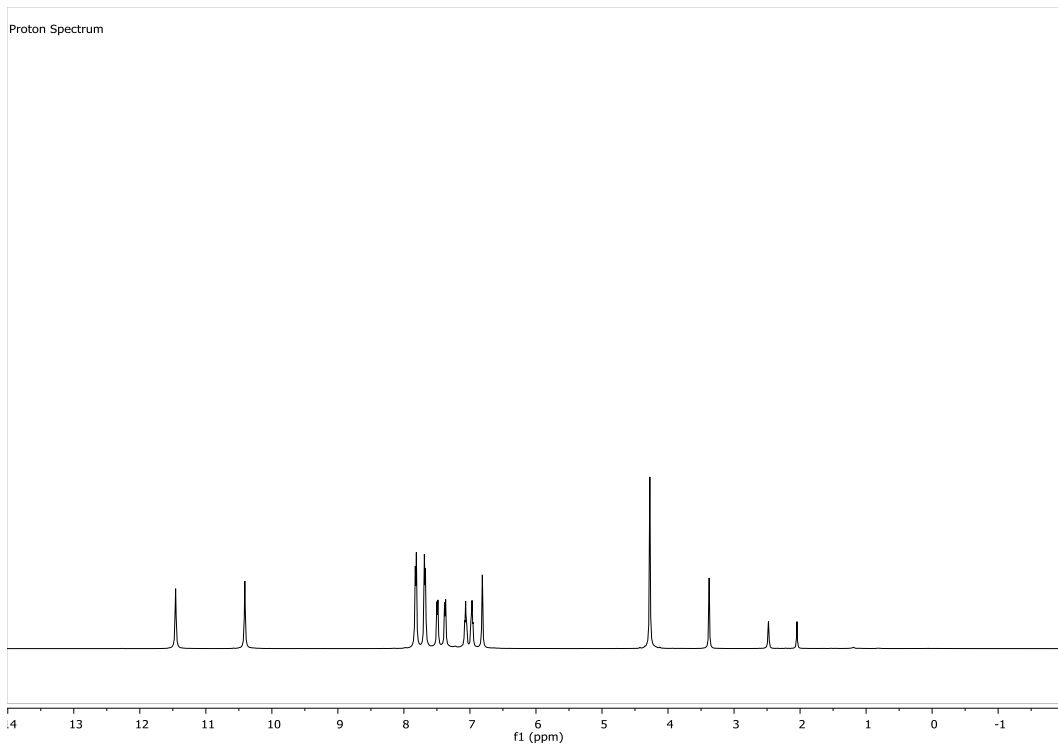


4.2

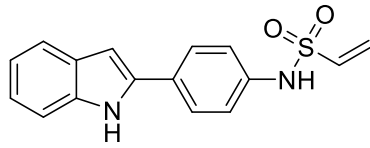




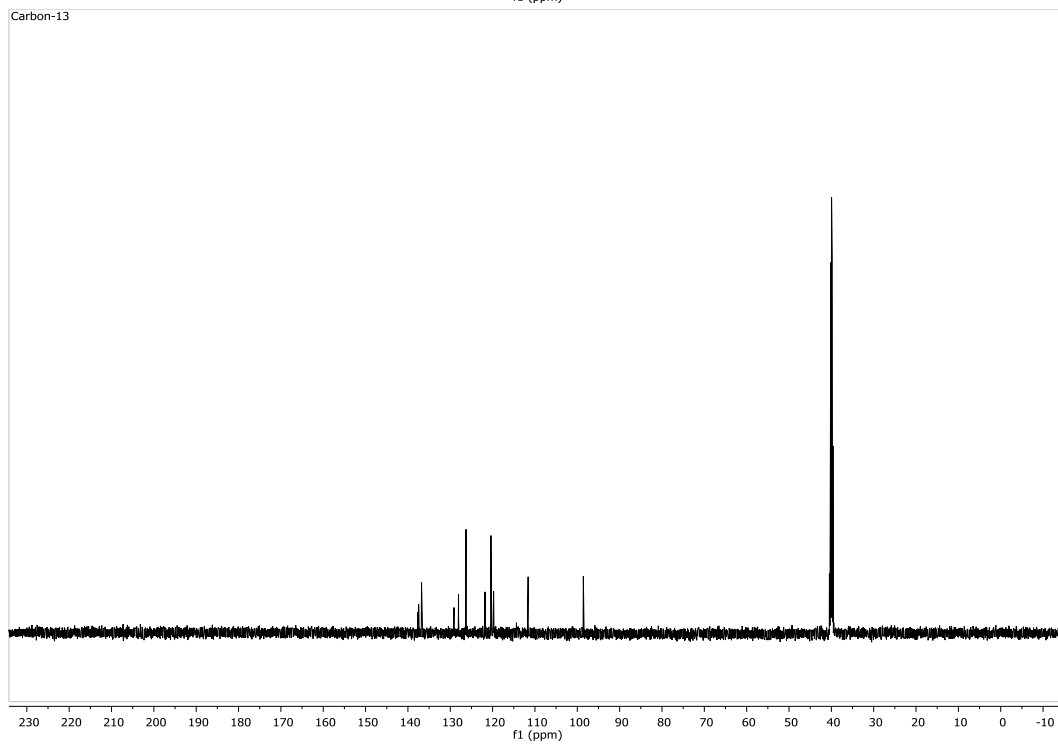
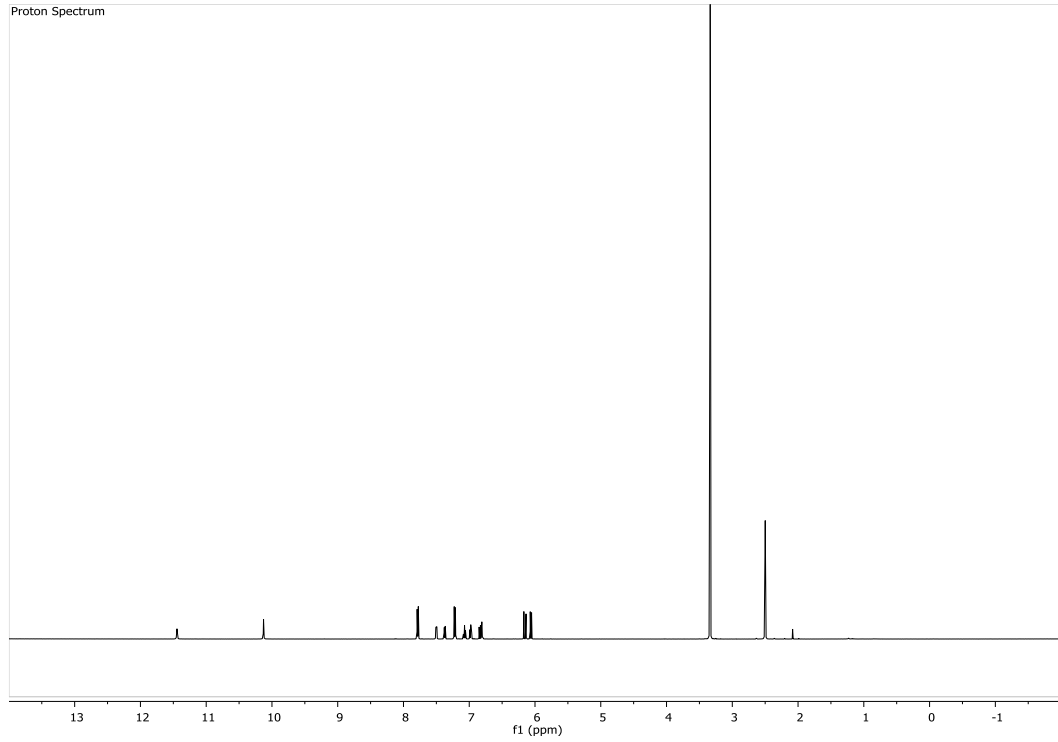
4.3

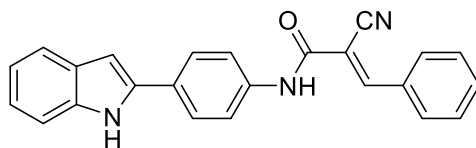




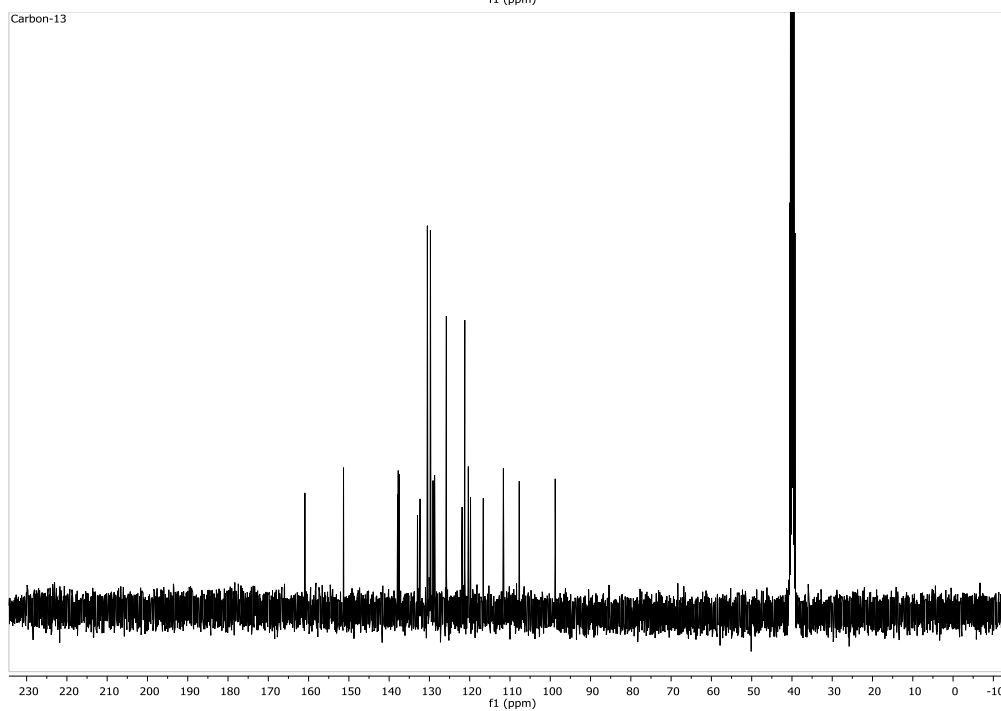
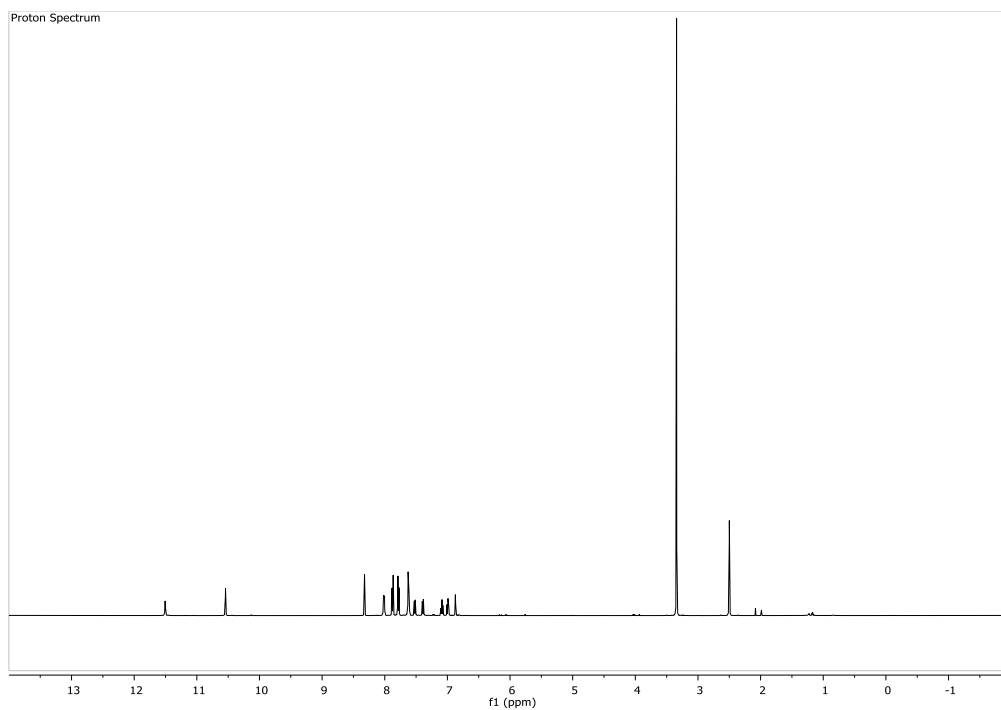


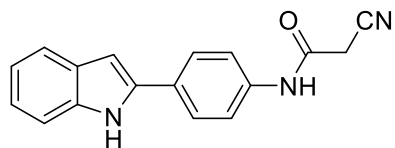
4.4



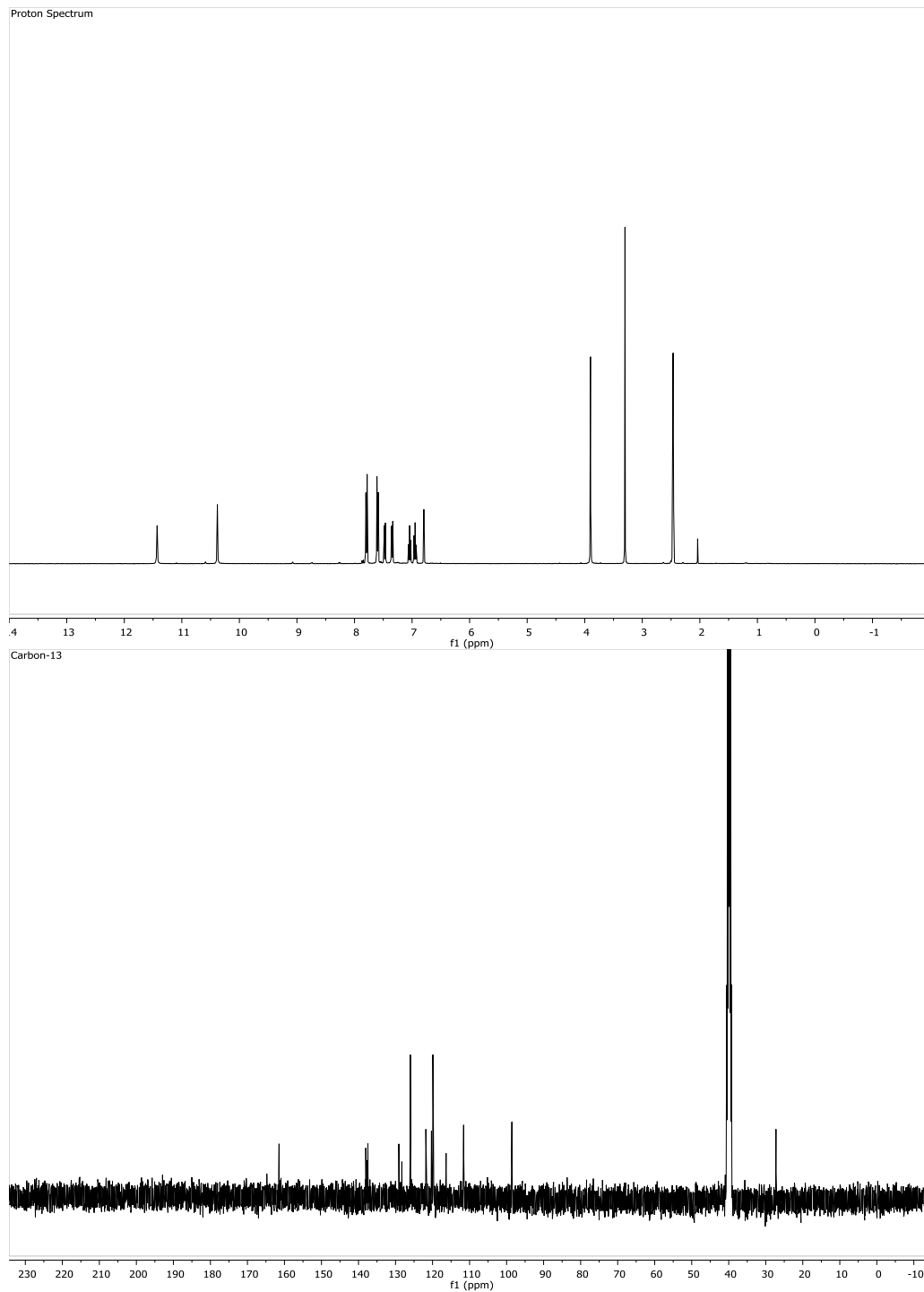


4.5





4.6



## C.2. InFarmatik Electrophile Fragment Library

Cmpd	Structure	Cmpd	Structure	Cmpd	Structure	Cmpd
EL-1002		EL-1027		EL-1051		EL-1086
EL-1003		EL-1028		EL-1052		EL-1092
EL-1004		EL-1029		EL-1053		EL-1098
EL-1005		EL-1030		EL-1054		EL-1104
EL-1006		EL-1031		EL-1055		EL-1105
EL-1007		EL-1032		EL-1056		EL-1106
EL-1009		EL-1033		EL-1057		EL-1108
EL-1010		EL-1034		EL-1058		EL-1109
EL-1011		EL-1035		EL-1059		EL-1113

EL-1012		EL-1036		EL-1061	
EL-1015		EL-1037		EL-1062	
EL-1016		EL-1038		EL-1063	
EL-1018		EL-1039		EL-1064	
EL-1019		EL-1040		EL-1065	
EL-1020		EL-1041		EL-1068	
EL-1021		EL-1044		EL-1069	
EL-1022		EL-1046		EL-1071	
EL-1023		EL-1047		EL-1074	
EL-1024		EL-1048		EL-1083	
EL-1025		EL-1050		EL-1084	

	Cmpd	Structure	Cmpd	Structure	Cmpd	Structure
	EL-1086		EL-1140		EL-1167	
	EL-1092		EL-1141		EL-1168	
	EL-1098		EL-1142		EL-1169	
	EL-1104		EL-1143		EL-1170	
	EL-1105		EL-1144		EL-1171	
	EL-1106		EL-1145		EL-1174	
	EL-1108		EL-1146		EL-1175	
	EL-1109		EL-1147		EL-1176	
	EL-1113		EL-1148		EL-1177	

	EL-1114		EL-1151		EL-1178	
	EL-1115		EL-1152			
	EL-1119		EL-1153			
	EL-1123		EL-1155			
	EL-1124		EL-1156			
	EL-1125		EL-1157			
	EL-1126		EL-1160			
	EL-1132		EL-1161			
	EL-1134		EL-1162			
	EL-1135		EL-1163			
	EL-1137		EL-1164			

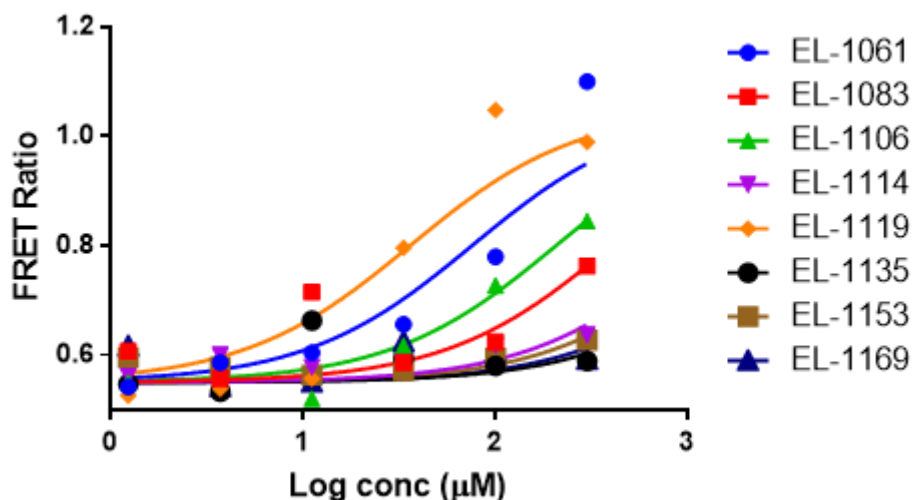
### C.3. Percent Inhibition Values from Fragment Screen

EL-1002	23.4397	EL-1016	5.017601	EL-1029	10.40367	EL-1040	5.289309	EL-1055	12.26516
EL-1003	23.4397	EL-1018	2.560673	EL-1030	19.59164	EL-1041	1.186666	EL-1056	12.26516
EL-1004	8.261333	EL-1019	12.5301	EL-1031	14.37781	EL-1044	17.77771	EL-1057	8.798419
EL-1005	7.453818	EL-1020	3.655214	EL-1032	2.286391	EL-1046	9.066585	EL-1058	3.928205
EL-1006	-3.81408	EL-1021	6.914212	EL-1033	5.289309	EL-1047	12.5301	EL-1059	14.64079
EL-1007	9.602168	EL-1022	7.992413	EL-1034	7.184141	EL-1048	1.461988	EL-1061	79.18494
EL-1009	0.911084	EL-1023	2.286391	EL-1035	19.84982	EL-1050	1.737049	EL-1062	17.77771
EL-1010	5.289309	EL-1024	-4.37503	EL-1036	11.99997	EL-1051	18.55653	EL-1063	12.26516
EL-1011	11.73454	EL-1025	-1.85916	EL-1037	17.51762	EL-1052	14.90353	EL-1064	14.64079
EL-1012	10.93676	EL-1027	7.184141	EL-1038	1.461988	EL-1053	7.184141	EL-1065	3.655214
EL-1015	-3.81408	EL-1028	-0.47075	EL-1039	2.286391	EL-1054	6.373595	EL-1068	5.831961

EL-1069	0.635241	EL-1108	58.9909	EL-1134	7.184141	EL-1148	6.64403	EL-1164	10.67034
EL-1071	18.81567	EL-1109	15.16603	EL-1135	74.59944	EL-1151	22.16286	EL-1167	6.102905
EL-1074	-16.1155	EL-1113	5.560763	EL-1137	13.5874	EL-1152	5.560763	EL-1168	6.64403
EL-1083	114.5248	EL-1114	91.47721	EL-1140	5.017601	EL-1153	96.15066	EL-1169	97.49706
EL-1084	7.184141	EL-1115	11.46886	EL-1141	9.602168	EL-1155	11.73454	EL-1170	7.184141
EL-1086	17.51762	EL-1119	81.03707	EL-1142	3.381966	EL-1156	39.28425	EL-1171	-10.3304
EL-1092	66.26212	EL-1123	12.5301	EL-1143	-6.62959	EL-1157	6.914212	EL-1174	17.25729
EL-1098	62.76205	EL-1124	-10.3304	EL-1144	23.9488	EL-1160	18.55653	EL-1175	11.99997
EL-1104	4.473416	EL-1125	4.473416	EL-1145	2.286391	EL-1161	7.992413	EL-1176	3.10846
EL-1105	15.42828	EL-1126	5.017601	EL-1146	28.48942	EL-1162	15.16603	EL-1177	35.40783
EL-1106	102.2454	EL-1132	74.38903	EL-1147	13.32344	EL-1163	-2.13764	EL-1178	-1.30301

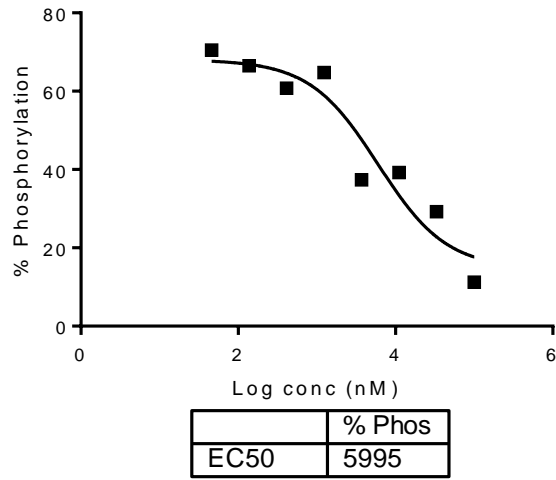
### C.4. Analytical Data for Determination of IC<sub>50</sub> Values

Follow-up of initial screening results



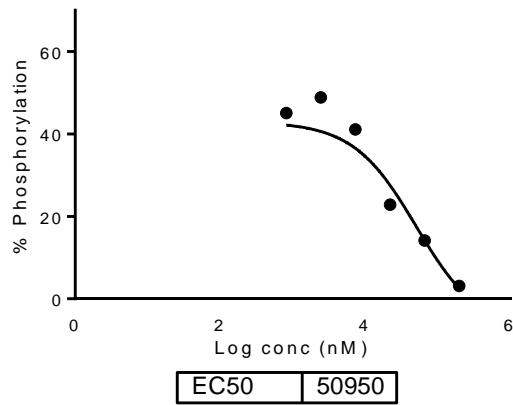


### Compound 4.1



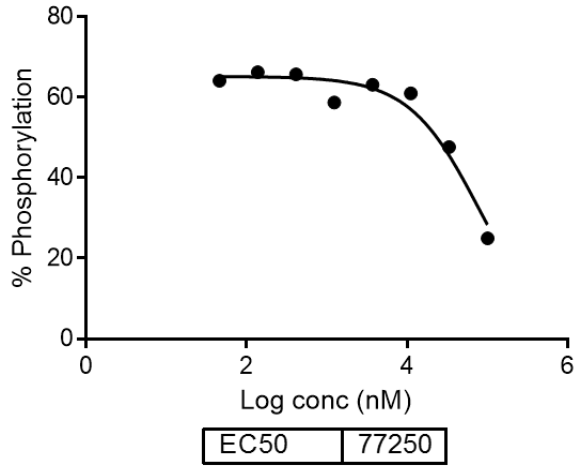
Avg IC<sub>50</sub> = 9.7 ± 3.7 μM

### Compound 4.2



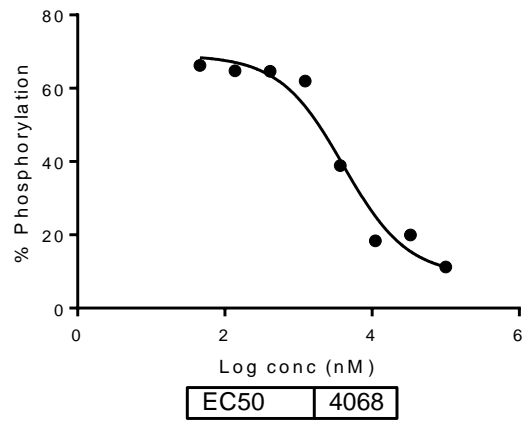
Avg IC<sub>50</sub> = 48 ± 2 μM

### Compound 4.3



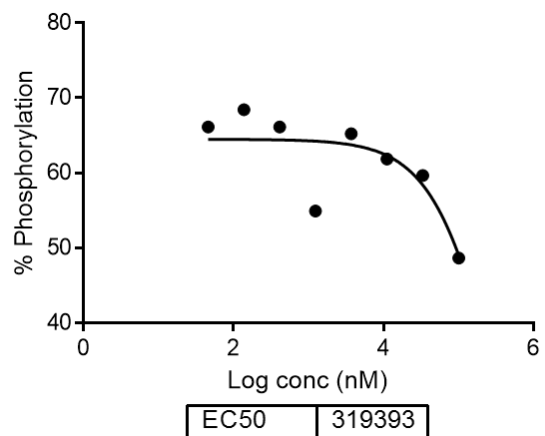
Avg  $IC_{50} = 83 \pm 6 \mu M$

### Compound 4.4



Avg  $IC_{50} = 4.4 \pm 0.3 \mu M$

### Compound 4.5



Avg  $IC_{50} = 274 \pm 45 \mu M$